Author:
Sharma, Shachi Dayal Gurumayum

Title:
Investigation of the surface interactions of polymer and surfactants in non-polar media

INVESTIGATION OF THE SURFACE INTERACTIONS OF POLYMER AND SURFACTANTS IN NON-POLAR MEDIA

by

Shachi Dayal Gurumayum Sharma

A thesis submitted to the University of Bristol in accordance with the requirements of the degree of Doctor of Philosophy in the School of Chemistry, Faculty of Science

Bristol, United Kingdom July 2002

ABSTRACT

Polymers and surfactants are usually added to Gasoline fuel formulations to help in the dispersion of carbonaceous particles formed during internal combustion. The polymer molecules are terminally functionalised, low molar mass polyisobutylenes (PIB) whilst the surfactants are alcohol or alkylphenol alkoxylate molecules. This study investigates the mechanism by which the molecules help reduce deposition. Adsorption isotherms of a PIB polymer, and surfactant molecules on stainless steel beads (~7 μm) and carbon particles (~ 214 nm) have been obtained. These isotherms show that the presence of a functional group increases adsorption. Surfactant molecules also reduce the adsorption of the polymer on steel. Modelling the isotherms shows the presence of aggregates on the surface with aggregation numbers ranging between 2 and 6. Interactions and aggregations in solutions have also been studied by using a hydrophilic dye, Rhodamine B, and the presence of a functional group appears to enhance aggregation. Flow-cell studies demonstrate the cleaning properties of the surfactants and indicate a synergistic interaction between the polymer and the surfactants. These studies clearly show that the presence of the polymer is necessary prior to deposition for the carbon particles to be removed afterwards. Atomic force microscopy and ellipsometry studies also show that the polymer is primarily the species providing a steric barrier.

Dedicated to my parents
for their encouragement and
continuing support and inspiration

ACKNOWLEDGEMENTS

At the very outset, I would like to thank my advisor, Professor Brian Vincent for his guidance and extremely valuable "surgeries" throughout the course of my doctoral research.

I would also like to thank my industrial advisor Dr. David Moreton, of Lubrizol UK, and my second assessor, Professor Terence Cosgrove for the interesting discussions and talks on the subject.

I would also like to thank Mr. Malcolm Macduff, Dr. Douglas Barr, and Mr. Rodney McAtee, all of Lubrizol UK for feedbacks and inputs into the project during regular group meetings. My thanks also go out to Dr. Roy Hughes {at the Bristol Colloid Centre (BCC)}, my MSc supervisor who continued to provide feedbacks and ideas during the course of my PhD, Dr. Jason Riley for thoughts on ellipsometry, Dr. Keith Bean (at the BCC) for help with the BET measurements, Dr. Manuel Romero (of Almeria University, Spain) for discussions on model fitting of the adsorption isotherms, and Dr. (soon!) Robin Mogford, who started work on adsorption on carbon and aggregation studies, and gave regular inputs into my work.

I would also like to thank Professor Paul Luckham, of Imperial College, London for giving me the opportunity to work in his lab using a `homemade` atomic force microscope. I also thank Miss Suraya Abdul Rashid who helped tremendously with the AFM experiments.

I would also like to thank Miss Ingrid Leveque for helping me out with the scanning electron microscopy studies of the flow cell plates. Here, my acknowledgements also go out to Mr. Charlie Murrey, Mr. Gwyn Jones, Mr. Phil Powell and Mr. Nigel Rich at the mechanical workshop for building the flow cell and the 'hot box tumbler' for me. I would also like to thank Miss Holly Alford, who did a good job of working with the

ubiquitous carbon particles as part of her undergraduate project. I would also like to thank Dr. Nisakorn Thongkon, Mr. Ian Nichols, and Mr. Chris Gill for help with the atomic absorption spectroscopy, refractometry, and Karl Fischer titration experiments, respectively.

I would also like to thank Mrs. Sarah Lawrence and Mrs. Sue Williams for helping me deal with the administrative necessities involved in carrying out any research study.

I would also like to thank all the wonderful members, past and present, of the Brian Vincent and Jeroen van Duijneveldt labs like Peter "Burnley" Dowding, James "Two" Weeks, Adrian "Guinness" Horgan, Alex "Cheerful" Routh, Laura "Germanic" Harnett, Tim "Aussie" Muster, Theresa "Manager" Wade, Patricia "Irish" Marr, Gerrit "Dutch" Vliegenthart, Shu-Dong "Soft-Spoken" Zhang, Bernd "Dribbling" Neumann, Matthew "Rugby" Hearn, Edward "High-Flyer" Leach, David "Monsieur" Voisin, Paul "Blue Skies" Seymour, Phillip "English" Dale, Ruth "In-Charge" Dunleavey, Darby "Yellow" Kozak, Pierre "Jolly" Starck, Kathryn "Welsh" Rees, Jessica "Polite" Tsiopani, John "Deep Thinking" Hardy, Claire "Smily" Pizzy, and Yves "Capoeira" Hennequin, to name some, for a wonderful three years in the lab. I also thank Brian for the times spent watching some wonderful cricket at Lord's! I have very much enjoyed the company of everyone in the lab and the department!

I would also like to thank The Lubrizol Corporation and the University of Bristol for providing the necessary funding to carry out this study.

Finally, I would like to thank my parents who are a continuing source of inspiration for me and to whom I dedicate this thesis.

AUTHOR'S DECLARATION

I declare that the work in this dissertation was carried out in accordance with the Regulations of the University of Bristol. The work is original except where indicated by special reference in the text and no part of the dissertation has been submitted for any other degree.

Any views expressed in the dissertation are those of the author and in no way represent those of the University of Bristol.

The dissertation has not been presented to any other University for examination either in the United Kingdom or overseas.

SIGNED: 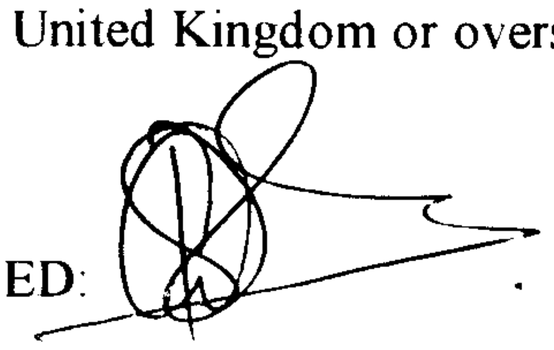 DATE: 31st July 2002

CONTENTS

LIST OF GRAPHS AND TABLES

CHAPTER 1: INTRODUCTION

1.1. Introduction

The oxidation and polymerisation of hydrocarbon fuel can lead to deposit formation on the surface of engine components, such as carburettor ports, fuel injectors, intake valves, etc. These deposits can also be formed due to the incomplete combustion of the mixture of air, fuel, and oil. Some of the problems caused by these deposits include stalling, poor acceleration, increase in fuel consumption and production of exhaust pollutants[1, 2]. The deposits can also lead to the formation of hot spots causing uncontrolled surface ignition[3]. These depositions are generally prevented by the addition of various additives in the fuel formulation. Thus, the development and understanding of the mechanism of interactions between the various additives form an integral part of passenger car motor oil development and in cutting the cost of formulation[4, 5]. In modern gasoline formulations, additives are added along with various other components like antiknocking agents (tetramethyl lead, ferrocene, etc.), octane improvers (ethyl *tert*-butyl ether), antioxidants (alkylated diphenyl amines), etc[6, 7]. The additives added generally consist of a functionalised PIB dispersant and alkoxylate surfactants, called "carrier fluids" in the additives industry.

The aim of this study is to understand the mechanism of interactions between a polyisobutylene polymer and a range of surfactants added to gasoline fuel formulations in order to help keep the inlet valve surface clean during the process of combustion. The polymer is a terminally functionalised polyisobutylene (PIB) molecule and the surfactants are alcohol or alkylphenol alkoxylate molecules. An understanding of their interactions could help in finding and developing new methods of analysis by which the additives used can be screened and tested before being marketed to the consumers.

1.2. Polyisobutylenes as stabilisers

The use of functionalised PIB as dispersants is a much studied subject. These dispersants stabilize the particles, formed during combustion, by strongly adsorbing on these particles while remaining soluble in the continuous solvent phase and, thus, help in reducing deposit formation on the engines surfaces[8-11]. The polymers prevent the flocculation of particles by overcoming the attractive van der Waals force between the particles[12, 13]. Though the effect of charges present on the particles in the stabilisation of these systems in non-polar media remains a subject of investigation[14-16], it is generally considered that the polymer stabilises the particles by providing a steric barrier between them[10, 17], as schematically represented in figure 1.1.

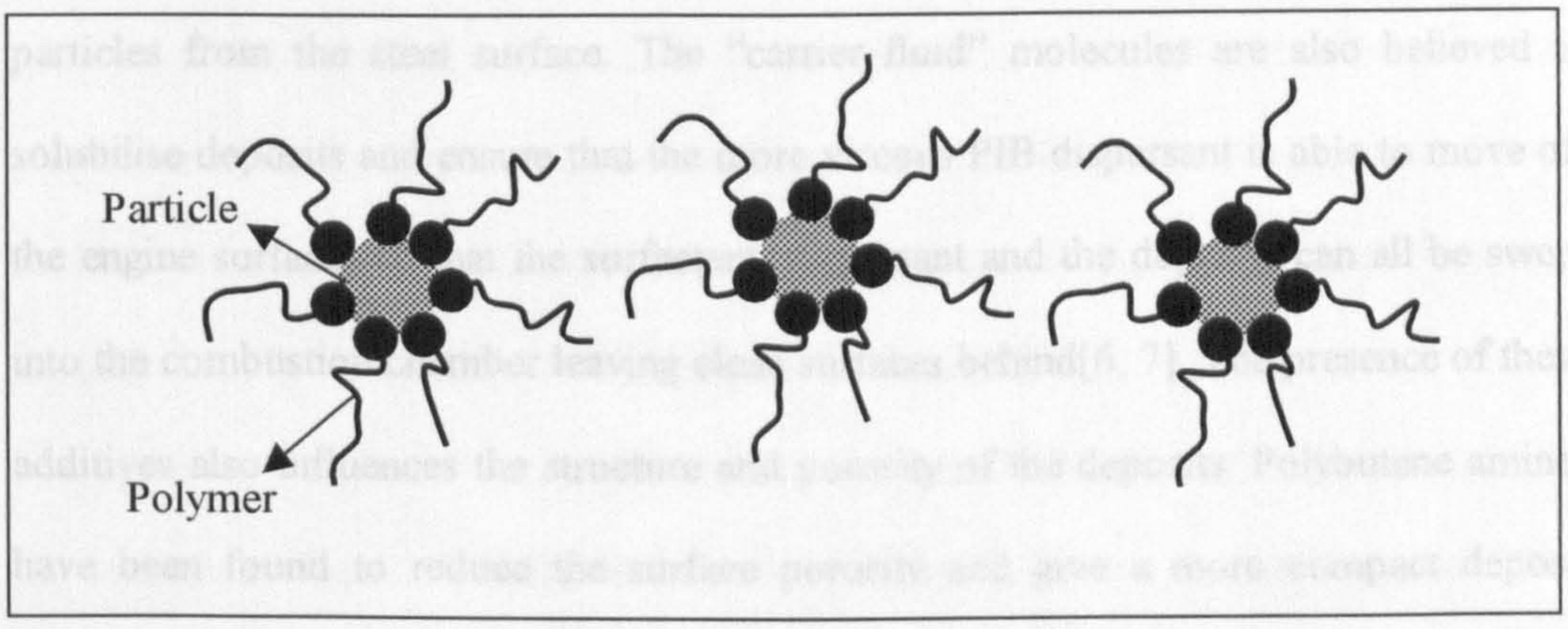

Figure 1.1: Schematic representation of steric stabilisation of carbonaceous particles by PIB dispersants

1.3. Polyisobutylene dispersant and carrier fluids

The interaction of PIB dispersants with carbon surfaces and their role in the dispersion of carbonaceous particles in nonpolar media is relatively well understood, as compared to the interactions of these polymers with stainless steel surfaces. Even less understood is the reason why PIB dispersants function more efficiently in the presence of certain of the "carried fluids". For example, in the US, an alkyl butoxylate surfactant with a propylene amine headgroup (represented as S3 in chapter 2) can play the role of a dispersant and help in keeping the intake valve surface clean. The same surfactant does

not work efficiently in European car engines and needs the presence of a PIB dispersant. This has been attributed to the fact that cars travel faster and shorter distances in Europe than in the US putting a larger load on the smaller European car engines.

The exact role played by the surfactants along with the PIB dispersant is not understood and this study is one of the first investigations carried out to gain an insight into the mechanism. A possible synergistic behaviour of the PIB dispersant and the surfactant molecules has been hypothesised. The PIB dispersant is expected to provide a steric barrier between the particles and the steel surface whilst the surfactant molecules are believed to play a major role in the removal of deposited or adsorbed particles from the steel surface. The "carrier fluid" molecules are also believed to solubilise deposits and ensure that the more viscous PIB dispersant is able to move off the engine surfaces so that the surfactant, dispersant and the deposits can all be swept into the combustion chamber leaving clean surfaces behind[6, 7]. The presence of these additives also influences the structure and porosity of the deposits. Polybutene amines have been found to reduce the surface porosity and give a more compact deposit structure as compared to polyether amine surfactants. The surface pores in the deposits formed may also be able to absorb the PIB dispersant and surfactants which, during combustion, may themselves burn and burn off the deposits. Though the mechanism of deposit structure formation is not clear, it has been suggetsed that the structure has a definite role in the effectiveness of the additives in removing the deposits[3].

1.4. Objectives

The primary objective of this work was to study the surface interactions of a functionalised PIB dispersant and a range of alkoxylate surfactants in a nonpolar medium, i.e. isooctane. The effect of these interactions on the deposition and removal of carbon particles from steel surfaces has also been studied. In chapter 2, the polymer and surfactants used have been described along with a schematic representation of their synthetic routes. The steel beads and carbon particles used have been characterised by the adsorption of nitrogen and statistically analysed by using the BET method[18]. The adsorption isotherms of the polymer and surfactants have been carried out on the steel beads as well the carbon particles (chapter 3) in order to understand the surface affinity of the additives used. This also gives information on the build-up of the polymer/surfactant molecules at the solid/isooctane interface and the aggregation at the surface can be calculated by theoretically fitting the data. Adsorption experiments of the polymer plus a surfactant have also been carried out.

The presence of a polar head group and a hydrocarbon tail give rise to the possibility of the polymer/surfactant forming reverse micellar aggregates in a nonpolar medium. This has been investigated using vapour pressure osmometry and a water soluble dye; the results are reported in chapter 4.

The adsorption of polymer molecules at the solid/liquid interface and the thickness of the adsorbed polymer layer can also be studied by using an atomic force microscope. The experiments have been carried out by using a carbon coated glass bead as a probe and the results have been presented in chapter 5. Information on structural conformations as diagrammatically represented in figure 1.2 can be obtained from the force profile curves.

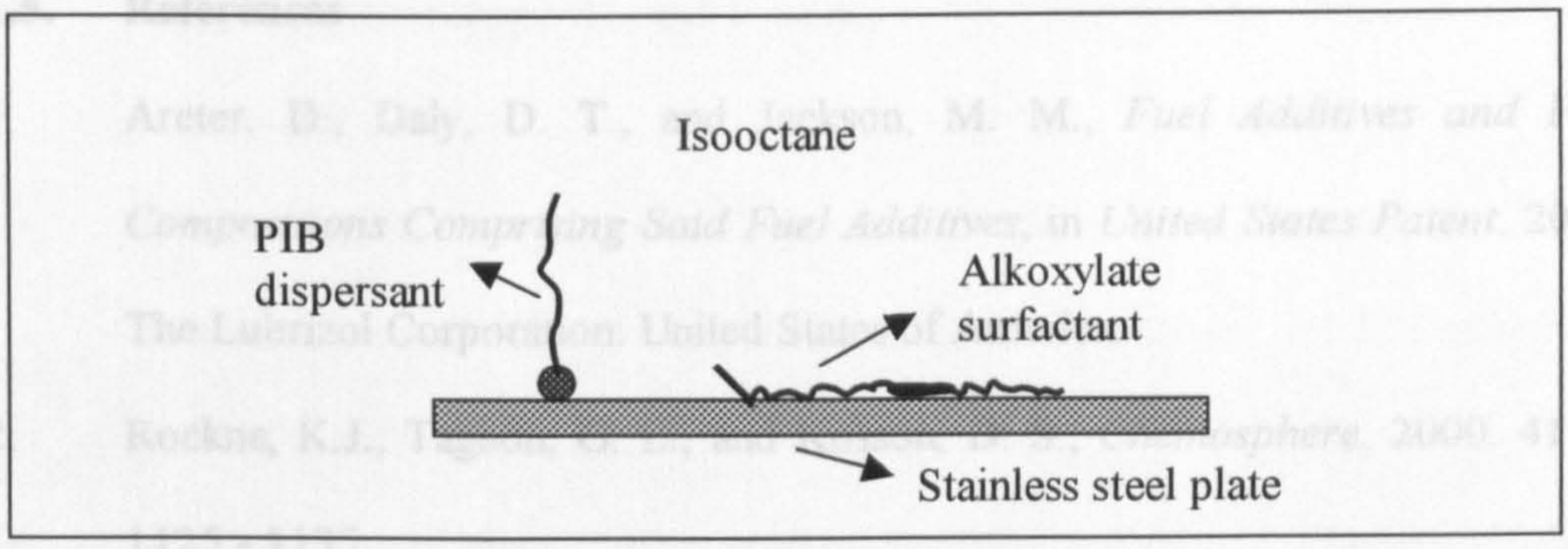

Figure 1.2: Conceivable conformations of the PIB dispersant and the surfactant at the steel/isooctane interface

In chapter 6, the growth and thicknesses of various polymer/surfactant layers at the steel/isooctane interface studied by ellipsometry have been reported. Ellipsometry experiments, carried out *in-situ*, helps in the understanding of the geometry of configuration of the different species at the interface as already represented in figure 1.2.

As part of this study, a flow cell was built to study the deposition of carbon particles on stainless steel plates. Removal experiments were also carried out using various combinations of the polymer and surfactant solutions. These experiments and image analyses of the digital pictures (of deposition and removal experiments) have been outlined in chapter 7.

Chapter 8 gives the overall conclusions of this study by correlating the adsorption, atomic force microscopy, ellipsometry, flow cell and aggregation studies. A clearer understanding of the interactions between the PIB dispersant and the alkoxylate surfactants has now been achieved. Synergistic behaviour is observed not only during the deposition of particles, but also during the removal process. These developments should lead to the ability to screen and select a combination of a polymer and a surfactant for enhanced performance in gasoline engines.

1.5. References

1. Areter, D., Daly, D. T., and Jackson, M. M., *Fuel Additives and Fuel Compositions Comprising Said Fuel Additives*, in *United States Patent*. 2001, The Lubrizol Corporation: United States of America.
2. Rockne, K.J., Taghon, G. L., and Kosson, D. S., *Chemosphere*, 2000. **41**: p. 1125 - 1135.
3. Zerda, T.W., Yuan, X., and Moore, S. M., *Carbon*, 2001. **39**: p. 1589 - 1597.
4. Roby, S.H., *Journal of the Society of Tribologists and Lubrication Engineers*, 1996: p. 787.
5. Mortier, R.M., and Orszulik, S. T., ed. *Chemistry and Technology of Lubricants*. Second ed. 1997, Blackie Academic and Professional: London.
6. Batt, R. *Performance Additives*. in *Additives 2001*. 2001. Oxford: Associated Octel Co. Ltd.
7. Field, I. *Lubricating Oil Additives*. in *Additives 2001 (RSC Training Day)*. 2001. Oxford: Infineum.
8. Pugh, R.J., and Fowkes, F. M., *Colloids and Surfaces*, 1984. **11**: p. 423 - 427.
9. Cox, A.R., *The Effect of Polymer Chain Architecture on the Adsorption and Dispersion Properties of Polyisobutylene*, in *Department of Chemistry*. 1998, University of Bristol: Bristol.
10. Cox, A.R., Mogford, R., Vincent, B and Harley, S., *Colloids and Surfaces A: Physicochemical and Engineering Aspects*, 2001. **181**: p. 205-213.
11. Aleman-Vazquez, L.O., and Villagomez-Ibarra, J. R., *Fuel*, 2001. **80**: p. 965-968.
12. Israelachvili, J.N., *Intermolecular and Surface Forces*. 1991: Academic Press.
13. Hunter, R.J., *Foundations of Colloid Science*. Vol. 1. 1995: Oxford University Press.

14. Pugh, R.J., Matsunaga, T., and Fowkes, F. M., *Colloids and Surfaces*, 1983. 7: p. 183 - 207.

15. Kornbrekke, R. *Charging and Colloidal Stability in Low Dielectric Liquids*. in *Gordon Research Conference, Chemistry at Interfaces*. 2002. Connecticut College, New London, USA.

16. Morrison, I., and Herb, C. *Charging of Particles in Nonpolar Media*. in *Gordon Research Conference, Chemistry at Interfaces*. 2002. Connecticut College, New London, USA.

17. Forbes, E.S., and Neustadter, E. L., *Tribology*, 1972. **5**: p. 72 - 77.

18. Brunauer, S., Emmett, P. H. and Teller, E., *Journal of American Chemical Society*, 1938. **60**: p. 309.

CHAPTER 2: MATERIALS

2.1. Introduction

During the course of this investigation, experiments have been carried out involving various types of polymer and surfactants, steel beads, carbon particles and steel plates for flow cell studies. Isooctane was used as the solvent throughout the study unless mentioned otherwise. In this chapter a brief description of the materials used will be given.

2.2. Polymer and surfactants

2.2.1. Synthesis

The polymer and surfactants used in this study have all been commercially synthesised at Lubrizol UK. The company manufactures and markets fuel additives. The polymer used was a terminally functionalised relatively low molar mass polyisobutylene (PIB) chain. PIB is a general purpose, hydrocarbon rubber produced in the molecular weight typically 500-3000 and is used in a range of applications such as automotive inner tubes, wire insulation, sealants and also, as in this study, as gasoline additives[1, 2]. PIB is widely used in the latter context because it is economical to manufacture and solubilises well in apolar solvents. The primary structure of these gasoline dispersants is as shown in figure 2.1[3]:

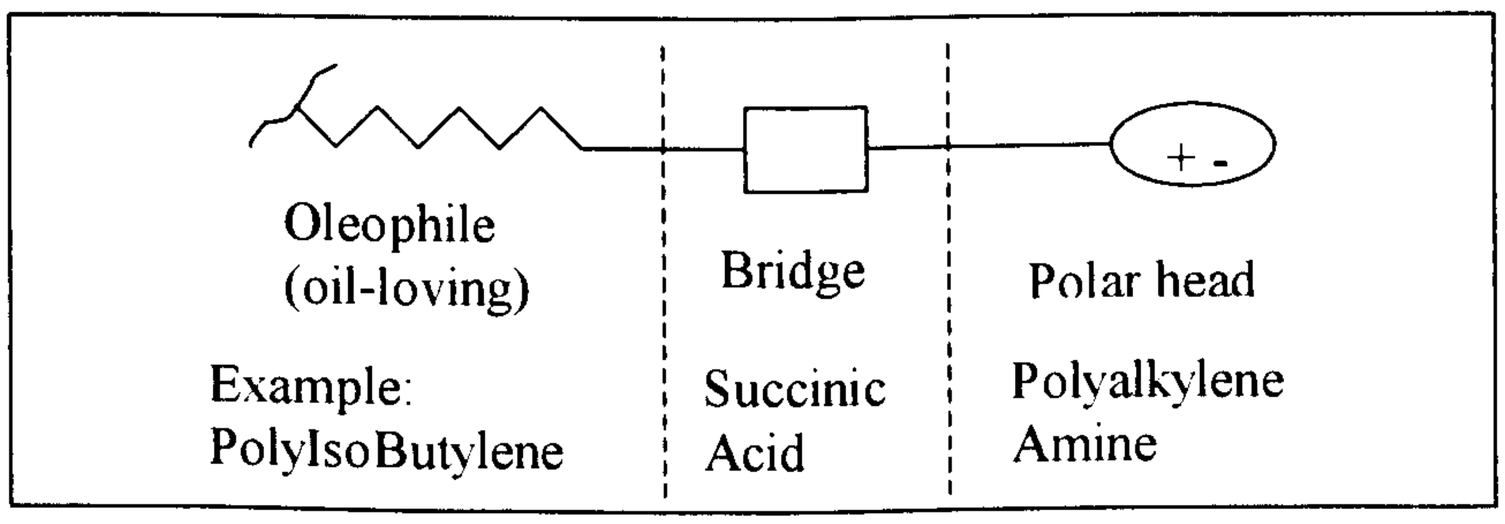

Figure 2.1: The primary structure of a dispersant

The different structures and molecular weights of the polymer and surfactants used in this study are as shown in figure 2.2:

Species Name	Structure	Mol. Wt./(g mol^{-1})
P1	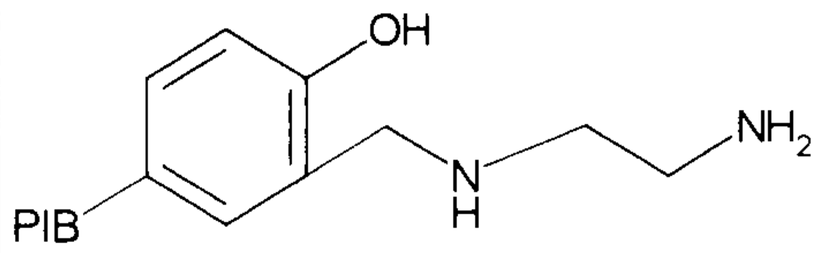	1174
S1	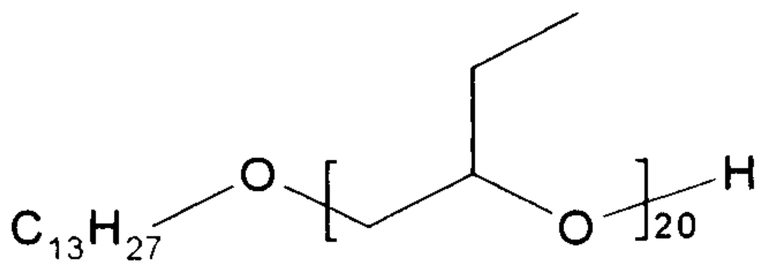	1640
S2	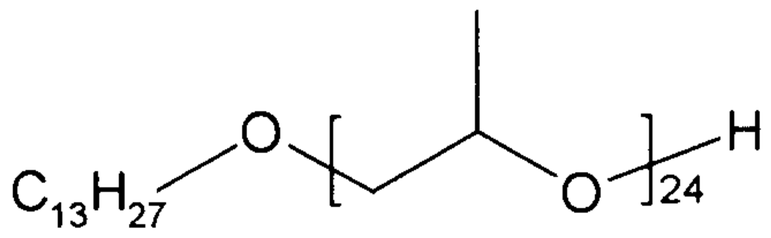	1592
S3	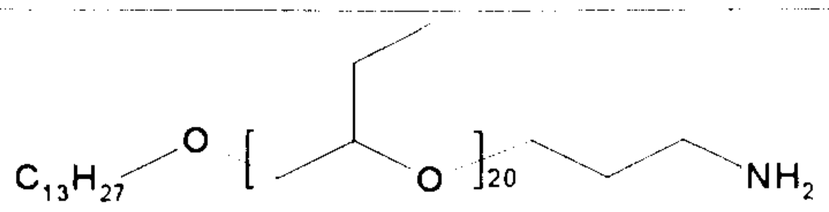	1697
S4	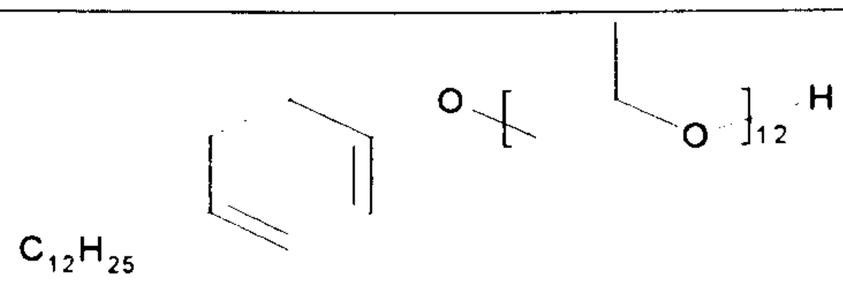	958
S5	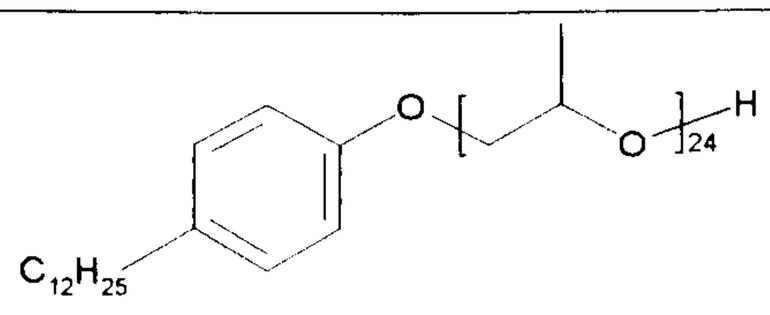	1654

Figure 2.2: Structures and molecular weights of the polymer and surfactants used

The polymer used in this study, termed P1, was synthesised by first alkylating phenol using the Friedel Crafts reaction with vinylidene polyisobutylene to give PIB phenol. This reaction uses BF_3 as a catalyst and normally has around 97% conversion. The PIB

phenol was then reacted with ethylene diamine (EDA) in the presence of formaldehyde to give the desired Mannich product as outlined in the mechanisms in figure 2.3[4]:

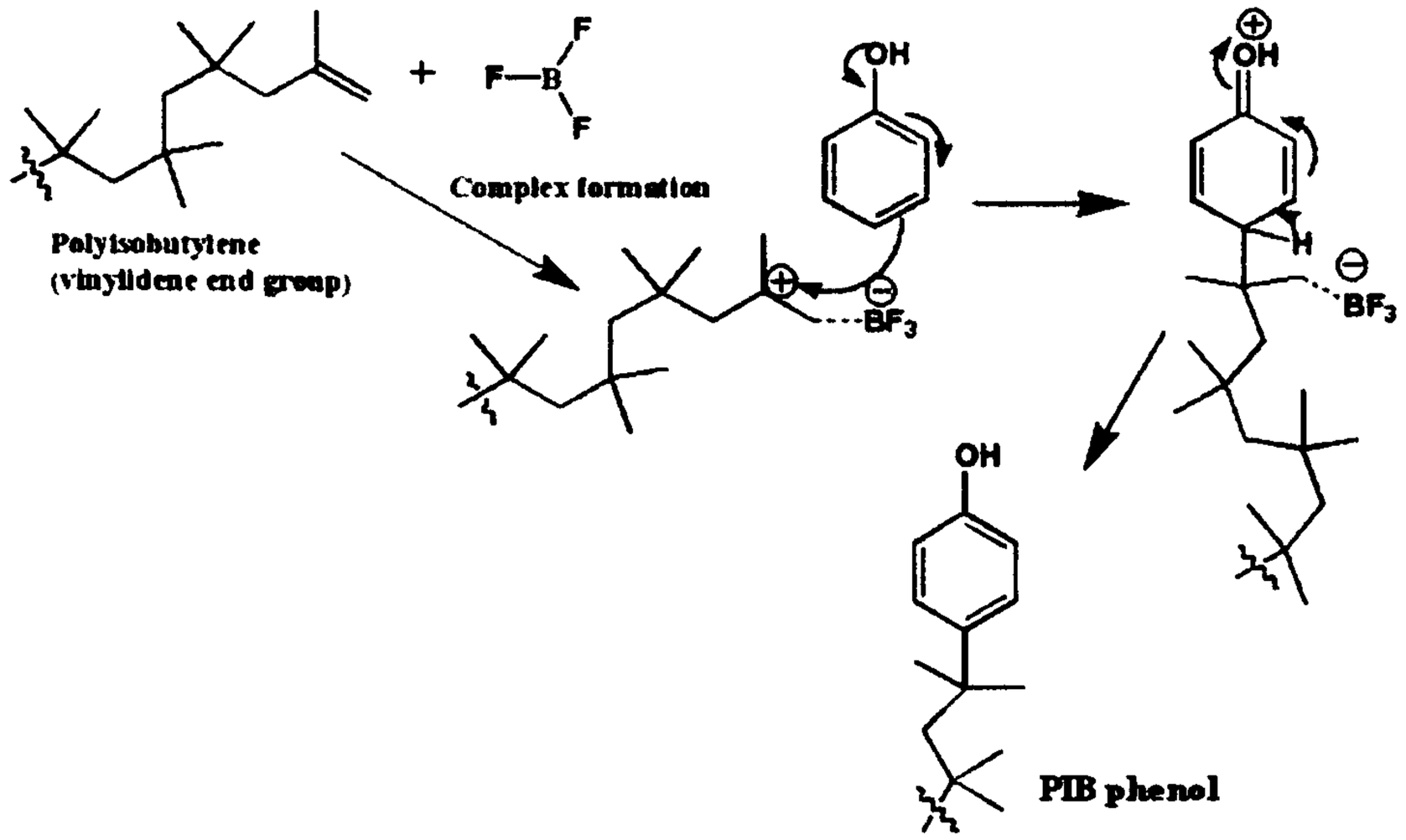

Figure 2.3: Alkylation of Phenol to obtain PIB phenol by Friedel Crafts reaction. The –OH group is strongly electron donating and ortho-para directing.

The second reaction which was the conversion of the PIB phenol to the final product could occur via two mechanisms depending on whether EDA was added first or not. When formaldehyde was added before the EDA, a methylol intermediate could be formed which then reacted with EDA to give the final product. On the other hand, if EDA was added to the formaldehyde, the mechanism could be via the formation of the Mannich adduct which then reacted with PIB phenol to give the final product. These mechanisms are shown in figures 2.4 and 2.5[5]:

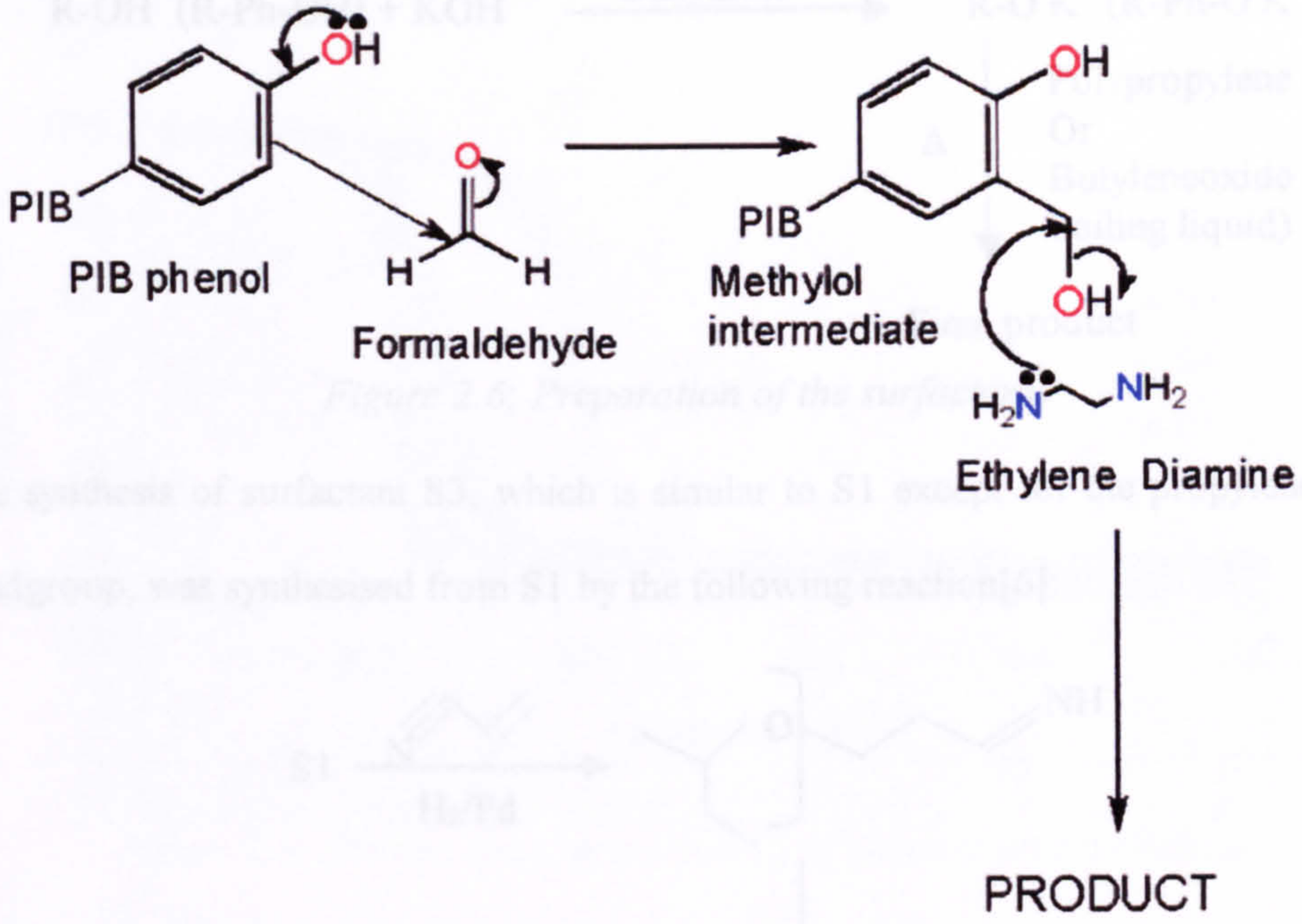

Figure 2.4: Mannich reaction via the formation of methylol intermediate when formaldehyde is added first

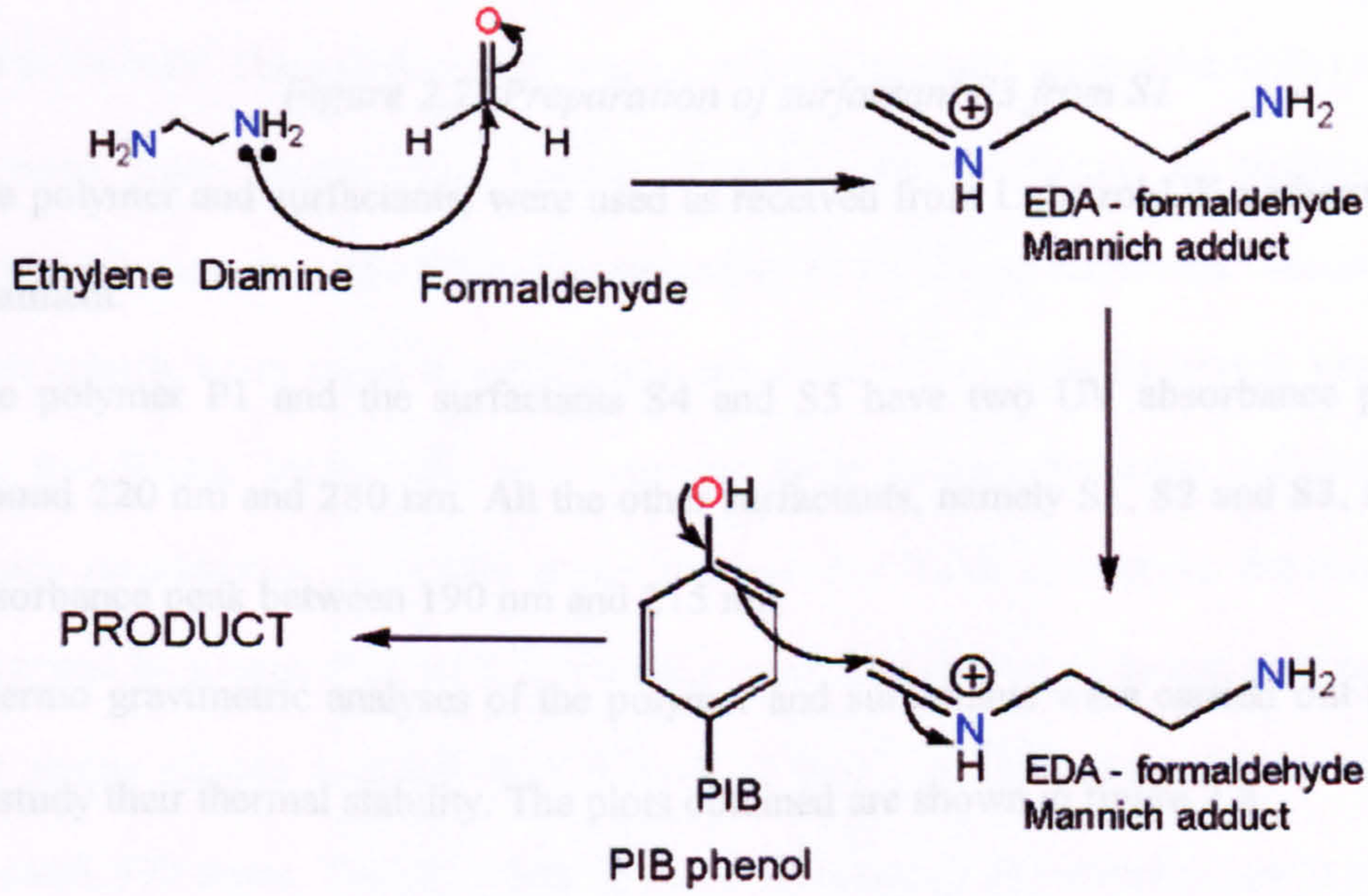

Figure 2.5: Mannich reaction mechanism via the formation of Mannich adduct when ethylene diamine is added first to the formaldehyde

The surfactants used in this study were also synthesised at Lubrizol UK. These were prepared by reacting the appropriate alcohol or alkyl phenol with alkoxylates catalysed by NaOH or KOH at about 120 °C and are summarised in figure 2.6:

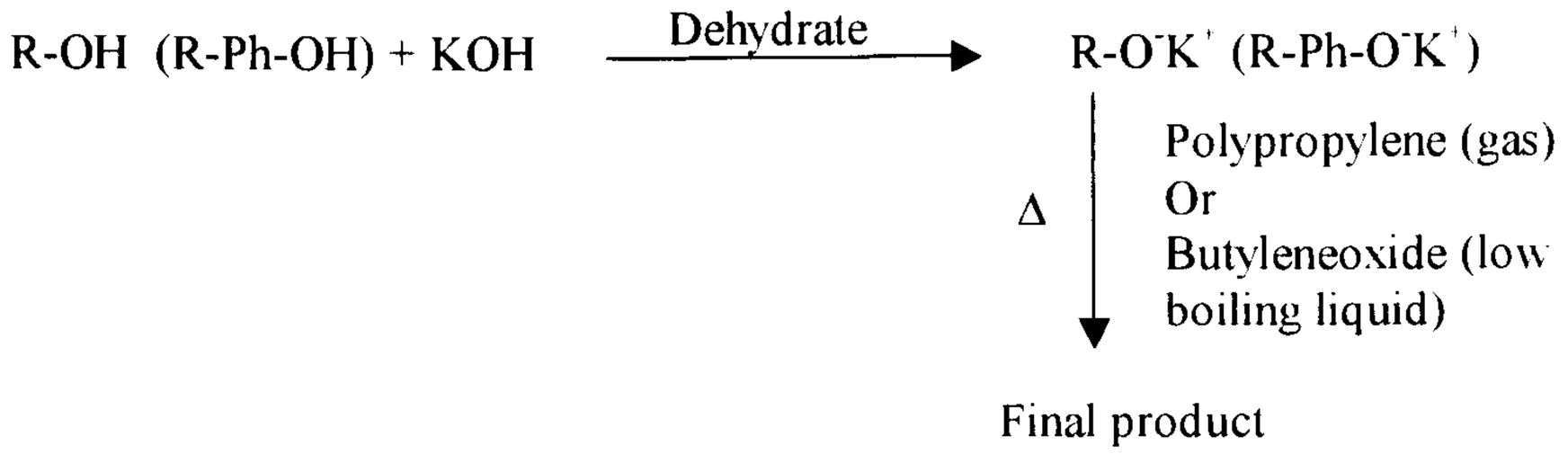

Figure 2.6: Preparation of the surfactants

The synthesis of surfactant S3, which is similar to S1 except for the propylene amine headgroup, was synthesised from S1 by the following reaction[6]:

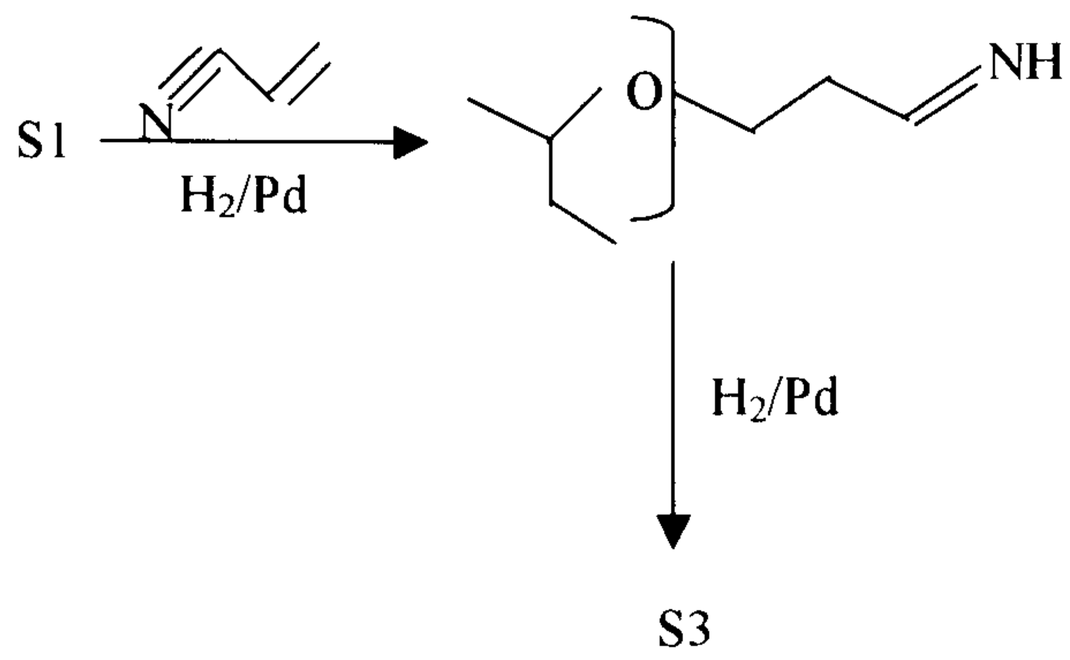

Figure 2.7: Preparation of surfactant S3 from S1

The polymer and surfactants, were used as received from Lubrizol UK without further treatment.

The polymer P1 and the surfactants S4 and S5 have two UV absorbance peaks at around 220 nm and 280 nm. All the other surfactants, namely S1, S2 and S3, show an absorbance peak between 190 nm and 215 nm.

Thermo gravimetric analyses of the polymer and surfactants were carried out in order to study their thermal stability. The plots obtained are shown in figure 2.8.

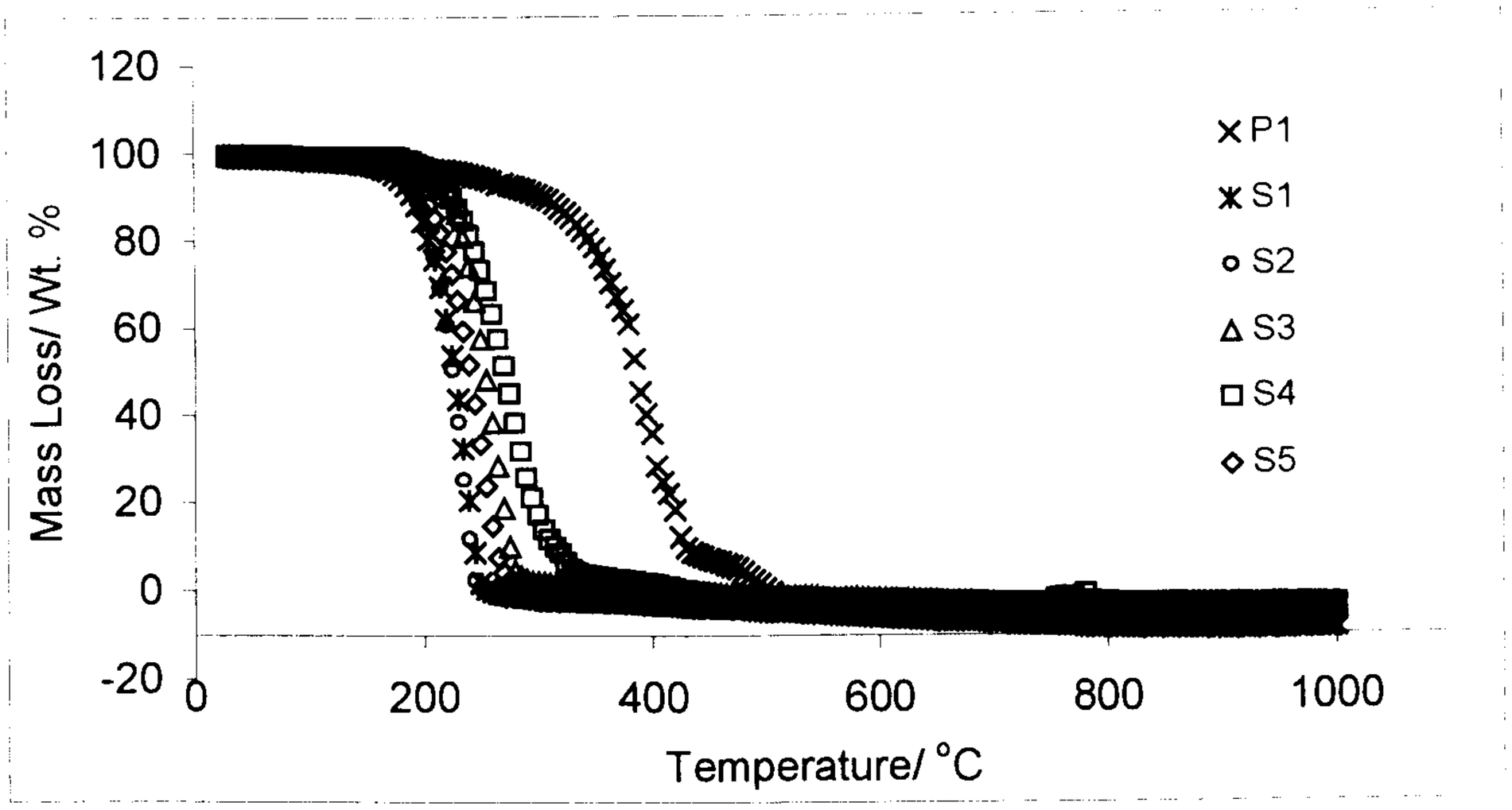

Figure 2.8: Thermo gravimetric profile of polymer and surfactants

2.2.2. Molecular modelling

In order to gain some insight into the molecular structures of the polymer and the different surfactants used in this study, some molecular modelling studies were carried out in vacuum. The software used was a CAChe (Computer Aided Chemistry) software obtained from Fujitsu. The various structures were obtained by performing an optimised geometry calculation corresponding to an energy minimum. Terms for the bond stretch, bond angle, dihedral angle, improper torsion, torsion stretch, bend bend, van der Waals, electrostatic and hydrogen bond interactions were included in the energy minimisation procedure except that van der Waals interactions between atoms separated by greater than 9.00 Å were excluded. The optimisation was continued until the energy change was less than 0.0042 kJ mol^{-1}, or until the structure had been updated 300 times. The structures obtained after energy minimisation are as shown in figure 2.9. However, the structures may undergo changes when interacting with solvent molecules.

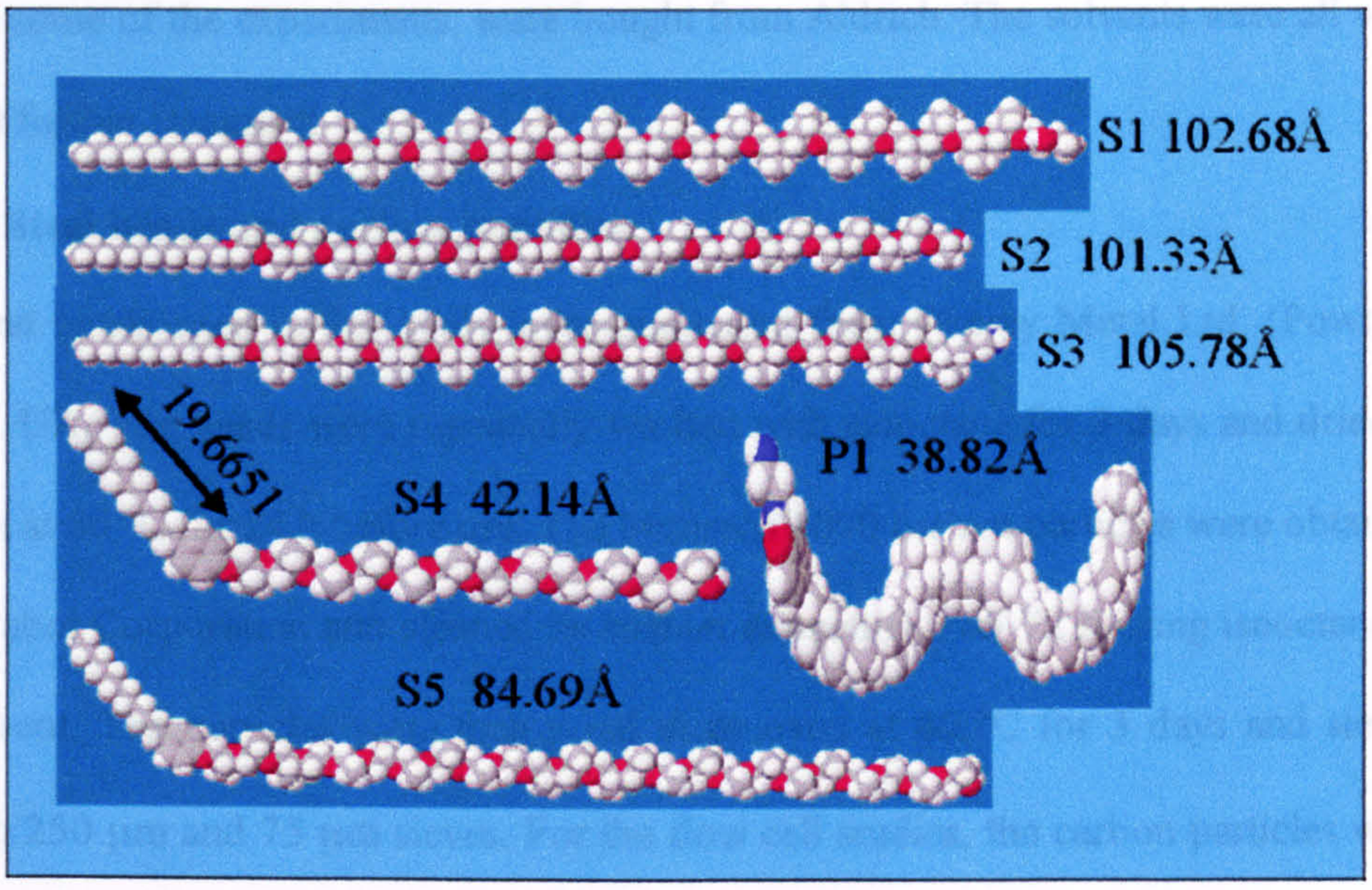

Figure 2.9: Structures of the polymer and surfactants used. The numbers given are the lengths of the individual polymers.

Interestingly, surfactants S1 and S3 also formed a globular structure on energy minimisation as shown in figure 2.10.

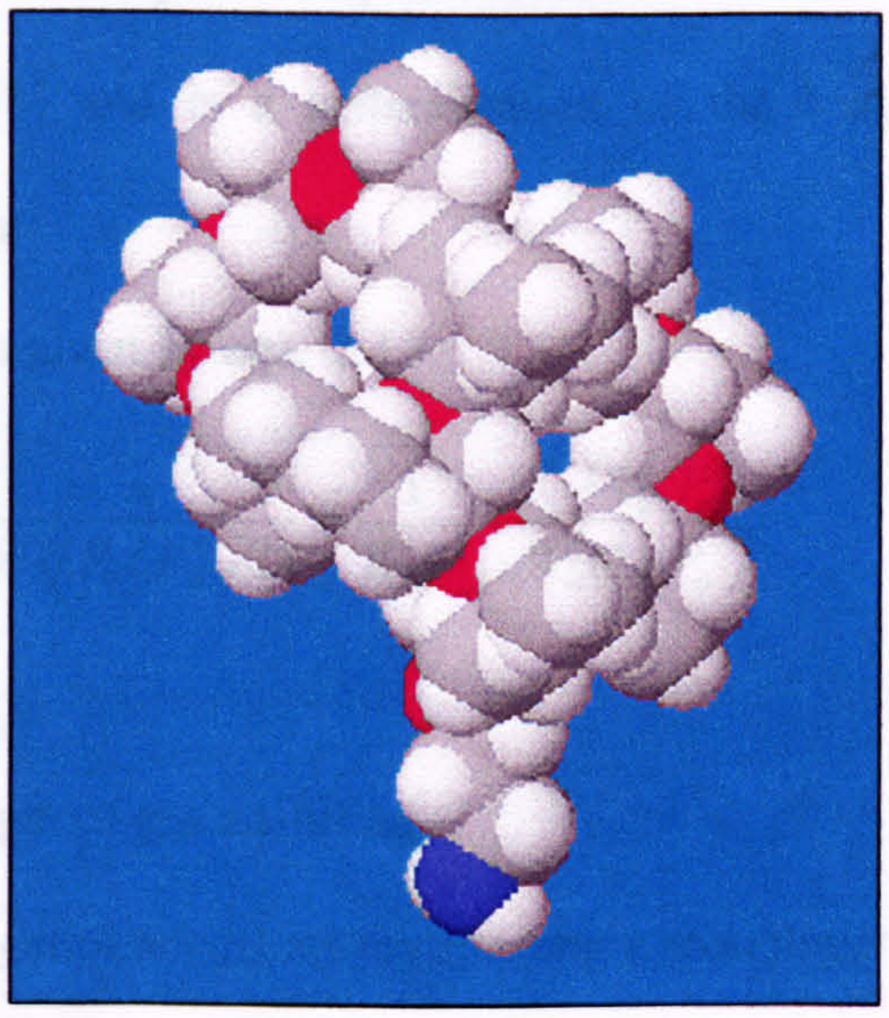

Figure 2.10: The folded structure of S3

2.3. Solvents

The solvent used primarily in this study was isooctane, purchased from Rathburn, UK. Karl Fischer analysis of the solvent gave a water content of the stock material of around 43 ppm. Other solvents, namely hexadecane, o-xylene and toluene, which were

used in some of the experiments, were bought from Aldrich. The solvents were all used without further treatment.

2.4. Steel beads and carbon particles

The steel beads used in this study were purchased from Osprey Metal Ltd. (Powders group), UK. The beads were repeatedly washed with isooctane for 3 days and dried in an oven at 80 °C for 24 h before use. The Monarch 1000 carbon particles were obtained from Cabot Corporation and cleaned by soxhlet extraction over 72 h using isooctane as the solvent. The particles were then dried in an oven at 80 °C for 3 days and sieved through 250 μm and 75 μm sieves. For the flow cell studies, the carbon particles were washed repeatedly in isooctane for 3 days and then dried and sieved.

2.4.1 Determination of the specific surface area of the beads and particles

The BET method allows the measurement of the surface area and porosity of solid particles by the physical adsorption of gaseous species such as nitrogen[7]. This method of analysing multilayer adsorption isotherms was first developed by Brunauer, Emmett and Teller[8] and is a generalisation of the Langmuir's treatment[9] for adsorbed monolayers.

The BET equation is given by eqn. 2.1.

$$\frac{1}{W((P_0/P)-1)} = \frac{1}{W_m C} + \frac{C-1}{W_m C}\left(\frac{P}{P_0}\right) \qquad \text{(Eqn. 2.1)}$$

where,

W = weight of gas adsorbed

W_m = weight of adsorbate constituting a monolayer of adsorbed molecules

P = pressure of gas

P_0 = saturated vapour pressure

C = BET constant which gives an indication of the magnitude of interactions between the adsorbate and the adsorbent and can be

expressed as the difference in adsorption energy in the first layer and subsequent layers[10, 11])

The BET equation is normally linearised as a plot of $1/W((P_0/P)-1)$ against P/P_0. If N_2 is used as the adsorbate, P/P_0 is usually restricted in the range of 0.05 to 0.35[12]. The weight of the monolayer of adsorbate, W_m, can then be obtained from the slope, s, and intercept, i, of the BET plot as shown in equations 2.2 and 2.3:

$$s = \frac{C-1}{W_m C} \qquad \text{(Eqn. 2.2)}$$

$$i = \frac{1}{W_m C} \qquad \text{(Eqn. 2.3)}$$

By combining equations 2.2 and 2.3 and eliminating C, W_m can be calculated as shown in equation 2.4

$$W_m = \frac{1}{s+i} \qquad \text{(Eqn. 2.4)}$$

The specific surface area, S_{BET}, is then expressed as:

$$S_{BET} = \frac{W_m N A_{cs}}{M} \qquad \text{(Eqn. 2.5)}$$

where,

N = Avogadro's number (6.023×10^{23} mol^{-1})

M = molecular weight of the adsorbate

A_{cs} = molecular cross sectional area of the adsorbate molecules

The cross sectional value for nitrogen, assuming a hexagonal close packed monolayer, at its boiling point (77K) is 16.2Å^2[13].

2.4.2. Porosity of solids obtained by gas adsorption

Porosity is defined as the total volume of pores per unit mass of a substance. It may also be expressed as the percentage of the total volume of the substance, i.e. $(V_{pores}/V_{substance}).100$ %[14]. Different techniques such as mercury porosimetry, X-ray

diffraction and gas adsorption exist for determining porosity. The most common gas used for adsorption studies is nitrogen; the small size of the molecules enables small pores to be penetrated.

Pores are classified into three main groups depending on their radius as follows[15]:

a) Macropores – pores with radii greater than 50 nm

b) Mesopores – pores with radii between 2 nm and 50 nm

c) Micropores – pores with radii less than 2 nm

Adsorption isotherms of nitrogen on the adsorbent are obtained by adsorbing known volumes of nitrogen at different equilibrium pressures[11]. Similarly, desorption isotherms can be obtained by monitoring the amount of gas removed on lowering the relative pressure. The adsorption isotherms thus obtained may be grouped into one of the five types. These different types are discussed in Chapter 3. Of the five types, type I is displayed by those with micropores such as activated carbons and molecular sieve zeolite. Type IV and V, on the other hand, are associated with adsorption by mesoporous surfaces.

The adsorption isotherms of porous materials exhibit a hysteresis loop because the adsorption and desorption curves do not coincide. Though generally associated with mesoporous structures, where capillary condensation can occur, microporous structures have also been shown to exhibit hysteresis at the lower pressure regime. For microporous materials, the amount of gas adsorbed increases very little after the pores have been filled with increased pressure and a plateau is obtained (type I of the five types)[14]. The various factors affecting adsorption hysteresis are not fully understood but the hysteresis shapes can be associated with various pore structures. Such connections were first exhibited by de Boer who identified five types of hysteresis loops as shown in figure 2.11[7, 16]:

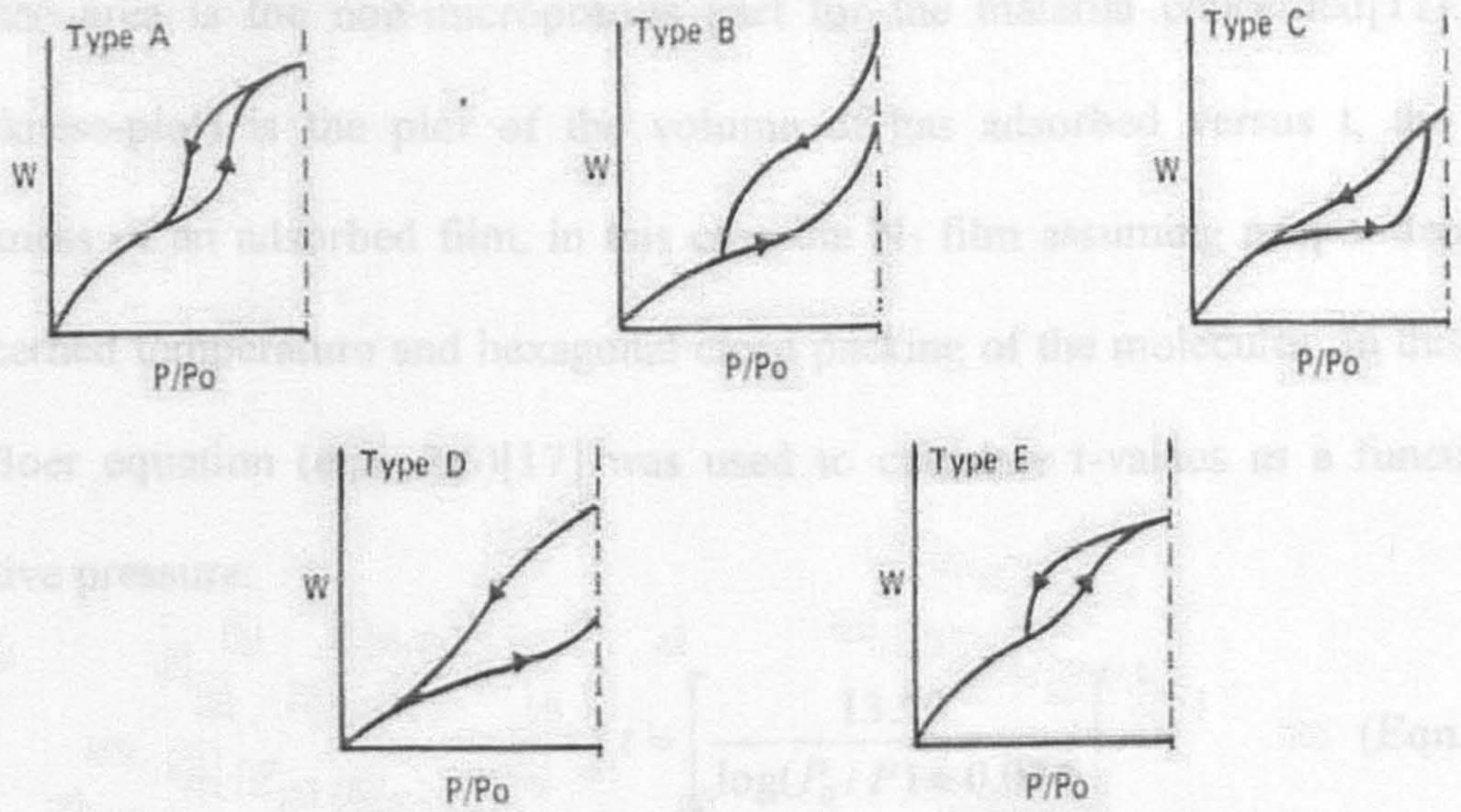

Figure 2.11: de Boer's five types of hysteresis[7]

Type A represents cylindrical pores open at both ends

Type B is associated with slit-shaped pores

Type C is related to tapered/wedged shaped pores with open ends

Type D represents tapered/wedged pores with narrow necks at one or both ends

Type E is attributed to bottleneck pores

In general, for adsorption on porous materials, the hysteresis loops closes before reaching a relative pressure of ~0.3. However, this is not the case with microporous substances where outgassing the adsorbent at higher temperatures may even be necessary to effect desorption[15].

2.4.3. t-Method of Micropore Volume and Surface Area Calculation

The surface area obtained from the BET method includes the micropore surface area. However, the polymer and surfactants used in this study were too large to adsorb into these pores. Thus, the microporous area was subtracted to obtain the representative area for these molecules. The t-method of de Boer was used to calculate the micropore volume and surface area in the presence of mesopores. The procedure is similar to the BET surface area determination, but with the t-method the pressure range is extended

to higher values which permits the calculation of the matrix surface area. The matrix surface area is the non-microporous part for the material concerned[11]. A t-plot (thickness-plot) is the plot of the volume of gas adsorbed versus t, the statistical thickness of an adsorbed film, in this case the N_2 film assuming proper density at the concerned temperature and hexagonal close packing of the molecules. In this study the de Boer equation (eqn. 2.6)[17] was used to calculate t-values as a function of the relative pressure:

$$t = \left[\frac{13.99}{\log(P_0 / P) + 0.034} \right]^{1/2} \qquad \text{(Eqn. 2.6)}$$

where t is defined as the statistical depth that is proportional to the number of monolayers present in the film regardless of how the molecules may be stacked[7].

In the absence of any micropores on the surface, the t-plot can be extrapolated to the origin since the slope represents the total surface area, S_t of the mesopores and macropores[17] as shown in eqn 2.7:

$$S_t = \frac{V_{ads}^{STP}(15.47)}{t} \qquad \text{(Eqn. 2.7)}$$

where,

V_{ads}^{STP} = The volume of gas adsorbed corrected to standard conditions of temperature and pressures

15.47 = a constant representing the conversion of the gas volume to liquid

Using the slope, s, obtained from the linear t-plot, Eqn. 2.7 can be reduced to Eqn. 2.8:

$$S_t = s \times 15.47 \qquad \text{(Eqn. 2.8)}$$

The presence of micropores gives rise to a positive intercept in the t-plot. This intercept, i, when converted to a liquid volume can be used to calculate the micropore volume, V_{MP}.

$$V_{MP} = i \times 0.001547 \qquad \text{(Eqn. 2.9)}$$

The micropore surface area, S_{MP}, can then be calculated (equation 2.10) by taking the difference between the BET surface area (S_{BET}) obtained and the surface area of all pores obtained from the t-plot (S_t)[11].

$$S_{MP} = S_{BET} - S_t \qquad \text{(Eqn. 2.10)}$$

2.4.4. Results

The plots of nitrogen adsorption and desorption isotherms on the steel beads and carbon particles are as shown in figures 2.12 and 2.13, respectively:

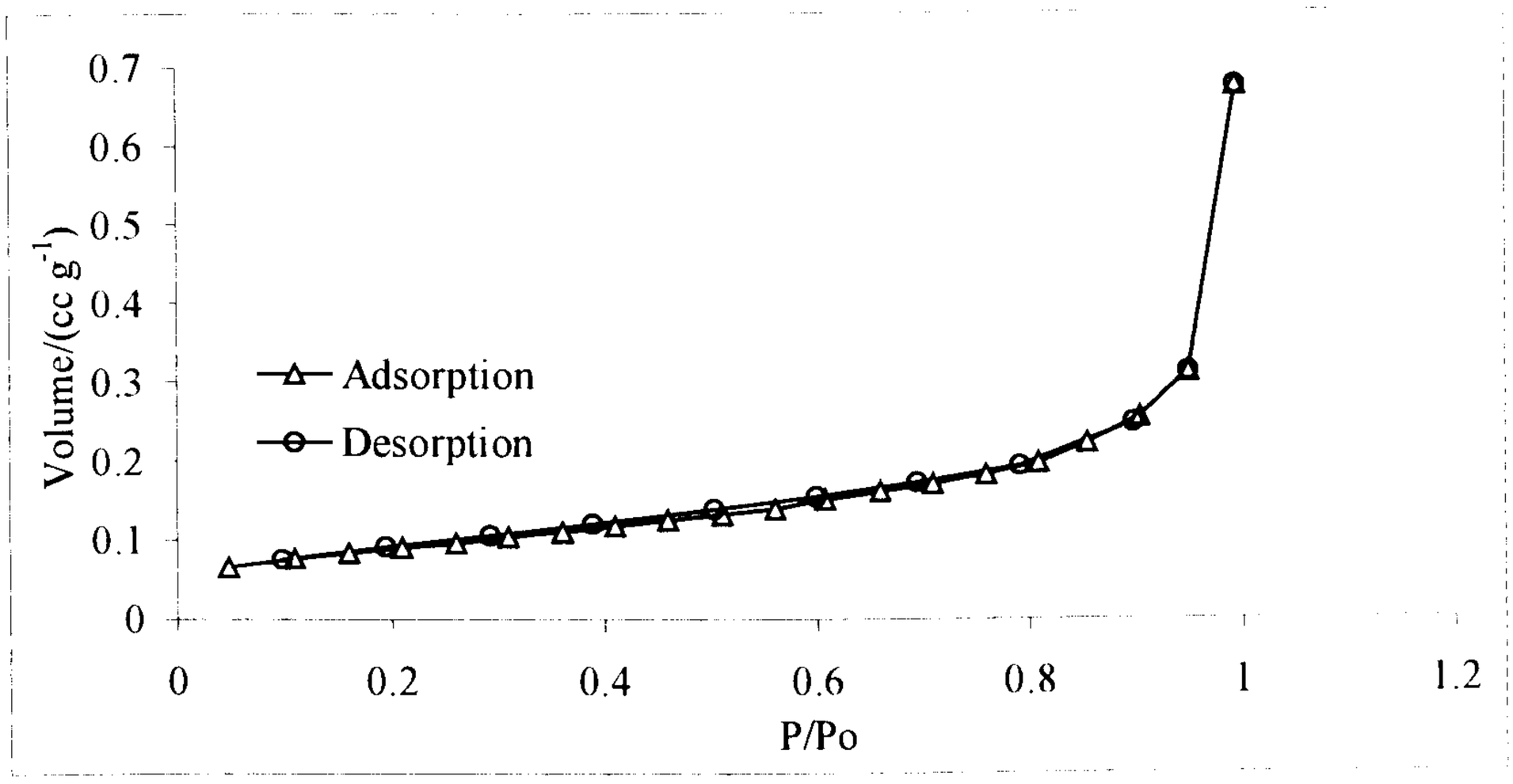

Figure 2.12: The adsorption-desorption isotherm of nitrogen on stainless steel 316 L

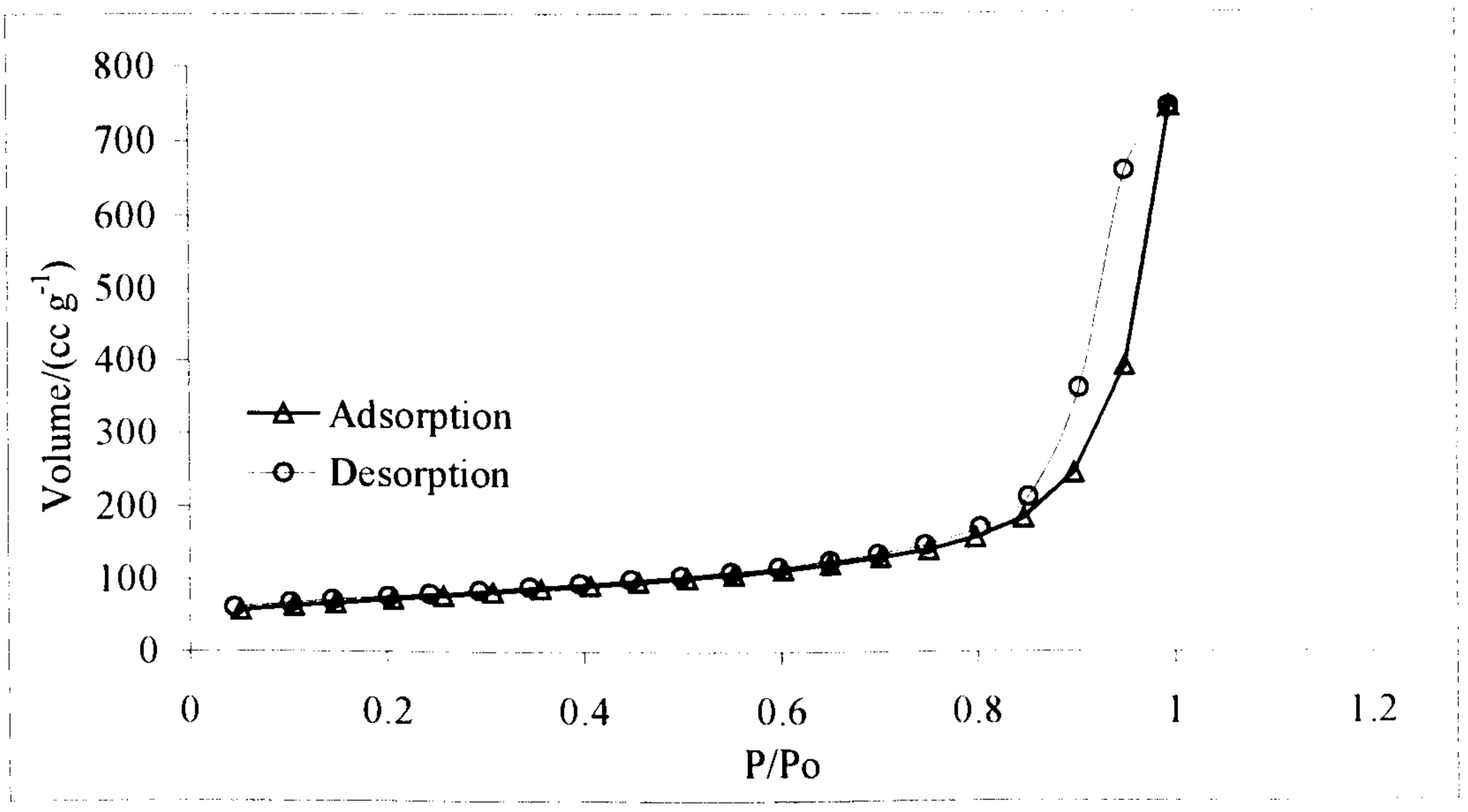

Figure 2.13: The adsorption-desorption isotherm of nitrogen on carbon particles showing a hysteresis loop

The isotherm for steel (fig. 2.12) does not show any hysteresis, indicating a non-porous surface for the steel beads. On the other hand, the plot for carbon (fig. 2.13) shows hysteresis, suggesting a porous surface. The hysteresis loops are of type A or C,

corresponding to cylindrical pores with open ends or tapered/wedge shaped pores with open ends, respectively

The BET plots used to obtain the surface areas of the two sets of particles are as shown in figures 2.14 and 2.15.

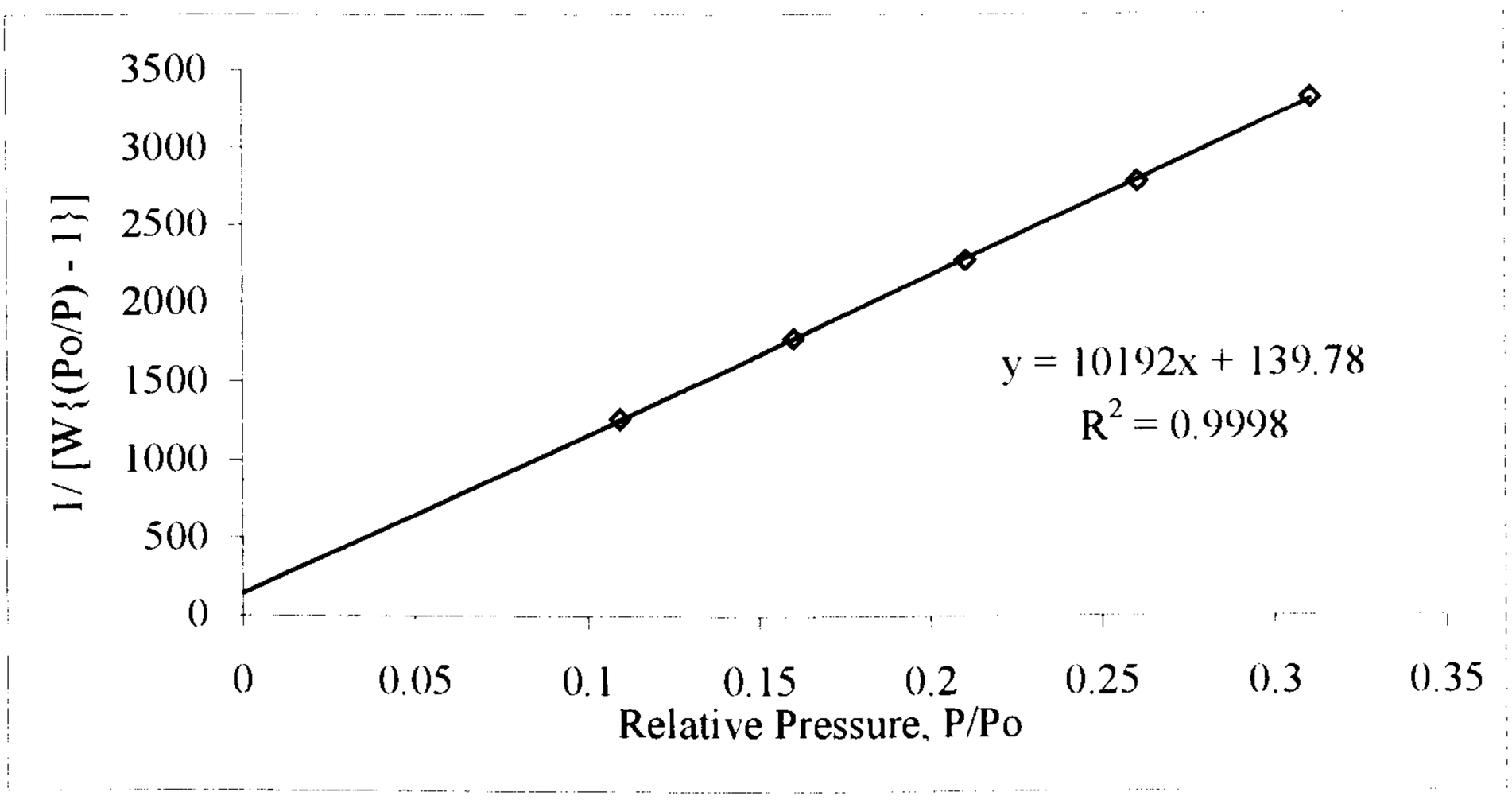

Figure 2.14: The BET plot for 316 L stainless steel beads

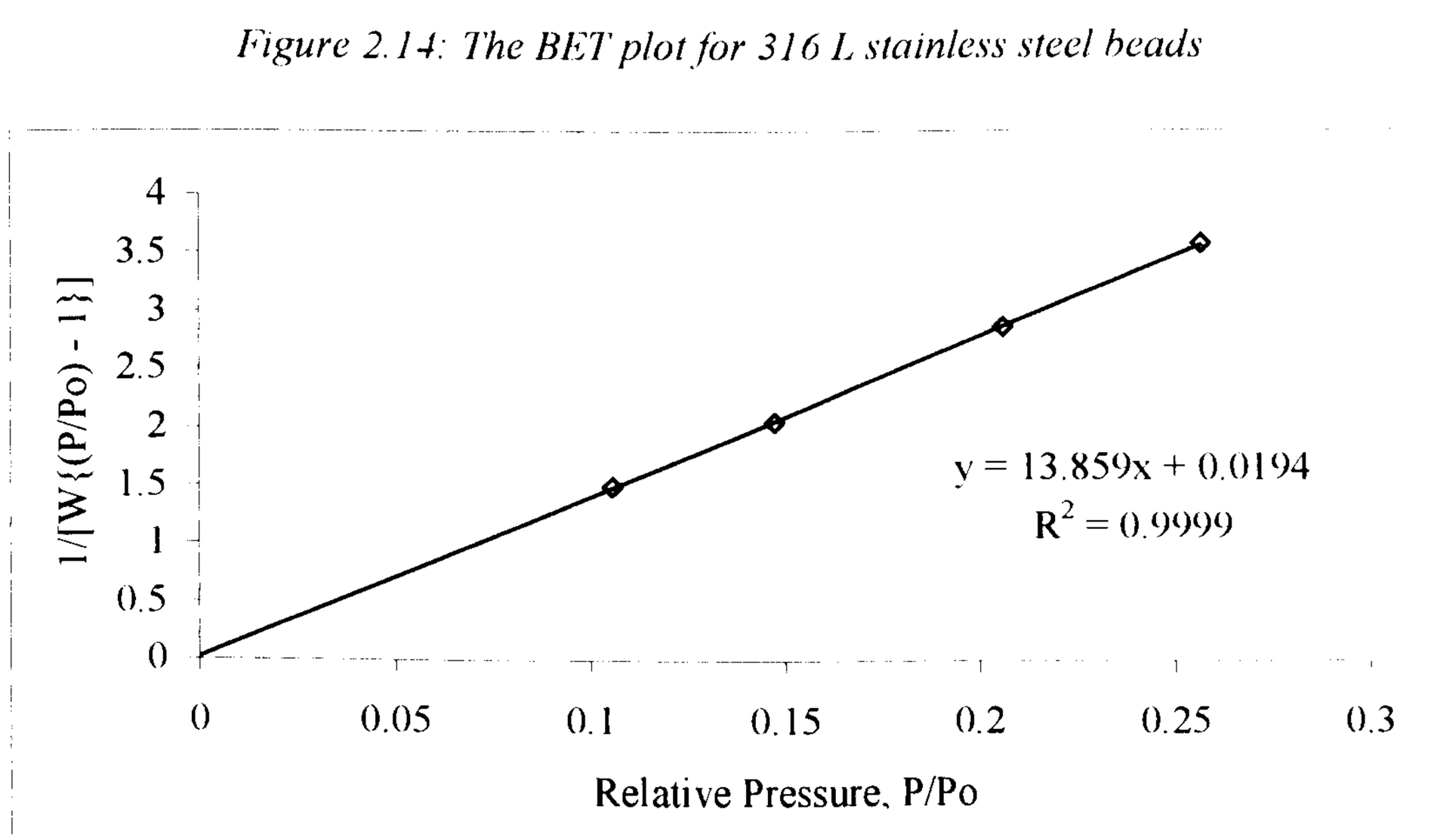

Figure 2.15: The BET plot for carbon particles

The BET plots gave surface areas of 0.34 $m^2 g^{-1}$ and 250.95 $m^2 g^{-1}$ for the steel beads and carbon particles, respectively. These surface areas include the surface areas of all the pores of the particles. As mentioned earlier, the polymers and surfactants used were

too big to adsorb in the microporous region and thus, the effective area for adsorption is the total specific surface area minus that for micropores. The micropore areas have been obtained from the t-plots as shown in figures 2.16 and 2.17.

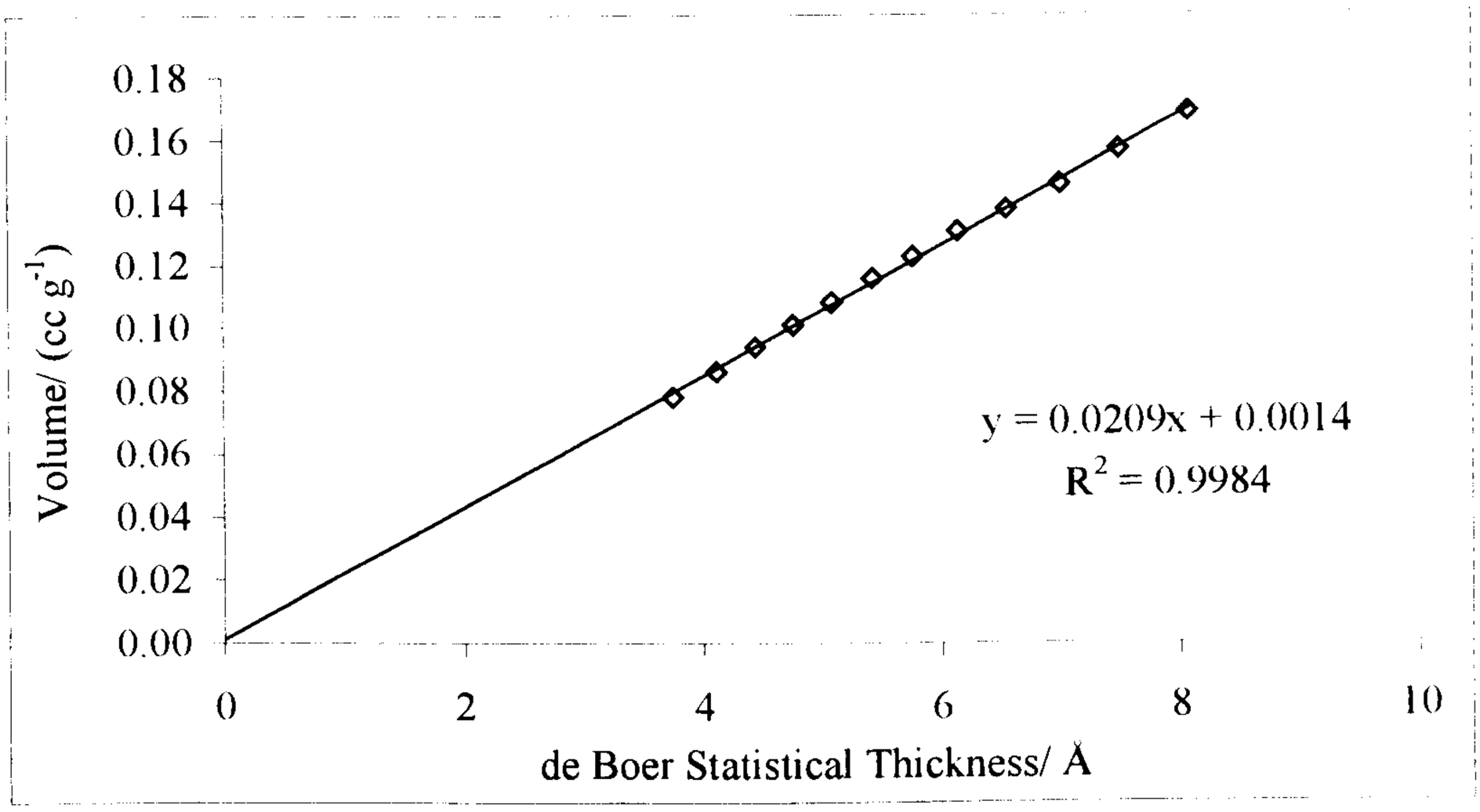

Figure 2.16: The V-t plot for 316 L stainless steel beads

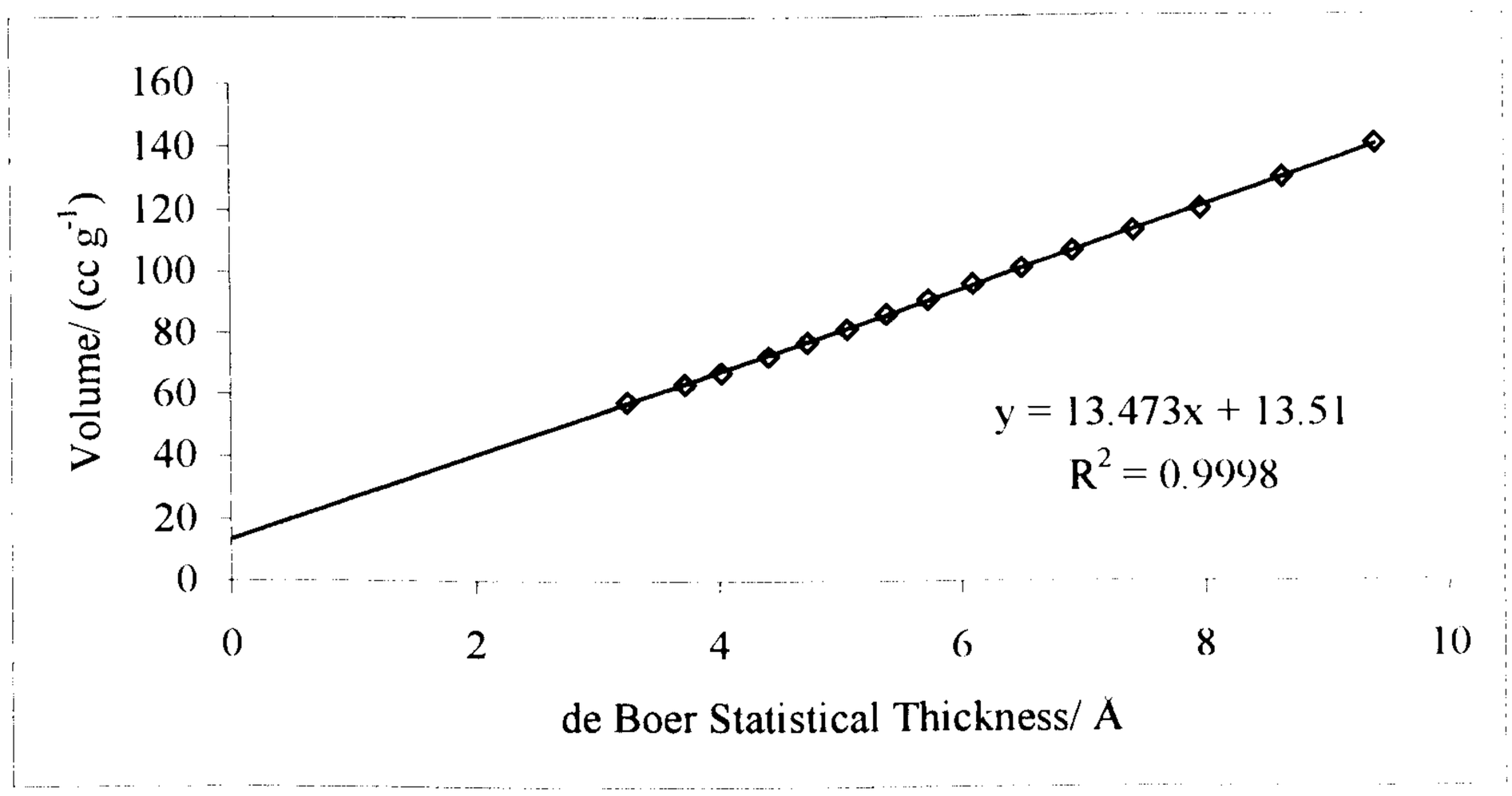

Figure 2.17: The V-t plot for carbon particles

The micropore volume and surface area determined from the V-t plot are 2.740×10^{-6} cc g^{-1} and 0 .0154 $m^2 g^{-1}$, respectively for the steel beads, and 2.057×10^{-2} cc g^{-1} and 42.04 $m^2 g^{-1}$, respectively for the carbon particles.

Subtracting the micropore areas from the respective total surfaces areas gave a surface area of 0.3217 $m^2 g^{-1}$ and 208.9 $m^2 g^{-1}$ for the steel beads and the carbon particles respectively.

2.5. SEM study of stainless steel beads and carbon particles

The steel beads were studied using a *JEOL 5600* scanning electron microscope to investigate the sizes and the nature of the surfaces. The particles were all spherical in shape and were mostly in the range of 2 –5 μm as shown in figure 2.18. Energy dispersive X-ray analysis (EDXA) were also carried out to analyse the surface composition of the beads and it showed the presence of chromium, as expected for stainless steel as shown in figure 2.19.

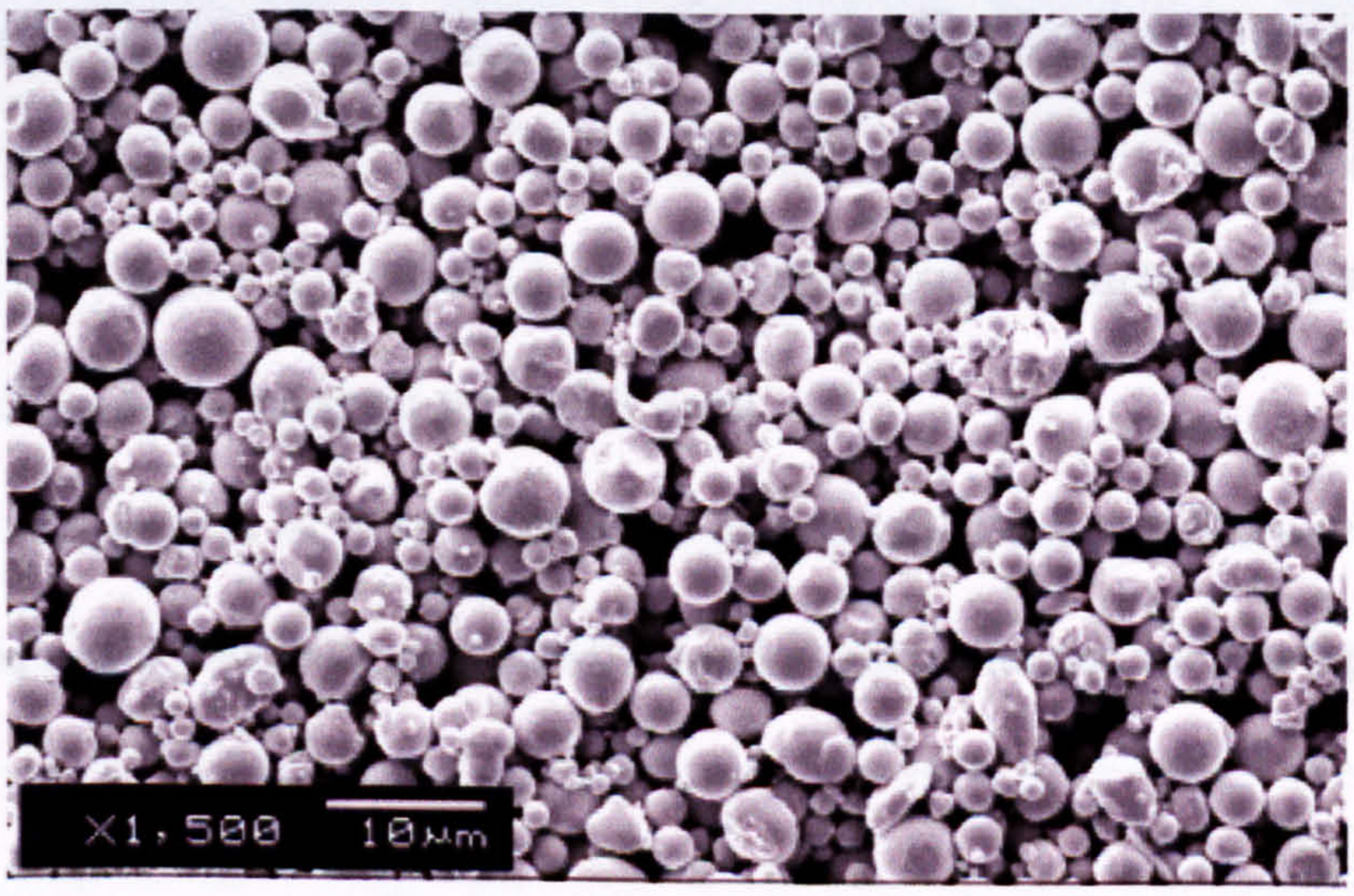

Figure 2.18: A scanning electron micrograph of the 316 L stainless steel beads

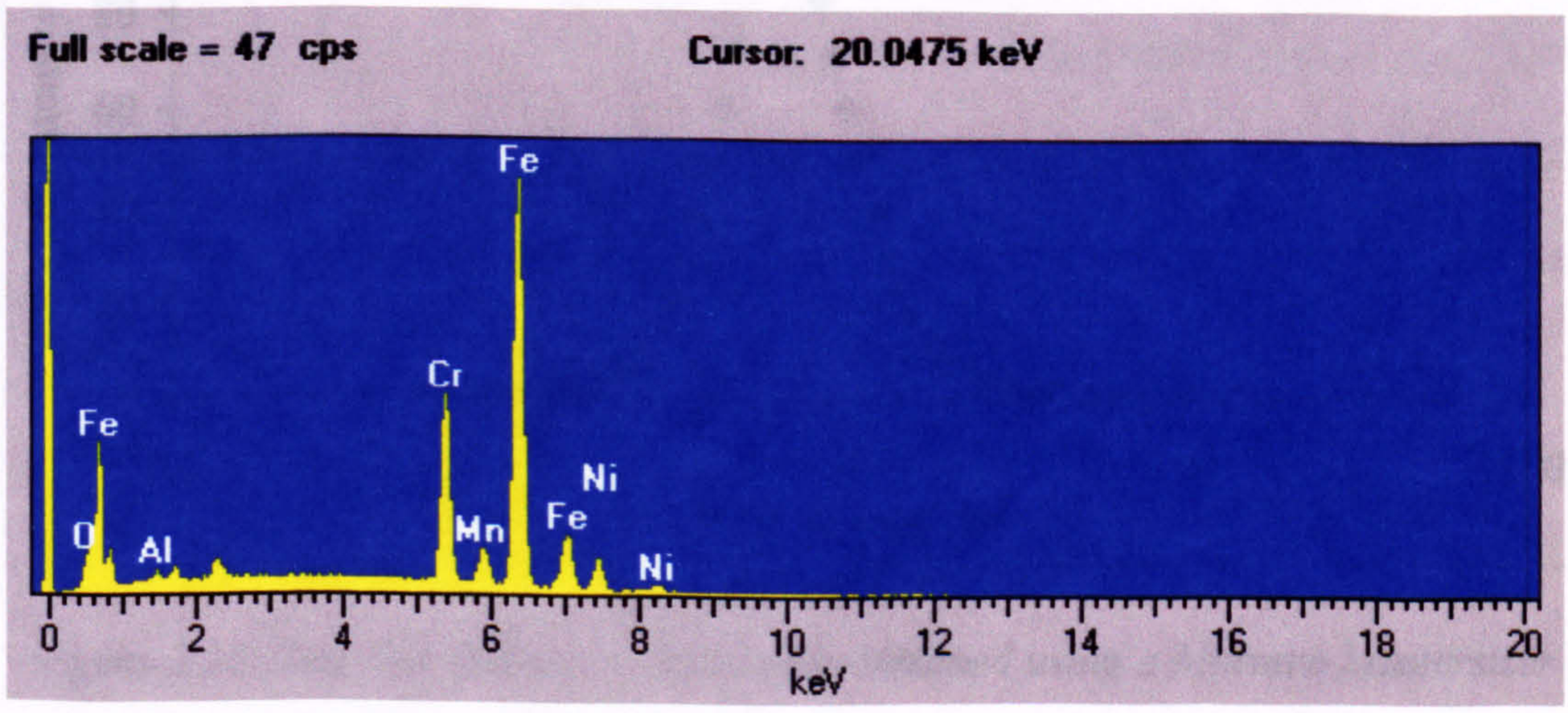

Figure 2.19: EDXA analysis of the 316 L stainless steel beads surface

The carbon particles were also studied using the *JEOL 5600* scanning electron microscope to investigate the sizes and the nature of the surfaces. The particles agglomerated on drying and individual particles could not be seen by the SEM. The EDXA graph of the carbon particles can be seen in figure 2.20. In the figure, the aluminium (Al) peak seen is from the SEM stub.

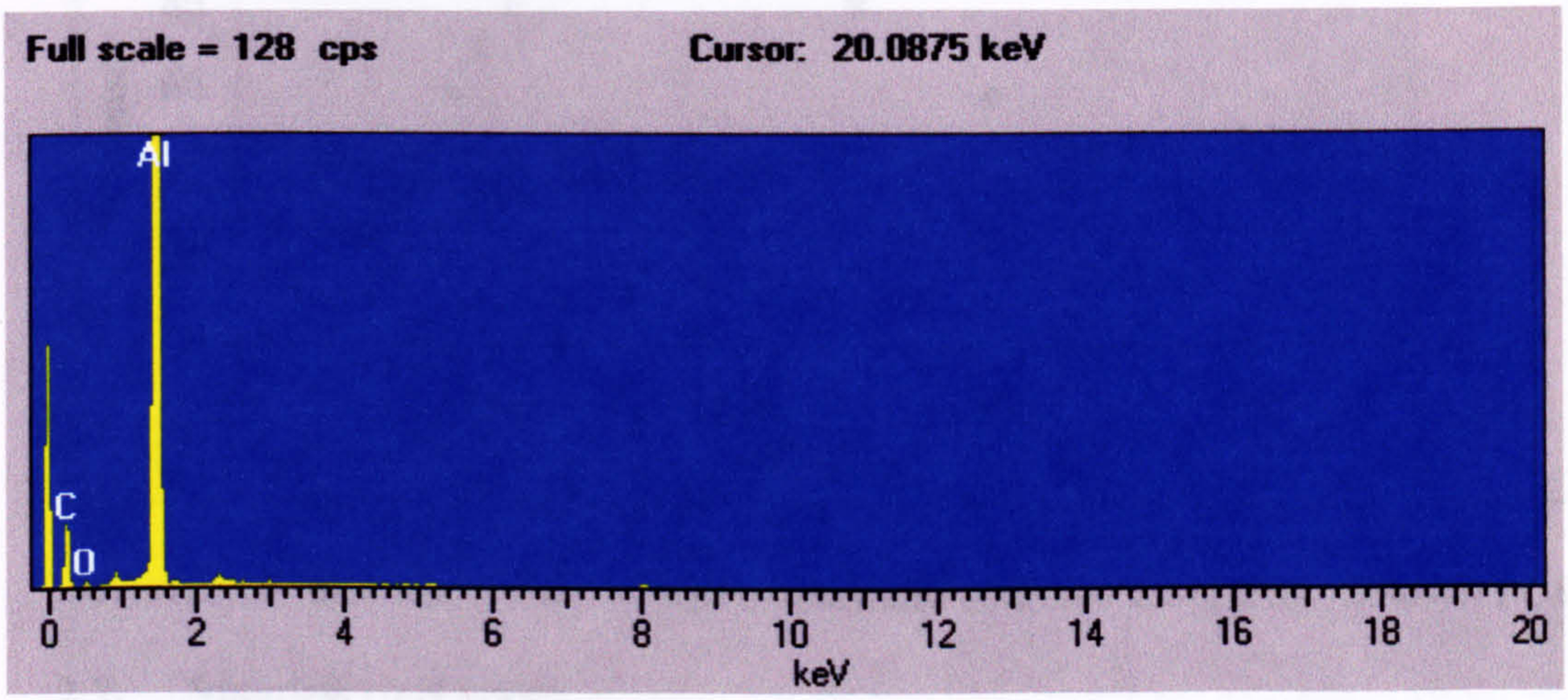

Figure 2.20: EDXA analysis of the carbon particle surface

2.6. Steel beads and carbon particles sizes

The average distribution of steel bead sizes were studied using a *Malvern Mastersizer* which showed a size distribution centred around 7 μm as may be seen in figure 2.21.

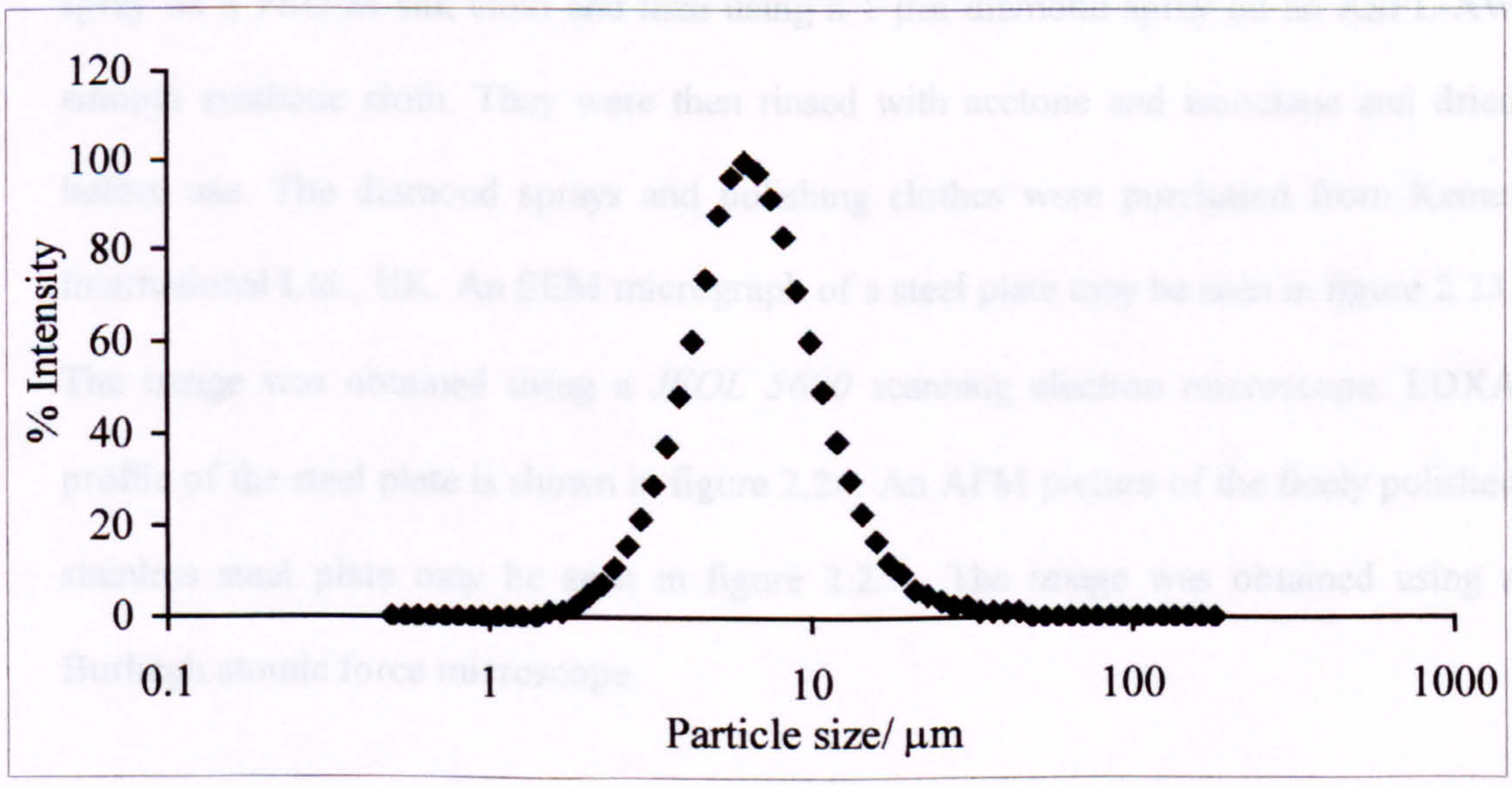

Figure 2.21: Size distribution of steel beads obtained using a Malvern Mastersizer

The average distribution of carbon particle sizes were studied using a *Brookhaven PCS* which showed a size distribution with a modal value of 214 nm as shown in figure 2.22.

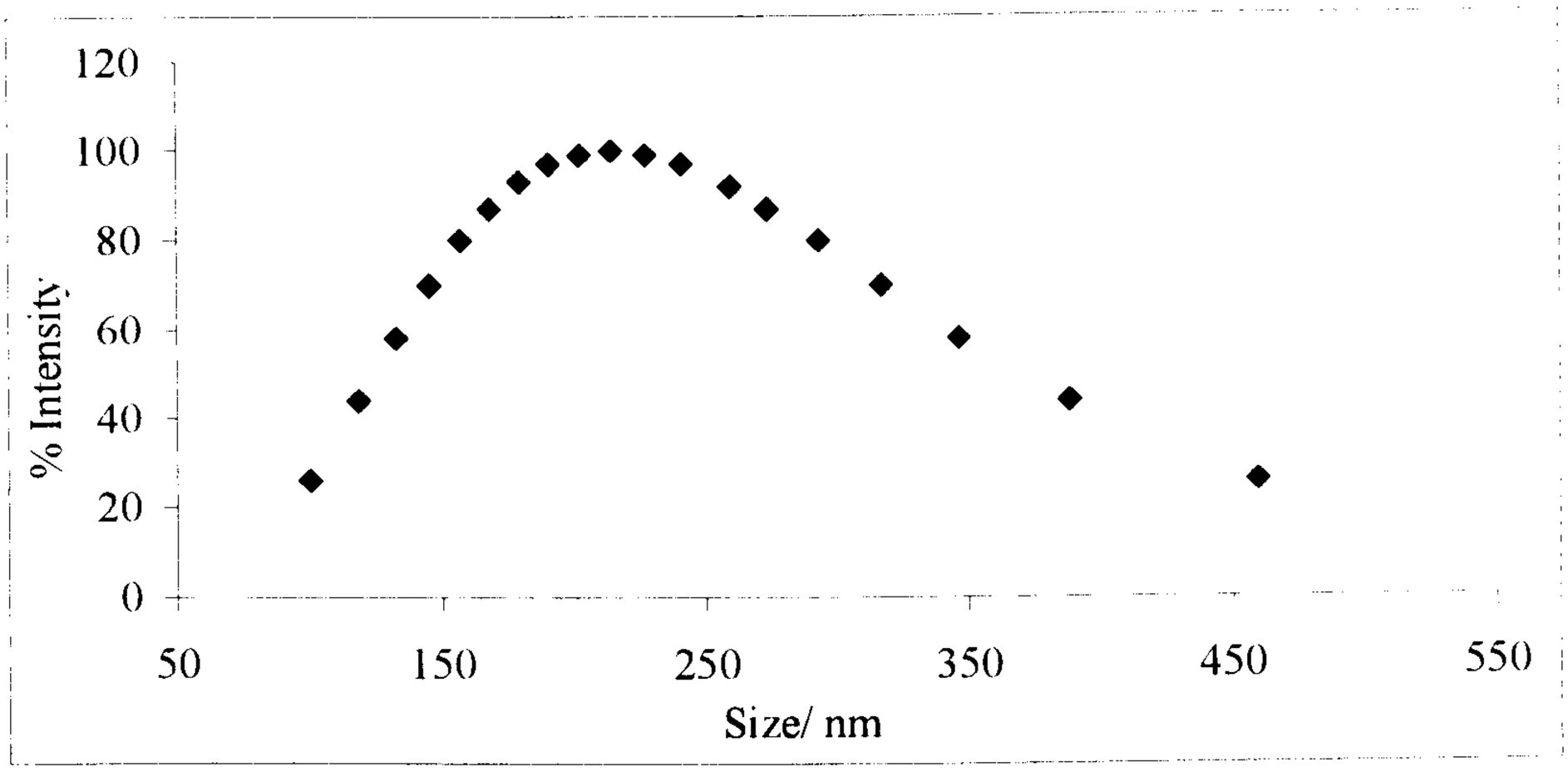

Figure 2.22: Size distribution of carbon particles obtained using a Brookhaven PCS

2.7. Stainless steel plates

Stainless steel plates, of area 1 cm^2, were used for studying the deposition properties of carbon particles on steel using a 'home-made' flow cell. The stainless steel plates were cut from metals obtained from Taybroh Metals, UK. They were initially polished using 600 and 1000 grid sandpapers, and then fine-polished, first using a 6 μm diamond spray on a PSU-M silk cloth and then using a 1 μm diamond spray on an ASFL-AW smooth synthetic cloth. They were then rinsed with acetone and isooctane and dried before use. The diamond sprays and polishing clothes were purchased from Kemet International Ltd., UK. An SEM micrograph of a steel plate may be seen in figure 2.23. The image was obtained using a *JEOL 5600* scanning electron microscope. EDXA profile of the steel plate is shown in figure 2.24. An AFM picture of the finely polished stainless steel plate may be seen in figure 2.25. The image was obtained using a Burliegh atomic force microscope.

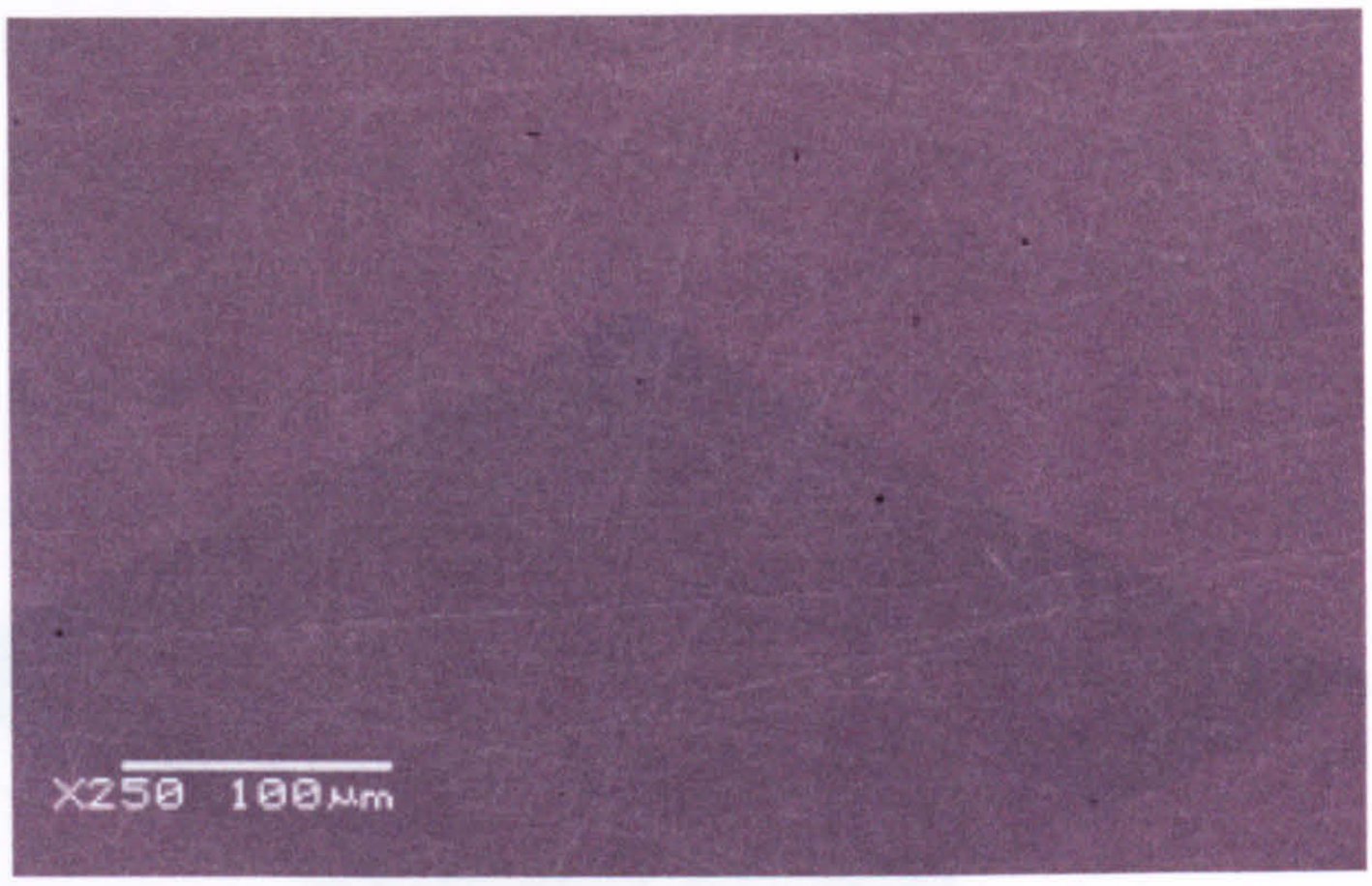

Figure 2.23: SEM picture of the surface of a stainless steel plate

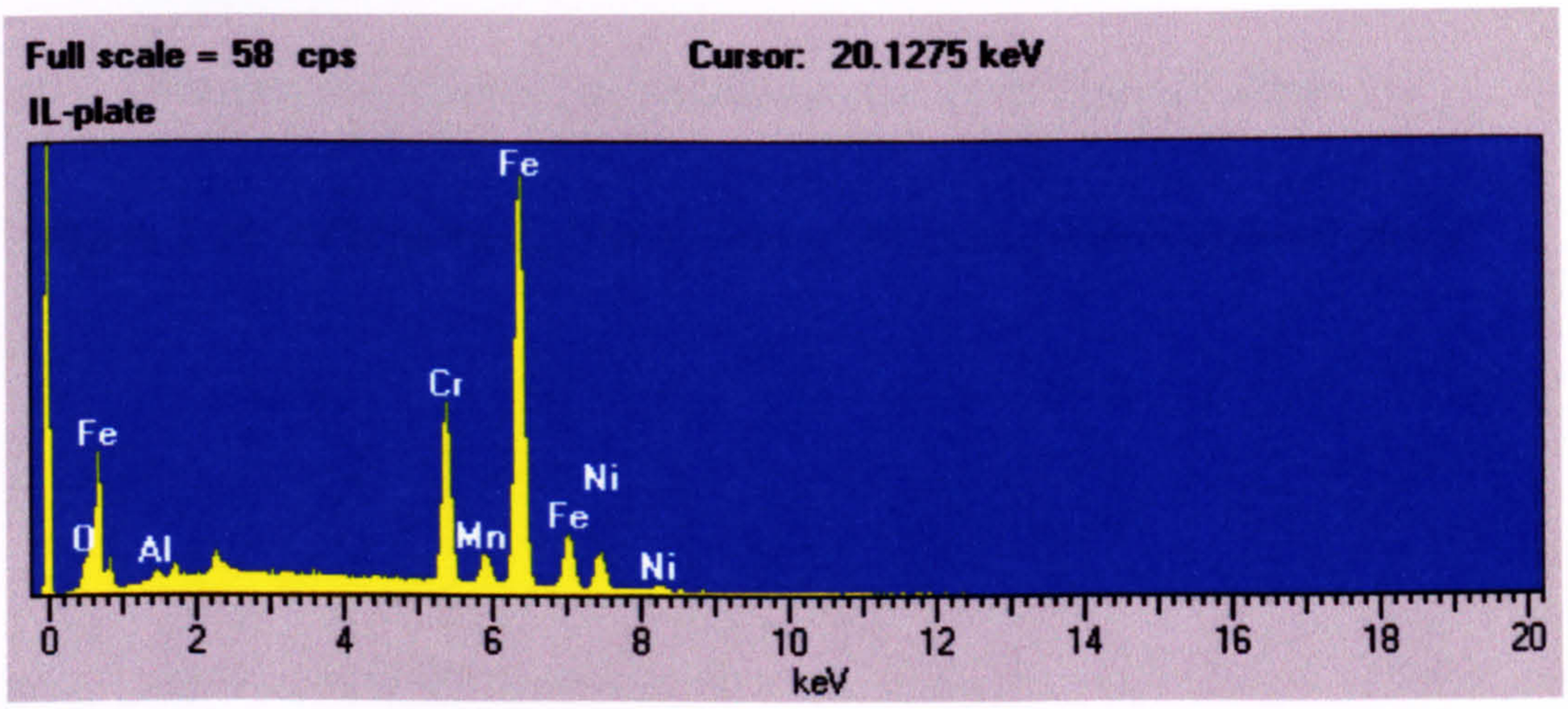

Figure 2.24: EDXA analysis of the steel plate surface

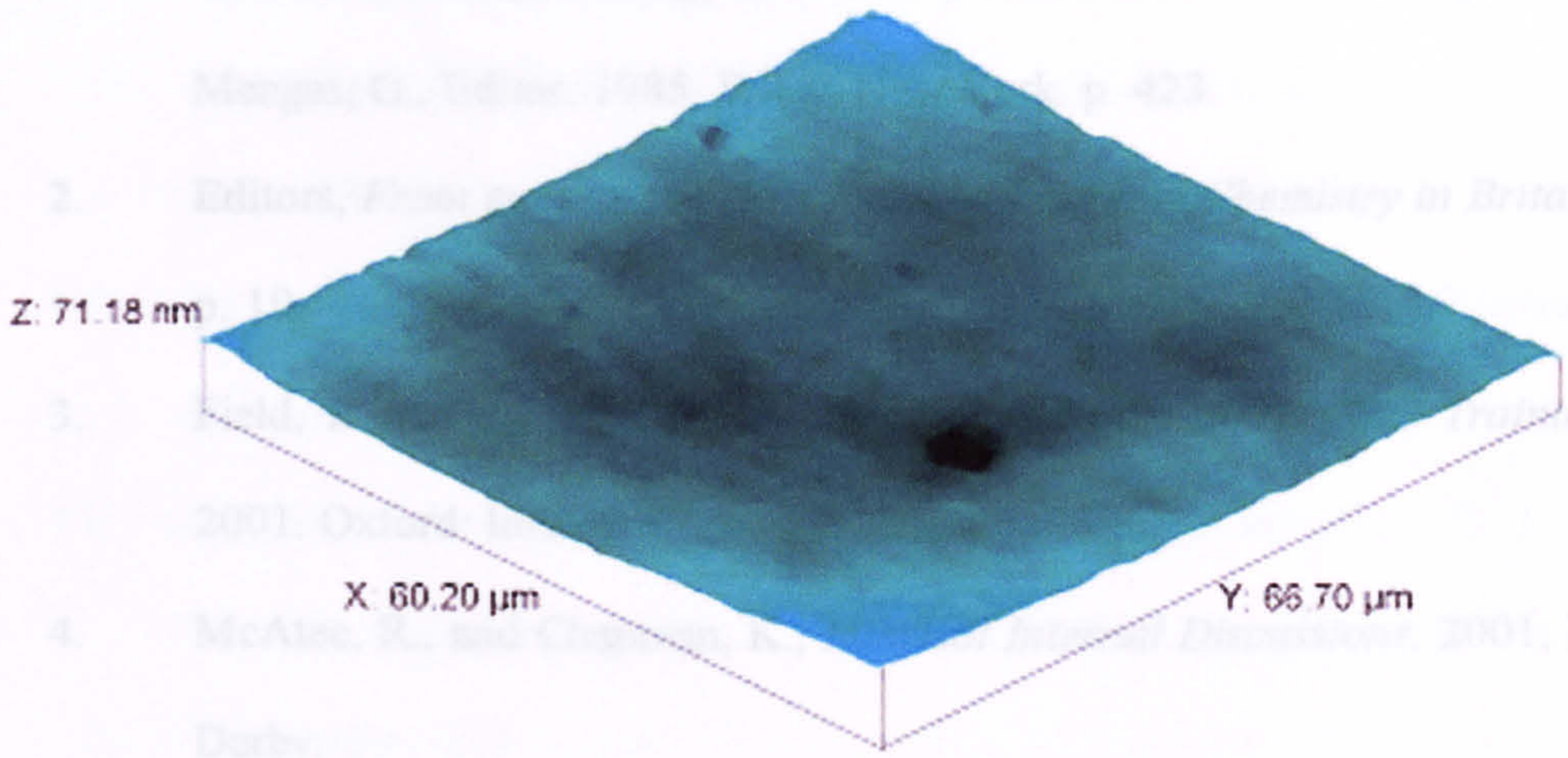

Figure 2.25: AFM picture of the surface of the polished stainless steel plates

2.8. References

1. Kresge, E.N., Schatz, R. H. and Wang, H. C., in *Encyclodpedia of Polymer Science and Engineering*, H.F. Mark, Bikales, N. M. Overberger, C. G. and Menges, G., Editor. 1985, Wiley: New York. p. 423.
2. Editors, *From gum to gas: PIB fuels the future*, in *Chemistry in Britain*. 2000. p. 19.
3. Field, I. *Lubricating Oil Additives*. in *Additives 2001 (RSC Training Day)*. 2001. Oxford: Infineum.
4. McAtee, R., and Chapman, K., *Lubrizol Internal Discussions*. 2001, Lubrizol: Derby.
5. Moreton, D., *Lubrizol Internal Discussions*. 2001, Lubrizol: Derby.
6. Moreton, D., and McAtee, R., *Lubrizol Internal Discussions*. 1999 - 2002: Derby.
7. Lowell, S., *Introduction to Powder Surface Area*. 1979, New York: John Wiley & Sons.
8. Brunauer, S., Emmett, P. H. and Teller, E., *Journal of American Chemical Society*, 1938. **60**: p. 309.
9. Langmuir, I., *Journal of the American Chemical Society*, 1918. **40**: p. 1361 - 1403.
10. Lowell, S., Shields, J., Charalambous, G., and Manzione, J., *Journal of Colloid and interface Science*, 1982. **86**: p. 191 - 195.
11. Autosorb, Q., *Manual*. p. II-1 to II-18.
12. Gregg, S.J., and Sing, K. S. W., *Adsorption, Surface Area and Porosity*. 1967, London and New York: Academic Press.
13. Atkins, P.W., *Elements of Physical Chemistry*. Second ed. 1999: Oxford University Press.

14. Ponec, V., Knor, Z. and Cerny, S., *Adsorption on solids*. 1974, London: Butterworths & Co. (Publishers) Ltd.

15. Sing, K.S.W., Everett, D. H., Haul, R. A. W., Moscou, L., Pierotti, R. A., Rouquérol, J. and Siemieniewska, T., *Pure and Applied Chemistry*, 1985. **57**: p. 603-619.

16. de Boer, J.H., *The Structure and Properties of Porous Materials*. 1958, London: Butterworths.

17. de Boer, J.H., Lippens, B. C., Linsen, B. G., Broekhoff, J. C. P., van der Heuvel, A. and Osinga, Th. J., *Journal of Colloid and Interface Science*, 1966. **21**: p. 405 - 414.

CHAPTER 3: ADSORPTION STUDIES

3.1. Introduction

Adsorption is the process by which molecules are attracted to an interface[1] and the corresponding build-up of this concentration at that interface[2]. Their presence at the interface renders the physical properties of the molecules different from those in the bulk, and this has been of great interest for fundamental and applied research. Adsorption has been applied for various diverse purposes such as the protective coating of Teflon on metals plates, the adsorption of colour pigments on fabrics, and the selective separation of components from a mixture. Adsorption also plays a significant role in the pharmaceutical and biotechnology industries[3, 4]. The adsorption of nitrogen gas onto solids is a fundamental and widely used method for the determination of surface areas and porosity.

3.2. Adsorption at a Solid/Gas Interface

Adsorption at a solid/gas interface occurs when a gas or a vapour is brought into contact with a clean solid surface. Some of the molecules in the gas/vapour phase (*the adsorptive*) become attached to the solid surface (*the adsorbent*). This overall process is termed *adsorption*; the molecules that leave the adsorptive and becomes attached to the adsorbent are the *adsorbate*. The reverse of the adsorption process is *desorption*. Most solids, especially highly porous adsorbents with large internal surface areas, such as carbon, silica and finely-divided powders, are capable of adsorbing high amounts of gas-phase molecules. The amount of gas adsorbed, per gram of solid, at equilibrium, Γ_{eqm}, depends on the temperature, T, the equilibrium pressure of the gas, P, and the effective surface area of the solid[5]. It also depends on the nature of the gas[6].

In general, the free energy, entropy and enthalpy of adsorption are all negative. The Gibbs free energy of adsorption is given by eqn 3.1:

$$\Delta G_{ads} = \Delta H_{ads} - T\Delta S_{ads} \qquad \text{Eqn. 3.1}$$

where,

ΔG_{ads} = change in Gibbs free energy

ΔH_{ads} = change in enthalpy of adsorption

ΔS_{ads} = change in entropy

T = temperature

The enthalpy of adsorption can be measured by direct calorimetric methods. Alternatively, in many cases, the isosteric (constant adsorption) enthalpy of adsorption, can be derived from adsorption isotherms, using the Clausius-Clapeyron (eqn. 3.5), e.g., for a Langmuir isotherm,

$$\frac{\theta}{1-\theta} = KP \qquad \text{Eqn. 3.2}$$

where,

$$\theta = \frac{\Gamma}{\Gamma_{max}} \qquad \text{Eqn. 3.3}$$

Γ and Γ_{max} are the equilibrium adsorbed amount and the maximum adsorbed amount respectively

K = constant of adsorption

P = pressure

Inversing eqn. 3.2 and substituting for θ gives

$$\frac{1}{\Gamma} = \frac{1}{\Gamma_{max}} + \frac{1}{KP\Gamma_{max}} \qquad \text{Eqn. 3.4}$$

The value of K can be obtained by plotting $\frac{1}{\Gamma}$ against $\frac{1}{P}$. The enthalpy of adsorption can be obtained if the experiment is carried out at different temperatures as shown in eqn. 3.5.

$$\left(\frac{\partial \ln K}{\partial T}\right)_{\Gamma} = \frac{-\Delta H_{ads}}{RT^2} \qquad \text{Eqn. 3.5}$$

where,

T = temperature

R = gas constant

3.2.1. Chemical adsorption and physical adsorption

Two different types of adsorption processes can occur, depending on the strength of the bonds involved. *Chemical adsorption* or *chemisorption* involves chemical interactions between the adsorbate and adsorbent, and the enthalpy of adsorption is greater than 100 kJ mol^{-1}. Spectroscopic analysis can be used to confirm change in chemical bonding of the gas/vapour molecules after reacting with the surface. High activation energies are involved in chemisorption, making the overall process slow and not readily reversible. The formation of chemical bonds in the adsorbed layer, leads to a localisation of the adsorbate molecules and is therefore limited to monolayer coverage. The extent of chemisorption may be used to determine the number of active sites on a solid[5, 7, 8].

Physical adsorption or *physisorption*, occurs when, associative intermolecular forces are involved rather than chemical bonds between the adsorbate and the adsorbent. Lower heats of adsorption (~ 10 kJ mol^{-1}) and low activation energies are characteristic of this type of adsorption. The process is readily reversible and equilibrium is in general achieved rapidly, except in porous materials. Multilayers are possible, as the adsorbate molecules are not restrained to specific sites and are free to translate on the surface. This means that physisorbed gases are useful for the determination of surface area of a solid[5, 8, 9].

There are many forces which may be involved in the physisorption of gas molecules onto solids, of which the most prominent are *dispersion forces*. Dispersion forces,

which arise from fluctuations in the electron density cloud, occur when the associated rapid oscillating dipoles of neighbouring molecules couple creating a net attracting potential. In the gas of molecules interactions with a solid, the first adsorbed layer of molecules will be strongly held whilst, above it other, subsequent layers are held with energies comparable to the latent enthalpy of sublimation or of vaporisation of the corresponding solid or liquid phase of those adsorbing molecules. Other forces involved in adsorbate-adsorbent interactions include *ion-dipole, ion-induced dipole, dipole-dipole* and *quadrapole* interactions[1, 7, 8].

To summarise these two adsorption mechanisms better, the schematic potential energy interaction curves for the adsorption of a diatomic gas X_2 on a metal M is shown in fig. 3.1[5]:

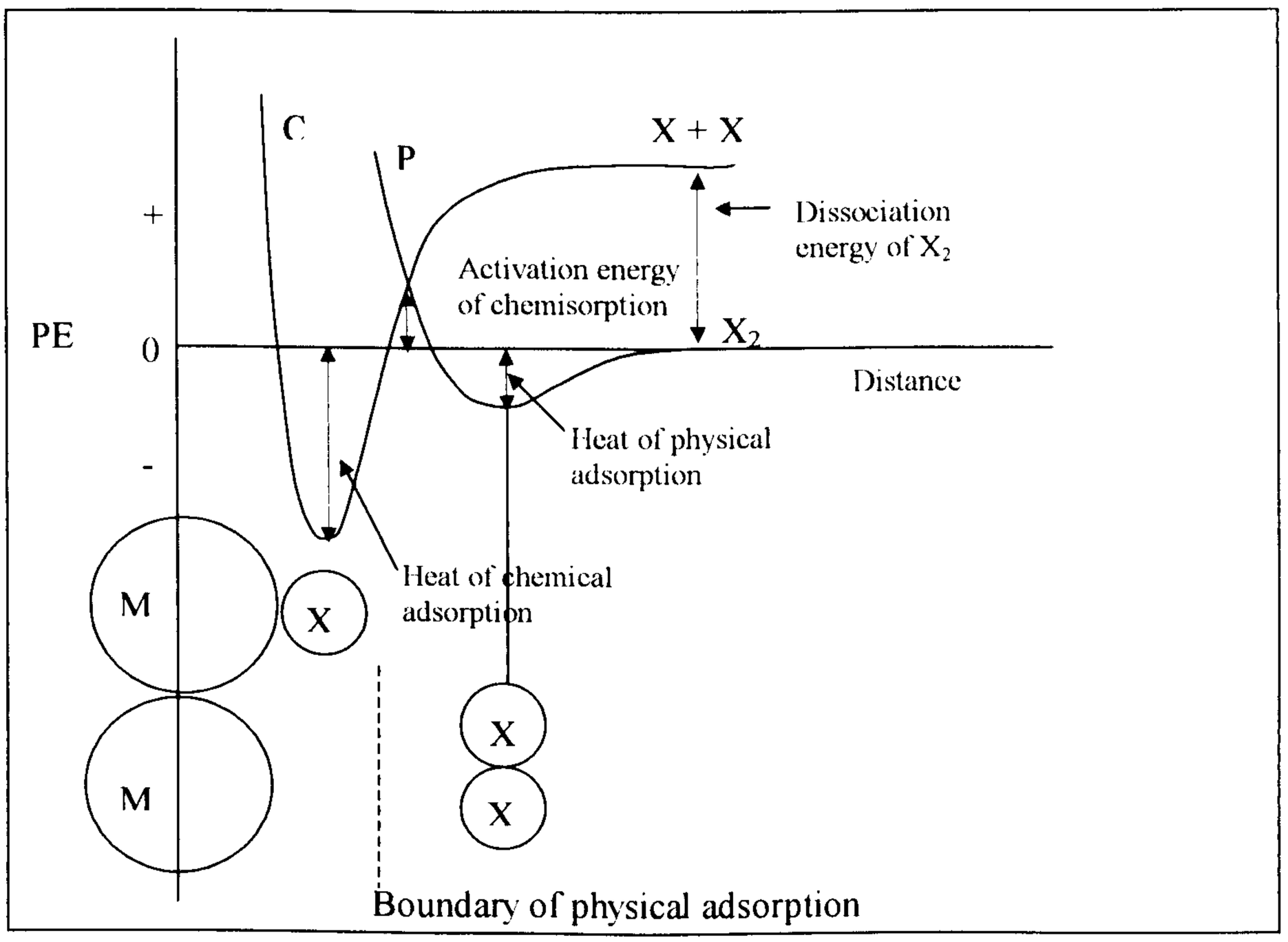

Figure 3.1: Potential energy curves for physical adsorption and chemical adsorption

In figue 3.1, curve P profiles the physical interaction energy between the metal and the gas molecule, associated, for example, with London-van der Waals dispersion forces. At short distances, electron cloud overlap gives rise to Born repulsion. Curve C, on the

other hand, represents chemisorption, where the gas molecule first dissociates to 2X. which is represented by a positive interaction energy at a large separation. The curve also has a relatively deep minimum at a distance much closer to the metal surface as compared to that of physisorption. This corresponds to the enthalpy of chemisorption. The point at which the physisorption curve and the chemisorption curve intersects represents the effective activation energy required for transition from physical adsorption to chemical adsorption of species X molecules.

3.2.2. Types of adsorption isotherms

Brunauer, Deming, Deming and Teller[7, 10, 11] classified adsorption isotherms for the physisorption of gases into five classes, as illustrated in figure 3.2. In the figure, the amount of gas adsorbed is plotted against the equilibrium relative pressure (P/P_0) where P and P_0 are the equilibrium pressure and the saturated vapour pressure, respectively.

The *Type I* isotherm, sometimes known as the *Langmuir* isotherm, is concave to the P/P_0 axis, with a rapid rise initially in the adsorbed amount with increasing relative pressure, but reaching a limiting value as P/Po → 1, thus indicating monolayer coverage[7]. Adsorption isotherms involving chemisorption exhibit this type of curve when all surface sites are occupied. Type I isotherms have also been adapted for the physical adsorption of gases on solids with a micropore structure, and a relatively small external surface. The rapid increase in the adsorbed amount at low pressure is associated with the filling of pores of small dimensions. When all micropores become filled, little or no further adsorption occurs, leading to the observed plateau[8, 12].

Type II, S-shaped, sigmoid or *BET* adsorption isotherms involve adsorption on non-porous or macroporous surfaces. Type II isotherms account for the formation of multilayers where the *knee* or *inflection* point signals the completion of the first adsorbed layer and the beginning of multilayer adsorption[7].

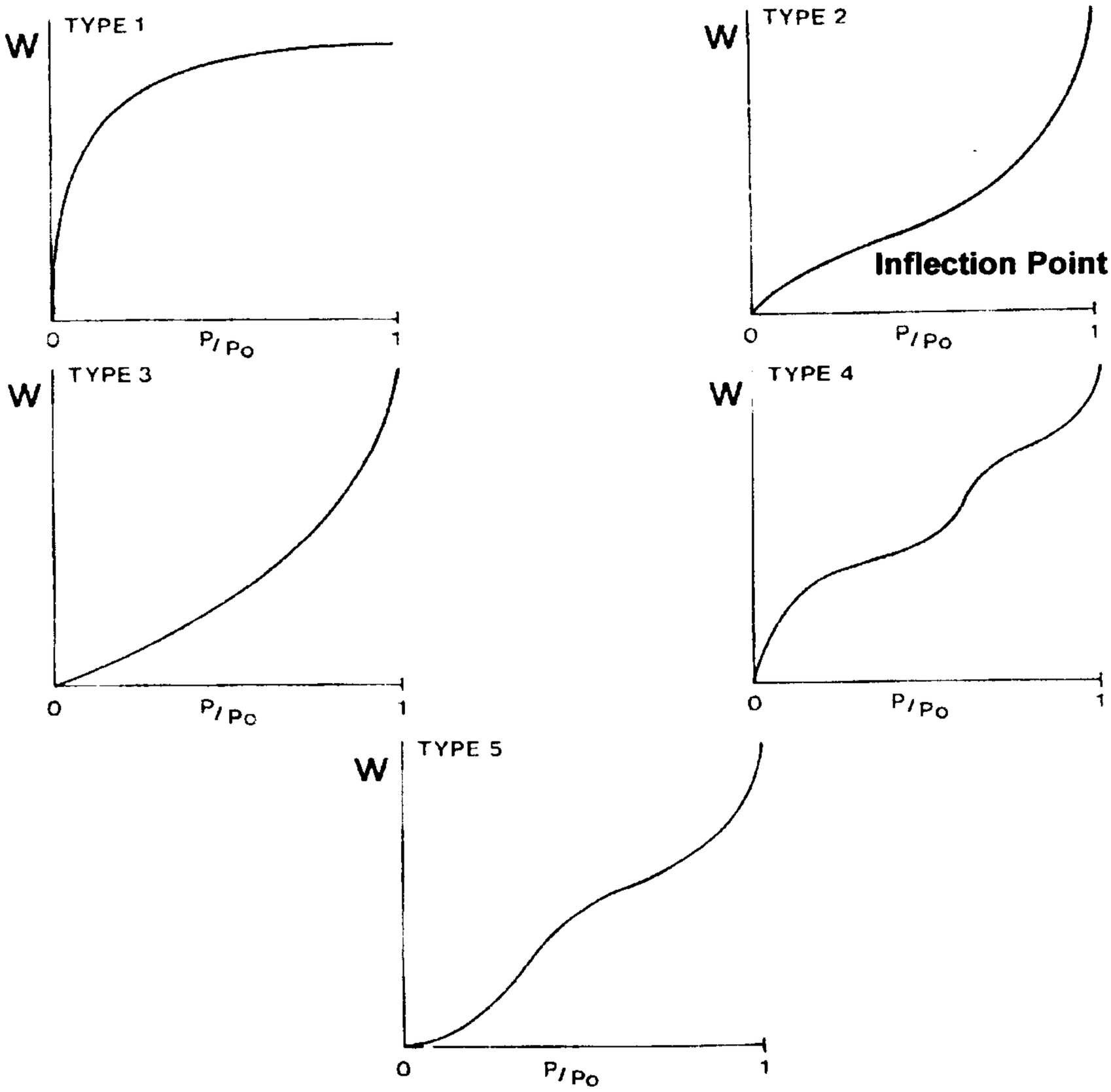

Figure 3.2: The five isotherm classifications according to Brunauer, Deming, Deming and Teller[8]

Type III isotherms are convex to the P/P_0 axis over their entire range and do not show any inflection point. They are characterised by enthalpy of adsorption, which are less than the adsorbate enthalpy of liquification. The weak adsorbent-adsorbate interactions indicate that strong lateral interactions between the adsorbed molecules are occurring, which can lead to the formation of aggregates on the surface[5, 7].

Type IV isotherms occur when adsorption proceeds on macroporous and mesoporous adsorbents with pores in the radius range of 15-1000Å. The slope of the isotherm increases at higher pressures indicating an increased uptake of the adsorbate as the pores are being filled. Like type II isotherms, type IV isotherms also exhibit an

inflection point indicating the completion of the first monolayer and the formation of multilayers[8].

Type V isotherms are uncommon and are related to type III isotherms. Like type III isotherms, the adsorbent-adsorbate interactions are weak, but type V isotherms involve adsorption on porous surfaces, as with Type IV isotherms[7].

3.3. Adsorption at a Solid/Liquid Interface

Many of the theories discussed in the previous section can be applied to the adsorption at a solid/liquid interface, as long as the adsorbate molecules, in the present case the oligomer and surfactants, are deemed to be *inflexible*. For oligomers, their low molecular weights puts them in this category[13].

Various techniques exist for measuring the total adsorbed amount of species from solution, such as ellipsometry and optical reflectometry (for that surface) or spectroscopic techniques which allow the measurement of the surface excess such as UV/Visible, FTIR and NMR (for particles). A measurement of the change in equilibrium bulk concentration, Δc, strictly leads to the "surface excess" but for dilute solutions this may be equated to the adsorbed amount.

The adsorbed amount, Γ, is related to Δc, in mg g^{-1} for this study, through eqn 3.6:

$$\Gamma = \frac{\Delta c M}{m a} \qquad \text{Eqn. 3.6}$$

where M is the mass of the liquid phase, m is the mass of the adsorbent and a is the specific surface area of the adsorbent.

Major problems associated with the solute depletion method are low accuracy at high solute concentrations, and the formation of particle aggregates, where there is no effective particle stabilisation mechanism. These problems may be resolved, to some extent, by scaling up the ratio of surface area to the volume of solution and by agitating

the sample, for example, using an ultrasonic bath, to disperse the particles in the latter case[2].

Spectroscopic methods are chemically specific and can distinguish different components in a complex system. Errors occurring in spectroscopic methods, especially UV/Visible spectroscopy, include non-linear extinction coefficients but can be observed from calibration plots. These allow the determination of the extinction coefficient, by plotting absorbance against concentration, in the low concentration regime, where the (linear) Beer-Lambert law (eqn. 3.7) is followed[14]:

$$A = \log\left(\frac{I_0}{I}\right) = \varepsilon C l \qquad \text{Eqn. 3.7}$$

where,

I_o = intensity of incident beam

I = intensity of transmitted beam

ε = absorption coefficient or molar extinction coefficient

C = concentration

l = path length

3.4. Factors affecting Polymer and Surfactant Adsorption

There are several factors that could affect the extent of polymer and surfactant adsorption onto an adsorbent. These include, the interaction of the polymer or surfactant with the substrate/adsorbent (the extent of adsorption increases with increasing affinity for the adsorbate with the surface) and the solvation of the polymer/surfactant in the solvent (the adsorption of the adsorbate increases with decreasing solubility)[13]. Variations in temperature and molecular weight can also affect the extent of adsorption. Lower molecular weight polymers in general show faster kinetics of adsorption, because of their ability to diffuse more rapidly through the medium[15, 16].

Previous work carried out on the adsorption of polyisobutylenes, with different functionalities, on carbon particles have shown that the strength of the attachment of a

molecule to an interface increases with the extent of the funtionalities[17]; this provides a stronger affinity for the surface. In particular, studies have indicated that the amine head groups in polymer dispersants ensure strong adsorption on an adsorbent [18].

3.5. The χ and χ_s parameters

When a *flexible* high molecular weight polymer chain adsorbs, there is a decrease in the conformational entropy, ΔS, of the chain segments in the interfacial region. However, the enthalpy of adsorption, ΔH, is normally sufficiently negative, that ΔG, the free energy of adsorption, is negative. The interactions between the polymer/surfactant segment and the solvent can be interpreted in terms of the Flory-Huggins parameter (or chi parameter) χ, which was originally defined as the energy change associated with the transfer of a segment from pure polymer to pure solvent.

When $\chi=0$ (the athermal case), the solvent is termed as "good" meaning that there is a strong chain expansion as the polymer chain walks through space avoiding itself[2].

The radius of gyration, R_g, for a self-avoiding walk (SAW) is proportional to N^{ν}, where $\nu=0.59$ (a universal exponent) in the limit of large N where N is the number of steps.

When $\chi>0$, resulting from a net segment- segment interaction, the excluded volume is smaller than the real volume, l^3, (where l corresponds to the bond length) of a polymer or surfactant segment. The excluded volume can be expressed as vl^3, where v is the dimensionless excluded volume parameter and is related to χ through eqn. 3.8:

$$v = 1 - 2\chi \qquad \text{Eqn. 3.8}$$

Therefore, when χ is 1/2, the net excluded volume is 0 and the chains behave ideally. This is known as the Θ point. χ is also dependant on temperature, the temperature corresponding to a Θ point is known as the Θ temperature[2]. For cases when $\chi<0$, the segments would be highly solvated and will have a low affinity for the surface.

The adsorption of a polymer onto a surface also depends on the interaction between the surface and the solvent or polymer. Such an interaction has been described by introducing a dimensionless adsorption energy parameter χ_s, which can be defined as the difference in the adsorption energies, in units of kT, of a solvent molecule and a polymer segment[2]. If a polymer adsorbs from the solvent, χ_s is positive and no adsorption occurs when χ_s is negative. If χ_s is zero or slightly positive, the lower conformational entropy of the polymer in the surface region hinders adsorption.

3.6. Experimental

3.6.1. Adsorption on stainless steel beads

The adsorption of the polymer/surfactants on stainless steel beads was carried out by tumbling a suspension of the beads in a solution of the polymer/surfactant in isooctane, for about 20 h, and then analysing the supernatant after the beads had settled. The UV/Visible absorbances of the polymer/surfactants were first calibrated by preparing a range of dilute solutions. A certain amount of the stock concentrated solution of a polymer/surfactant was added to 3 g of stainless steel, weighed into a sample vial. This was then diluted to 1.5 g with isooctane, giving a total mass of 4.5 g. This procedure was repeated to give various polymer/surfactant concentrations in the range 0.1 to 4 wt. %. The vials were sealed with Teflon tape and the samples were shaken vigorously for 5 min and then tumbled for 20 h. After 20 h, the samples were left standing for 10 min and then centrifuged at 5000 r.p.m. for 30 min. The supernatant was then diluted, as necessary, and analysed using a *HP8453* Diode Array UV/Visible Spectrophotometer to obtain the polymer/surfactant concentration. The reference cell used contained isooctane which had been tumbled for 20 h with the steel and centrifuged. The objective here was to reduce any response which may come from UV/Visible-active species, which may have leached out from the steel, present in the adsorption

experiment samples. For adsorption of mixtures of polymer and surfactants, a second stock solution, that of the second species, was added before dilution with isooctane.

3.6.2. Adsorption on carbon particles

For these experiments, 0.2 g of the carbon particles was weighed into a sample vial, followed by the addition of a certain amount of the stock polymer/surfactant solution. The total mass was then made up to 7 g by the addition of isooctane. The amount of the stock solution added was varied to give polymer concentrations in the range 0.05 wt. % to 4 wt. %. The vials were sealed and the samples were sonicated for 2 min, with occasional agitation to break up any weakly flocculated aggregates. The vials were tumbled for about 24 h, and the carbon particles allowed to settle for 30 min, before centrifuging at 15,000 r.p.m. for 120 min, or until a clear supernatant was obtained. The supernatant was then analysed for polymer/surfactant concentration.

3.7. Results

3.7.1. Adsorption on stainless steel beads

3.7.1.1. Calibration of the polymer and surfactant absorbances in isooctane

Various dilute solutions of the polymer and surfactants were prepared and their absorbances were measured at 25 °C to obtain the calibration plots as shown in figure 3.3. These calibrations were used for calculating the amount of polymer/surfactant adsorbed on steel.

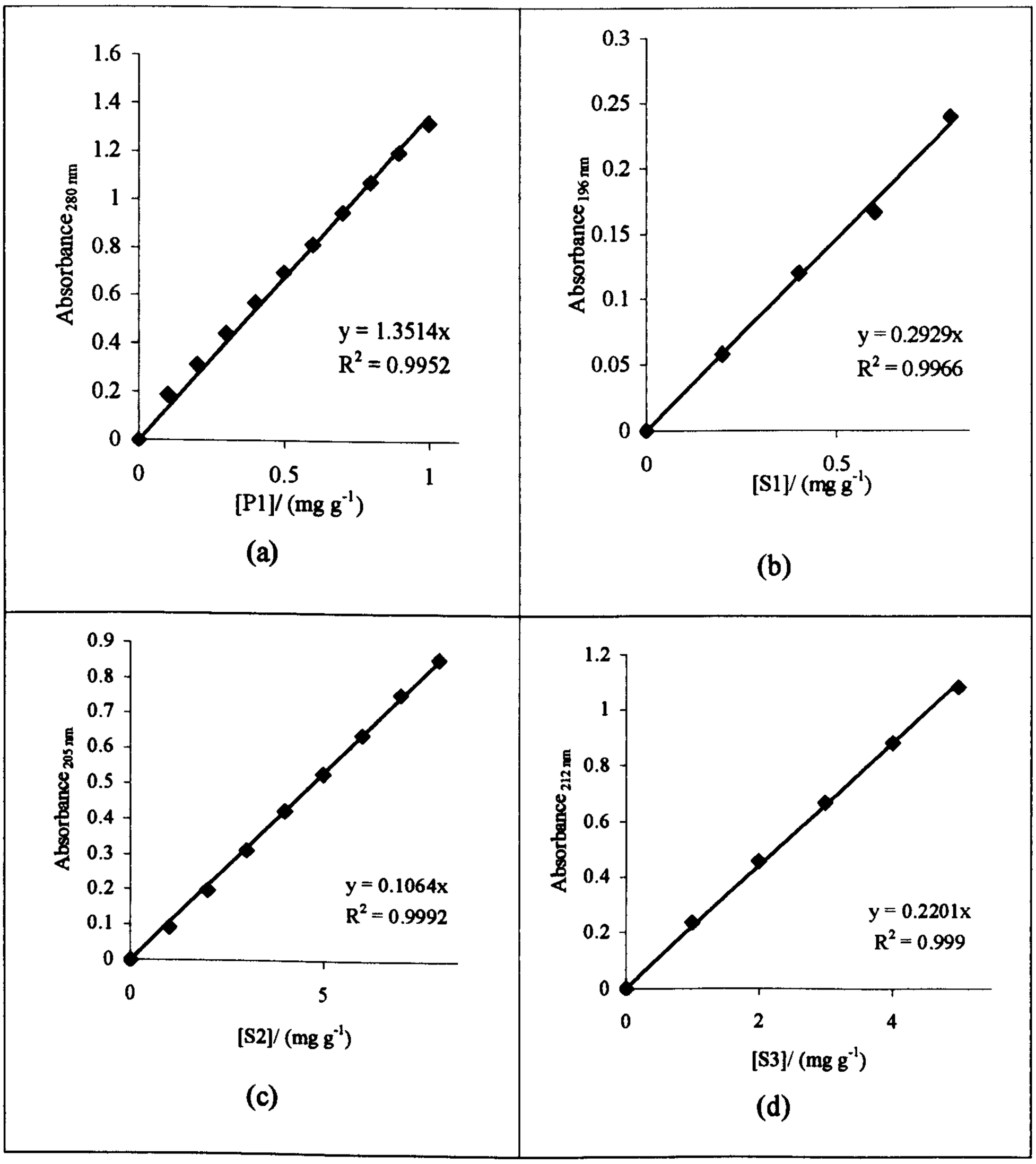

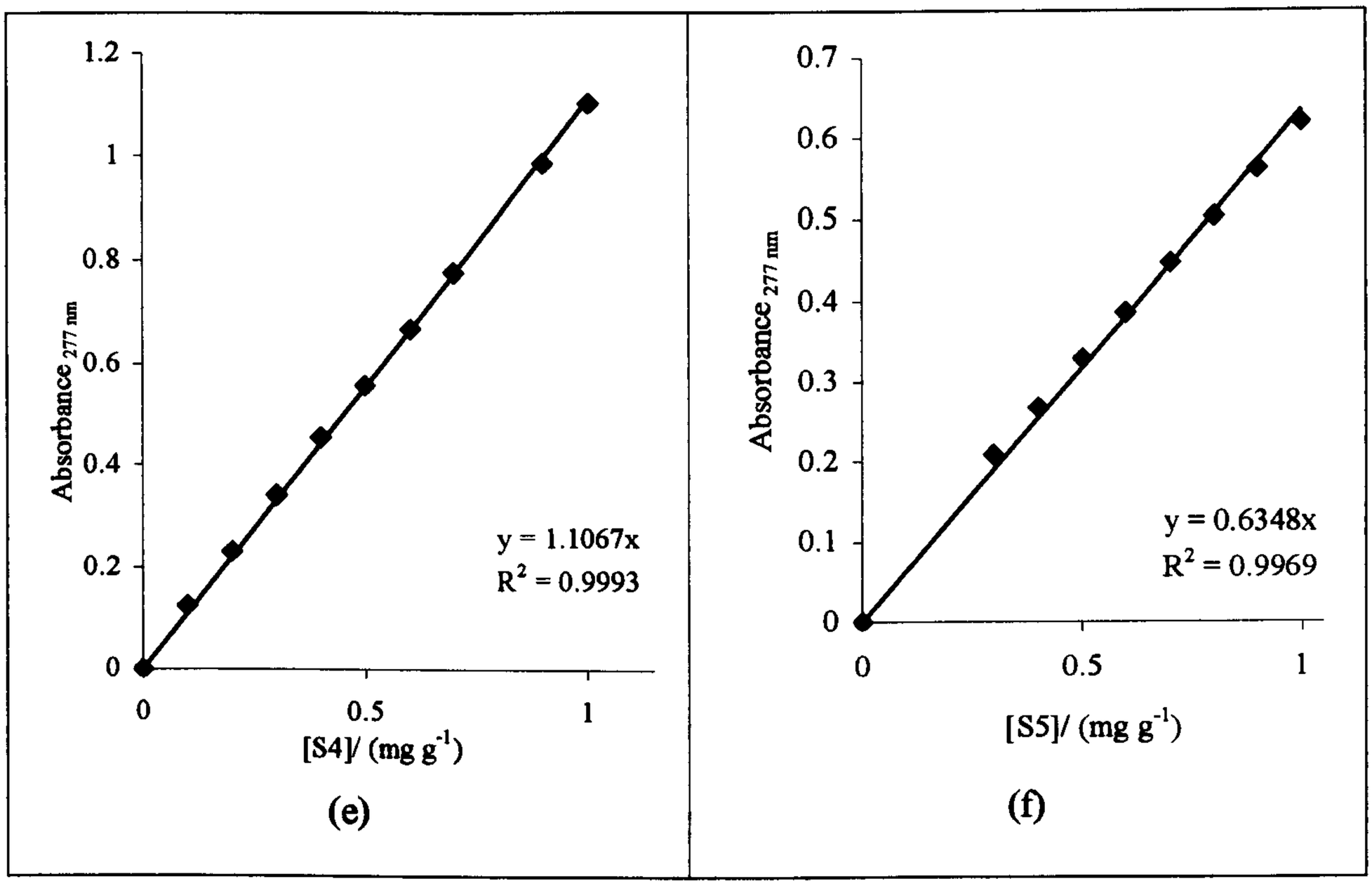

Figure 3.3: Calibration plots of P1, S1, S2, S3, S4 and S5

3.7.1.2. Adsorption kinetics of surfactant S3

The adsorbed amount of S3 on stainless steel was determined, at different times, for up to 8 hours. The results are shown in figure 3.4.

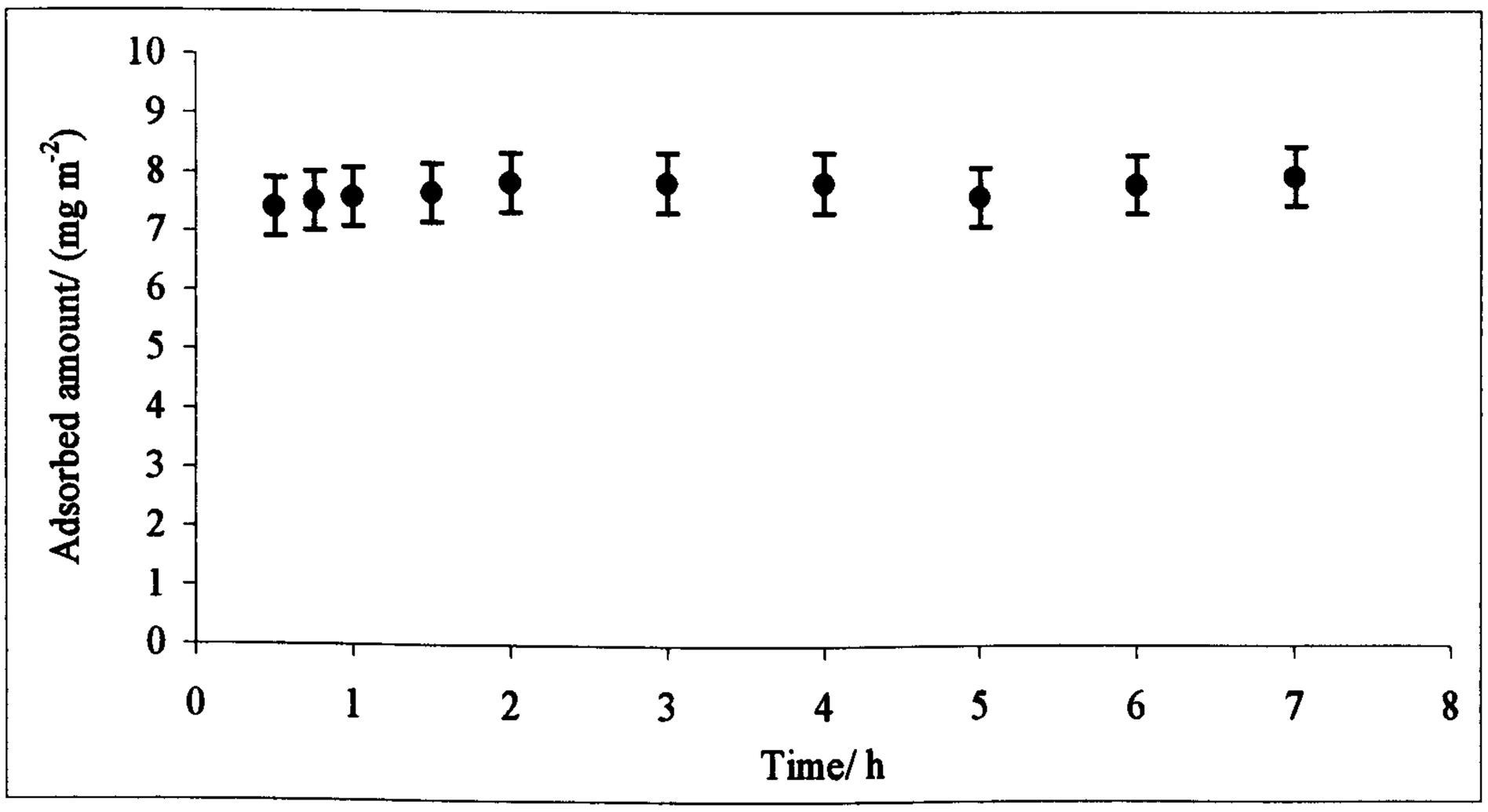

Figure 3.4: Adsorption kinetics of S3 up to 8 h

3.7.1.3. Adsorption isotherms of the polymer and surfactants on steel

The adsorption isotherms for the polymer and the various surfactants on stainless steel beads at 25 °C are shown in figure 3.5. The error involved is about 10%.

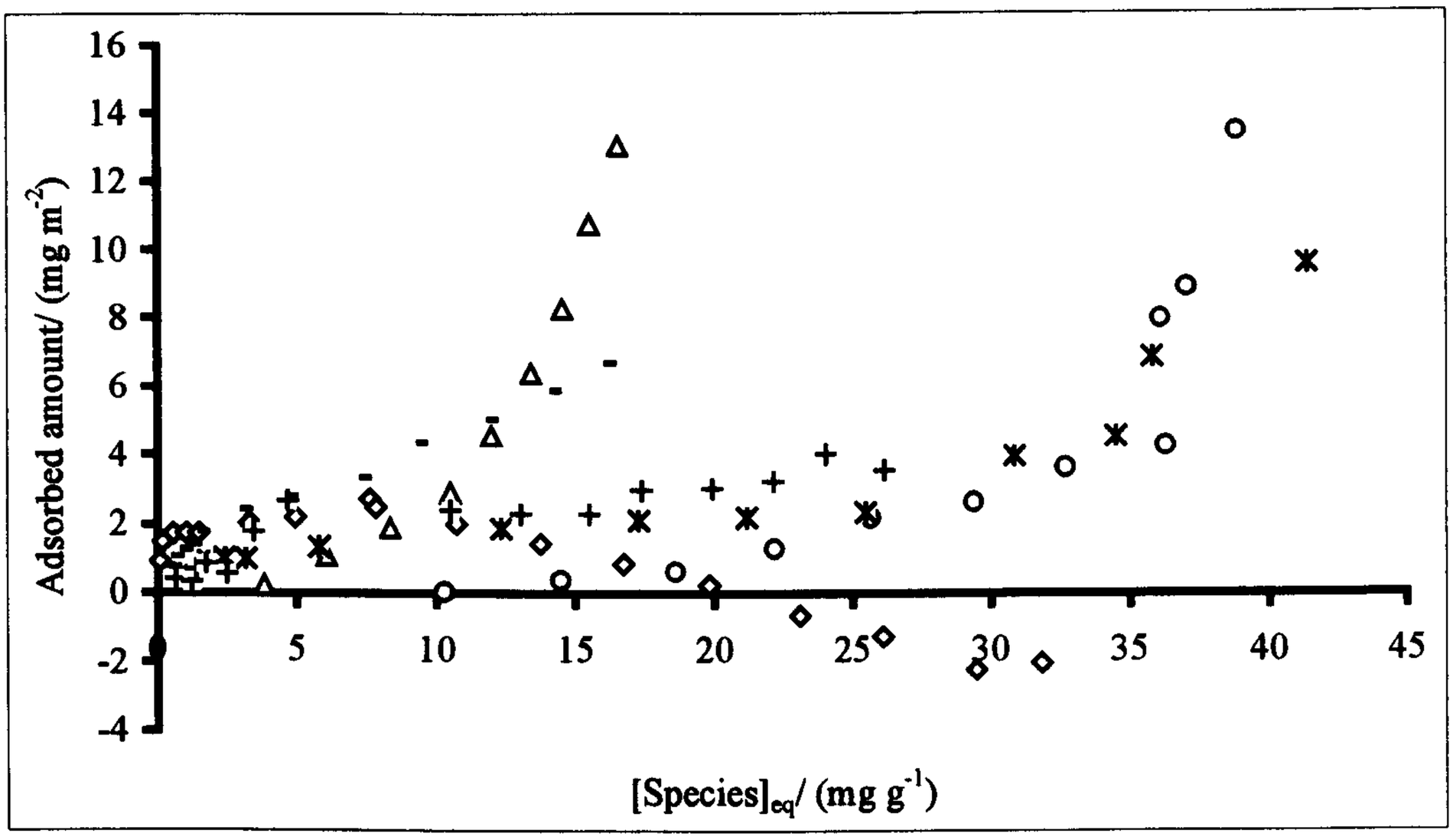

Figure 3.5: Adsorption isotherms of P1 (◊), S1 (Δ), S2 (O), S3 (*), S4(+) and S5(-)

The initial parts of the adsorption isotherms are shown in figure 3.6.

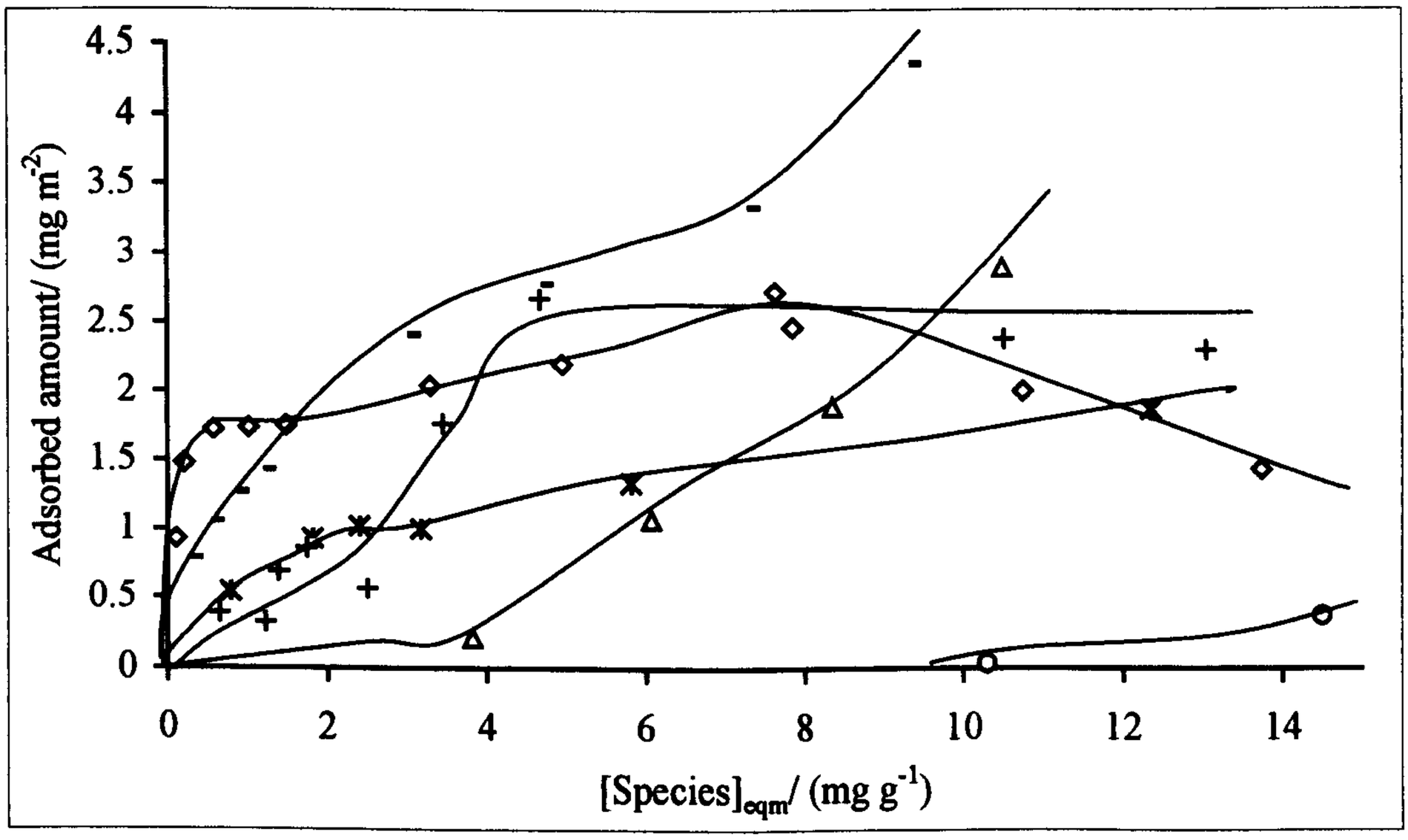

Figure 3.6: Initial region of the adsorption isotherms of P1 (◊), S1 (Δ), S2 (O), S3 (*), S4(+) and S5(-). The lines have been added for visual guidance.

3.7.1.4. Adsorption of polymer and surfactant mixtures

Adsorption isotherms of the polymer were also determined in the presence of surfactants S1, and S3 at 25 °C. The results are shown in figure 3.7.

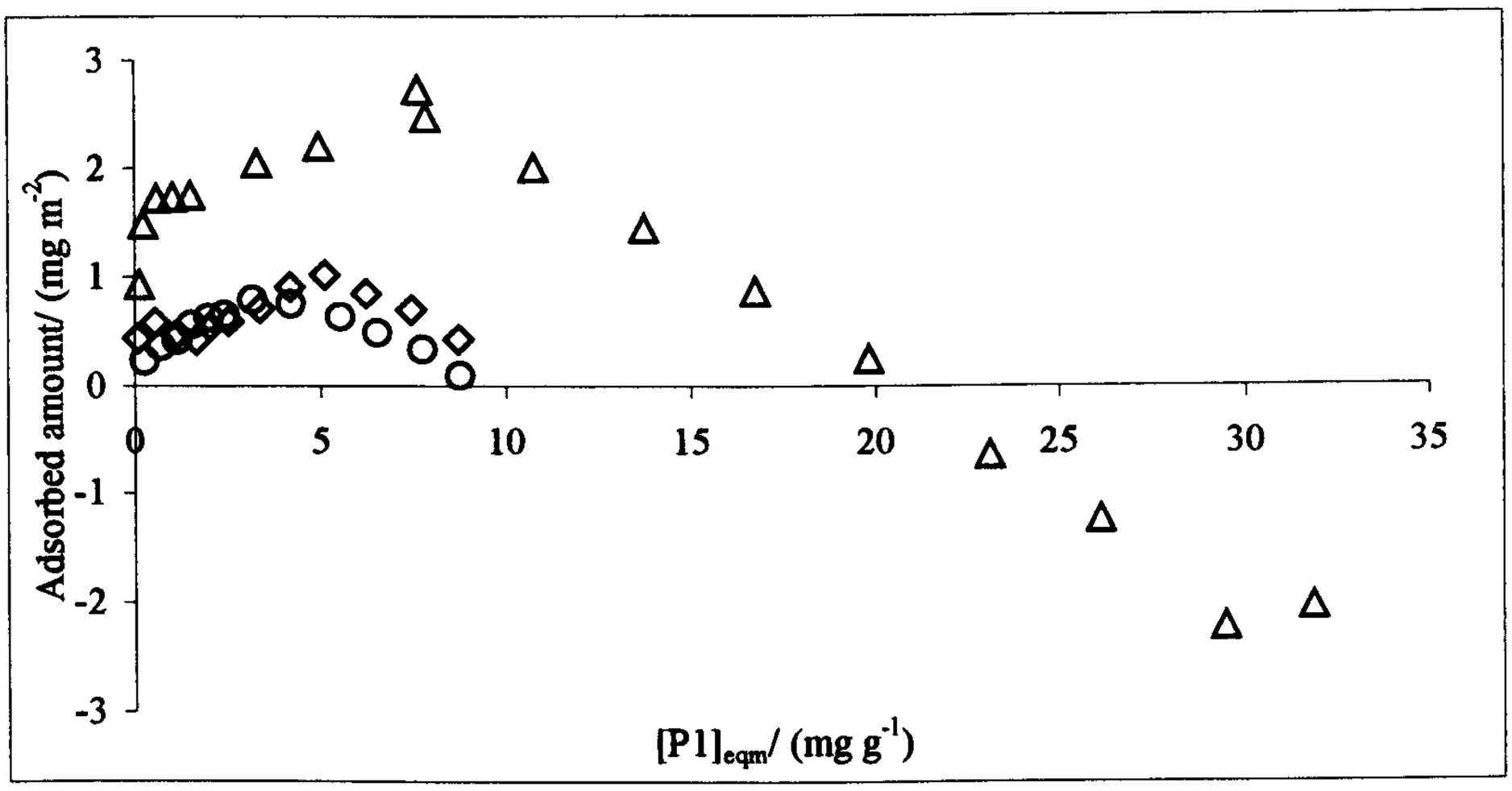

Figure 3.7: Adsorption isotherms of P1 (Δ), P1 and 0.3 wt. % S1 (◊), and P1 and 0.3 wt. % S3 (O)

3.7.1.5. Adsorption of surfactants S1 and S3 mixtures

Adsorption isotherms were also obtained for mixtures of S3 and S1 at 25 °C as shown in figure 3.8. The absorbance of 0.5 wt. % S1 at 212 nm was subtracted from the total absorbance before calculating the equilibrium concentration of S3.

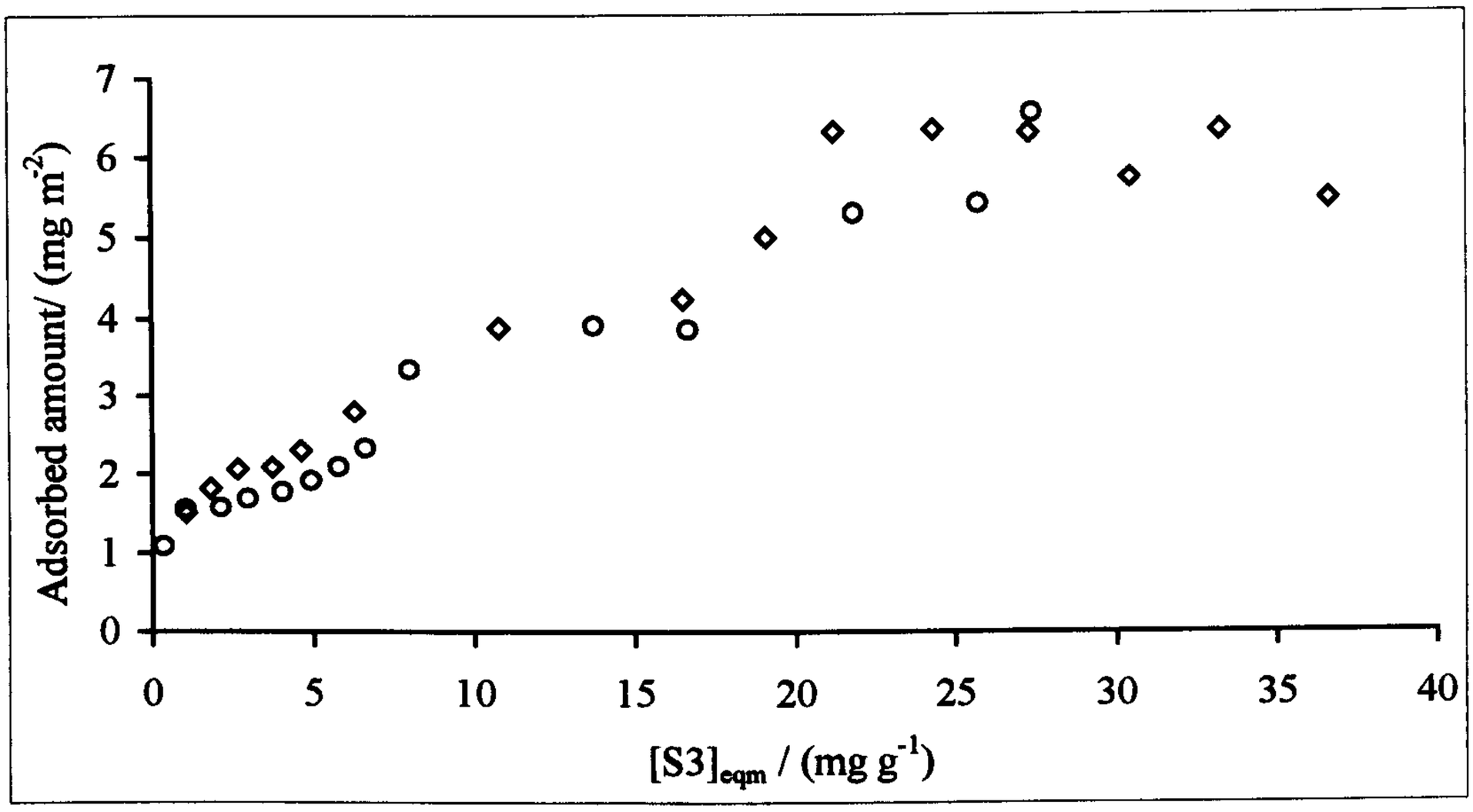

Figure 3.8: Adsorption isotherms of S3 (o) and S3 and 0.5 wt. % S1 (◊)

3.7.1.6. Adsorption of S3 on steel at 40 °C

Adsorption experiments of surfactant S3 (with the amine head group) were also carried out at 40 °C. However, it was found that isooctane (b.pt. 98.5 °C) evaporated very quickly. Hence, experiments were carried out at 25 °C and 40 °C in hexadecane, which has a much higher boiling point of 287 °C. The slope of the calibration plot of S3 in hexadecane at 25 °C was found to be 0.2472 and this value was used to calculate the surfactant concentrations. The adsorption isotherms so obtained are shown in figure 3.9.

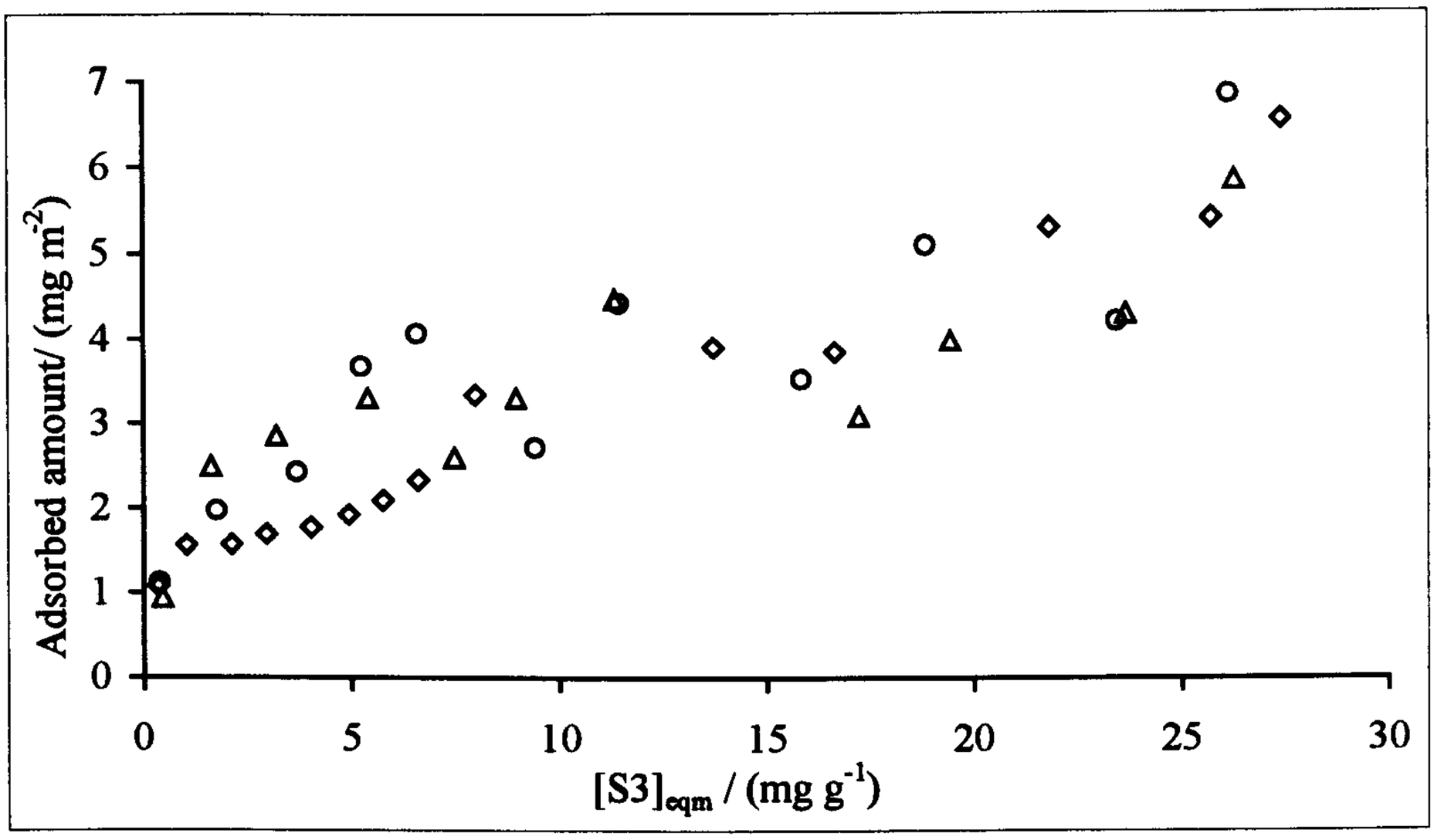

Figure 3.9: Adsorption isotherms of S3 at 25 °C (◊) in isooctane and at 25 °C (Δ) and 40 °C (O) in hexadecane

3.7.1.7. Adsorption isotherm of a polymer-iron complex

As may be seen in figure 3.7, the adsorption isotherm of P1 shows an unexpected decrease at around 10 mg g^{-1}. It was believed that this was due to the "leaching" effect of the polymer on steel. In order to investigate this, an already-complexed polymer was used to carry out the adsorption experiments, with the expectation that more of the P1-Fe complex would be required to leach the steel surface. The UV absorbance of P1-Fe at 274 nm was calibrated before carrying out the adsorption experiments. The slope of the plot and the regression value were found to be 1.4786 and 0.9996, respectively. The adsorption isotherm of P1-Fe is shown in figure 3.10.

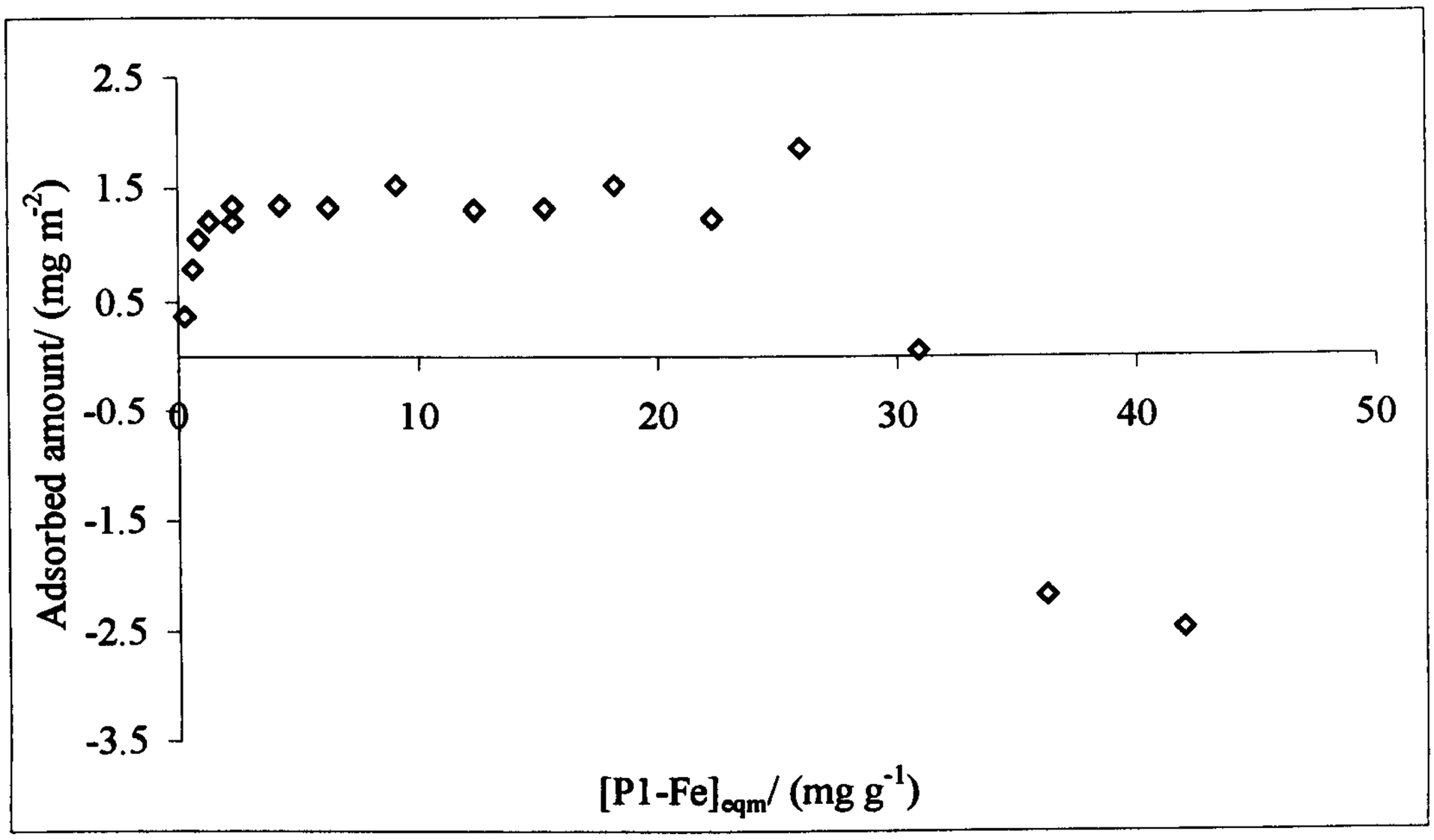

Figure 3.10: Adsorption isotherm of P1-Fe complex at 25 °C in isooctane

3.7.2. Adsorption on carbon particles

3.7.2.1. Calibration of the polymer and surfactant absorbances in isooctane

For the adsorption on carbon experiments, new calibration plots were established; the values of the slopes obtained are as given in table 3.1.

Species	Wavelength	Slope of the calibration plot	Regression
P1	280	1.1795	0.9987
S1	196	0.3602	0.9950
S2	205	0.1239	0.9995
S3	212	0.3033	0.9994
S4	277	1.0284	0.9992
S5	277	0.5962	0.9990

Table 3.1: Calibration slopes of P1, S1, S2, S3, S4 and S5

3.7.2.2. Adsorption isotherms of the polymer and surfactants on carbon

The adsorption isotherms of the polymer and the various surfactants on carbon particles are shown in figure 3.11 to 3.13.

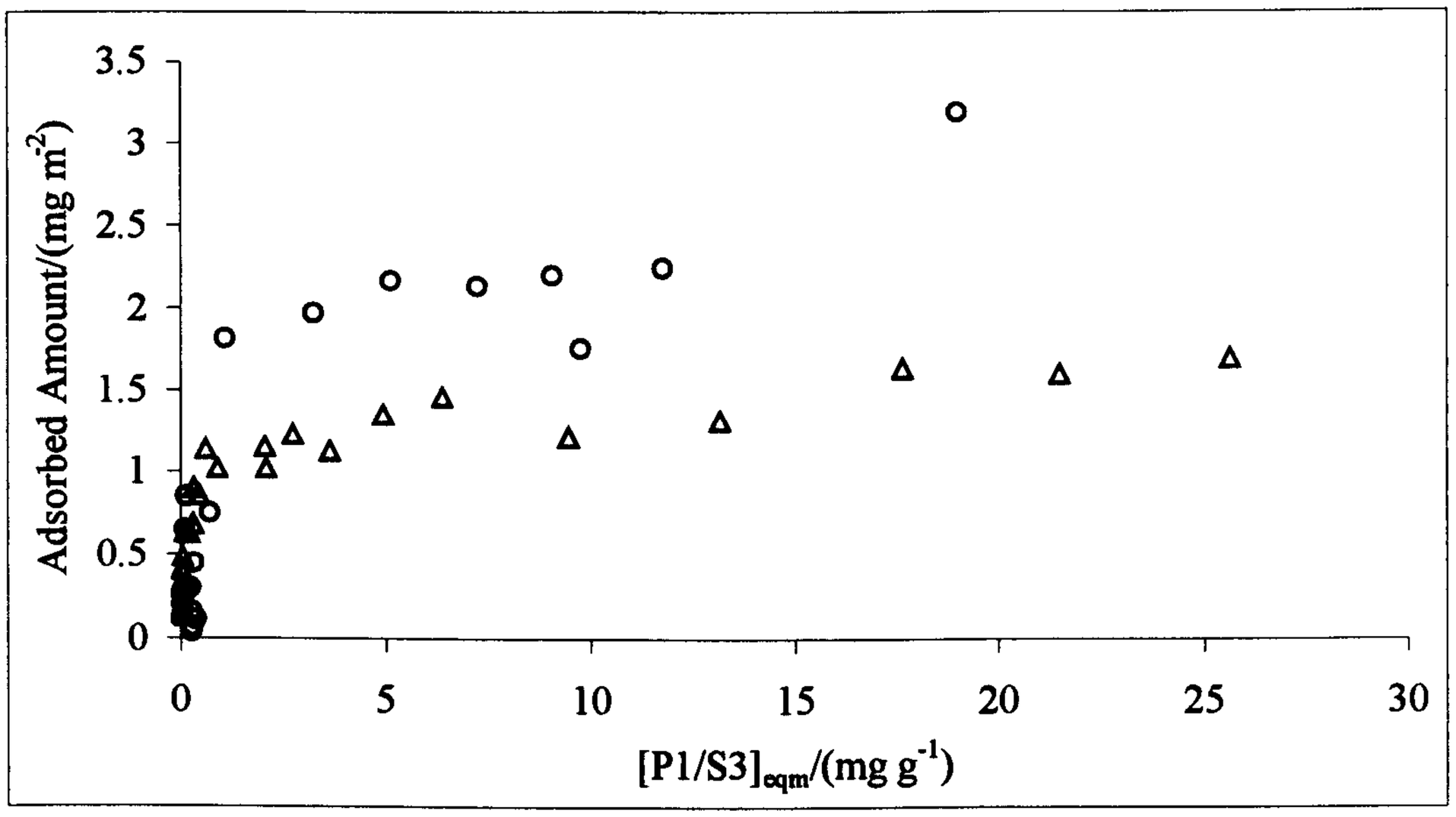

Figure 3.11: Adsorption isotherms of P1 (Δ) and S3 (O) on carbon at 25 °C

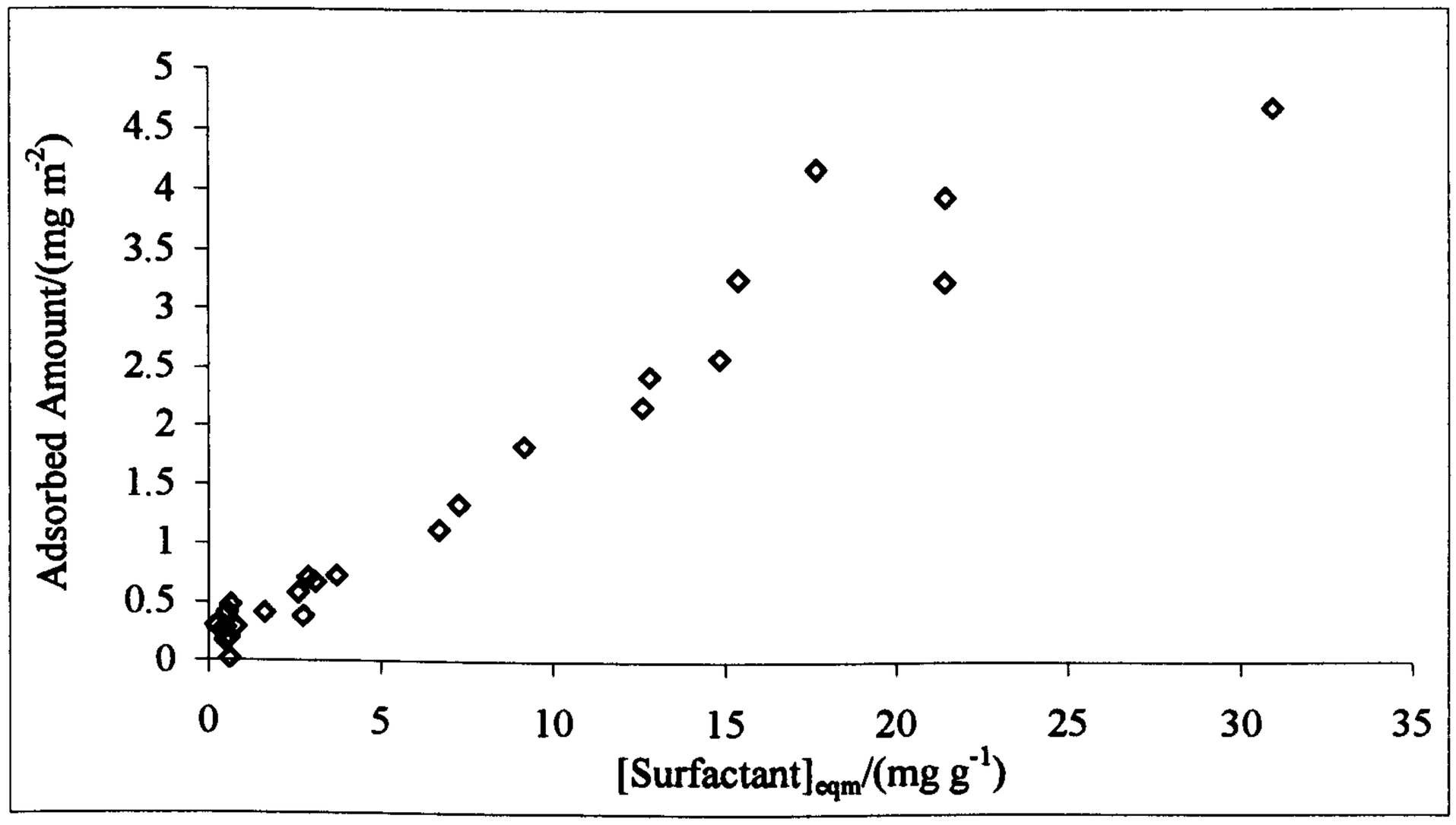

Figure 3.12: Adsorption isotherm of S2 (◊) on carbon at 25 °C

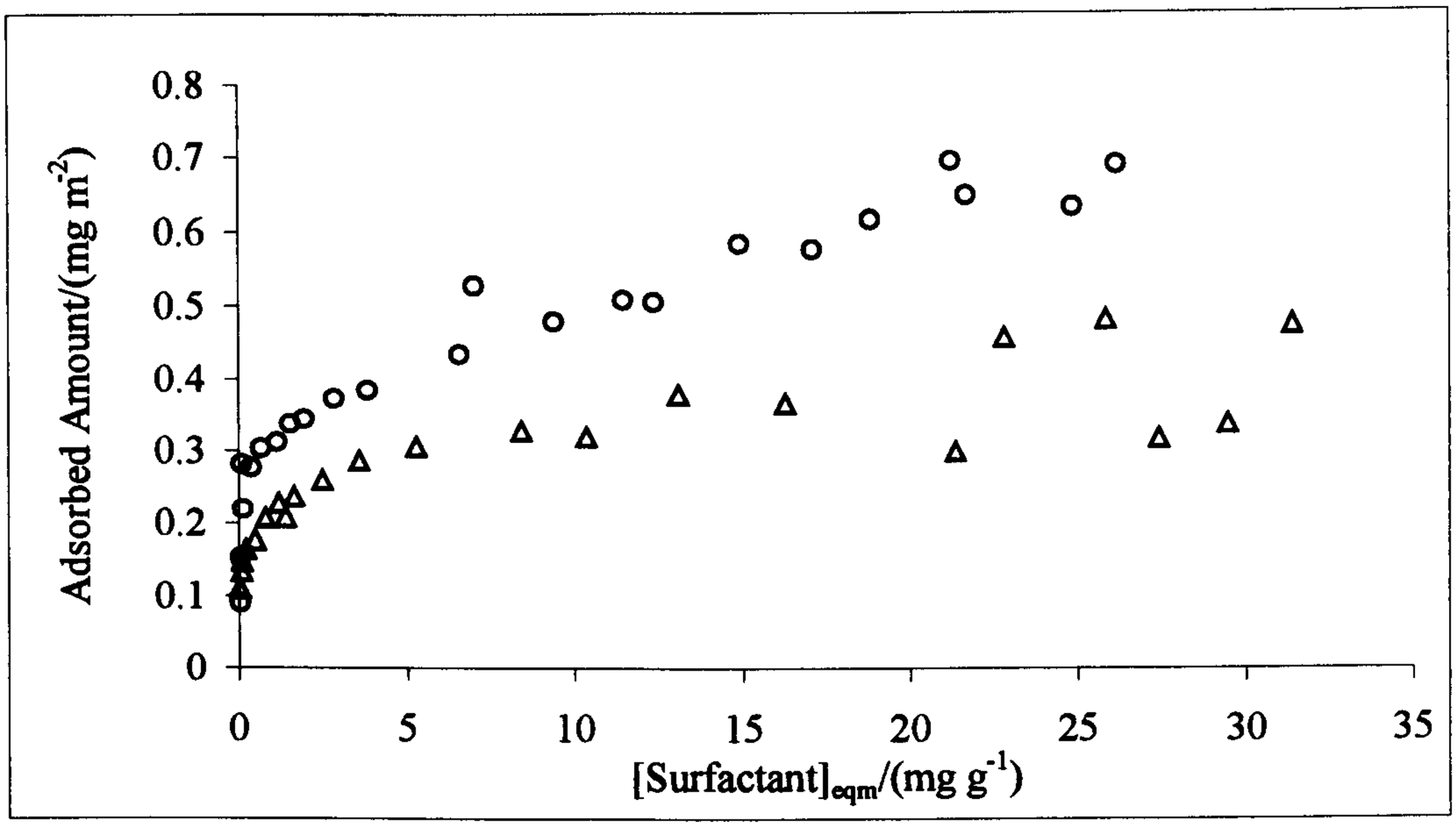

Figure 3.13: Adsorption isotherms of S4 (Δ) and S5 (O) on carbon at 25 °C

3.8. Analysis and Discussion

The calibration experiments (figure 3.3 and table 3.1) gave good linear fits, validating the use of UV/Vis spectroscopy as a technique for measuring the adsorbed amount. Attempts were also made to use IR spectroscopy to determine polymer concentration but this method was found to be much less precise. The kinetics experiment carried out with surfactant S3 (figure 3.4) showed that the adsorption process is relatively fast, with the equilibrium state reached within 30 min. However, in fact, all the samples were tumbled for 20 h. The adsorption isotherms (figures 3.5, 3.6, 3.11, 3.12 and 3.13) clearly show that the presence of an amine unit in the head group increases the adsorbed amount, as can be seen by comparing the isotherms for P1 and S3 with those of the other surfactants. Similar behaviour has already been reported[17, 18]. The isotherms are mostly of type II and type III[8] indicating multilayer or aggregate formation at the interface. Moreover, the sharp rises in some of the adsorption isotherms at low concentrations may be indicative of an incipient phase transition at the interfacial region[19]. Surprisingly, P1 adsorption seems to decrease around 1 wt. %. By way of explanation, it is thought that the polymer causes "leaching" of metal ions from the steel surface, with the formation of metal complexes in solution. This would lead to an increase in the total light absorbance of the supernatant solution, and hence the decrease in adsorption an artefact. Indeed, atomic absorption spectroscopy studies showed the presence of various metal ions in the supernatant solution and, a visible change in the colour of the supernatant at 1 wt. % P1 and above was also observed. To further test the complexation hypothesis, adsorption studies were carried out using an iron-complex form of P1, termed Fe-P1. The adsorption isotherm so obtained may be seen in figure 3.10. The apparent decrease in the adsorbed amount is now extended to around 3 wt. %. This implies that a higher concentration of the complexed polymer molecules is required before they start leaching the surface effectively.

The adsorption isotherm of S5 rises rapidly and much earlier than for S4 which has the same type of polymer backbone, but a lower molecular weight. Similar molecular weight dependence of adsorbed amount, albeit for much higher molecular weight ranges, has been reported in other adsorption studies[20]. However, it is not clear as to why the adsorption isotherm rises much faster for S1 than S2 even though they have similar molecular weights. The explanation might lie in the different structures of the backbone chains namely, the propoxylate and the butoxylate units on S2 and S1, respectively. Also, the solvency of the non-polar solvent on the polar propoxylate units in S3 would be poor in comparison to the solvation of the PIB chain of the polymer. This would lead to an increased adsorption of S3 as compared to P1, as can be seen in figure 3.11. A similar explanation could also be given for the increased adsorbed amount of S5, as compared to S4 which has only half the number of propoxylate units as S5. Similar reasoning can also be used to explain the difference in the adsorbed amounts of S4 and S5 on stainless steel (figure 3.5). This effect of the 'selective' nature of the solvent has also already been reported[20].

The adsorption isotherms for P1 in the presence of S1 or S3 show a decrease in the adsorbed amount of P1, as compared to P1 alone (figure 3.7). This would imply that the surfactant molecules are replacing some of the polymer molecules at the interface. However, the presence of the amine group on surfactant S3 does not seem to differentiate it from S1 in its ability to displace the polymer molecules. Thus, the butoxylate units seem to be the deciding factor in this process. This hypothesis is also further supported by the fact that the presence of surfactant S1 does not seem to affect the adsorbed amount of S3 (figure 3.8). However, it is unlikely for the strongly adsorbing polymer to be completely displaced by the surfactant. Thus, the surfactant molecules may be interacting with the loosely bound polymer molecules at the steel/isooctane interface to form aggregates which are then solubilised in the solvent.

This might also be an effect of the solvent/surfactant interactions, where the polar butoxylate units are less soluble in the non-polar solvent, i.e. isooctane. Thus, the competitive adsorption[21] taking place in the mixed system could be driven by the different solvent/surfactant (χ) and surfactant/surface (χ_s) interactions. Though there is a slight difference in the molecular weights of the polymer (1174 g mol^{-1}) and S1 (1640 g mol^{-1}) and S3 (1697 g mol^{-1}), it is unlikely that such small differences could lead to large differences in the adsorbed amount, as reported in some cases[15, 16]. More importantly, the polymer and surfactants do not have the same backbone chemistry.

Figure 3.9 shows the adsorption isotherms of S3 at 25 °C and 40 °C carried out in hexadecane, which has a much higher boiling point than isooctane and thus, a lower vapour pressure. However, there seemed to be no significant differences in the amount of surfactant adsorbed on steel at these two temperatures.

As already mentioned, the adsorption isotherms are mostly type II and III which suggest aggregation or multilayer formation at the interface. Similar observations have been made for the adsorption of polystyrene-hydrogenated polyisoprene AB-type diblock copolymers at the cyclohexane/carbon black interface[20]. There are various models available which can be used to analyse these type of adsorption isotherms. In this study, a model developed by Zhu and Gu[22] has been used to fit the data, and hence obtain the aggregation numbers at the interface. This model considers that adsorption takes place in two distinct steps; the first step involves the adsorption of the molecules on the surface and the second one involves interactions between adsorbed molecules. The general form of isotherm is given in eqn. 3.9:

$$\frac{\Gamma}{\Gamma_{max}} = \frac{K_1 C\left(\frac{1}{n} + K_2 C^{n-1}\right)}{1 + K_1 C\left(1 + K_2 C^{n-1}\right)} \qquad \text{Eqn. 3.9}$$

where,

Γ = amount of surfactant adsorbed

Γ_∞ = limiting adsorption at high concentrations

C = concentration of surfactant

K_1 and K_2 = equilibrium constants

n = aggregation number

One such model fit is shown in figure 3.14. For this fit, the values of equilibrium constants K_1 and K_2 are 3.53×10^3 and 9.43×10^{10}, respectively. The aggregation number, n, is equal to 6.22.

The values obtained for the aggregation numbers of the different surfactants at the interface are given in table 3.2. The table shows that the aggregation numbers are in the range 2 to 6 for most systems. A good fit could not be obtained for the polymer adsorption on steel and S1 adsorption on carbon using the Zhu-Gu model due to a lack of sufficient data points.

The value of Γ_∞ used in each model fit was that of the adsorbed amount at the highest equilibrium concentration for each adsorption isotherm. It is likely that the fits and the aggregation numbers obtained will change with different values of Γ_∞.

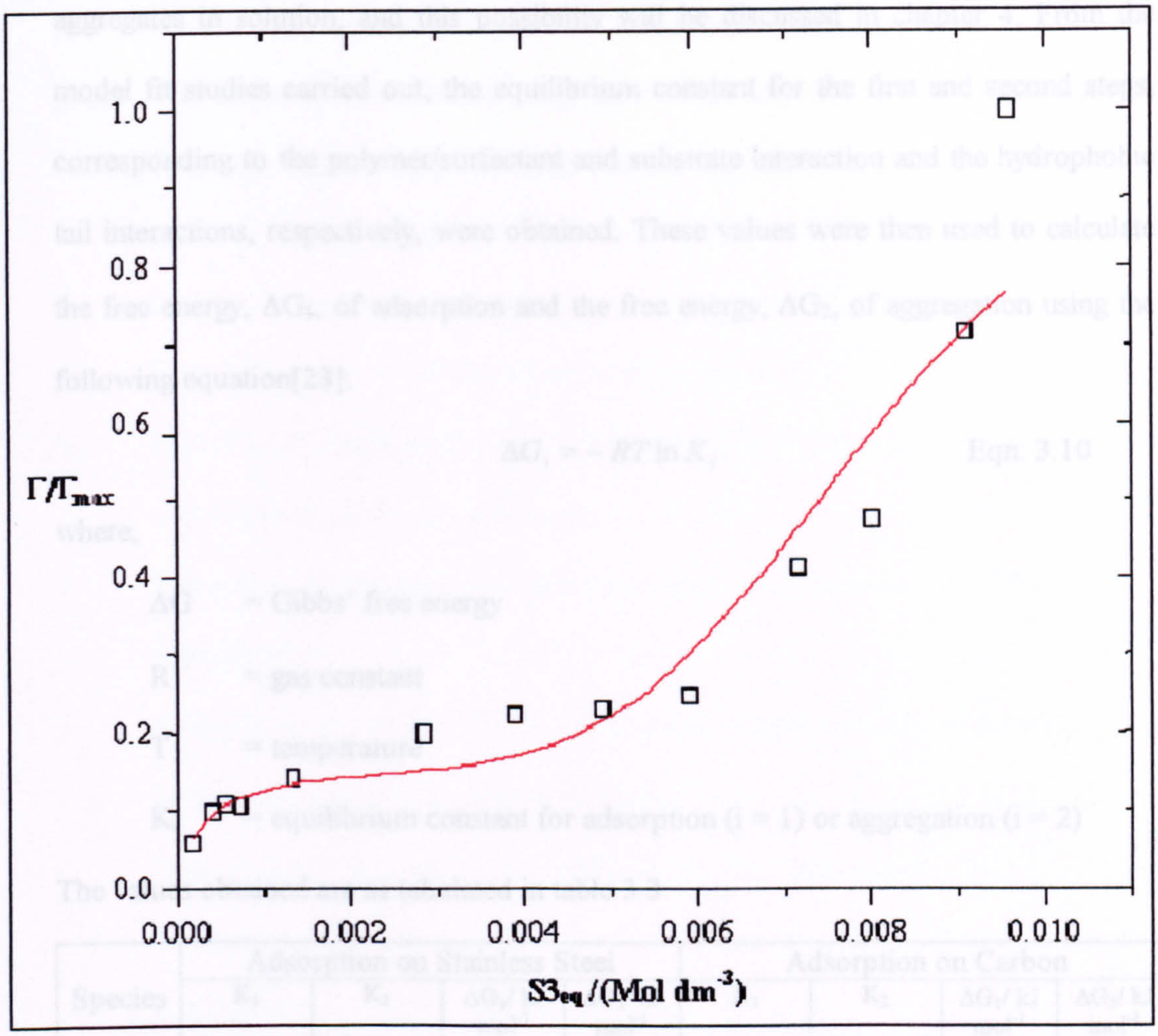

Figure 3.14: Theoretical Zhu-Gu model fit to the adsorption isotherm of S3 on stainless steel surface

Species Name	Calculated Aggregation Number	
	Adsorption on steel	Adsorption on carbon
P1	Not enough data points	2
S1	6	Not enough data points
S2	6	4
S3	6	1
S4	2	2
S5	3-4	3

Table 3.2: Aggregation numbers of the various species adsorbed on stainless steel beads and carbon particles

It is clear from the type of the adsorption isotherms and the aggregation numbers obtained that the polymer and the surfactants are aggregating at the steel/isooctane and carbon/isooctane interfaces. These aggregates could well be in equilibrium with similar

aggregates in solution, and this possibility will be discussed in chapter 4. From the model fit studies carried out, the equilibrium constant for the first and second steps, corresponding to the polymer/surfactant and substrate interaction and the hydrophobic tail interactions, respectively, were obtained. These values were then used to calculate the free energy, ΔG_1, of adsorption and the free energy, ΔG_2, of aggregation using the following equation[23]:

$$\Delta G_i = -RT \ln K_i \qquad \text{Eqn. 3.10}$$

where,

ΔG = Gibbs' free energy

R = gas constant

T = temperature

K_i = equilibrium constant for adsorption (i = 1) or aggregation (i = 2)

The values obtained are as tabulated in table 3.3:

Species	Adsorption on Stainless Steel				Adsorption on Carbon			
	K_1	K_2	ΔG_1/ kJ mol^{-1}	ΔG_2/ kJ mol^{-1}	K_1	K_2	ΔG_1/ kJ mol^{-1}	ΔG_2/ kJ mol^{-1}
P1	Not enough data points				2.52×10^4	232.48	-25.11	-13.50
S1	27.42	2.50×10^{12}	-8.23	-70.73	Not enough data points			
S2	8.61	1.55×10^{11}	-5.33	-63.84	970.93	8.20×10^6	-17.04	-39.44
S3	3.53×10^3	9.43×10^{10}	-20.24	-62.61	975.21	0	-17.05	
S4	330.61	5.40×10^{01}	-14.37	-9.88	4.84×10^4	1.36×10^3	-26.73	-17.88
S5	6.83×10^3	2.48×10^6	-21.87	-36.48	1.70×10^{45}*	1.57×10^4	-258.03	-23.94

Table 3.3: Free energies of the adsorption and interfacial aggregation processes of the different species on stainless steel beads and carbon particles. * = S5 adsorption on carbon is a very steep slope for the first step which the model has taken to be almost normal to the x axis.*

The values for ΔG_1 were generally greater for species containing a functional amine group. The presence of a benzene ring also enhanced the first step of the process leading to greater values of the free energies within the concentration regime studied.

3.9. References

1. Wedler, G., *Chemisorption: An experimental approach*. 1976, London: Butterworths.
2. Fleer, G.J., Cohen Stuart, M. A., Scheutjens, J. M. H. M., Cosgrove, T and Vincent, B, *Polymers at interfaces*. 1993: Chapman & Hall.
3. Kim, J.C., and Lund, D. B., *Biotechnol. Prog.*, 1998. **14**: p. 951 - 958.
4. Du, Y.J., Cornelius, R. M. and Brash, J. L, *Colloids and Surfaces B: Biointerfaces*, 2000. **17**: p. 59 - 67.
5. Shaw, D.J., *Colloid and Surface Chemistry*. 4th Edition ed. 1989: Butterworth Heinemann.
6. Gregg, S.J., and Sing, K. S. W., *Adsorption, Surface Area and Porosity*. 1967, London and New York: Academic Press.
7. Sing, K.S.W., Everett, D. H., Haul, R. A. W., Moscou, L., Pierotti, R. A., Rouquérol, J., and Siemieniewska, T., *Pure and Applied Chemistry*, 1985. **57**: p. 603-619.
8. Lowell, S., *Introduction to Powder Surface Area*. 1979, New York: John Wiley & Sons.
9. Sing, K.S.W., *Colloids and Surfaces A*, 1989. **38**: p. 113 - 124.
10. Brunauer, S., Emmett, P. H. and Teller, E., *Journal of American Chemical Society*, 1938. **60**: p. 309.
11. Brunauer, S., Deming, L. S., Deming, W. E., and Teller, E., *Journal of the American Chemical Society*, 1940. **62**: p. 1723 - 1732.
12. Autosorb, Q., *Manual*. p. II-1 to II-18.
13. Cox, A.R., *The Effect of Polymer Chain Architecture on the Adsorption and Dispersion Properties of Polyisobutylene*, in *Department of Chemistry*. 1998, University of Bristol: Bristol.

14. Banwell, C.N., and McCash, E. M., *Fundamentals of Molecular Spectroscopy*. Fourth ed. 1995, New Delhi: Tata McGraw-Hill Publishing Company Limited.

15. Cohen Stuart, M.A., Waajen, F. H. W. H., Cosgrove, T., Vincent, B. and Crowley, T. L., *Macromolecules*, 1984. **17**: p. 1825.

16. Santore, M., and Fu, Z., *Macromolecules*, 1997. **30**: p. 8516 - 8517.

17. Cox, A.R., Vincent, B, Harley, S. and Taylor, S. E., *Colloids and Surfaces A: Physiochemical and Engineering Aspects*, 1999. **146**: p. 153 - 162.

18. Dubois-Clochard, M.-C., Durand, J. -P., Delfort, B., Gateau, P., Barré, L., Blanchard, I., Chevalier, Y. and Gallo, R., *Langmuir*, 2001: p. 5901 - 5910.

19. Findenegg, G.H., Koch, C. and Liphard, M., *Adsorption of decan-1-ol from heptane at the solution/graphite interface*, in *Adsorption from solution*, R.H. Ottewill, Rochester, C. H. and Smith, A. L., Editor. 1983, Academic Press.

20. Shar, J.A., Cosgrove, T, Obey, T. M., Warne, M. R. and Wedlock, D. J., *Langmuir*, 1999. **15**: p. 7688 - 7694.

21. van der Beek, G.P., M. A. Cohen Stuart, Fleer, G. J. and Hofman, J. E., *Macromolecules*, 1991. **24**: p. 6600.

22. Zhu, B.-Y., and Gu, T., *J. Chem. Soc., Faraday Transactions 1*, 1989. **85**(11): p. 3813-3817.

23. Atkins, P.W., *Elements of Physical Chemistry*. Second ed. 1999: Oxford University Press.

CHAPTER 4: AGGREGATION STUDIES

4.1. Introduction

In chapter 3, it was shown that the polymer and the surfactants associate at the interface of steel and isooctane to form aggregates with up to 6 molecules per aggregate. It was also mentioned that the polymer/surfactant most likely formed aggregates in solution too. This chapter will describe the investigations carried out to study the association of the polymer/surfactant molecules in isooctane. As the polymer and surfactant molecules have both hydrophilic and hydrophobic segments, and the solvent used is non-polar, i.e. isooctane, they are expected to form aggregates where the hydrophilic segments will form the core surrounded by the hydrophobic segments, similar to reverse micelles. The formation of micellar aggregates by polyisobutylene-polystyrene-polyisobutylene (PIB-PS-PIB) triblock copolymer in hexane has previously been studied[1]. It was shown that PIB chains extended into hexane while the PS units formed the core. Other studies have also shown the formation of reverse micelles in various non-polar solvents, including isooctane, the solvent used in this study[2-6].

Various techniques may be employed in the study of aggregation of surfactants in solution and reverse micelles such as small-angle neutron scattering[3], light scattering[7, 8], vapour pressure osmometry[9, 10], infrared spectroscopy[11], thermometric investigations[12], and the solubilisation of iodine[2]. In this investigation, two methods were used to study the aggregation of the polymer/surfactants in isooctane namely, vapour pressure osmometry (VPO), and aggregation studies using a water soluble dye.

4.2. VPO Experimental

4.2.1. Vapour Pressure Osmometry

A *Gonotec Osmomat 070/090-SA* was used to measure the vapour pressure of the different solutions. A schematic diagram of the instrument is shown in figure 4.1.

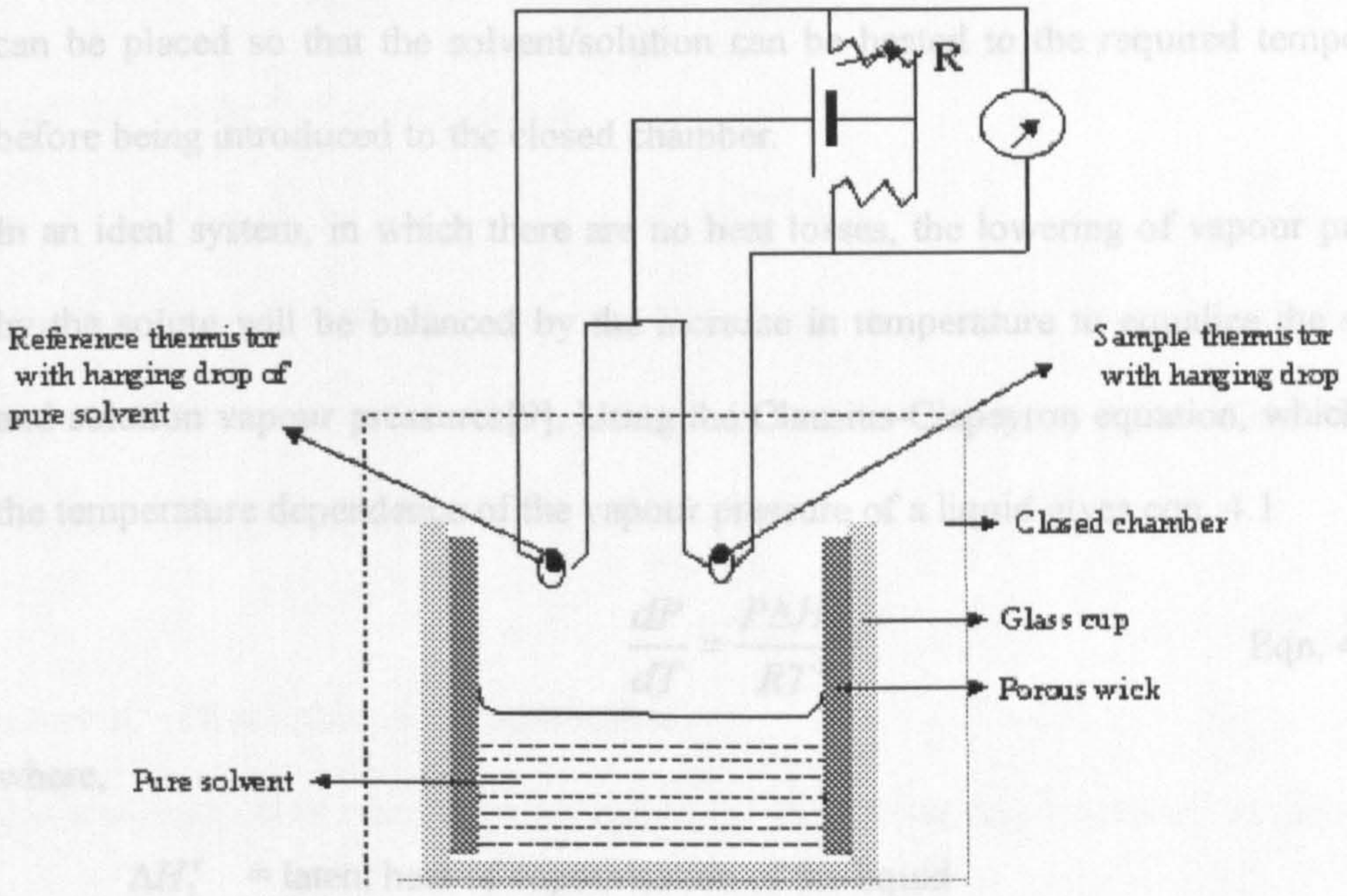

Figure 4.1. Schematic diagram of a vapour pressure osmometer

The apparatus consists of a solvent reservoir, two thermistors, a wick to disperse the solvent and a Wheastone bridge circuit. The solvent reservoir at the bottom and the porous wick helps in maintaining saturation vapour pressure in the cell. The two thermistors are connected as arms of the Wheatstone bridge as shown in figure 4.1. R is a variable resistor which can be used to null any off-balance voltage across the arms. The presence of a solute in a solvent lowers vapour pressure of the solvent and when a drop of the solution is exposed to the vapour of the pure solvent, condensation of solvent from the vapour phase takes place. The heat of condensation increases the temperature of the solution drop and will, theoretically, increases the solution vapour pressure to that of the solvent pressure to attain equilibrium. If a drop of the pure solvent is placed on one thermistor and a drop of the solution is placed on the other

thermistor, this increase in temperature can be easily recorded as a change in balancing resistance, ΔR, across a Wheatstone bridge circuit. The instrument is first calibrated with a standard of known molar mass before starting an experiment. It also has a thermal chamber above the closed chamber where solvent/solution containing syringes can be placed so that the solvent/solution can be heated to the required temperature before being introduced to the closed chamber.

In an ideal system, in which there are no heat losses, the lowering of vapour pressure by the solute will be balanced by the increase in temperature to equalize the solvent and solution vapour pressures[9]. Using the Clausius-Clapeyron equation, which gives the temperature dependence of the vapour pressure of a liquid gives eqn. 4.1

$$\frac{dP}{dT} = \frac{P\Delta H_1^v}{RT^2} \qquad \text{Eqn. 4.1}$$

where,

ΔH_1^v = latent heat of vapourisation of the liquid

P = pressure

T = temperature

R = gas constant

If the vapour pressure of the solution is P and that of the pure solvent is P_o and the temperature changes from T_1 to T_2, then, assuming an involatile solute, eqn. 4.1 can be integrated to obtain eqn. 4.2 and eqn. 4.3.

$$\int_{P_o}^{P} \frac{dP}{P} = \frac{\Delta H_1^v}{R} \int_{T_1}^{T_2} \frac{dT}{T^2} \qquad \text{Eqn. 4.2}$$

$$\ln \frac{P}{P_o} = \ln a_1 = -\frac{\Delta H_1^v}{R}\left[\frac{1}{T_2} - \frac{1}{T_1}\right] \qquad \text{Eqn. 4.3}$$

where a_1 is the activity of the solvent. For a small change in temperature, i.e., T_2 - T_1 (= Δ T) with respect to the operating temperature T, the eqn. 4.3 can be rearranged to give eqn. 4.4.

$$\Delta T = -\frac{RT^2}{\Delta H_1^v} \ln a_1 \qquad \text{Eqn. 4.4}$$

Eqn. 4.4 can be further rewritten as

$$\Delta T = -K^{"} \ln a_1 \qquad \text{Eqn. 4.5}$$

where K" is a constant. Also, since ΔR (the change in balancing resistance measured by the Wheastone bridge circuit) is proportional to ΔT, the activity of the solvent will be related to ΔR by eqn. 4.6.

$$\Delta R = -K' \ln a_1 \qquad \text{Eqn. 4.6}$$

where K' is a constant of proportionality.

For a dilute polymer solution, the activity of the solvent can be related to the volume fraction of the solute u_2 by the following virial equation:

$$\ln a_1 = -\frac{u_2}{m} - \alpha u_2^{\,2} - \beta u_2^{\,3} \ldots \qquad \text{Eqn. 4.7}$$

where m is the ratio of the molar volumes of polymer and solvent.

The solute concentration c_w (in weight of solute per unit weight of solution) for a dilute polymer system can be related to u_2 as shown in eqn. 4.8.

$$u_2 = c_w \frac{\bar{v}_1}{\bar{v}_2} \text{ and } \frac{u_2}{m} = c_w \frac{M_1}{M_2} \qquad \text{Eqn. 4.8}$$

where $\bar{v}_1$ and $\bar{v}_2$ are the partial specific volumes and M_1 and M_2 are the molar masses of the solute and solvent, respectively. As vapour pressure lowering is a colligative property, the value of M_2 can be approximated to the number average value $\overline{M_n}$ for a polydisperse solute. Eqn. 4.8 can then be rewritten as:

$$\Delta R = K' c_w \frac{M_1}{\overline{M}_n} + K' \alpha \left(\frac{\overline{v}_2}{v_1} \right)^2 c_w{}^2 + K' \beta \left(\frac{\overline{v}_2}{v_1} \right)^3 c_w{}^3 + \ldots \quad \text{Eqn. 4.9}$$

Eqn. 4.9 can be rewritten to a convenient form, Eqn. 4.10.

$$\frac{\Delta R}{c_w} = \left(\frac{\Delta R}{c_w} \right)_0 \left(1 + \Gamma_2 c_w + \Gamma_3 c_w{}^2 + \ldots \right) \quad \text{Eqn. 4.10}$$

where $$\left(\frac{\Delta R}{c_w} \right)_0 = \frac{K}{\overline{M}_n} \quad \text{Eqn. 4.11}$$

and $K = K'M_1$ is a constant.

In a reasonably dilute system, third virial coefficient contributions to non-ideality are not common for polymers whose molar masses are lower than 25000 g mol^{-1} and hence, plotting a graph between $\left(\frac{\Delta R}{c} \right)$ and c, the concentration, should give a straight line whose intercept is $\left(\frac{\Delta R}{c} \right)_0$ and whose slope gives Γ_2. If K is known from the calibration experiment, $\overline{M}_n$ can be calculated.

4.2.2. Experimental details

A sufficient volume of isooctane was added to the reservoir and the instrument was left to stabilise for 30 min at 40 °C to create an equilibrium solvent vapour environment in the chamber. Before experiments were carried out with either the polymer or one of the surfactants, the instrument was first calibrated using solutions of squalane in the concentration range 0.4 g kg^{-1} (0.001 mol kg^{-1}) to 4.0 g kg^{-1} (0.01 mol kg^{-1}) in isooctane. Syringes containing isooctane and the various solutions were placed in the thermal chamber and left to stabilise and attain the set temperature for 30 min. After 30 min, a drop of isooctane was placed on each of the thermistor tips taking maximum care that the drops were of the same size. After 2 min, three values of ΔR were measured at a set interval of 2 min; the average of these values is the baseline value.

After the baseline measurement, a drop of most dilute squalane solution was placed at the tip of one of the thermistors and left for 2 min to stabilise. Three values of ΔR were then measured again at intervals of 2 min and the average taken to obtain the ΔR value for that particular solution. The thermistor was then flushed with isooctane and a drop of the second most dilute solution was placed at the tip of the thermistor. ΔR values were measured again and this procedure was repeated for all the solutions, with the most concentrated solution measured last. The values were corrected for baseline shift and a plot of $\left(\frac{\Delta R}{c}\right)$ against c, where c is the concentration, was obtained. This plot was used to calculate the calibration constant, K, of the instrument as the molecular weight of Squalane is known.

The same procedure was repeated with solutions of the polymer and the surfactants in the concentration range 2 g kg^{-1} to 16 g kg^{-1}.

4.2.3. Results

4.2.3.1. Calibration plot of VPO signal against concentration using squalane

The plot of ΔR/c as a function of concentration for the calibration of the instrument using squalane is shown in figure 4.2.

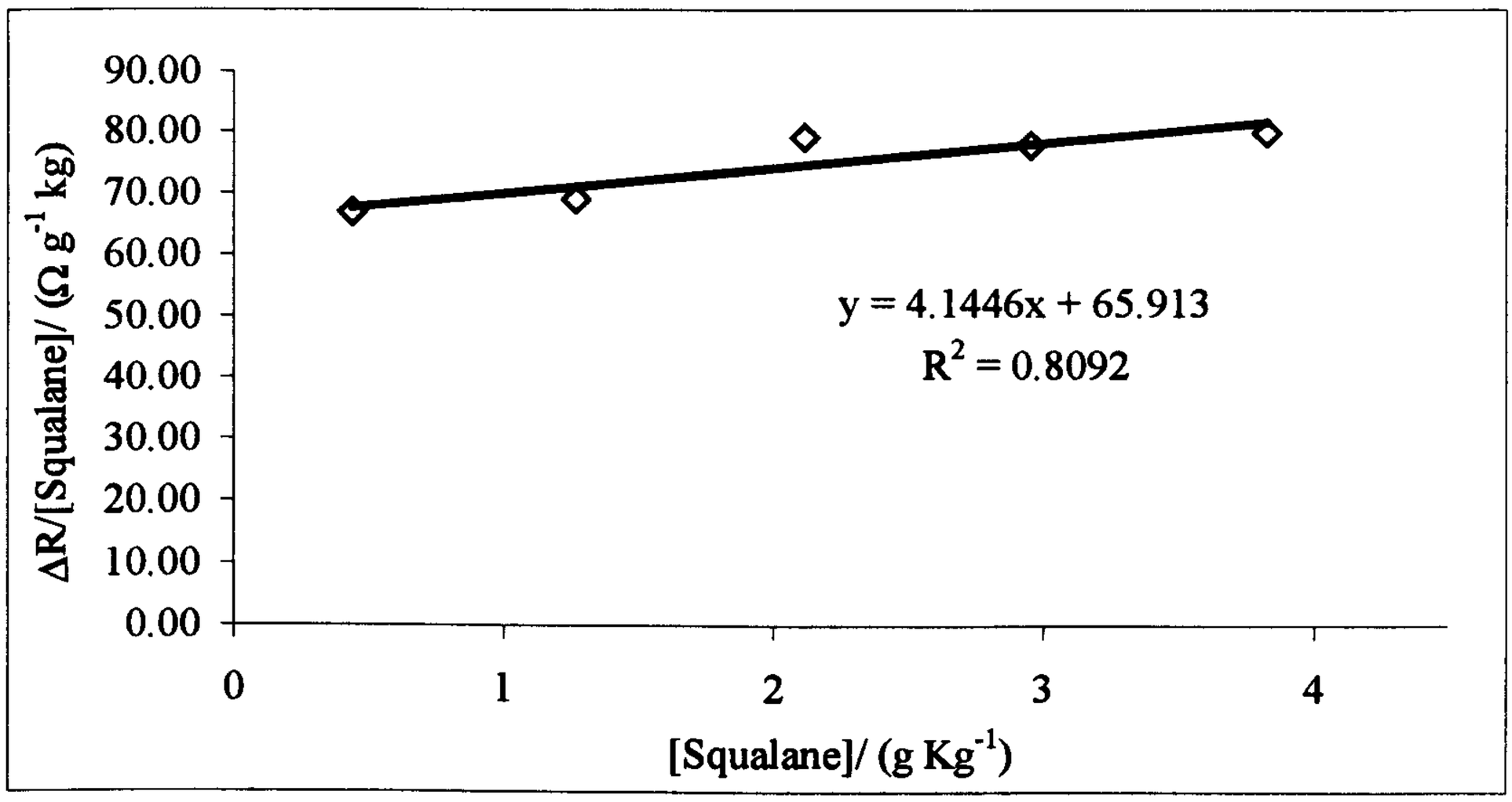

Figure 4.2: Plot of VPO signal against concentration for squalane

4.2.3.2. Plot of VPO signal against concentration for P1

The plot of ΔR/c as a function of concentration for P1 is shown in figure 4.3

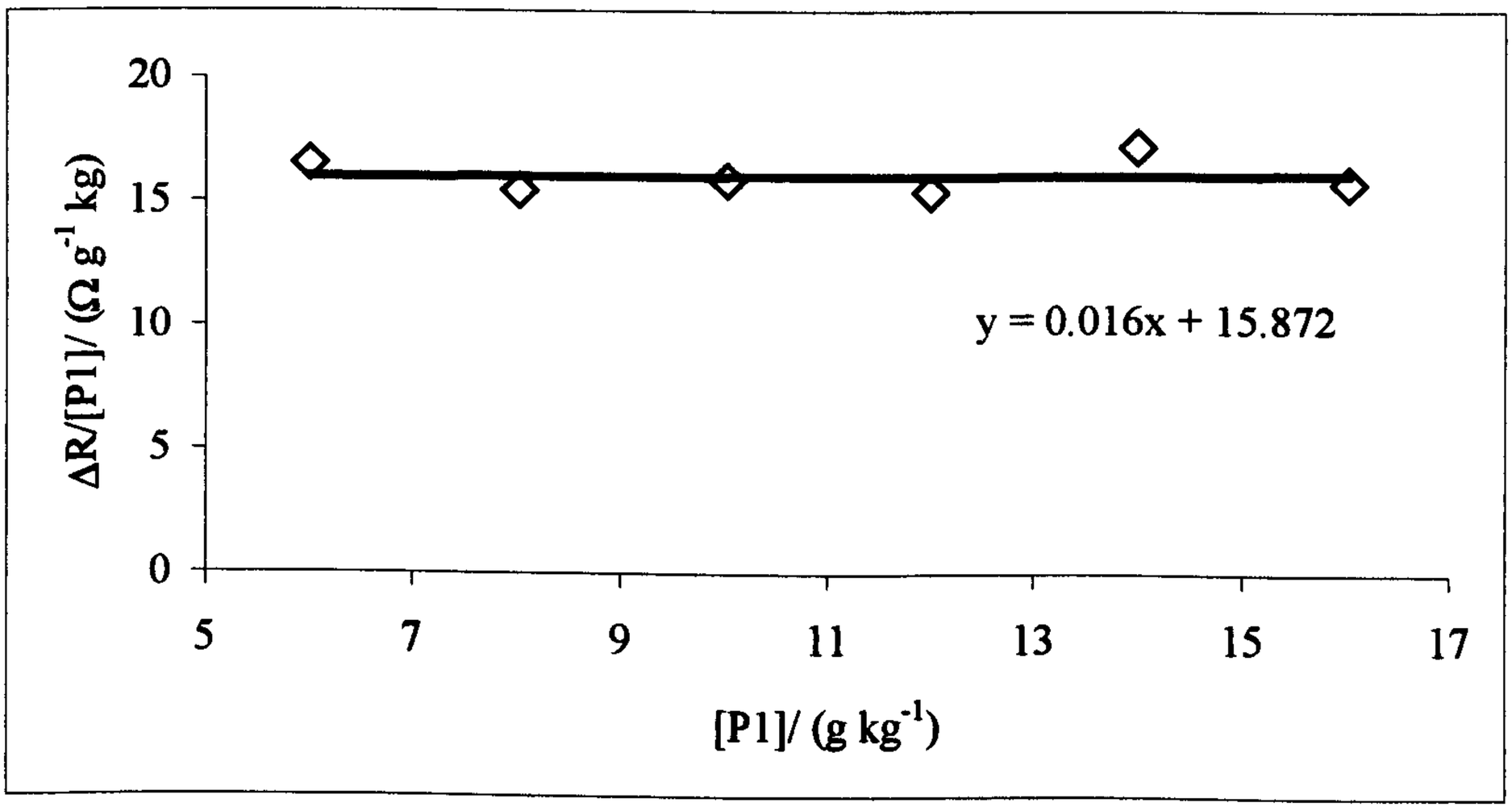

Figure 4.3: Plot of VPO signal against concentration for P1

4.2.3.3. Plot of VPO signal against concentration for surfactants S1, S2, S3, S4 and S5

The plot of ΔR/c as a function of concentration for S1, S2, S3, S4 and S5 are shown in figure 4.4 to 4.8, respectively.

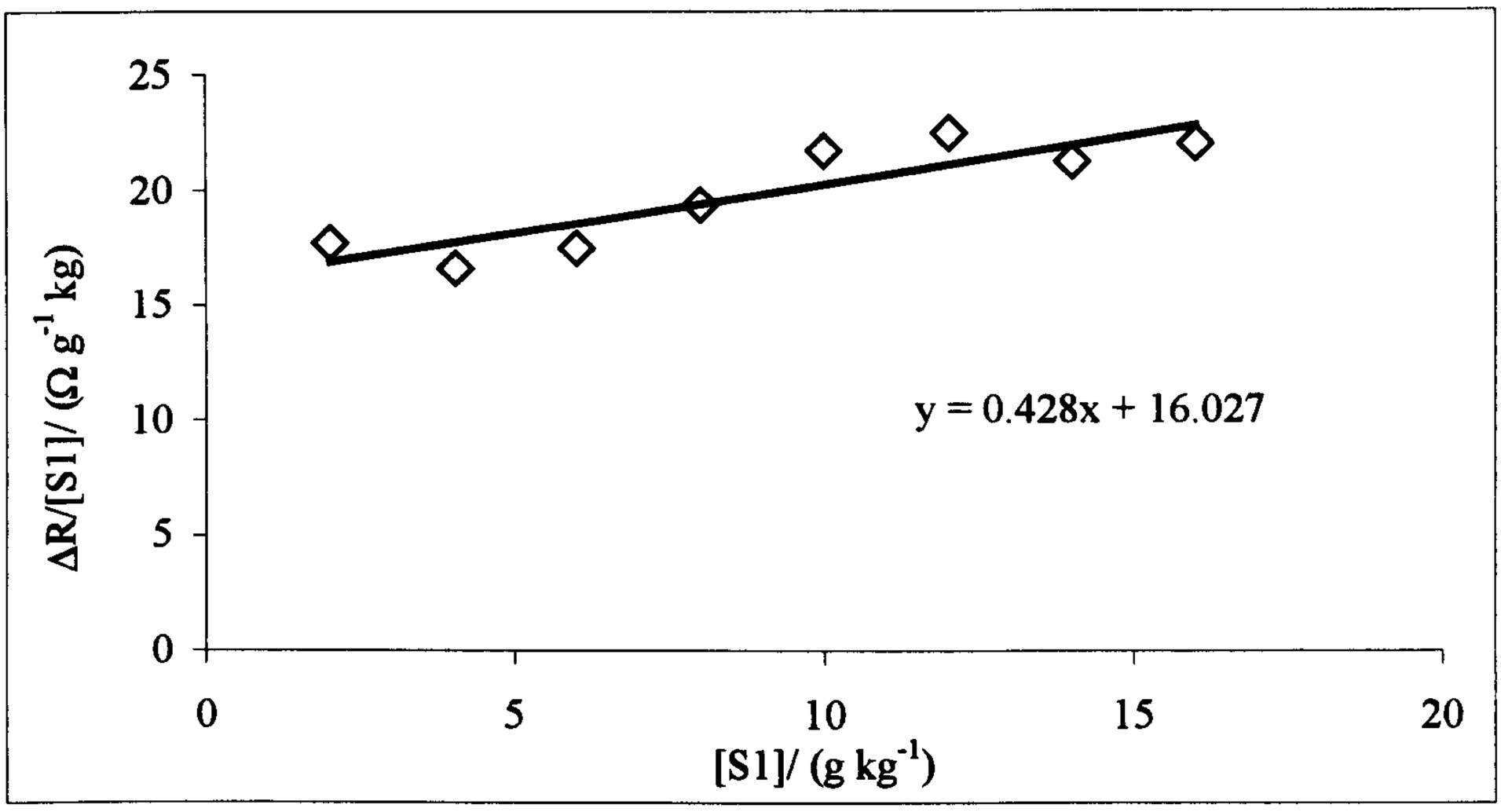

Figure 4.4: Plot of VPO signal against concentration for S1

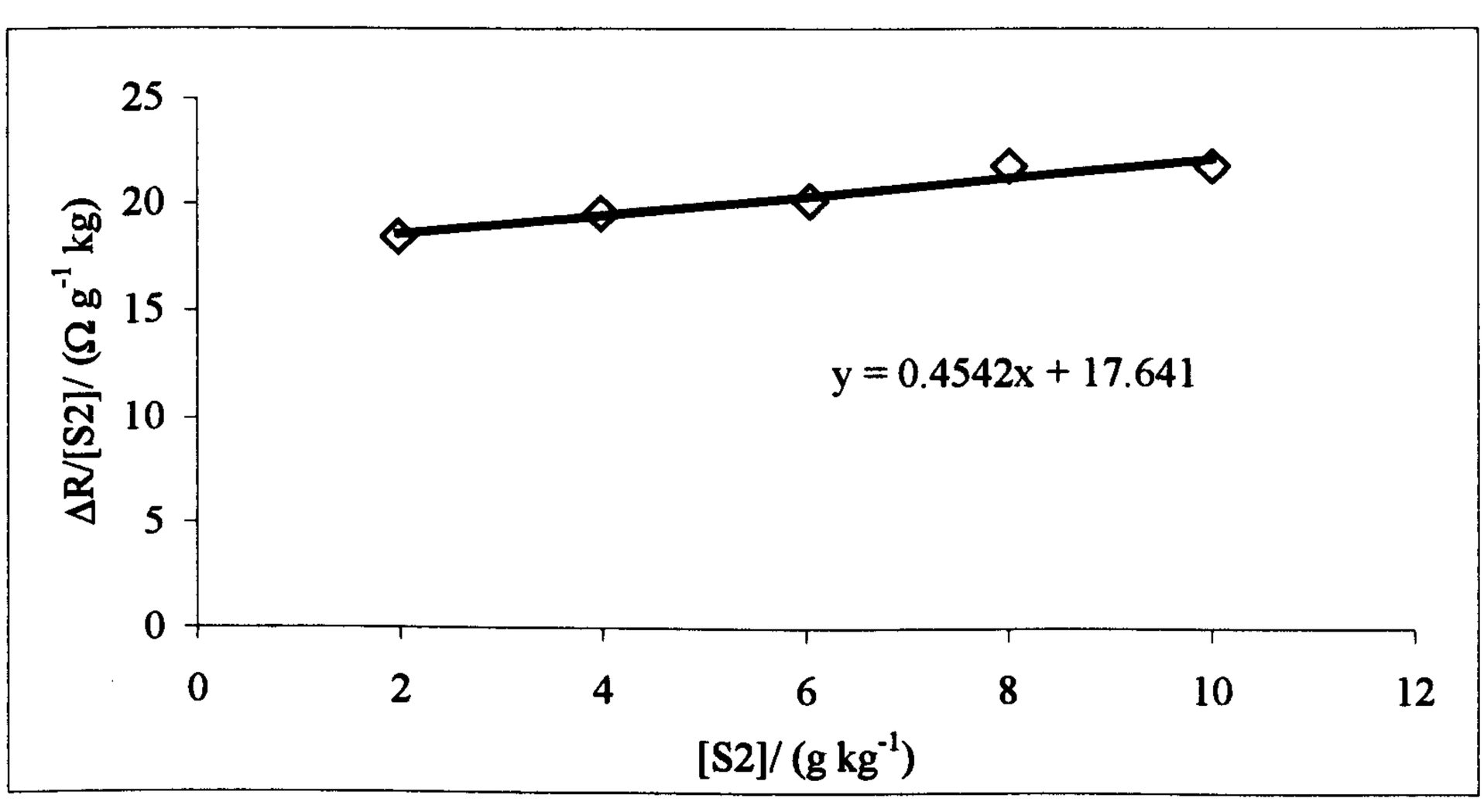

Figure 4.5: Plot of VPO signal against concentration for S2

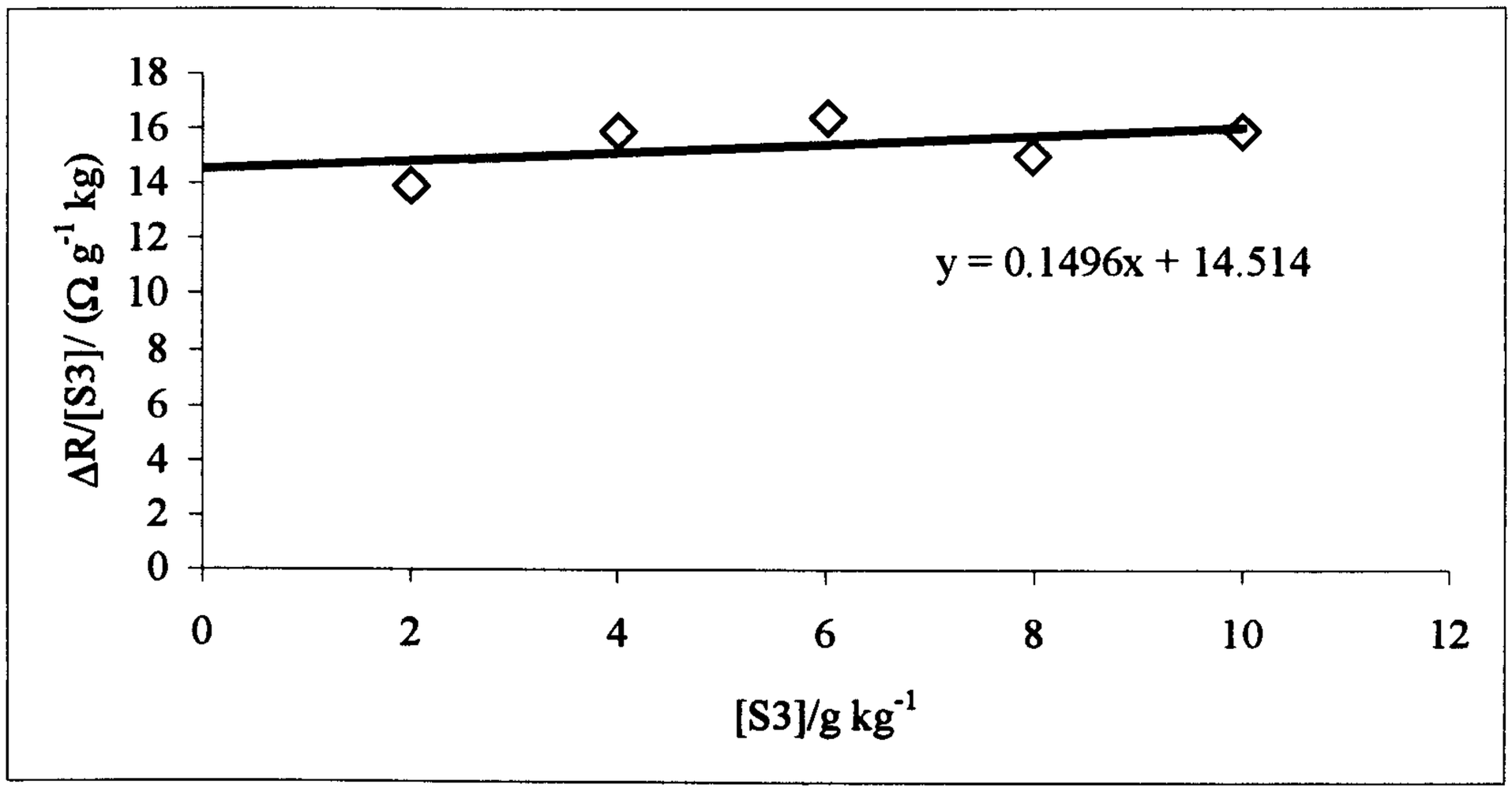

Figure 4.6: Plot of VPO signal against concentration for S3

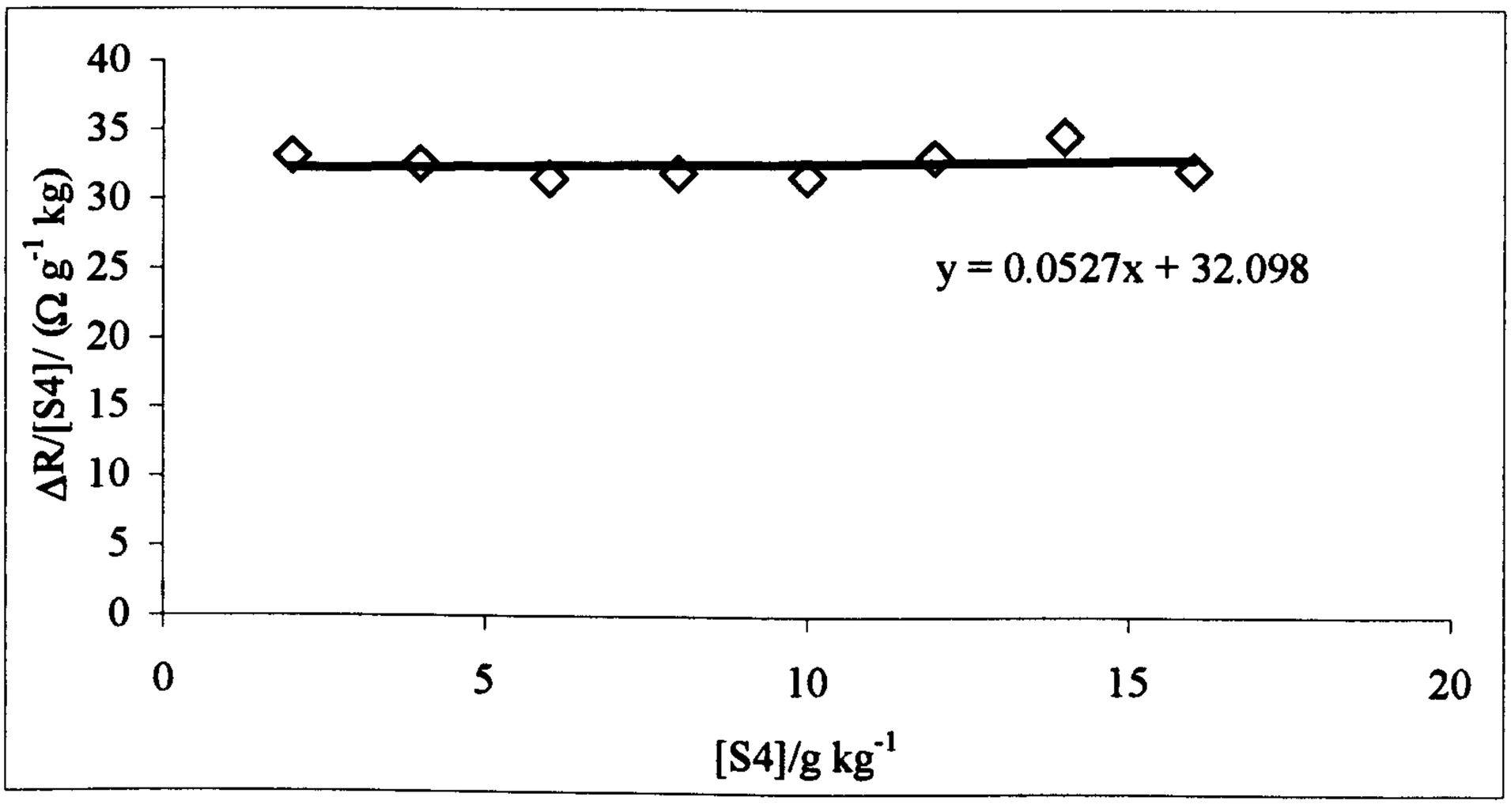

Figure 4.7: Plot of VPO signal against concentration for S4

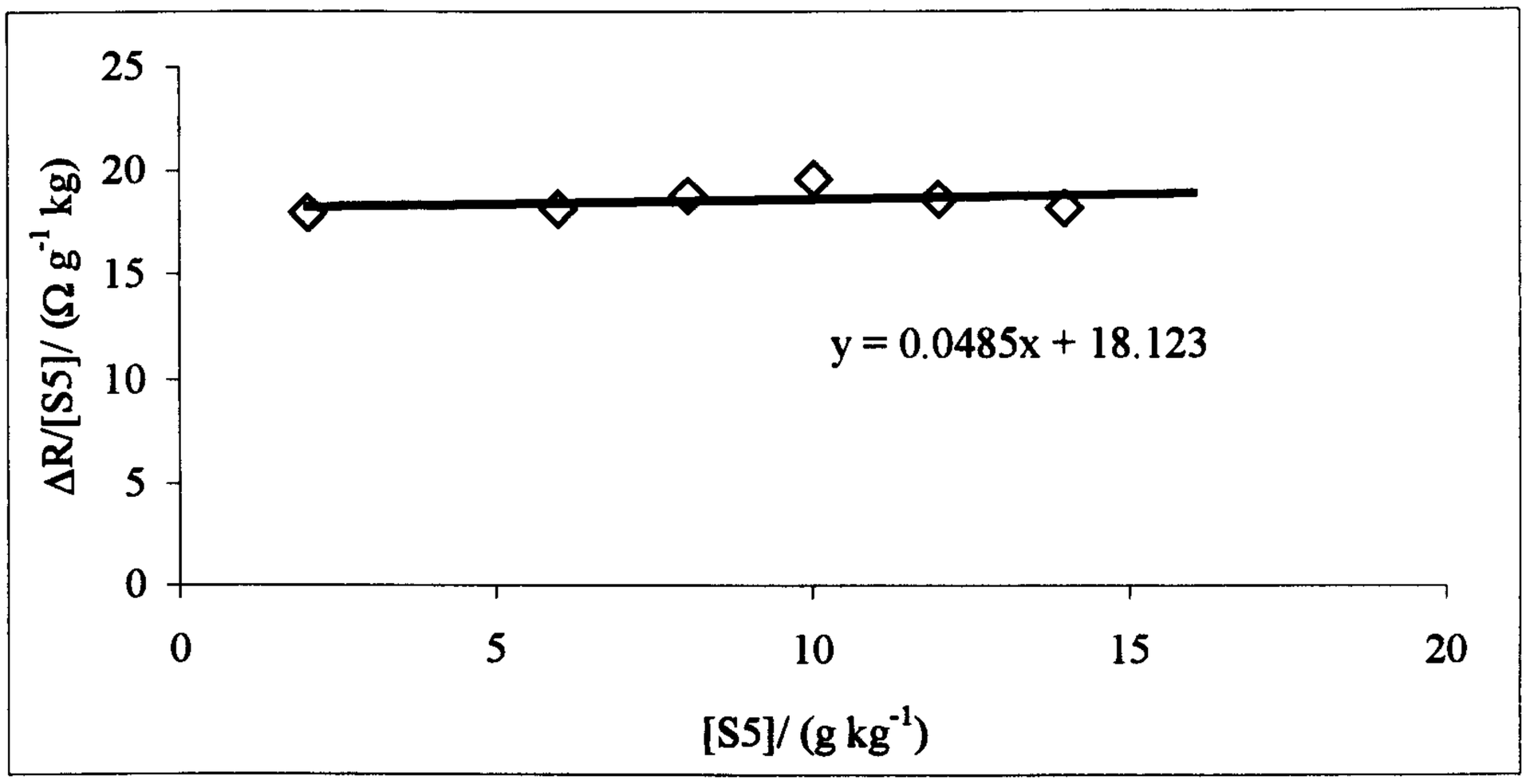

Figure 4.8: Plot of VPO signal against concentration for S5

4.2.3.4. Calculation of aggregation number

The value of the cell constant obtained from the calibration experiment carried out using squalane as the solute in isooctane was found to be 27870 Ω mol^{-1} kg. Using this in equation 4.11, the value of $\overline{M_n}$ for the polymer and the various surfactants were calculated. Dividing the $\overline{M_n}$ value by the molecular weight of the corresponding polymer/surfactant gives the value of the aggregation number in isooctane. The values are shown in table 4.1.

S. No.	Species	Calculated Molecular Weight/ (g mol^{-1})	$\overline{M_n}$ (±30)/ (g mol^{-1}) from VPO experiments	Aggregation number, n
1	P1	1174	1756	1.5
2	S1	1640	1740	1.1
3	S2	1592	1580	1.0
4	S3	1697	1920	1.1
5	S4	958	868	0.9
6	S5	1654	1538	0.9

Table 4.1: $\overline{M_n}$ and aggregation numbers of the polymer and various surfactants

4.3. Dye Absorption Study Experimental

4.3.1. Dye Absorption by Aggregates

When amphiphilic molecules are added to a non-polar solvent, the molecules form aggregates in solution such that the polar head groups are embedded in the core of the aggregate and the hydrocarbon tails are dispersed in the medium forming a shell around the core. This is schematically represented in figure 4.9.

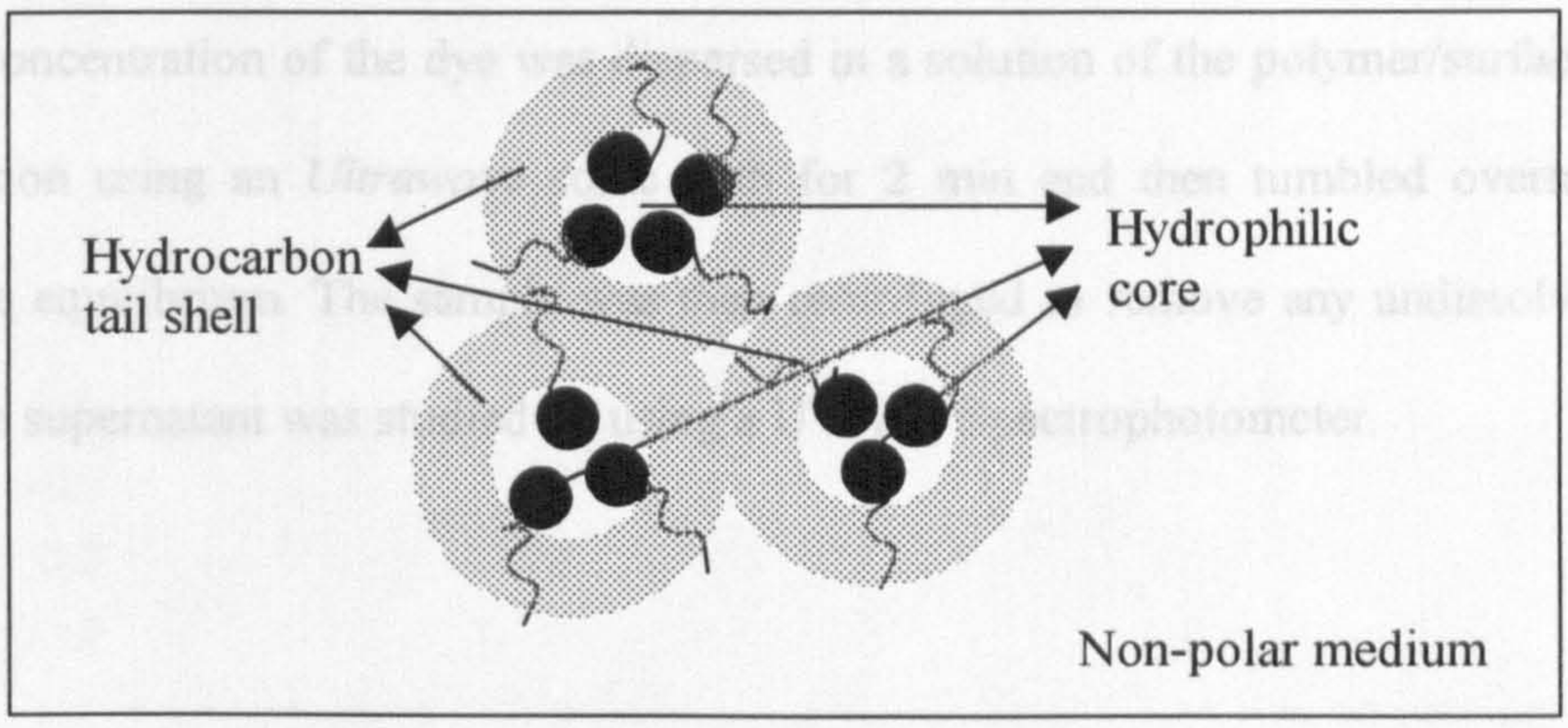

Figure 4.9: Schematic representation of reverse micelles

However, discussions have been made over the process of aggregate formation in non-polar media; whether the aggregation can be characterized by a monomer $\rightleftharpoons$ n-mer as postulated in aqueous micelles or whether a multiple equilibrium model applies, where a stepwise formation of aggregates is assumed in an indefinite association process such that monomer $\rightleftharpoons$ dimer $\rightleftharpoons$ trimer $\rightleftharpoons$ ... n-mer[4].

If a water soluble dye is added to the solution, it would be solubilised in the hydrophilic core of the aggregates[2] and its uptake into solution can be monitored by measuring the absorbance at the wavelength of maximum absorption in water, λ_{max}, using a UV/VIS spectrophometer. This, though, introduces the possibility of the dye acting as a core surface site on which the polymer/surfactant molecules can adsorb.

4.3.2. Experimental details

Rhodamine B, a water soluble dye was used to study the aggregation of the polymer/surfactant in solution. Experiments were first carried out to study if the aggregation was induced by the dye itself. In order to do this, the dye concentration in the solution of the polymer was gradually increased whilst keeping the polymer concentration constant. In order to study the aggregation of the polymer/surfactant, a fixed concentration of the dye was dispersed in a solution of the polymer/surfactant by sonication using an *Ultrawave* sonic bath for 2 min and then tumbled overnight to achieve equilibrium. The sample was then centrifuged to remove any undissolved dye and the supernatant was studied by using a UV/VIS Spectrophotometer.

4.3.3. Results

4.3.3.1. Absorption at λ_{max} as a function of dye concentration

In order to test if the dye induced aggregation, experiments were carried out with increasing dye concentrations and the absorbance of the dye in solution at λ_{max} was measured using a UV/VIS spectrophotometer. The result is shown in figure 4.10.

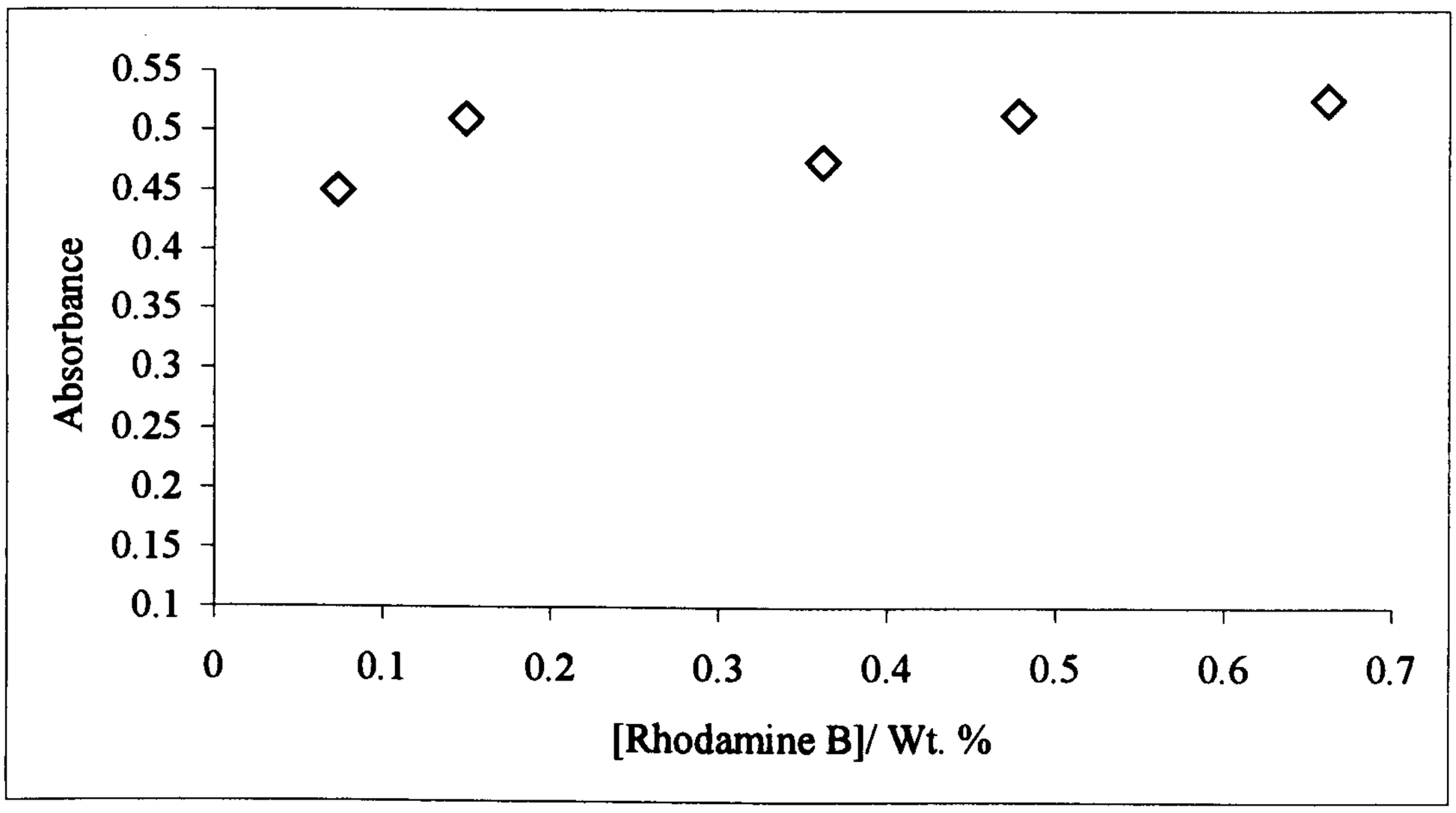

Figure 4.10: Absorbance at 551 nm of the dissolved dye versus the amount initially added at a fixed P1 concentration of 0.1 wt. %

4.3.3.2. Absorption at λ_{max} as a function of P1 concentration

The effect of gradually increasing P1 concentration at a fixed concentration of 0.25 wt % Rhodamine B on the absorbance of the solution is shown in figure 4.11.

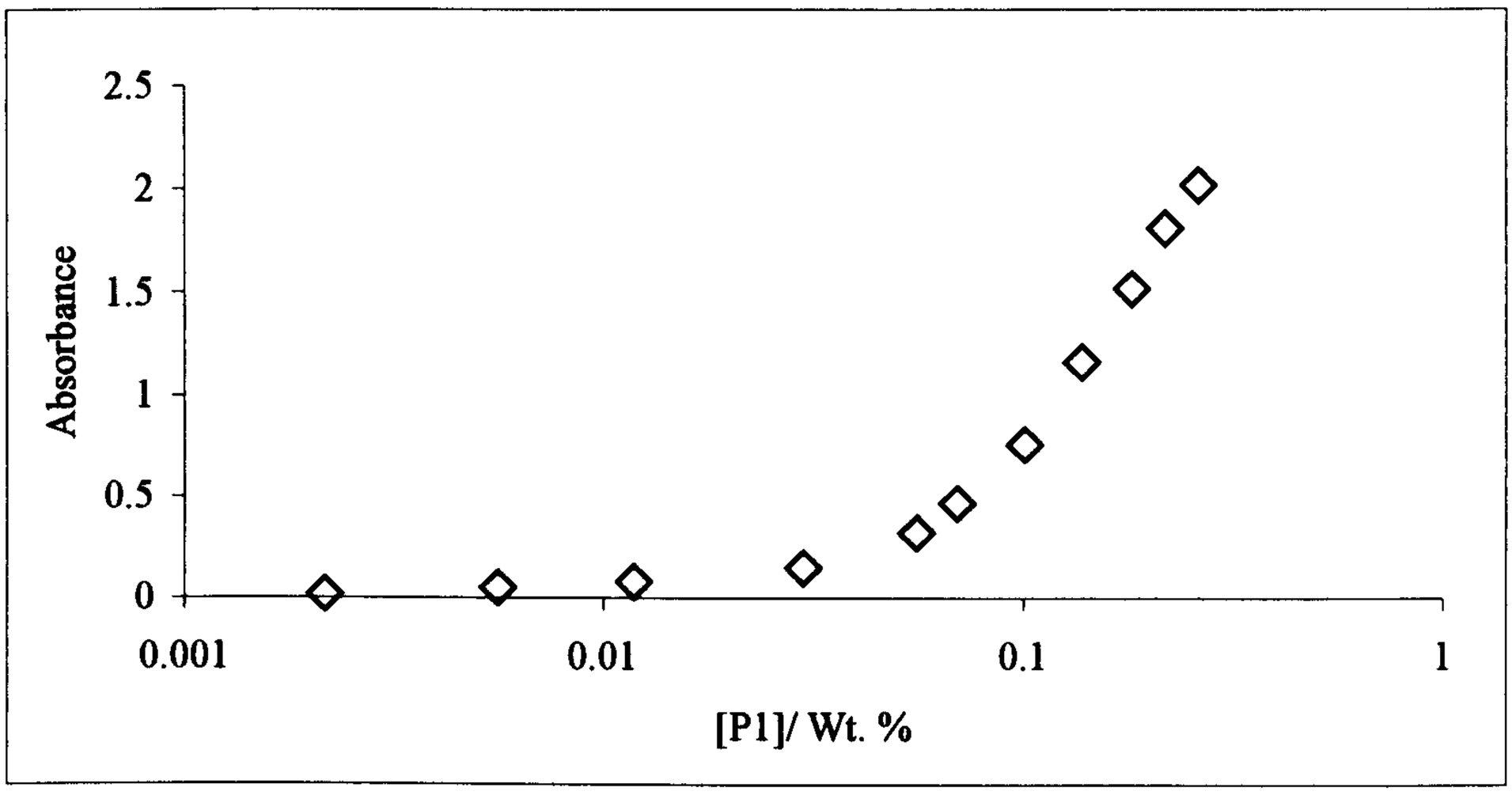

Figure 4.11: Absorbance at 553 nm of the dissolved dye as a function of P1 concentration

4.3.3.3. Absorption at λ_{max} as a function of P1 concentration in the presence of a fixed amount of S1 or S3 or S4

The effect of either S1, S3, or S4 on the absorbance of the dissolved dye at gradually increasing P1 concentrations is shown in figure 4.12.

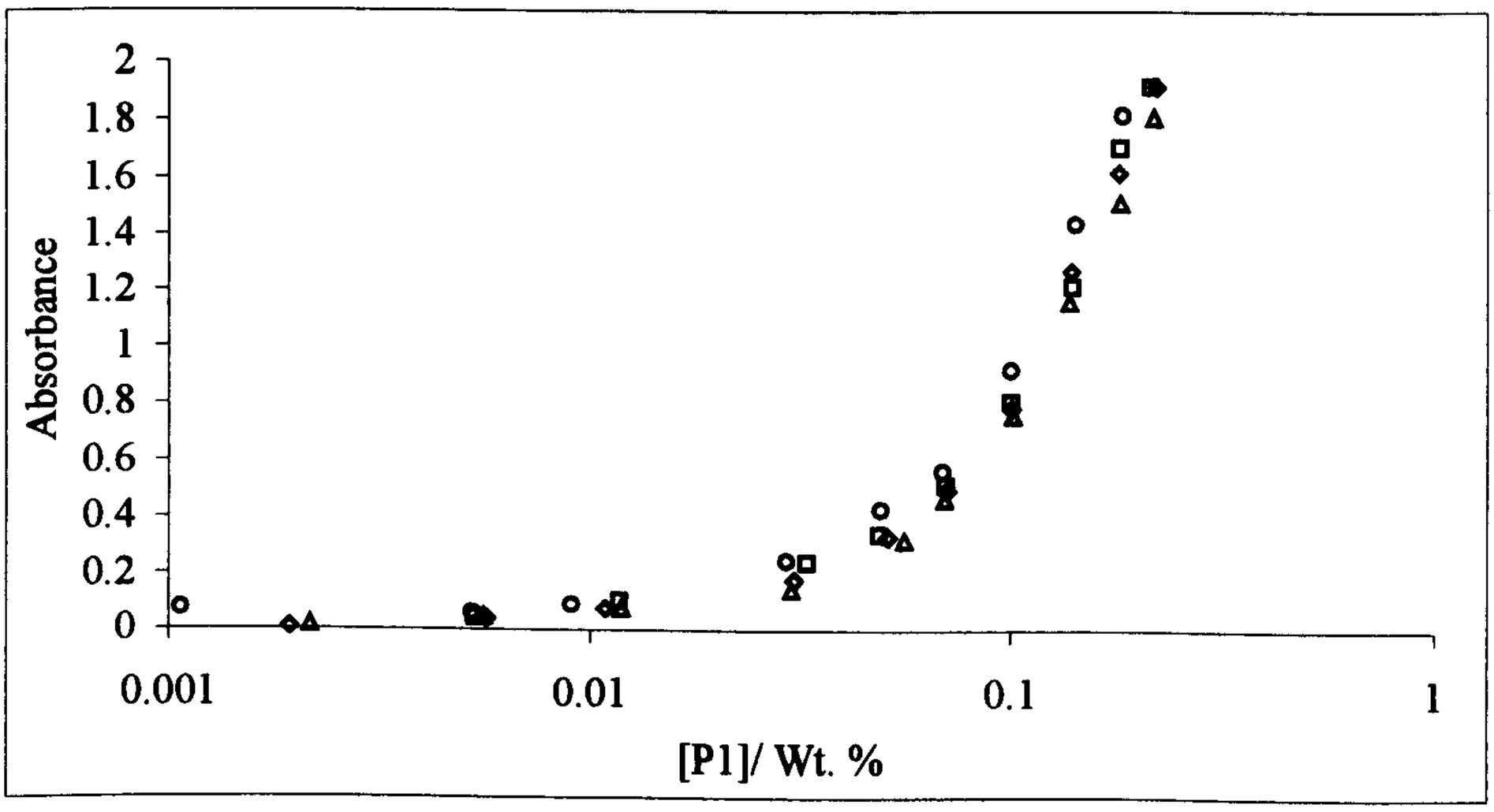

Figure 4.12: Absorbance at 553 nm of the dissolved dye as a function of P1 concentration (Δ) and in the presence of 0.1 wt. % S1 (◊) or S3 (O) or S4 (□)

4.4. Analysis and Discussion

The results of the aggregation studies carried out using vapour pressure osmometry indicate very little aggregation of the polymer or surfactant in solution as indicated in table 4.1. The extremely small slopes of the plots (figures 4.3 to 4.8) also indicate that the polymer/surfactant is in a thermodynamically poor solvent[13]. However, aggregation studies carried out by following the solubilisation of Rhodamine B, a water soluble dye, in isooctane with increasing polymer concentration indicate that there is aggregation taking place in solution. The "flat" nature of the plot in figure 4.10 shows that aggregation is independent of the dye concentration. Thus, the increase in absorbance as seen in figure 4.11 with increasing P1 concentration must correspond to an increased uptake of the dye by the aggregating polymer molecules. The surfactants with the less polar headgroups could not effectively solubilise Rhodamine B in isooctane to enable a systematic study. Their effect on the aggregation of P1 is also minimal as shown in figure 4.12 though S3, with the amine headgroup, seems to have a slightly stronger influence. However, one needs to be cautious in interpreting the results as the dye itself could be acting as a surface site facilitating adsorption and the solubilisation of the polymer molecules in the solvent. The anomaly in the results obtained from osmometry and dye study could be due to the difference in sensitivity of the techniques used. Previous VPO studies carried out with higher molecular weight polymers of the same kind as studied here have showed the presence of aggregates in solution[10]. Therefore, the possible aggregation suggested by the dye study indicates the co-existence of aggregates at the interface (as already shown in chapter 3) and in solution as schematically represented in figure 4.13.

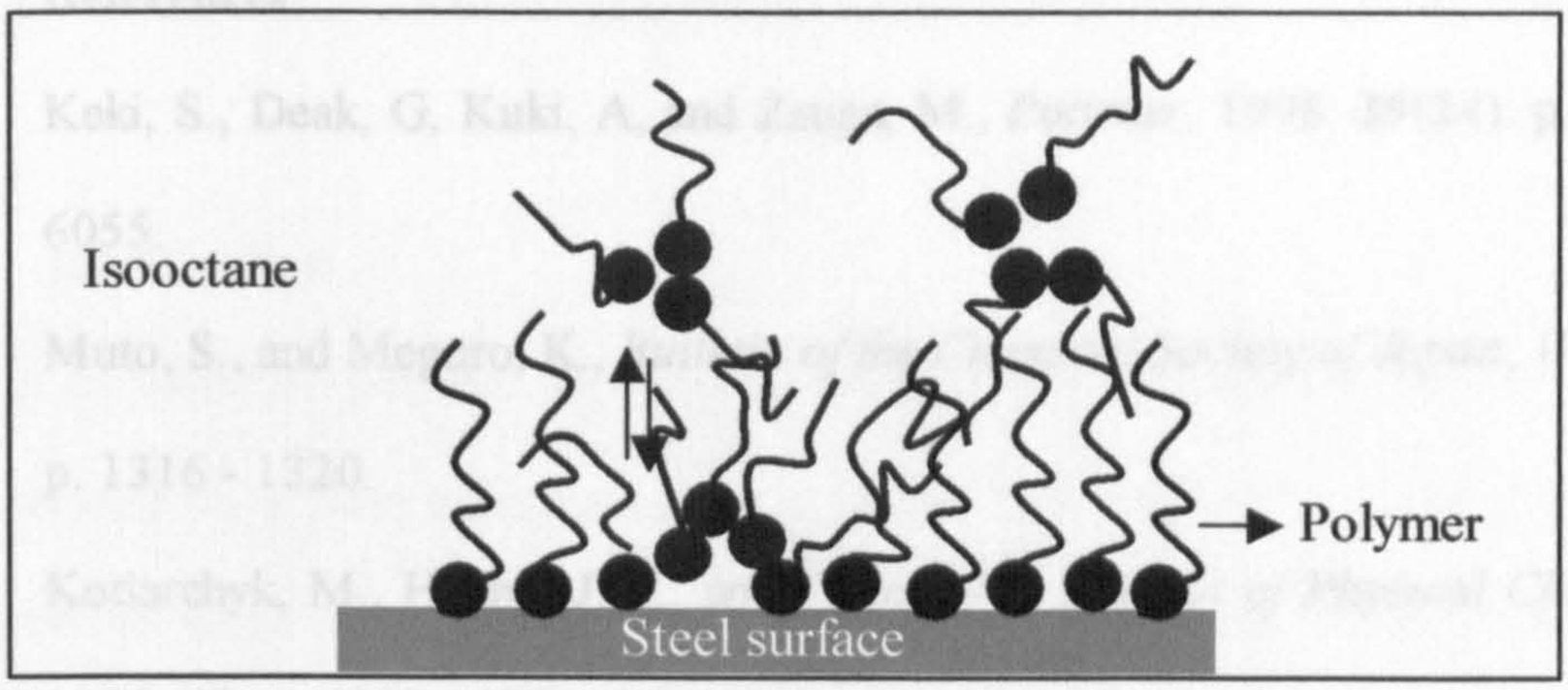

Figure 4.13: Schematic representation of the existence of polymer aggregates at the interface and in solution

4.5. References

1. Keki, S., Deak, G, Kuki, A, and Zsuga, M., *Polymer*, 1998. **39**(24): p. 6053 - 6055.
2. Muto, S., and Meguro, K., *Bulletin of the Chemical Society of Japan*, 1973. **46**: p. 1316 - 1320.
3. Kotlarchyk, M., Huang, J. S., and Chen, S-H, *Journal of Physical Chemistry*, 1985. **89**: p. 4382 - 4386.
4. Jean, Y-c., and Ache, H. J, *Journal of the American Chemical Society*, 1978. **100**: p. 6320 - 6327.
5. Hasegawa, M., Sugimura, T., Shindo, Y., and Kitahara. A., *Colloids and Surfaces A: Physicochemical and Engineering Aspects*, 1996. **109**: p. 305 - 318.
6. Krishnakumar, S., and Somasundaran, P., *Journal of Colloid and Interface Science*, 1994. **162**(2): p. 425 - 430.
7. Peri, J.B., *Journal of Colloid and Interface Science*, 1969. **29**: p. 6.
8. Mogford, R., *PhD Thesis*. To be submitted, University of Bristol.
9. Billingham, N.C., *Molar Mass Measurements in Polymer Science*. 1977, London: Kogan Page Limited.
10. Cox, A.R., Mogford, R., Vincent, B and Harley, S., *Colloids and Surfaces A: Physicochemical and Engineering Aspects*, 2001. **181**: p. 205-213.
11. Pacynko, W.F., Yarwood, J., and Tiddy, G. J. T., *Journal of Chemical Society; Faraday Transactions 1*, 1989. **85**(6): p. 1397 - 1408.
12. Saris, P., Rosenholm, J. B., Sjoeblom, E., and Henriksson, U., *Journal of Physical Chemistry*, 1986. **90**(4): p. 660 - 665.
13. Billingham, N., *Email correspondence on VPO results*. 2000: Bristol.

CHAPTER 5: ATOMIC FORCE MICROSCOPY STUDIES

5.1. Introduction

A layer of adsorbed polymer on colloidal particles provides a steric hindrance which helps to stop them from aggregating. To achieve this, the layer should be of sufficient thickness in order to overcome the attractive van der Waals forces between the particles. Repulsion between colloidal particles can also be achieved by introducing charges on the surfaces. This provides a long range repulsive Coulombic interaction between the electrical double layers at low ionic strengths[1]. However, in this study, the surfaces used bear little or no charge in non-polar media. The polymer and surfactants used are also neutral. An earlier study carried out on the interactions of carbon surfaces covered with a polyisobutenesuccinimide dispersant confirmed that the stabilisation effect of the polymer is essentially steric in nature[2]. The thicknesses of adsorbed layers of the polymer and the surfactants were studied in the present work using a modified atomic force microscope, which will be described in detail in the following sections.

5.2. Equipment and Theory

Atomic force microscopes[3] evolved from scanning tunnelling microscopes[4] and have been playing a vital role in the direct measurement of surface forces for a number of years[5-7]. A modified atomic force microscope[8] constructed in Professor Luckham's group at Imperial College, London was used to measure the force-distance profiles of the detergent and surfactant molecules adsorbed on stainless steel and carbon surfaces. The technique uses a probe attached to the tip of the cantilever instead of a normal AFM cantilever[2, 9]. A diagrammatic representation of the AFM equipment is as shown in figure 5.1:

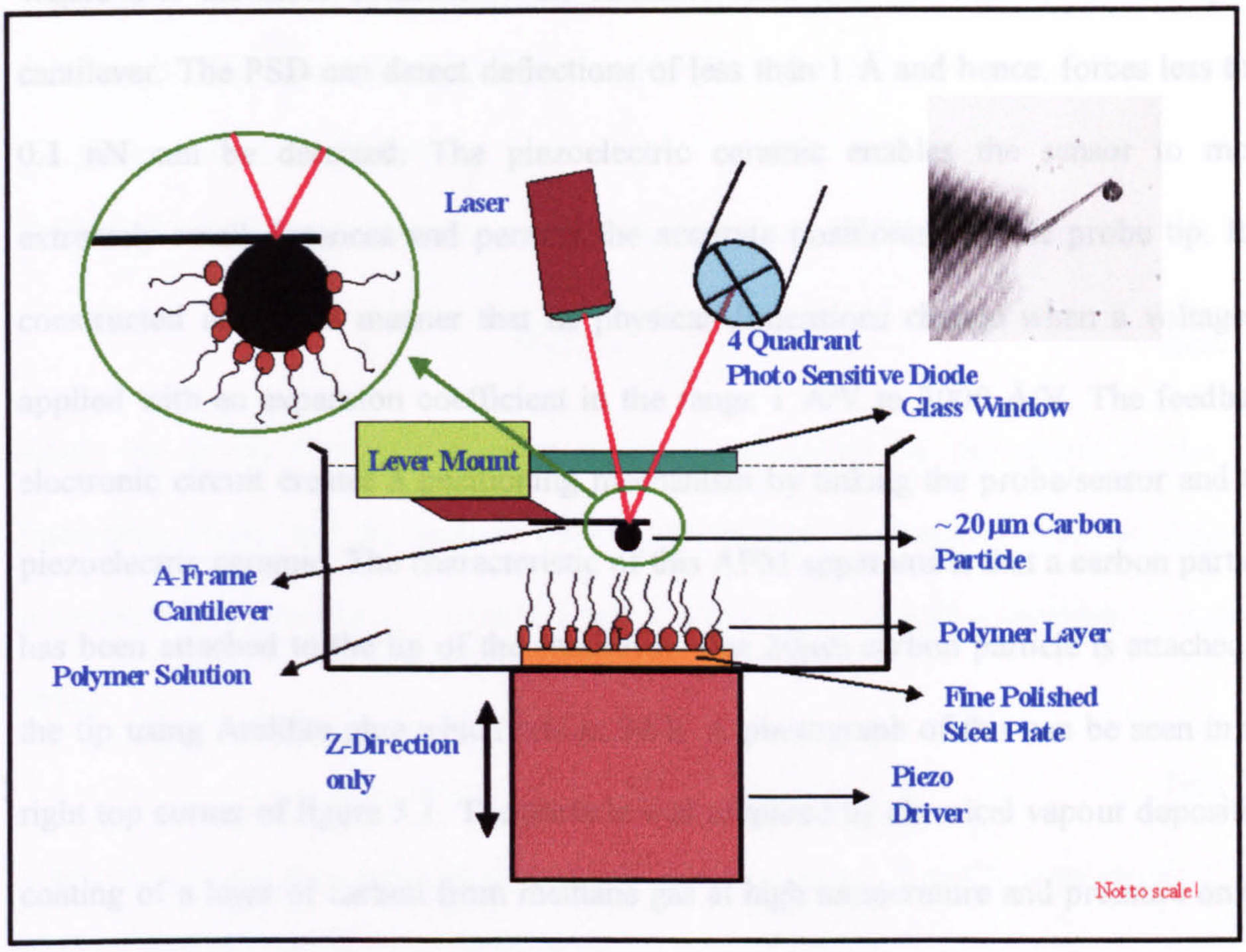

Figure 5.1: Schematic diagram of the AFM apparatus

The apparatus consists of a high resolution sensing probe, piezo electric ceramics, a feedback electronic circuit, and a computer for generating and presenting graphs. The colloidal probe and the stainless steel plate are both immersed in the solvent or polymer solution and the force is measured by following the deflection of a laser beam reflected from the tip of the probe. A glass window placed at the liquid air interface provides a stable interface through which the laser beam can transmit as can be seen in figure 5.1. The force sensor in the AFM measures the deflection of the cantilever through the help of a small laser beam which is reflected off the tip of the cantilever. The reflected beam moves across the face of a four-quadrant photo sensitive diode (PSD) which enables the calculation of the deviation of the cantilever by measuring the difference in light intensity at the sectors. The force, F, required to generate the deflection can be calculated using Hooke's law as follows:

$$F = -kx \qquad \text{Eqn. 5.1}$$

Where k is the force constant of the cantilever and x is the distance moved by the cantilever. The PSD can detect deflections of less than 1 Å and hence, forces less than 0.1 nN can be detected. The piezoelectric ceramic enables the sensor to move extremely small distances and permits the accurate positioning of the probe tip. It is constructed in such a manner that its physical dimensions change when a voltage is applied with an expansion coefficient in the range 1 Å/V to 3000 Å/V. The feedback electronic circuit creates a positioning mechanism by linking the probe/sensor and the piezoelectric ceramic. The characteristic of this AFM apparatus is that a carbon particle has been attached to the tip of the cantilever. The 20μm carbon particle is attached to the tip using Araldite glue which sets in 24 h. A photograph of this can be seen in the right top corner of figure 5.1. The particle was prepared by chemical vapour deposition coating of a layer of carbon from methane gas at high temperature and pressure on the surface of a glass bead. A fine polished steel plate is placed at the bottom of the watch glass containing the solvent or the polymer solution.

As already mentioned in section 5.1, van der Waals attractive forces act between all bodies. The AFM apparatus allows the measurement of this interaction and the contribution of an adsorbed layer on the net force of interaction. The total force of interaction is dependent on the area of interaction. Various equations have been derived for different bodies interacting such as two spheres, a sphere and a plate, a sphere and a cylinder, etc.[1]. However, the standard presentation of force-distance data is based on the Derjaguin approximation[10] which is applicable to a variety of interaction geometries by making use of the approximation that, at very close separation, any two macroscopic bodies, behave as two parallel plates.

For a sphere-plate interaction,

$$F(D)_{sphere-plate} = 2\pi RW(D)_{plate-plate} \qquad \text{Eqn. 5.2}$$

where F(D) is the force between a spherical surface and a flat surface separated by a distance D, R is the radius of curvature and W(D) is the interaction energy between two flat plates of the same material.

The van der Waals contribution to the interaction energy W(D) is given by eqn. 5.3:

$$W(D) = \frac{-A_H}{12\pi D^2} \qquad \text{Eqn. 5.3}$$

where A_H is the Hamaker constant which is dependent on the nature of the two interacting bodies and the medium between them. The net Hamaker constant, A_{132}, for a system which involves two bodies 1 and 2, interacting through a medium, 3, is given by[1]:

$$A_{132} = (A_1^{1/2} - A_3^{1/2}) * (A_2^{1/2} - A_3^{1/2}) \qquad \text{Eqn. 5.4}$$

where A_1, A_2 and A_3 are the Hamaker constants of media 1, 2 and 3, respectively.

Substituting eqn. 5.2 in eqn. 5.3 leads to

$$F(D) = \frac{-A_H R}{6D^2} \qquad \text{Eqn. 5.5}$$

The dependence of the force on the value and sign of the Hamaker constant in eqn. 5.4 can be shown by assuming three different values for the interaction between a particle of 20μm against a plate as shown in figure 5.2.

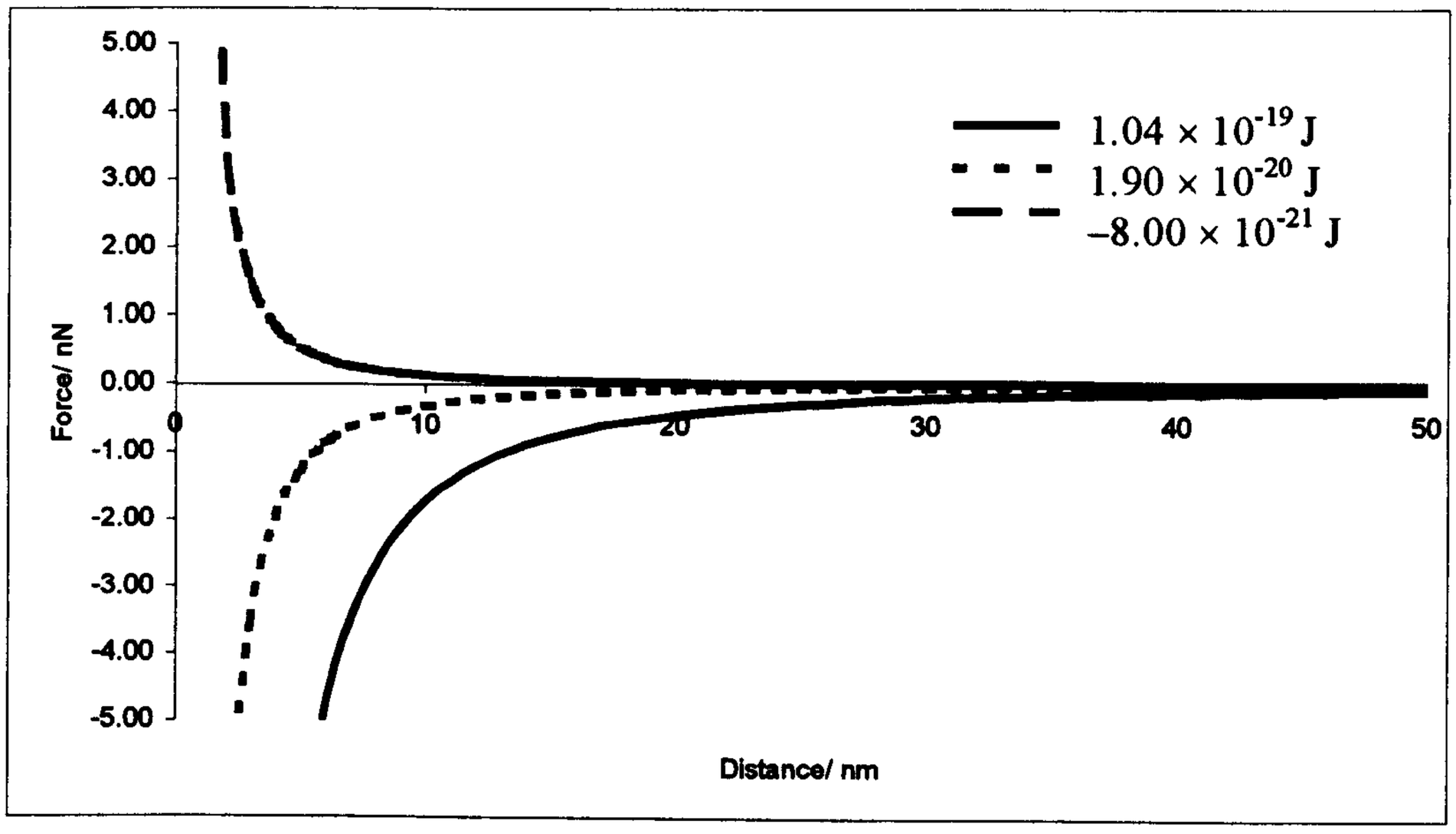

Figure 5.2: Force distance profiles of a 20 μm particle interacting with a plate at Hamaker constant values 1.04 × 10^{-19} J, 1.90 × 10^{-20} J and –8.00 × 10^{-21} J[11]. The plots corresponding to the different Hamaker constants have been indicated on the graph.

5.3. Experimental details

A 20 μm carbon bead was attached to a tipless A-frame cantilever using Araldite. This was done under an optical microscope with a camera attached to view the cantilever and the particle on a monitor. A small amount of Araldite was placed on a glass plate and spread with a pin so that a thin strip of glue was obtained on the glass plate. The cantilever was then held face down on a micrometer with both vertical and horizontal motion levers. The camera was focussed to obtain a clear picture of the cantilever on the screen. The cantilever was then slowly taken down towards the glue on the glass plate until it touched the glue. This way, the glue was placed on the cantilever. After this, the glass slide was replaced with another one with carbon particles scattered on it. The cantilever was placed right on top of a carbon particle and slowly taken down until it touched the particle and the carbon stuck to the cantilever. It was then allowed to dry for 24 h.

The cantilever was placed on the cantilever mount of the AFM. A fine polished steel plate was then stuck to the bottom of a watch glass using a piece of double-sided tape to hold the plate stable. As the tape was completely shielded by the steel plate, the solvent could not reach and dissolve the glue on it. Isooctane was then poured into the watch glass such that it immersed the bottom half of the glass window attached on the cantilever mount as shown in figure 5.1. The system was now ready for measurement. A baseline measurement was carried out first in order to measure the force distance profile of the interaction of the carbon particle with the steel plate. After this baseline experiment, the solvent was changed to a polymer solution for obtaining the force-distance interaction in the presence of adsorbed polymers on the surfaces. The cantilever was changed for every new polymer solution used.

5.4. Results

5.4.1. Force distance plot of carbon bead – steel plate interaction in pure isooctane and in the presence of adsorbed polymer layers

The profile of the interaction between a bare carbon bead and a bare stainless steel plate in pure isooctane was taken as the baseline measurement. The plot so obtained can be seen in figure 5.3.

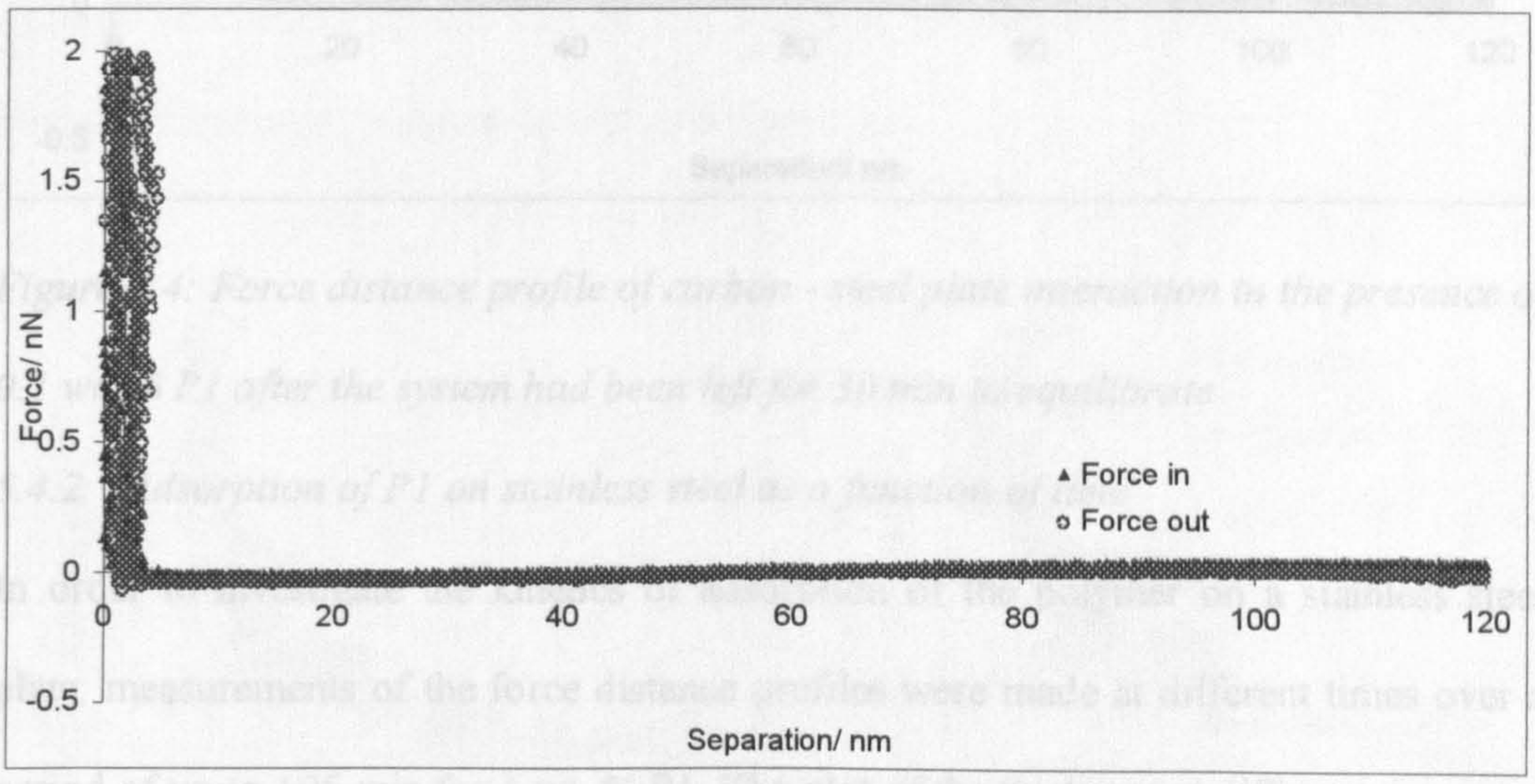

Figure 5.3: Force distance profile of bare carbon - bare steel plate interaction

This profile changes in the presence of the polymer in solution as can be seen in figure 5.4.

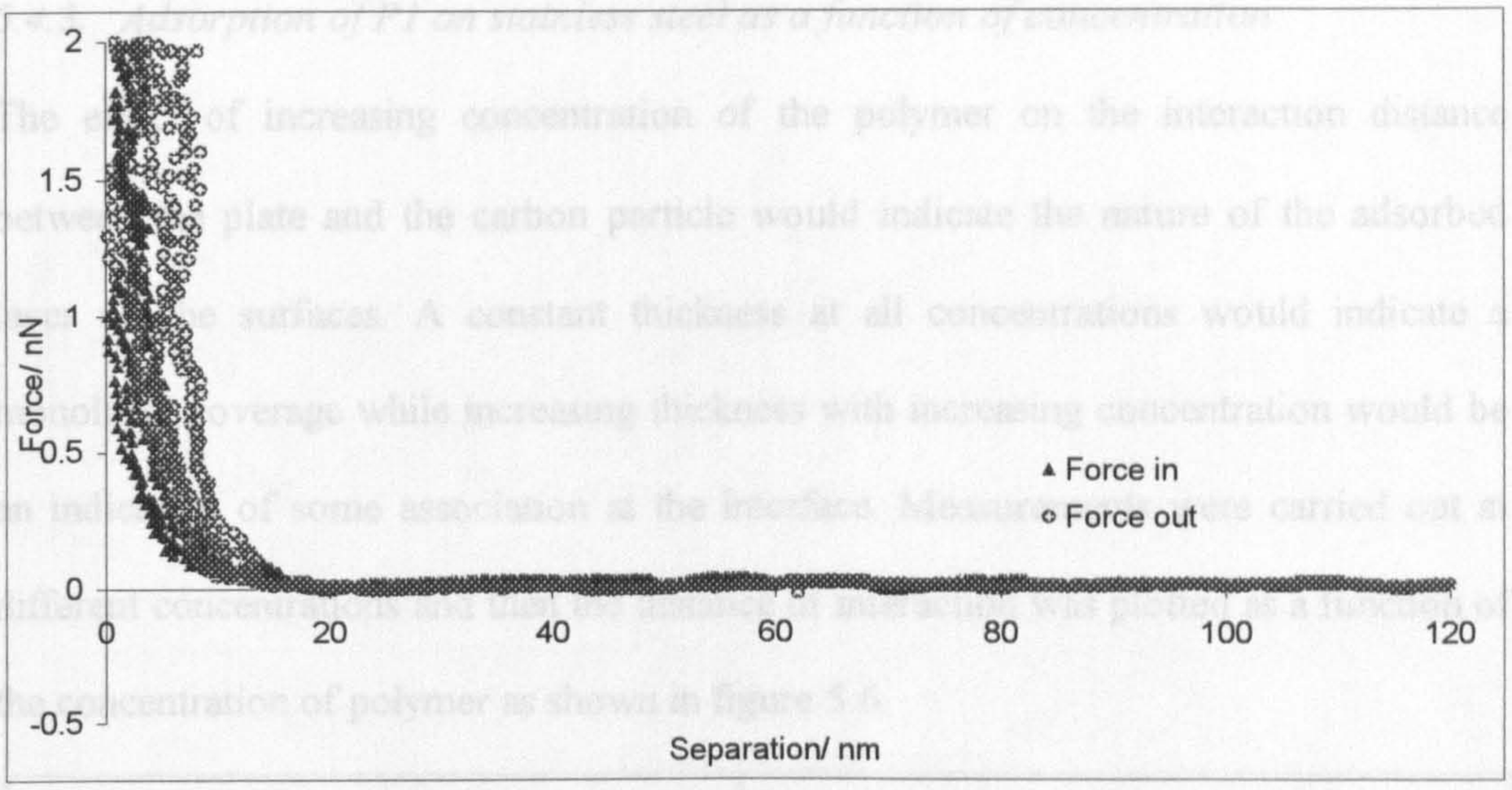

Figure 5.4: Force distance profile of carbon - steel plate interaction in the presence of 0.1 wt. % P1 after the system had been left for 30 min to equilibrate

5.4.2. Adsorption of P1 on stainless steel as a function of time

In order to investigate the kinetics of adsorption of the polymer on a stainless steel plate, measurements of the force distance profiles were made at different times over a period of up to 105 min for 1 wt. % P1. The plot of the thickness at different times can be seen in figure 5.5.

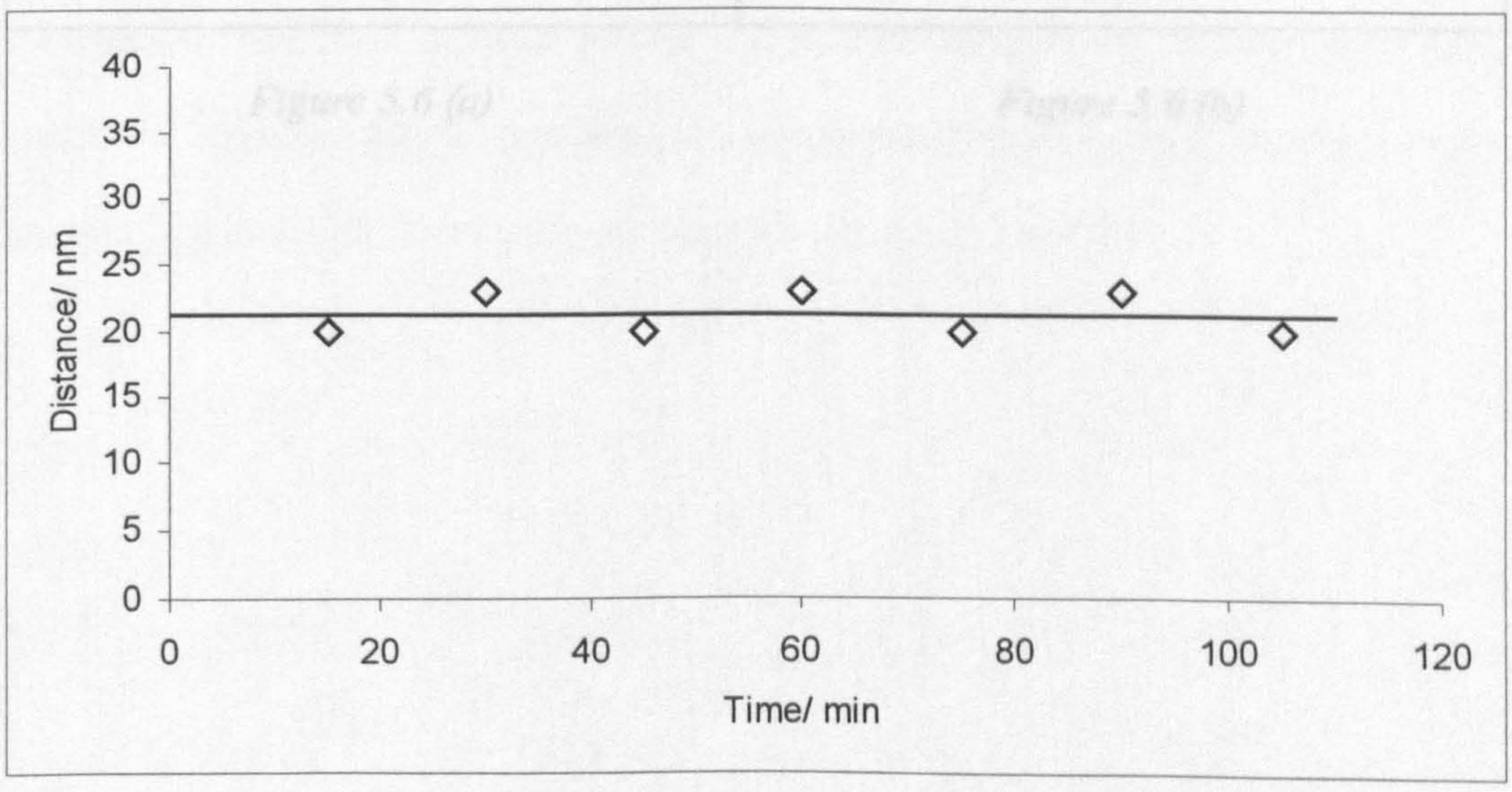

Figure 5.5: Thickness plot at different times for 0.25 wt. % P1 solution in isooctane on stainless steel plate

5.4.3. Adsorption of P1 on stainless steel as a function of concentration

The effect of increasing concentration of the polymer on the interaction distance between the plate and the carbon particle would indicate the nature of the adsorbed layer on the surfaces. A constant thickness at all concentrations would indicate a monolayer coverage while increasing thickness with increasing concentration would be an indication of some association at the interface. Measurements were carried out at different concentrations and then the distance of interaction was plotted as a function of the concentration of polymer as shown in figure 5.6.

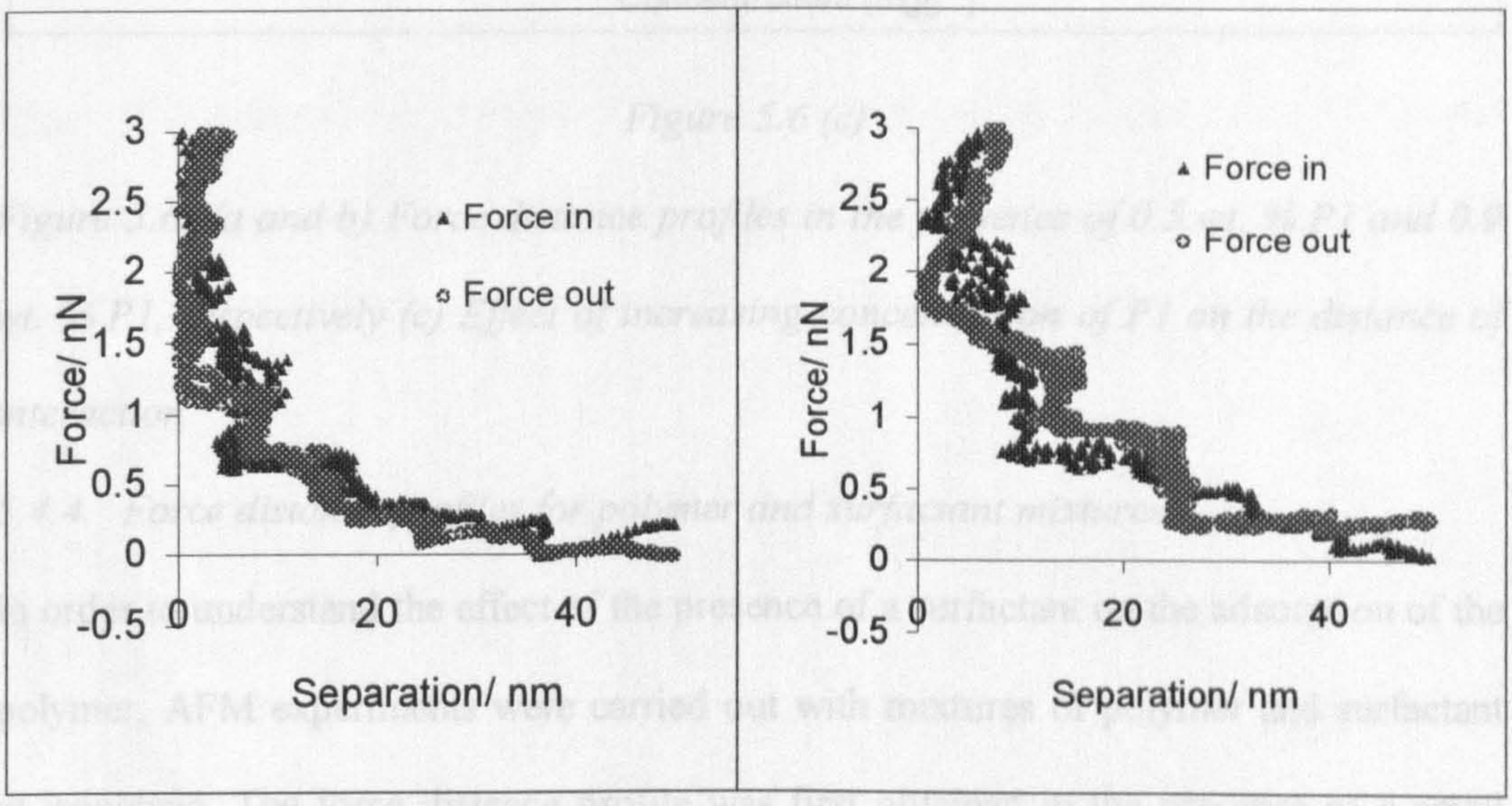

Figure 5.6 (a) *Figure 5.6 (b)*

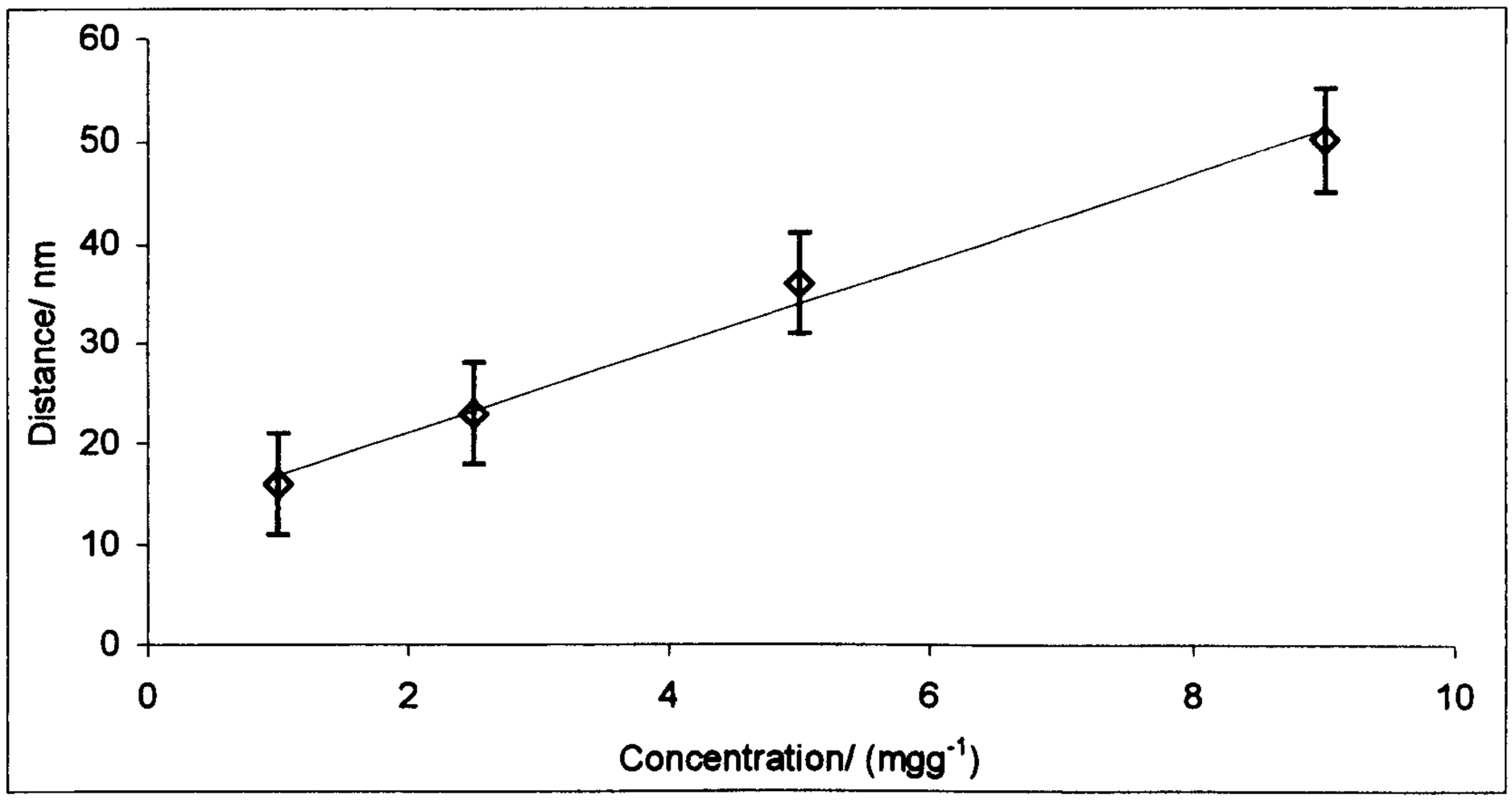

Figure 5.6 (c)

Figure 5.6: (a and b) Force distance profiles in the presence of 0.5 wt. % P1 and 0.9 wt. % P1, respectively (c) Effect of increasing concentration of P1 on the distance of interaction

5.4.4. Force distance profiles for polymer and surfactant mixtures

In order to understand the effect of the presence of a surfactant on the adsorption of the polymer, AFM experiments were carried out with mixtures of polymer and surfactant in isooctane. The force distance profile was first obtained in the presence of a small amount of surfactant S2. S2 concentration was then increased to study its effect on the distance of interaction. The results are shown in figures 5.7 and 5.8.

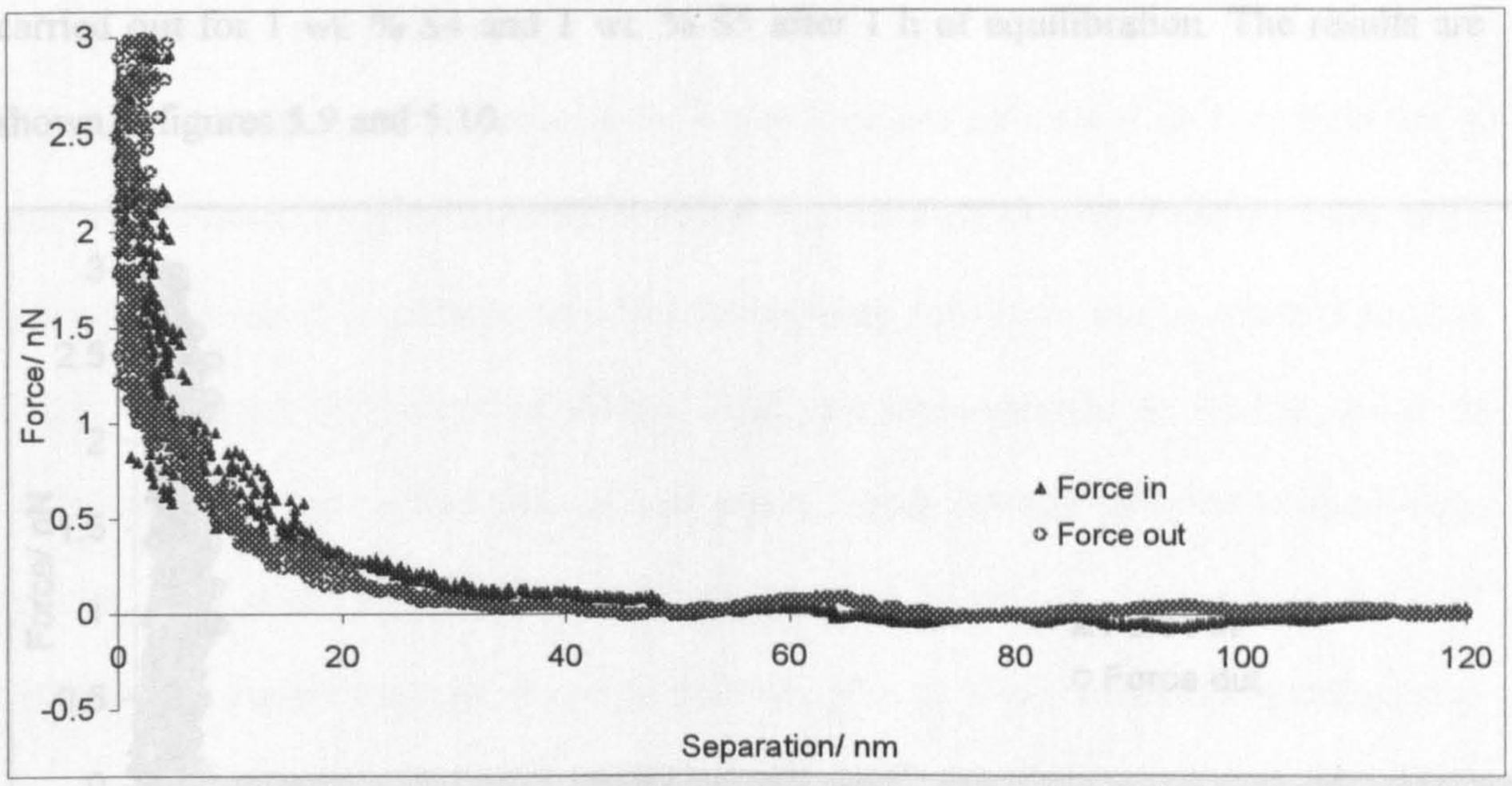

Figure 5.7: Force distance profile for a mixture of 0.8 wt. % P1 and 1.0 wt. % S2 after 1 h of equilibration

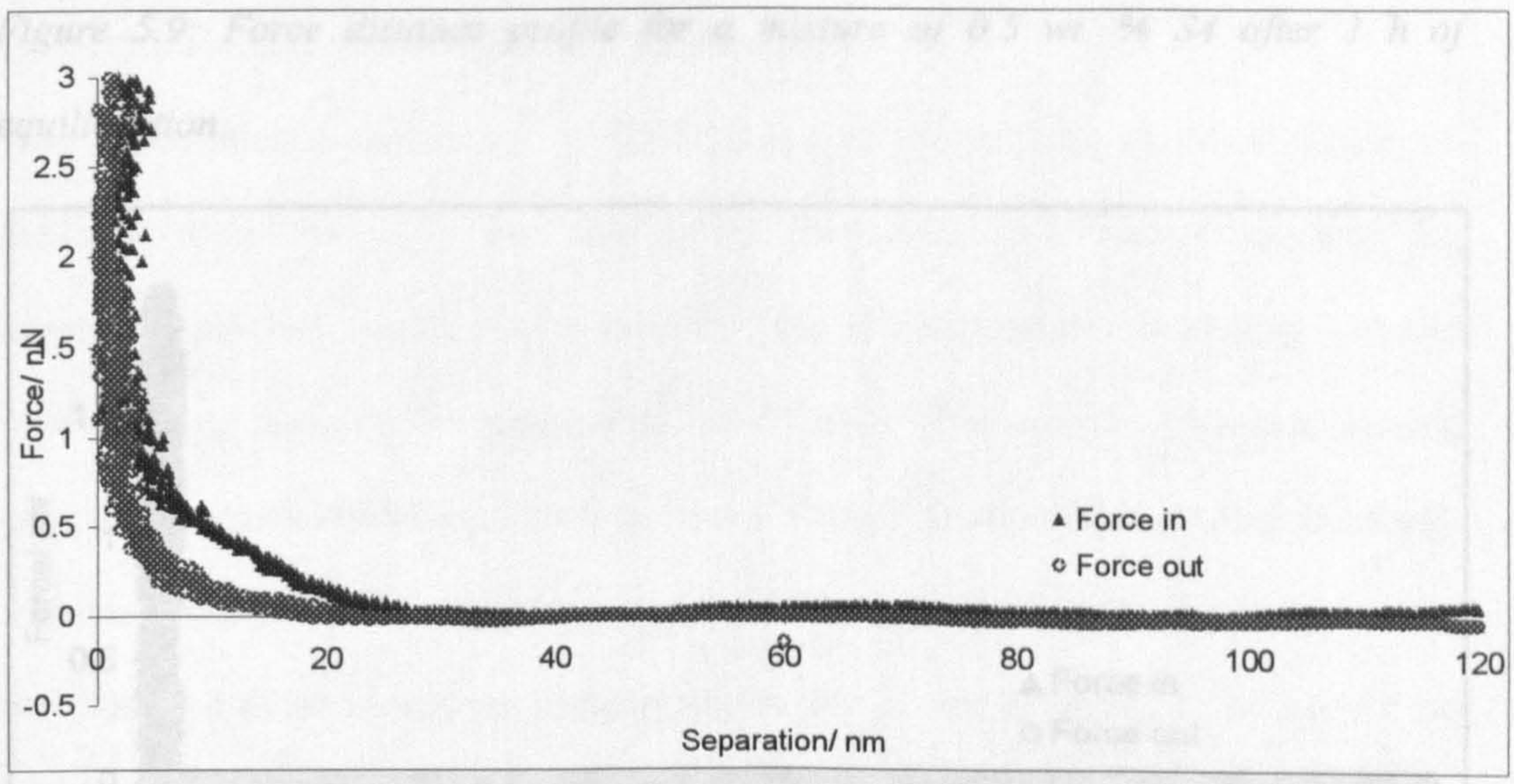

Figure 5.8: Force distance profile for a mixture of 0.6 wt. % P1 and 1.8 wt. % S2 after 1 h of equilibration

5.4.5. Force distance profiles of the adsorption of surfactants S4 and S5

Surfactants S4 and S5 have similar structures except that S5 has twice the number of propoxylate units as compared to S4. If they were to adsorb normal to an interface, S5 would give about twice the thickness of S4. In order to test this, measurements were

carried out for 1 wt. % S4 and 1 wt. % S5 after 1 h of equilibration. The results are shown in figures 5.9 and 5.10.

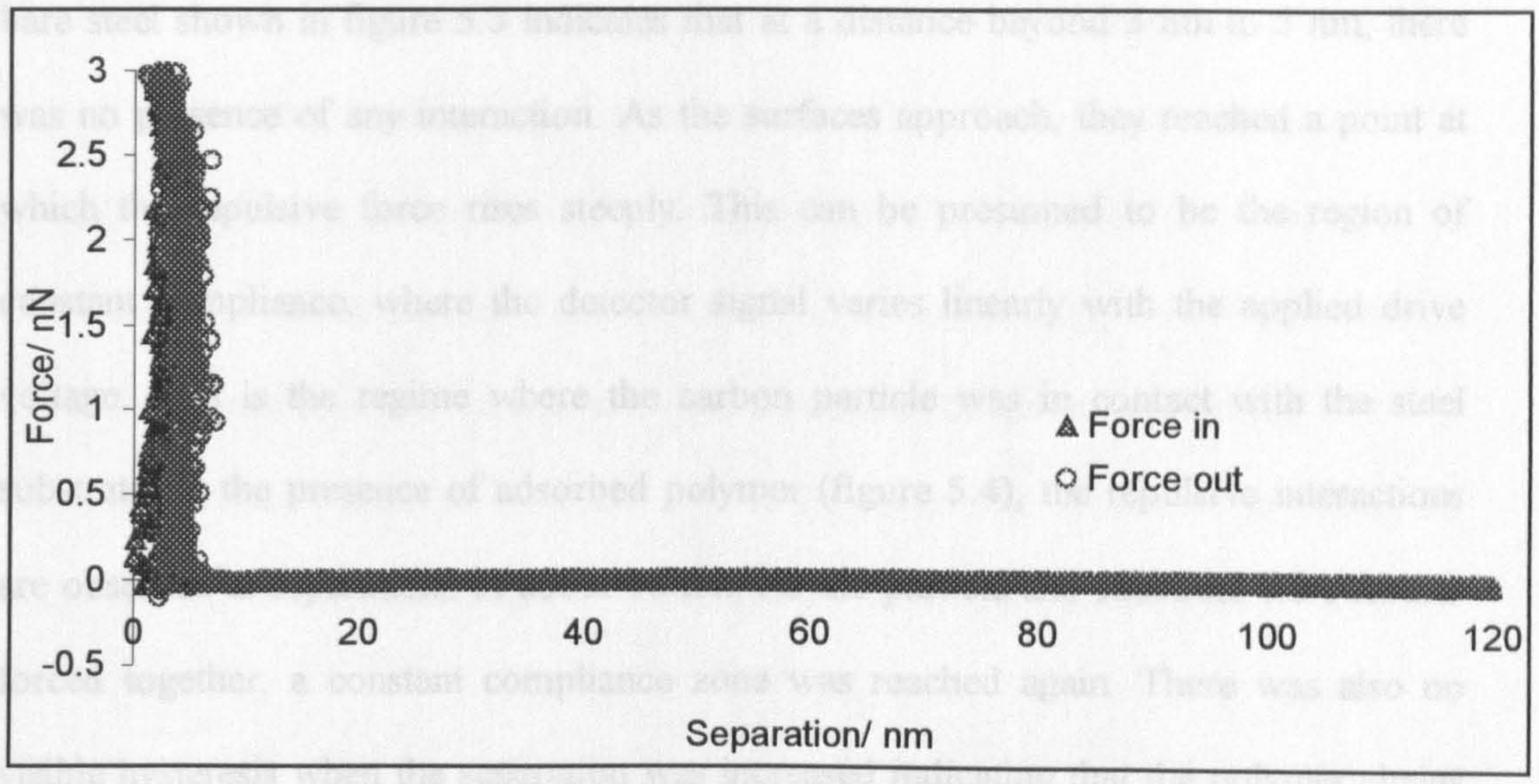

Figure 5.9: Force distance profile for a mixture of 0.5 wt. % S4 after 1 h of equilibration

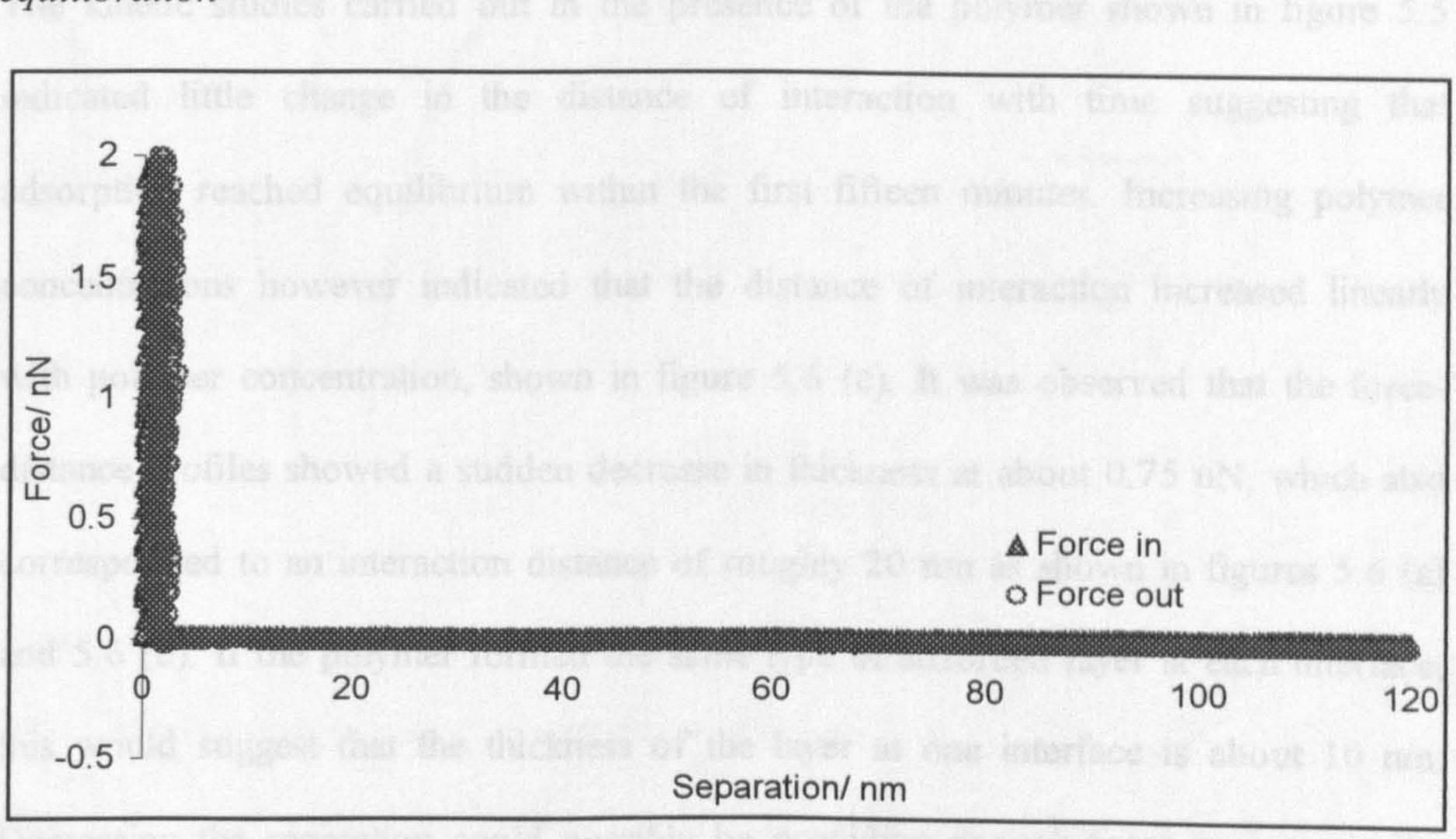

Figure 5.10: Force distance profile for a mixture of 0.5 wt. % S5 after 1 h of equilibration

5.5. Analysis and Discussion

The force-distance profile obtained for the interaction between a bare particle and a bare steel shown in figure 5.3 indicates that at a distance beyond 3 nm to 5 nm, there was no presence of any interaction. As the surfaces approach, they reached a point at which the repulsive force rises steeply. This can be presumed to be the region of constant compliance, where the detector signal varies linearly with the applied drive voltage. This is the regime where the carbon particle was in contact with the steel substrate. In the presence of adsorbed polymer (figure 5.4), the repulsive interactions are observed at separations of about 18 nm. As the particle and substrate were further forced together, a constant compliance zone was reached again. There was also no visible hysteresis when the separation was increased indicating that the polymer chains on the surfaces did not entangle with one another.

The kinetic studies carried out in the presence of the polymer shown in figure 5.5 indicated little change in the distance of interaction with time suggesting that adsorption reached equilibrium within the first fifteen minutes. Increasing polymer concentrations however indicated that the distance of interaction increased linearly with polymer concentration, shown in figure 5.6 (c). It was observed that the force-distance profiles showed a sudden decrease in thickness at about 0.75 nN, which also corresponded to an interaction distance of roughly 20 nm as shown in figures 5.6 (a) and 5.6 (b). If the polymer formed the same type of adsorbed layer at each interface, this would suggest that the thickness of the layer at one interface is about 10 nm. Decreasing the separation could possibly be providing enough force to squeeze the polymer layers between the steel substrate and the carbon probe surfaces thus giving the 'apparent' jump until it reached the constant compliance regime.

The polymer, usually added in gasoline formulations, was believed to form a protective coating on the valve surfaces and also disperse the carbonaceous particles formed

during combustion. For the polymer molecules to effectively disperse the particles, they should form a layer thick enough to provide steric hindrance and overcome the attractive van der Waals forces acting between the particles. The values of Hamaker constants for carbon (quartz), steel and an alkane of 8 carbons are around 6.50×10^{-20} J, 40.0×10^{-20} J and 4.50×10^{-20} J, respectively[12]. These values were used to calculate the Hamaker constants corresponding to the interactions between carbon and carbon, steel and steel and carbon and steel through an alkane medium using eqn. 5.4. The force distance profiles obtained for the interaction of a particle of radius 10 microns with a substrate obtained by using eqn. 5.5 are shown in figure 5.11:

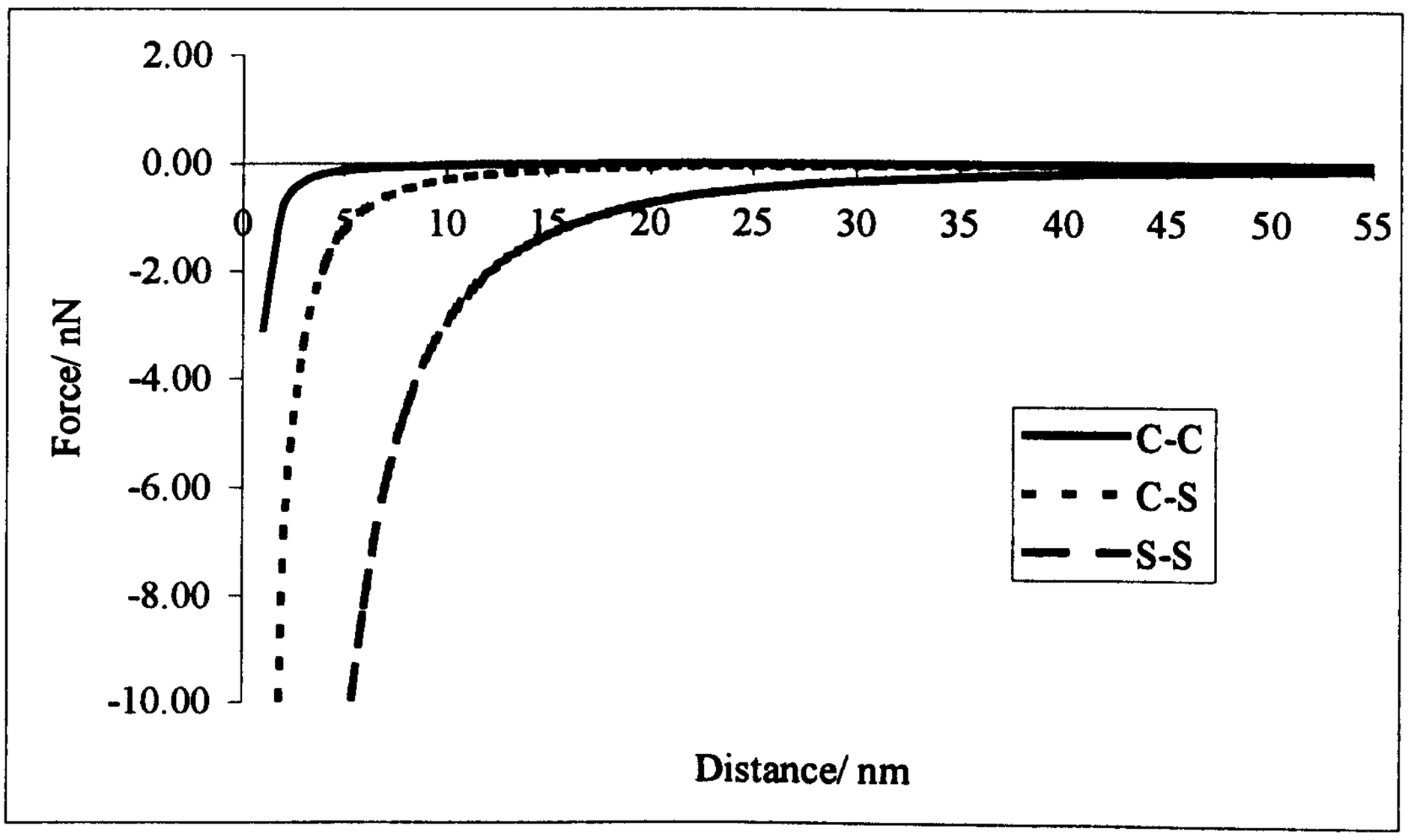

Figure 5.11: Theoretical force distance profiles for carbon – carbon, carbon-steel and steel – steel interactions through an alkane medium

The theoretical profile for carbon particle and steel interaction through an alkane medium showed that the minimum thickness required in order to overcome the van der Waals force was about 20 nm. Corresponding to a layer of at least 10 nm thick on each interface. From the experiments carried out using an atomic force microscope, it was shown that the polymer might provide a layer just thick enough to achieve this.

The thickness of the adsorbed layer of the polymer decreased in the presence of surfactant S2 (figures 5.7 and 5.8) suggesting some interaction between the surfactant and the polymer at the interface. However, it was unlikely for the surfactant with the poly(propylene oxide) chain to completely displace the polymer with the strongly hydrophilic amine and phenolic headgroups. The surfactant could be interacting with weakly bound polymer molecules at the interfaces and then these aggregates could themselves be solubilising in the solvent. The S2 molecules could also be displacing some of the polymer molecules on approaching the constant compliance regime. Interestingly, this was the only experiment where hysteresis was observed on separation. Poly(ethylene oxide) polymers have been shown to form bridges between glass substrates and glass probes in water in a similar experimental set-up[13]. This could be an explanation for the observed hysteresis where the propoxylate chain formed a bridge between the stainless steel plate and the carbon particle during full compression.

Surfactants S4 and S5 have the same structural units but S5 has twice the number of propoxylate units as compared to S4. Thus, if these molecules were to attach standing on the surfaces, S5 would give twice the thickness as that of S4. However, the force distance profiles for surfactants S4 and S5 were very similar and not very different from that of the bare substrate–bare probe interaction as shown in figures 5.9 and 5.10. This could only mean that the molecules, if they did adsorb, were lying in a flat configuration with the propoxylate units acting as the anchor points. Ellipsometry experiments also showed small thickness values for all the surfactants suggesting that this hypothesis is correct (chapter 6 of this thesis).

5.6. References

1. Hunter, R.J., *Foundations of Colloid Science*. Vol. I. 1985: Clarendon Press, Oxford.
2. Georges, E., Georges, J-M., and Hollinger, S., *Langmuir*, 1997. **13**: p. 3454 - 3463.
3. Binnig, G., Quate, C. F. and Gerber, C., *Phys. Rev. Lett.*, 1986. **56**(9): p. 930 - 933.
4. Binnig, G., and Rohrer, H., *Helv. Phys. Acta*, 1982. **55**: p. 726.
5. Ducker, W.A., Senden, T. J., and Pashley, R. M., *Nature*, 1991. **353**: p. 239 - 241.
6. Fleming, B.D., Wanless, E. J., and Biggs, S., *Langmuir*, 1999. **15**: p. 8719 - 8725.
7. Briscoe, W.H., and Horn, R. G., *Langmuir*, 2002. **18**: p. 3945 - 3956.
8. Braithwaite, G.J.C., Luckham, P. F., and Howe, A. M., *Langmuir*, 1996. **12**: p. 4224 - 4237.
9. Bowen, W.R., Lovitt, R. W. and Wright, C. J., *Journal of Materials Science*, 2001. **36**: p. 623 - 629.
10. Derjaguin, B.V., *Kolloid Zeitschrift*, 1934. **69**: p. 155.
11. Hartley, P.G., *Measurement of Colloidal Interactions Using the Atomic Force Microscope*, in *Colloid-Polymer Interactions: From Fundamentals to Practice*, Farinato, R.S., and Dubin, P. L., Editor. 1999, John Wiley & Sons, Inc.: New York.
12. Israelachvili, J.N., *Intermolecular and Surface Forces*. 1991: Academic Press.
13. Braithwaite, J.C., and Luckham, P. F., *J. Chem. Soc., Faraday Trans.*, 1997. **93**(7): p. 1409 - 1415.

CHAPTER 6: ELLIPSOMETRY STUDIES

6.1. Introduction

Ellipsometry is an optical technique used for the characterisation of film thicknesses and optical constants at an interface. It uses the optical polarisation transformation of a polarized light as it is reflected from, or transmitted through, a film or an interface. It is an indirect measurement technique which does not perturb the system, when an appropriate wavelength and intensity of the light beam is used[1]. Ellipsometry is a popular technique to study interfacial properties *in-situ* to study for example, the growth of polymer films[2, 3], associative interactions at interfaces[4], adsorption at an interface[5], etc.

A plane electromagnetic wave consists of an electric field and a magnetic field at 90 degrees to each other, which are both orthogonal to the direction of propagation of the beam as shown in figure 6.1.

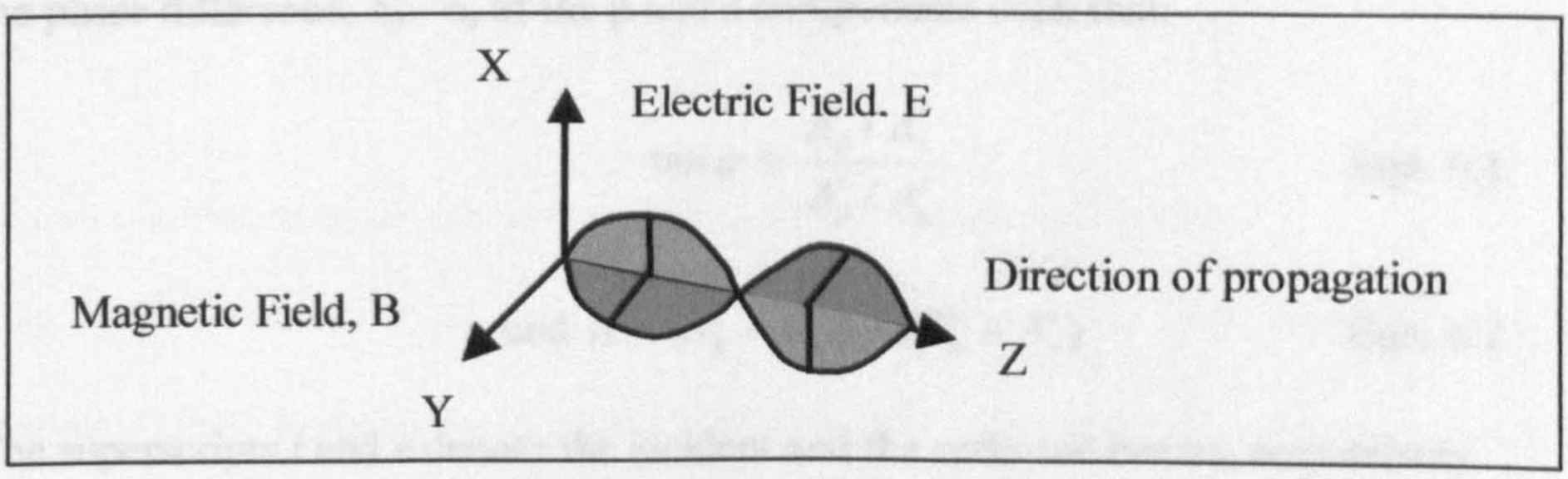

Figure 6.1: The two components of an electromagnetic wave

Polarization states of a beam are usually defined in terms of the direction and phase of the electric field vector only. In a non-charged and isotropic system, the components of the polarisation vector must lie in the plane perpendicular to the direction of propagation. Thus, the polarization state of a beam can be defined by any two orthogonal axes in the plane perpendicular to the direction of propagation. These two planes are usually denoted as the p- and s-planes. The p-plane lies in the plane of

incidence and is normal to the surface whereas, the s-plane lies parallel to the surface. The p-plane, s-plane and the direction of propagation define a right-handed Cartesian co-ordinate system[6]. This is illustrated in figure 6.2.

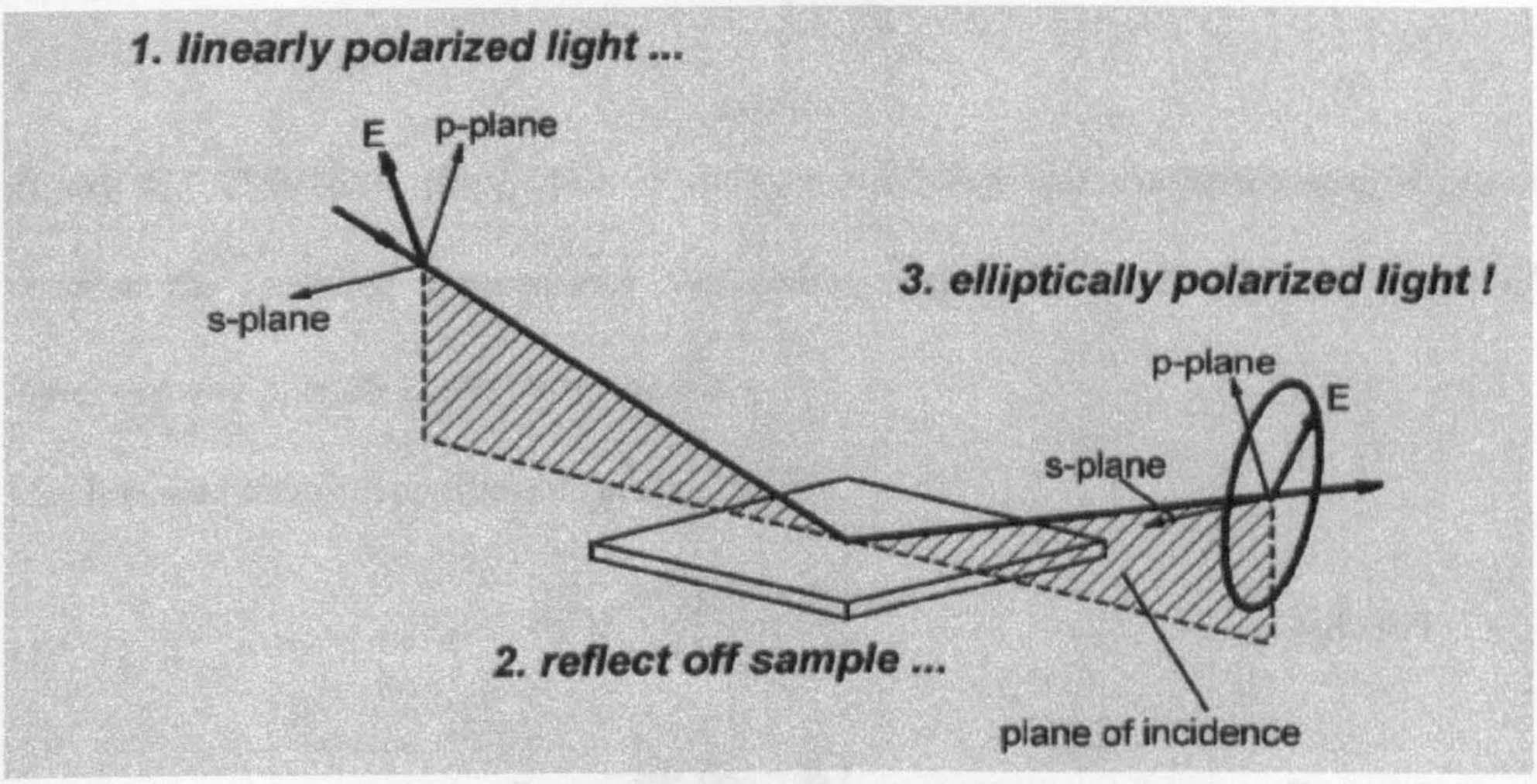

Figure 6.2: Schematic illustration of s- and p-planes and the geometric arrangement of an ellipsometric experiment[1]

The polarisation state of a light beam is characterised by the amplitude ratio, A_p/A_s and the phase difference, $\delta_p - \delta_s$ of the p and s components such that:

$$\tan\psi = \frac{A_p^r / A_s^r}{A_p^i / A_s^i} \qquad \text{Eqn. 6.1}$$

$$\text{and } \Delta = (\delta_p^r - \delta_s^r) - (\delta_p^i - \delta_s^i) \qquad \text{Eqn. 6.2}$$

The superscripts *i* and *r* denote the incident and the reflected beams, respectively.

The measured quantities in ellipsometry are Ψ, the amplitude component, and Δ, the phase component. Ψ and Δ are related to the ratio of Fresnel reflection coefficients R_p and R_s for p- and s-polarized light, respectively, as follows:

$$\rho = \frac{R_p}{R_s} = \tan(\psi)e^{i\Delta} \qquad \text{Eqn. 6.3}$$

R_p and R_s are derived from the oblique reflection and transmission of a plane wave at the interface between two semi-infinite media as represented in figure 6.3.

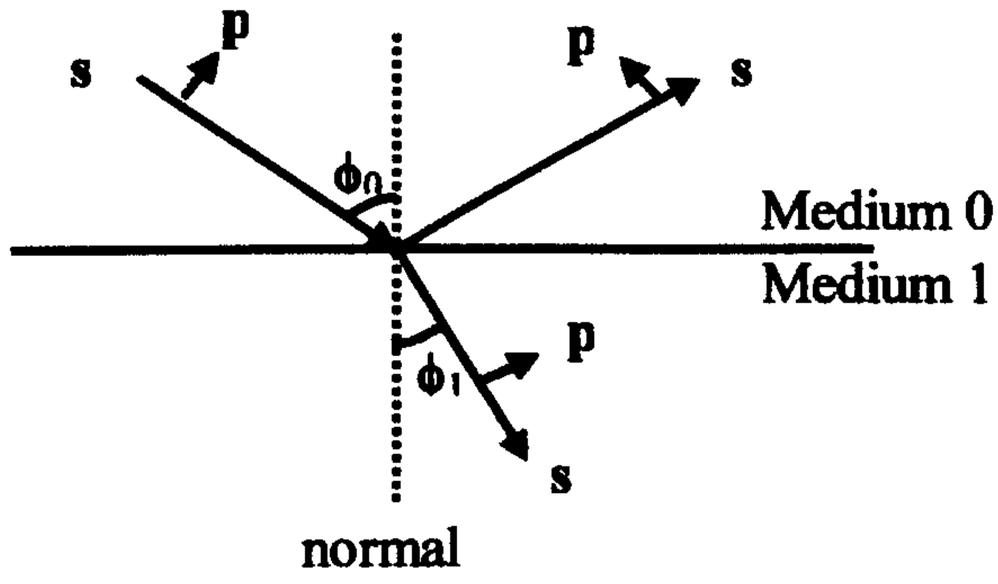

Figure 6.3: Schematic illustration of oblique reflection and transmission of a plane wave at the interface between two semi-infinite media 0 and 1. ϕ_0 is the angle of incidence and ϕ_1 is the angle of refraction.

The Fresnel reflection coefficients are given by:

$$R_p = \frac{\tan(\phi_0 - \phi_1)}{\tan(\phi_0 + \phi_1)} \qquad \text{Eqn. 6.4}$$

$$R_s = \frac{-\sin(\phi_0 - \phi_1)}{\sin(\phi_0 + \phi_1)} \qquad \text{Eqn. 6.5}$$

They also depend on the wavelength of the light, λ, and the optical properties of the reflecting system. The complex index of refraction, N, for each media can be expressed as shown in eqn. 6.6[7].

$$N = n + ik \qquad \text{Eqn 6.6}$$

Where n is the index of refraction and k is the extinction coefficient.

The angle at which R_p is minimum is called the Brewster angle. Reflection at the Brewster angle leads to maximum polarisation of the reflected light from the interface and the intensity of the reflected parallel polarisation is a minimum enabling accurate data acquisition[8, 9].

6.2. Instrumentation

The Ellipsometer used in this study is an M-2000U® Ellipsometer manufactured by J. A. Woollam Co., Inc. It is a spectroscopic ellipsometer and operates in the wavelength range of 235 nm to 1700 nm.

The instrument consists of the following units[1]:

1. Light Source
2. Polariser
3. Compensator
4. Sample Platform
5. Analyser
6. Detector

A range of light sources are available for the VASE M-2000U® Ellipsometer as listed below:

Lamp source	Wavelength range (nm)
Deuterium (D_2)	140 - 300
Xenon (Xe)	190 - 2000
Quartz Tungsten Halogen (QTH)	350 - 2000
Silicon carbide globar	1500 - 40000

Figure 6.4: The different light sources available for spectroscopic ellipsometers

The light beam is coupled between the various optical units of the ellipsometer by fiber optic cables of about 200 – 400 μm diameter suitable for UV and IR transmissions.

The polariser used is a calcite Glan-Taylor polariser which polarises a light beam to 1 part in 10^6, and transmits sufficiently in the range 230 nm to 2200 nm.

Compensators, placed in-between the polariser and the sample, convert linearly polarised light to circularly polarised light. An ideal compensator is an optical retarder that has a retardation of exactly 90° between the perpendicular components of the electric field of the light beam. Retarders are generally constructed from thin plates of a birefringent material or from polished crystal rhombs. The VASE M-2000®

ellipsometer has a rotating compensating configuration. White light is reflected from a sample through the analyser and to the detector.

The detector used in the M-2000® ellipsometer is a charge-coupled device (CCD) array which operates simultaneously at many wavelengths. Silicon arrays are used for wavelengths up to 1100 nm, but are replaced with InGaAs (Indium-Gallium-Arsenic mixture arrays) to cover the near infrared spectrum up to 1700 nm.

6.3. Experimentation

All the experiments using the ellipsometer were carried out at an incident angle 70°. Previous studies of similar systems had also used this angle[10]. A quartz sample cell, obtained from Hellma, Germany, with the transmitting sidewalls angled at 70° was used for all the *in-situ* measurements.

Steel plates of 1 cm^2 area, which have been previously fine polished (section 2.7 in chapter 2 of this thesis), were used as the substrates and all the samples were prepared in isooctane solvent and the experiments carried out at ambient room temperature. In order to facilitate the dispersion of concentrated samples added to the solvent/solution in the cell, a small overhead stirrer was built in the laboratory using a 1.5 – 4.5 V and 6550 r.p.m. motor. By using a dye solution, as a visible reference it was found that the stirrer was able to disperse the solution throughout the cell within 90 s. As a precaution to avoid bubble formation and splashing, only the tip (< 1 mm) of the stirrer was immersed in the solvent/solution. The cell was covered with a top, with an opening for the stirrer, to minimise evaporation of the solvent during the course of the experiment.

The plate and the cell had been previously cleaned by passing strong currents of dry air to remove any dust or particulate matter present on the plate or inside the cell. The wavelength range chosen for the current study was 500 nm to 1000 nm, which is the range where the polymer or any of the surfactants are non-absorbing, i.e. are spectroscopically inactive.

Measurements were started in the presence of a fixed mass of isooctane in the cell plus the steel plate. After some time, a known amount of concentrated polymer/surfactant solution was added to the cell to study the adsorption and polymer/surfactant layer build-up at the interface. The solution was dispersed using the "homemade" stirrer. Some of the experiments were started straight with a polymer/surfactant solution.

To analyse the data, a model describing the optical structure of the substrate, i.e. steel plate in isooctane, was constructed using the data analysis software package available with the instrument. This was taken as the base model representing the substrate. A layer, representing the polymer layer, was then added on top of the base model and was fitted with a theoretical model corresponding to an organic film. The models were iterated until the theoretical values of Ψ and Δ closely matched the measured values.

6.4. Results

6.4.1. Ellipsometric profile of ψ for *stainless steel/isooctane interface*

An initial study of the stainless steel and pure isooctane was carried out to study if there was any change in the value of ψ with time. The plot of ψ as a function of wavelength and time, is shown in figure 6.5.

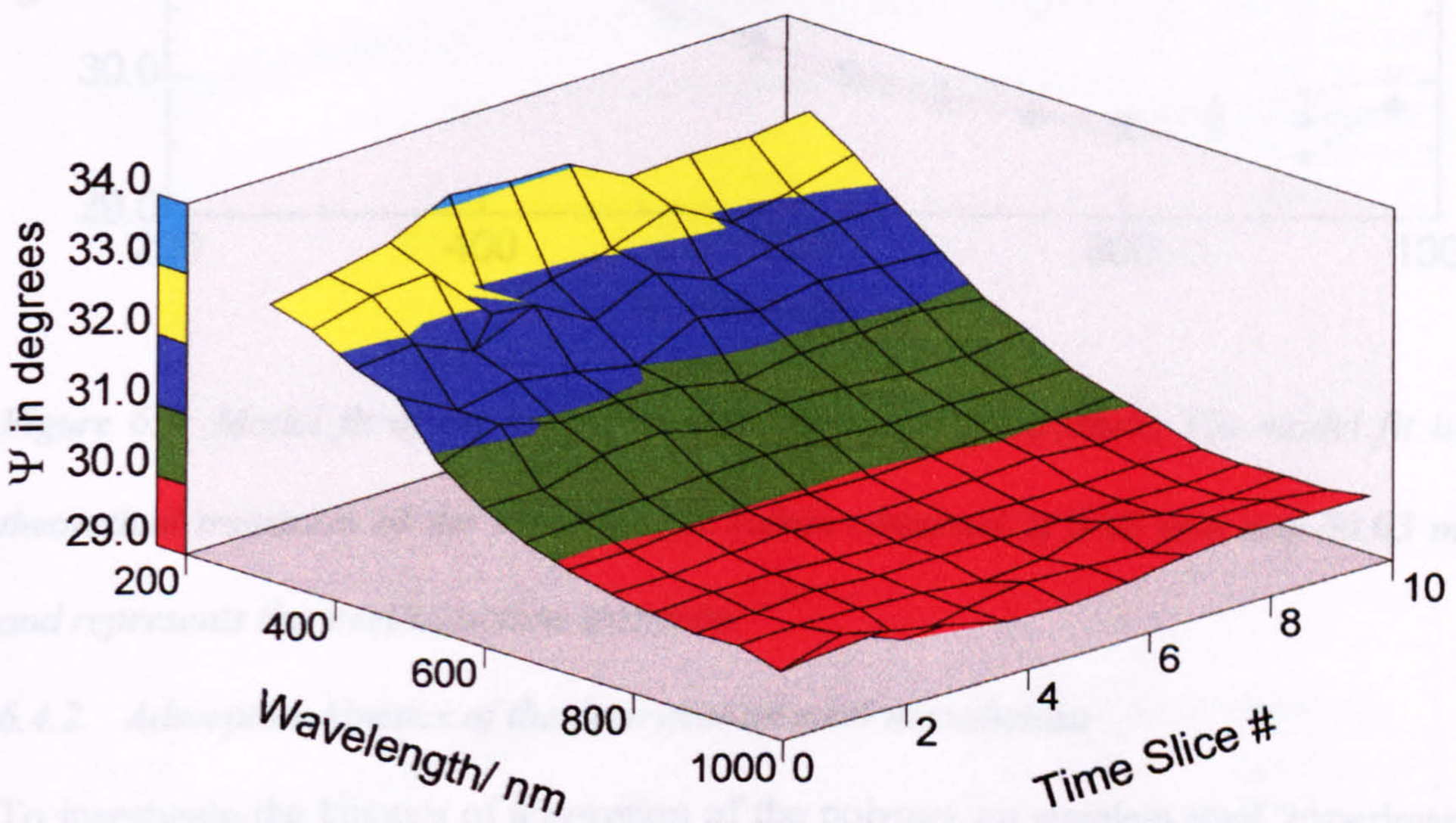

Figure 6.5: ψ as a function of wavelength and time every 20 min. The slices indicate the times of which the data have been plotted.

As this was the data from which base model, representing the steel isooctane interface, is generated, a theoretical base line model fit was carried out at 0 min and 80 min to study if the same model fitted the data collected at these different times. One model could fit the graphs obtained at different times as shown in figure 6.6.

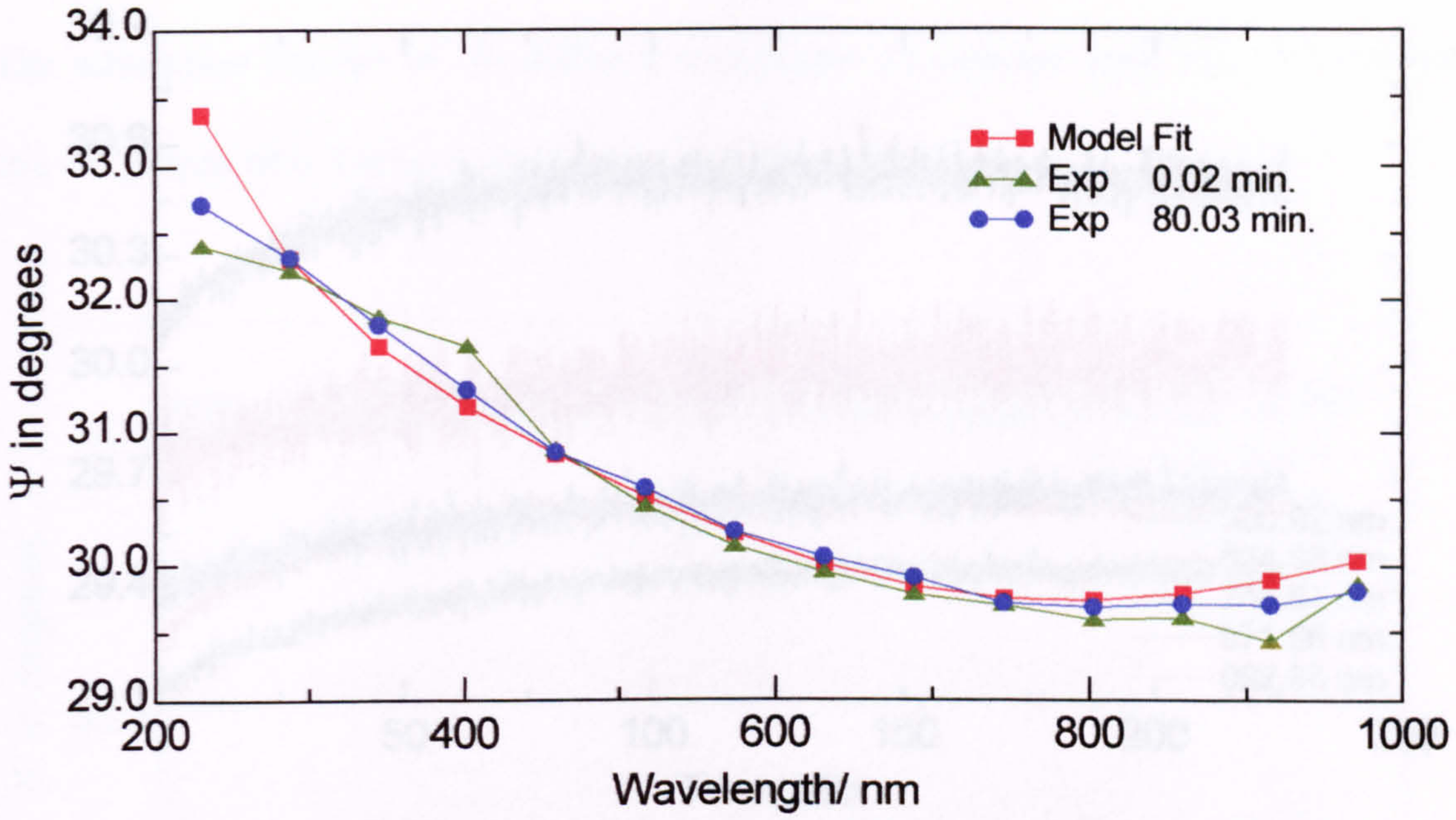

Figure 6.6: Model fit of the ψ graphs obtained at different times. The model fit is a theoretical treatment of the experimental values obtained at 0.02 min and 80.03 min and represents the steel/isooctane interface.

6.4.2. Adsorption kinetics of the detergent on steel in isooctane

To investigate the kinetics of adsorption of the polymer on stainless steel, experiments were carried out at different concentrations as a function of time. It was noticed that adsorption reached equilibrium condition in about 60 to 70 minutes, as can be seen in the following figures.

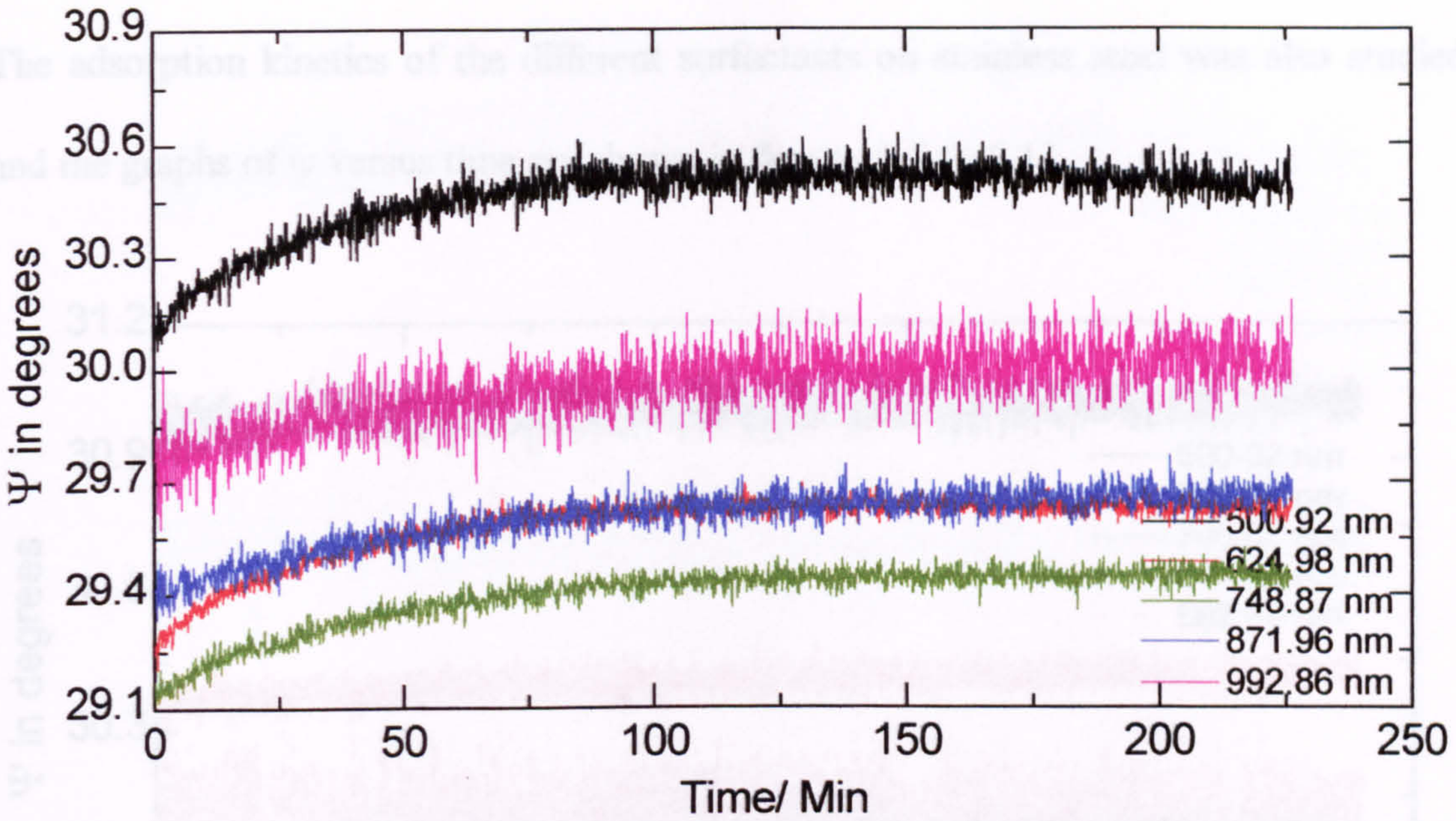

Figure 6.7: Plot of ψ as a function of time for 0.5 wt. % P1 solution

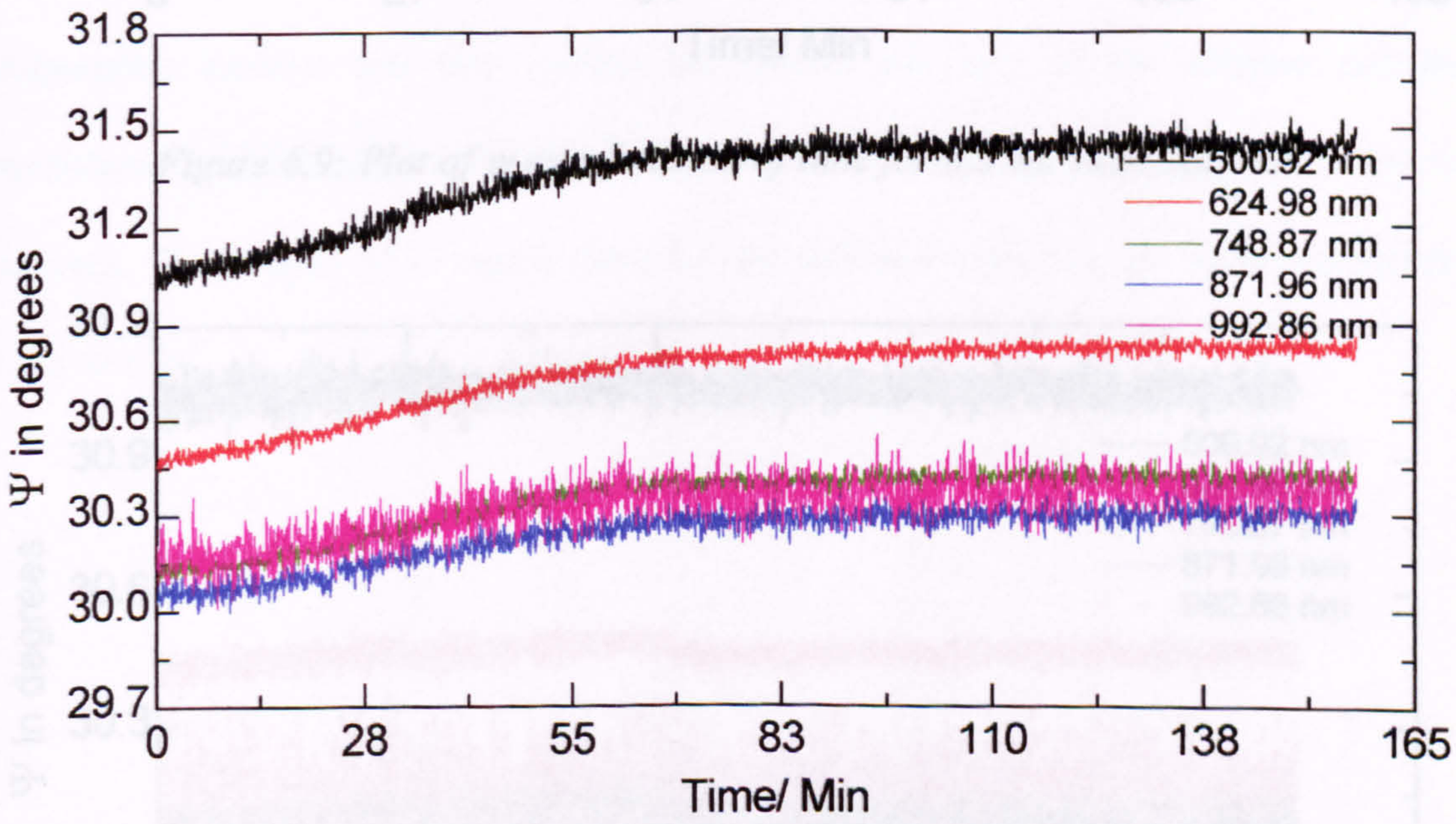

Figure 6.8: Plot of ψ as a function of time for 1.0 wt. % P1 solution

6.4.3. *Adsorption kinetics of the surfactants on steel in isooctane*

The adsorption kinetics of the different surfactants on stainless steel was also studied and the graphs of ψ versus time are shown in figures 6.9 to 6.11.

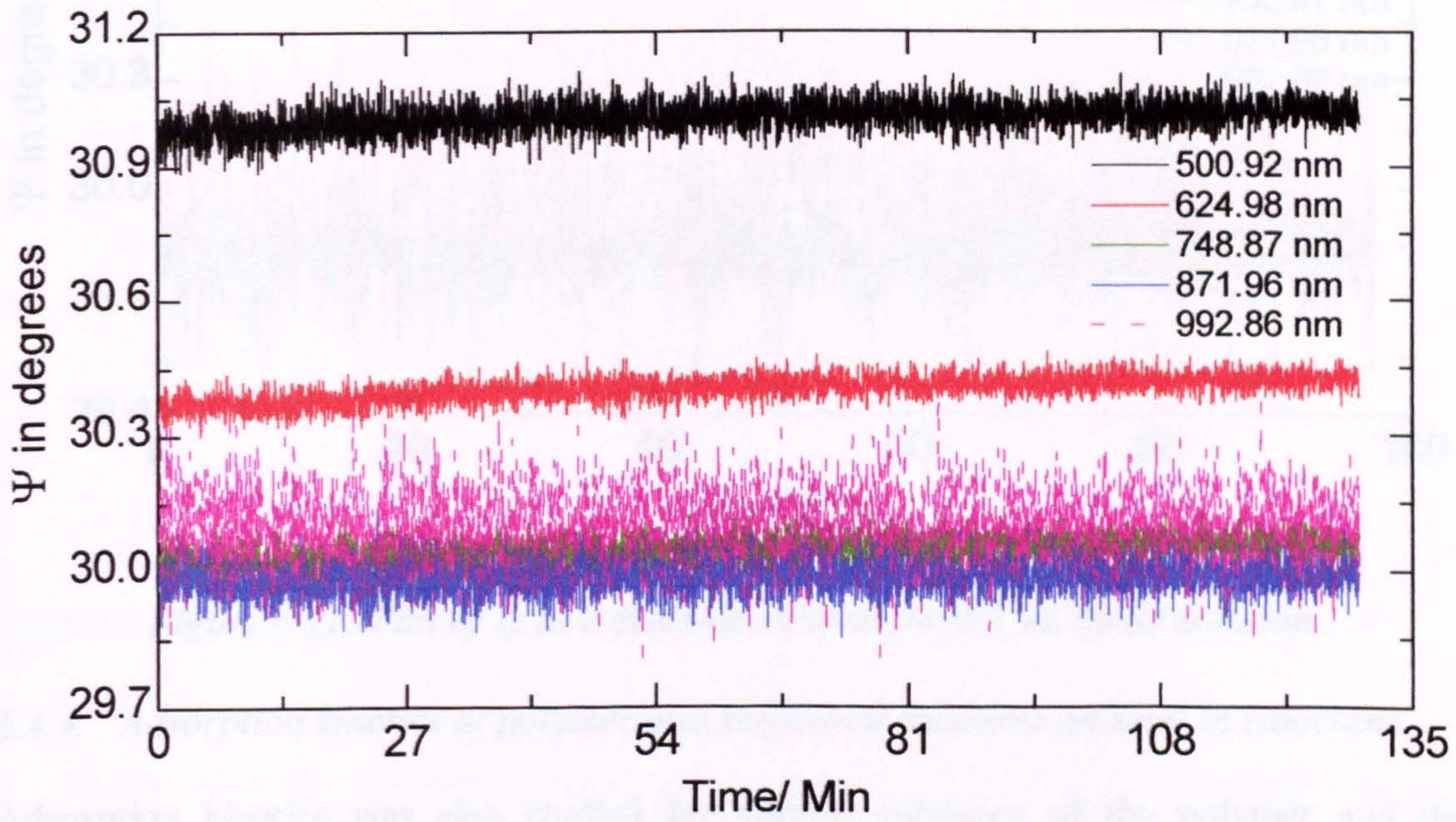

Figure 6.9: Plot of ψ as a function of time for 0.5 wt. % S1 solution

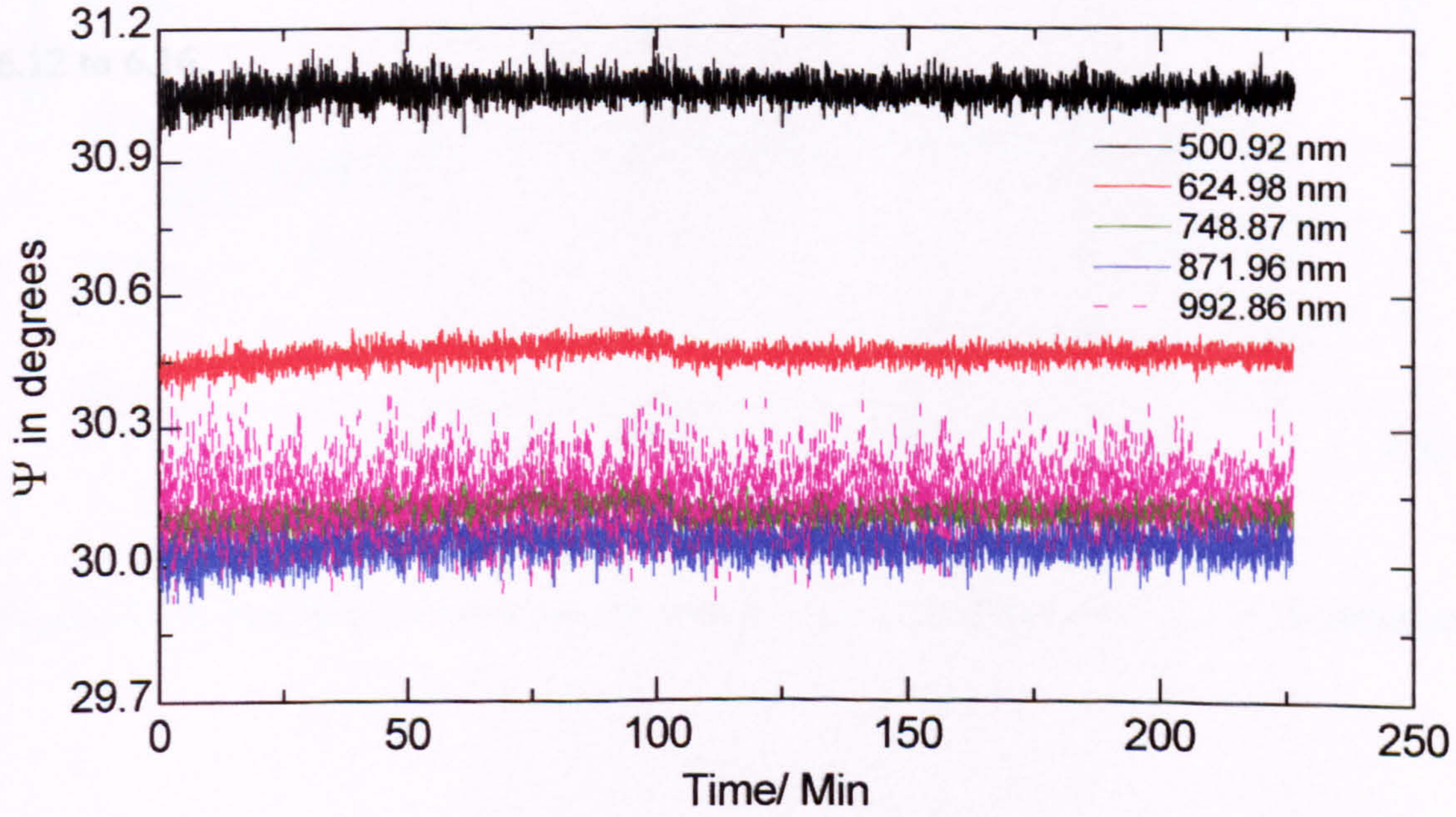

Figure 6.10: Plot of ψ as a function of time for 0.5 wt. % S3 solution

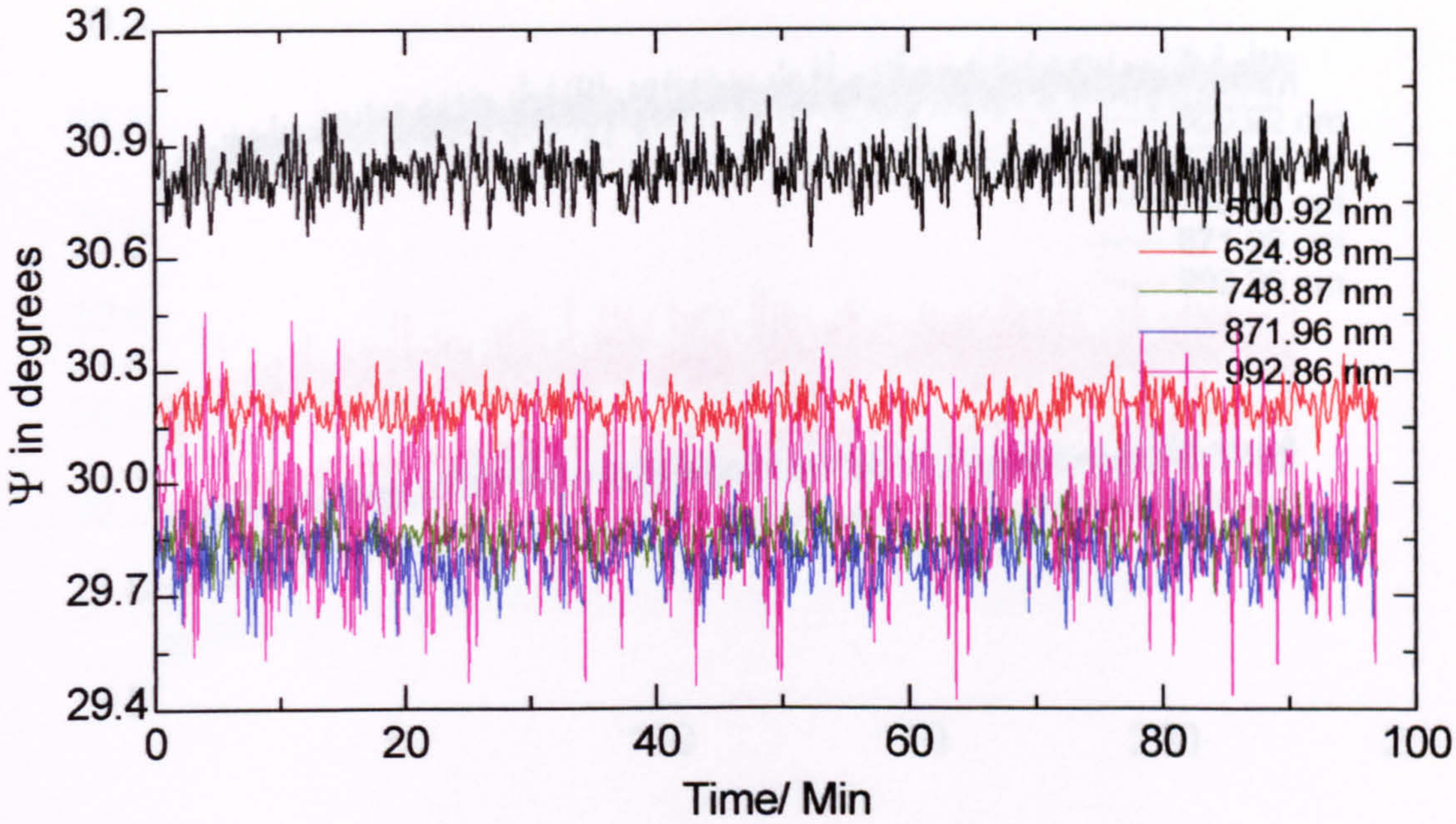

Figure 6.11: Plot of ψ as a function of time for 0.5 wt. % S5 solution

6.4.4. Adsorption kinetics of polymer and surfactant mixtures on steel in isooctane

Adsorption kinetics was also studied for various mixtures of the polymer and the surfactants and the graphs show equilibration after 70 minutes like for the polymer on its own. The graphs of ψ versus time for the different mixtures are shown in figures 6.12 to 6.16.

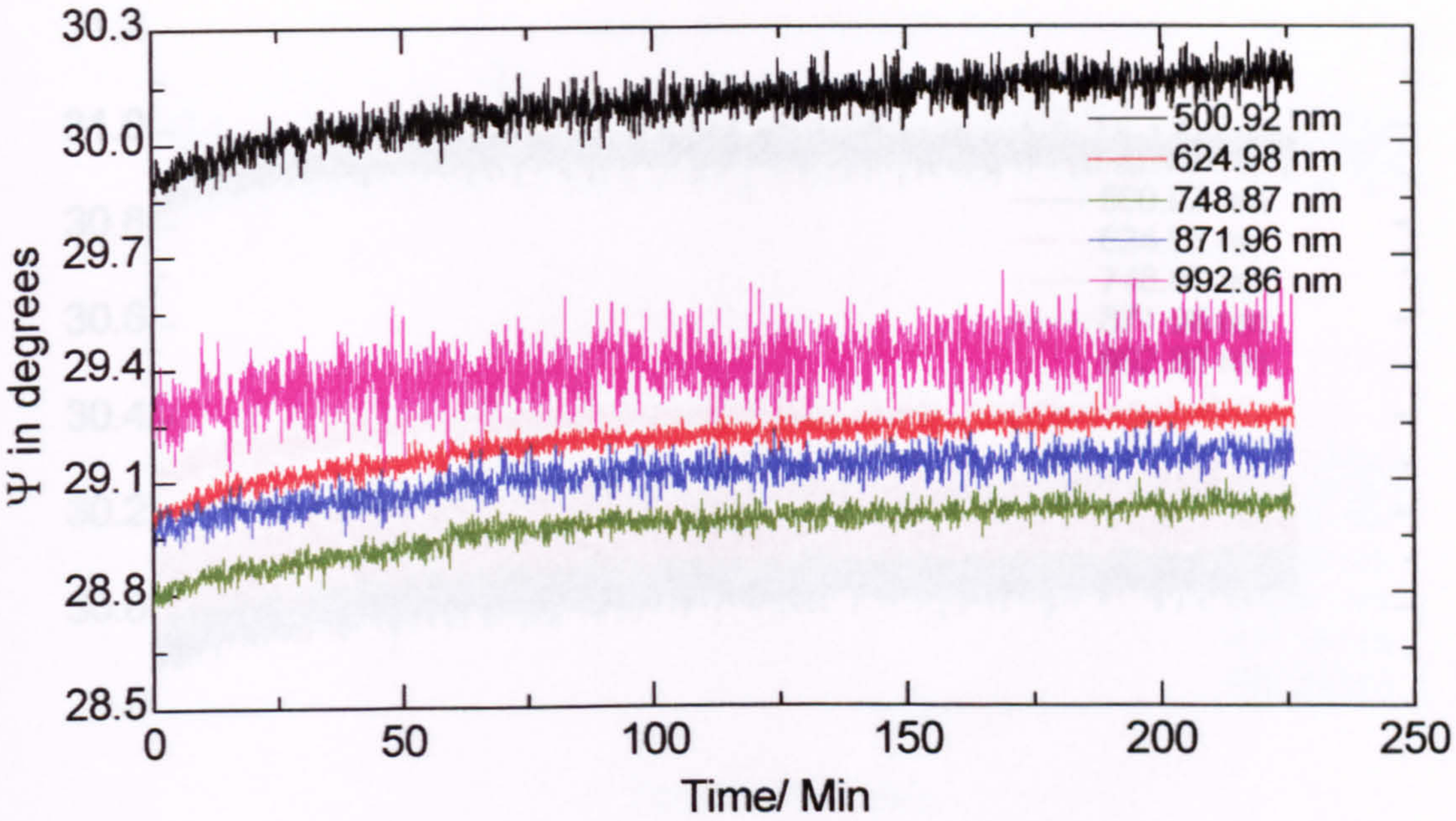

Figure 6.12: Plot of ψ as a function of time for 0.5 wt. % P1 and 0.5 wt. % S1 solution

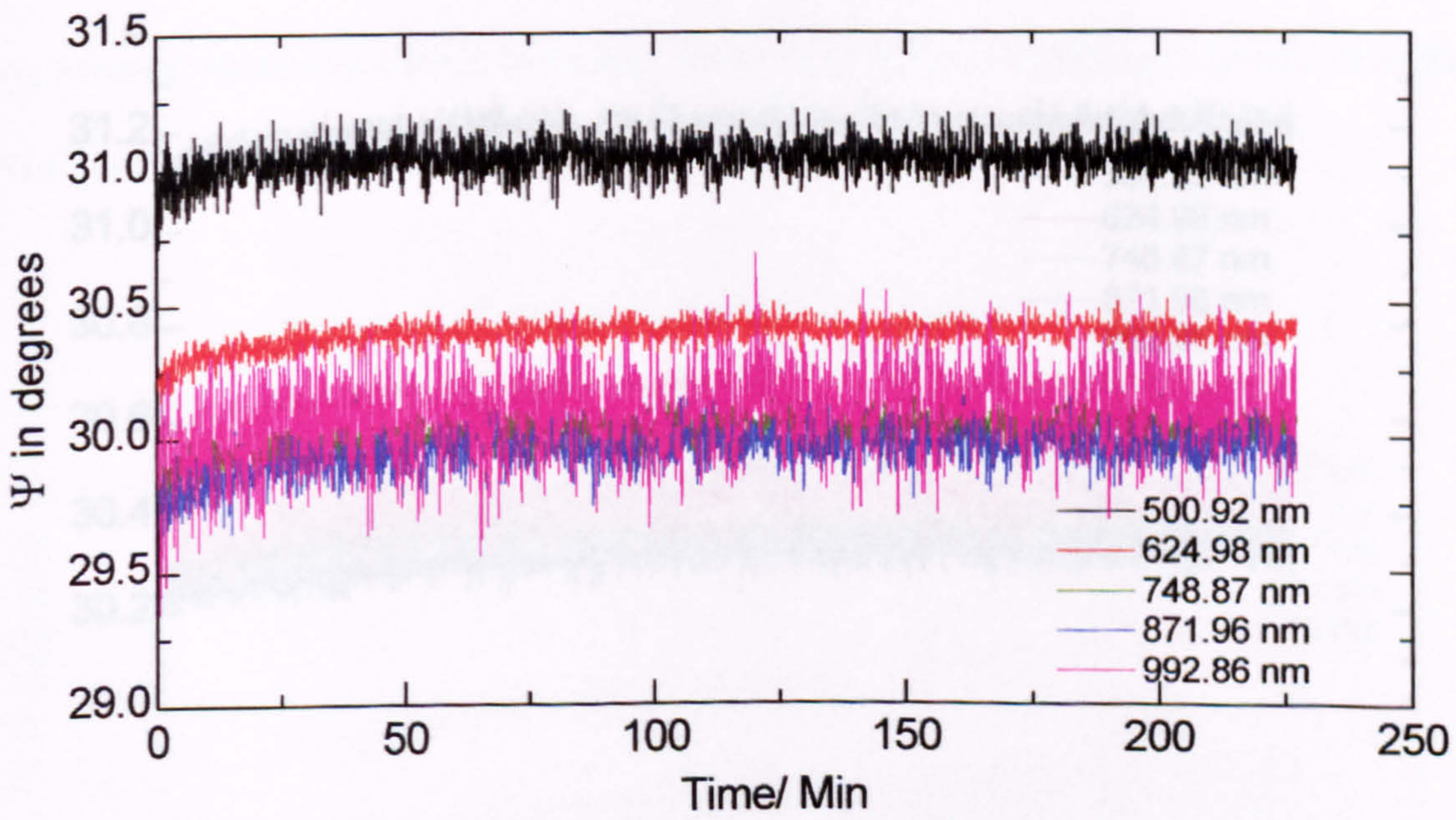

Figure 6.13: Plot of ψ as a function of time for 0.5 wt. % P1 and 0.5 wt. % S2 solution

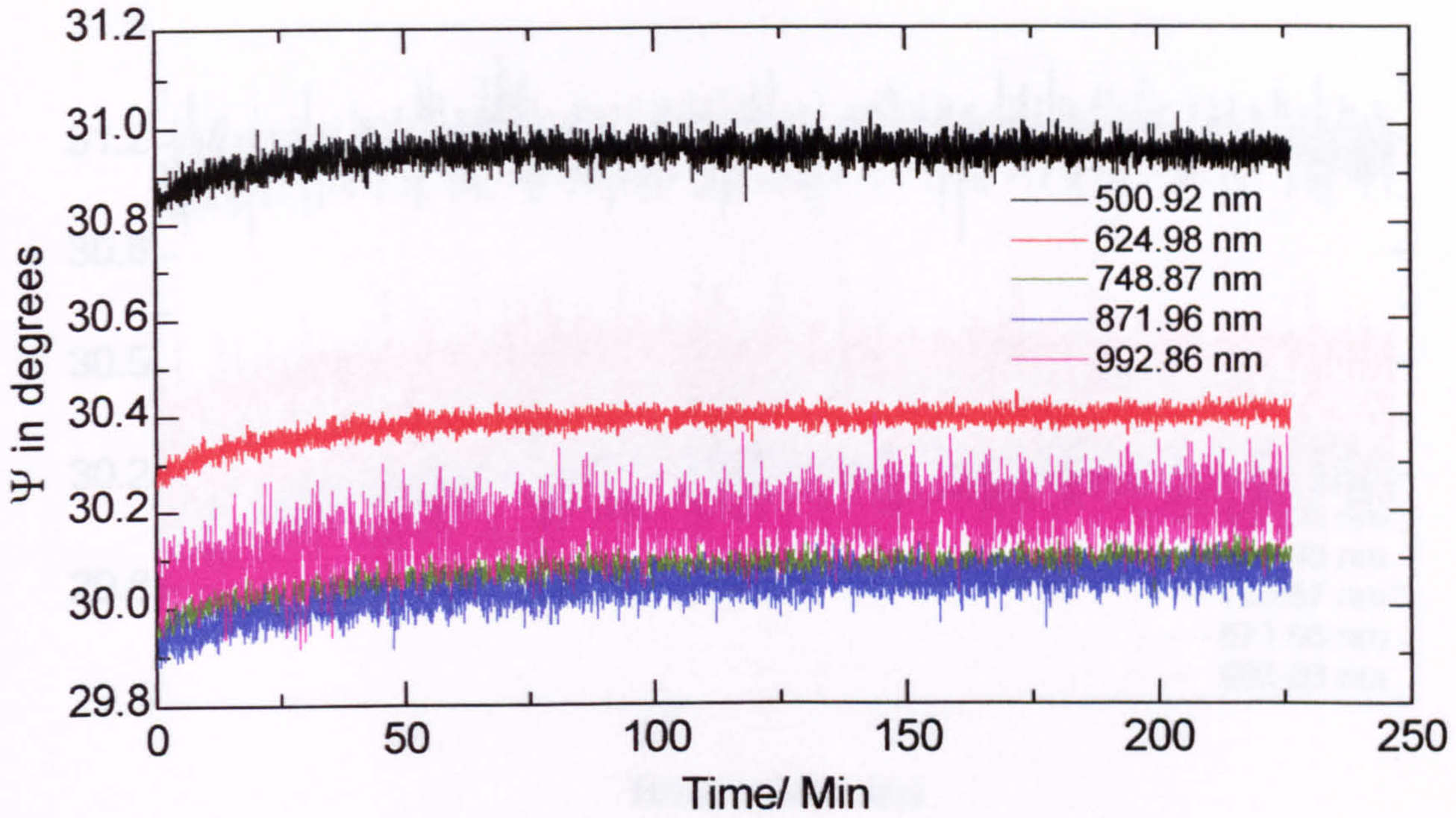

Figure 6.14: Plot of ψ as a function of time for 0.5 wt. % P1 and 0.5 wt. % S3 solution

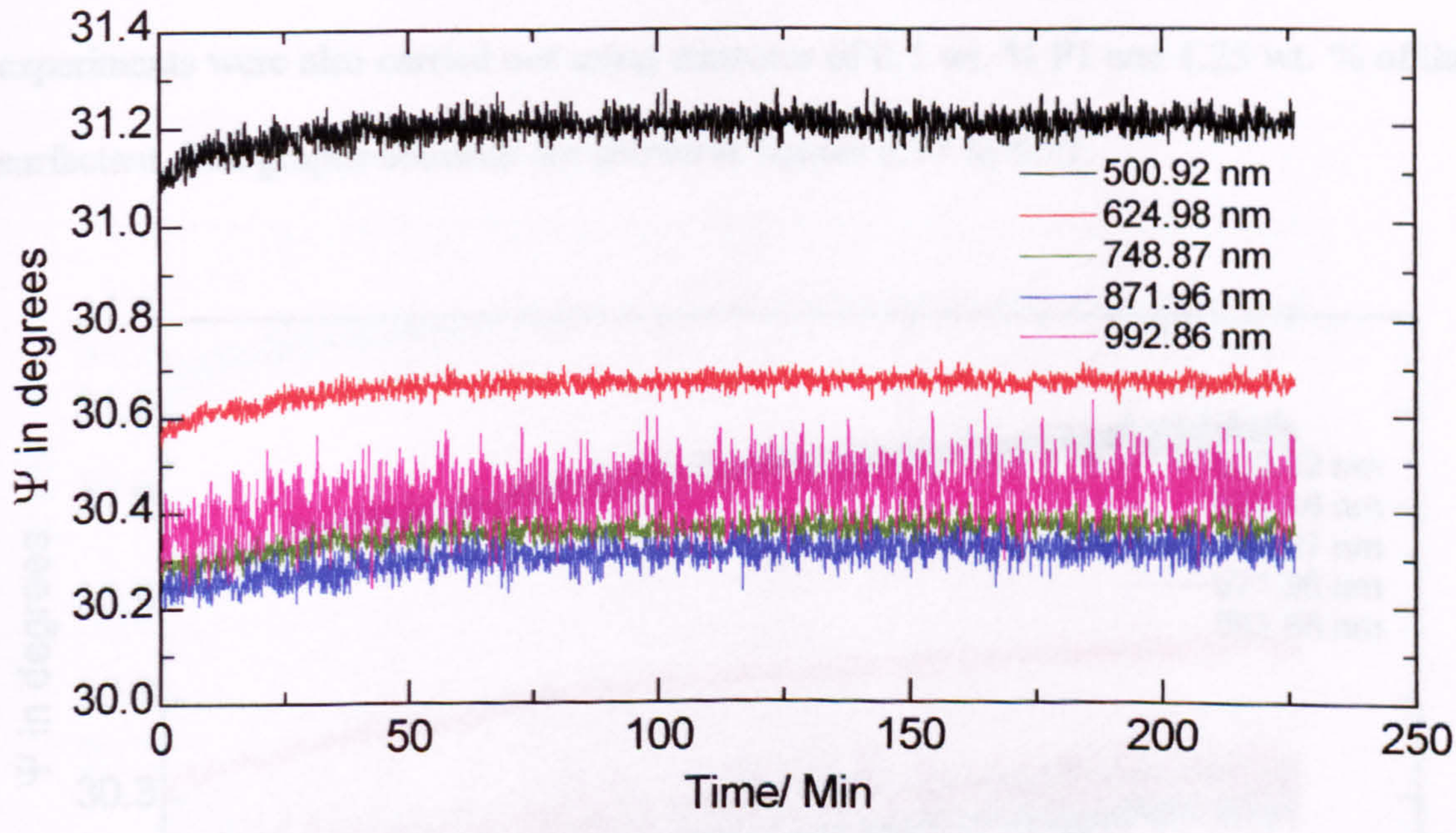

Figure 6.15: Plot of ψ as a function of time for 0.5 wt. % P1 and 0.5 wt. % S4 solution

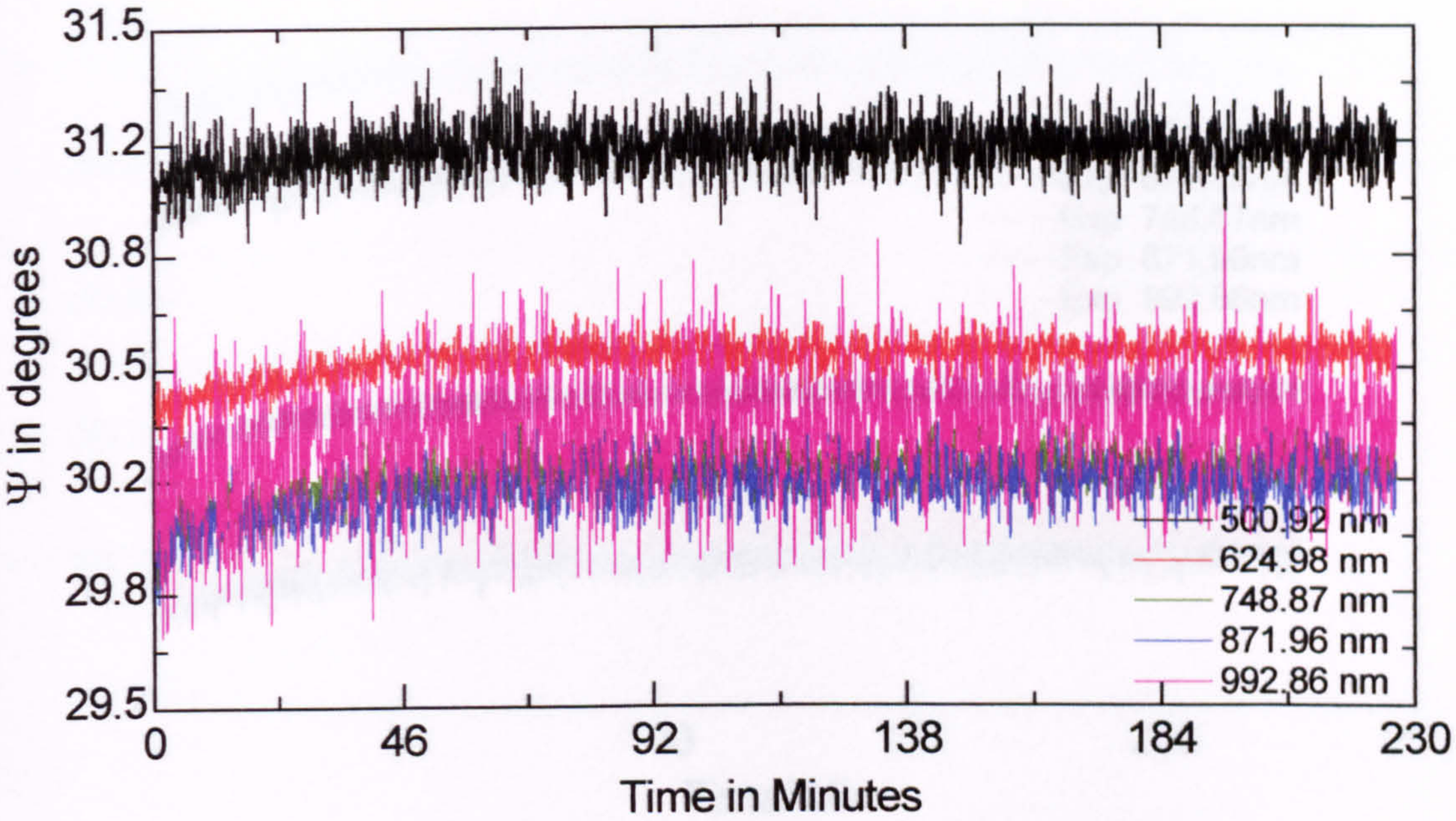

Figure 6.16: Plot of ψ as a function of time for 0.5 wt. % P1 and 0.5 wt. % S5 solution

To understand the effect of polymer-surfactant ratio on adsorption kinetics, experiments were also carried out using mixtures of 0.5 wt. % P1 and 1.25 wt. % of the surfactant. The graphs obtained are shown in figures 6.17 to 6.21.

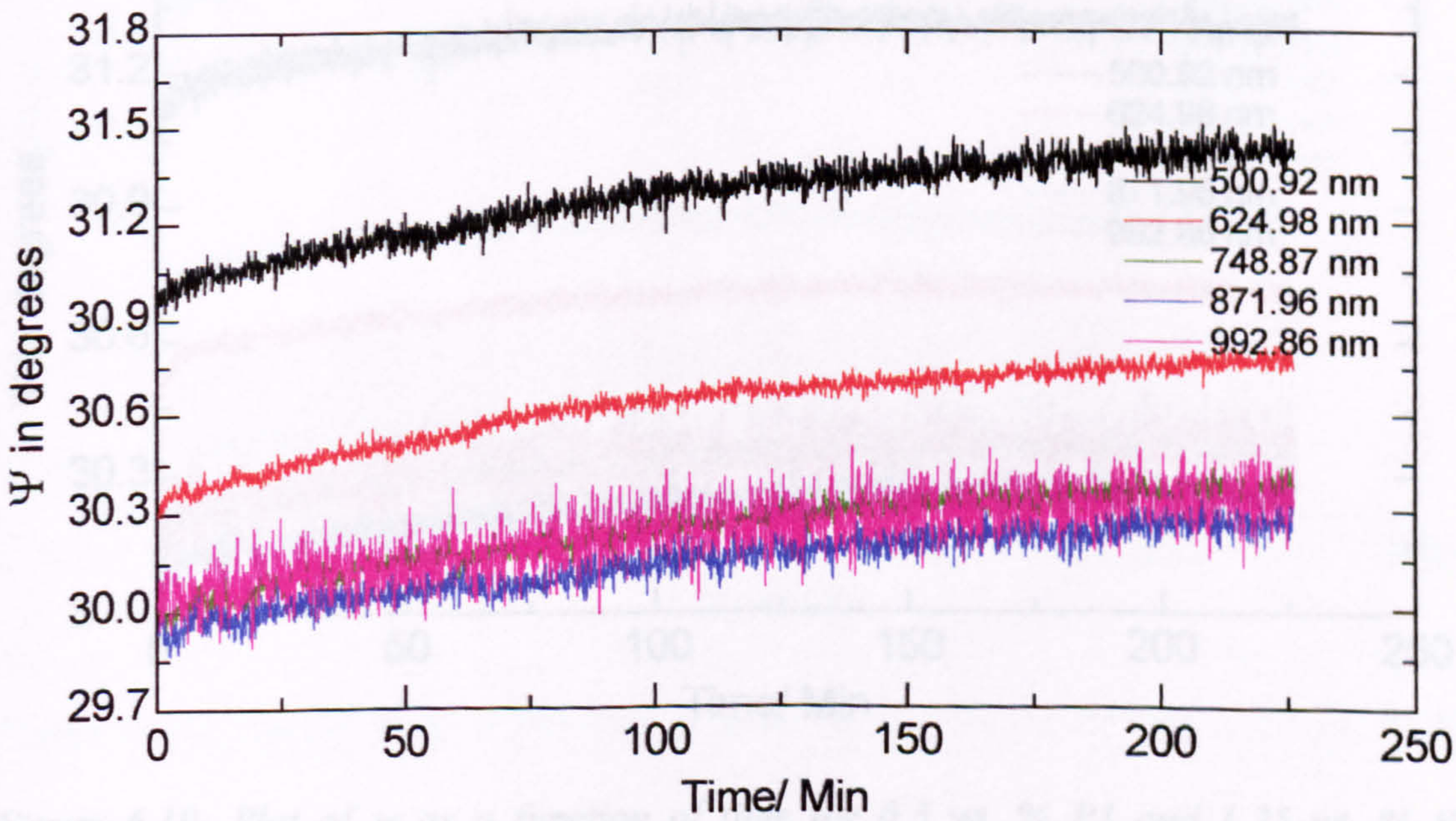

Figure 6.17: Plot of ψ as a function of time for 0.5 wt. % P1 and 1.25 wt. % S1 solution

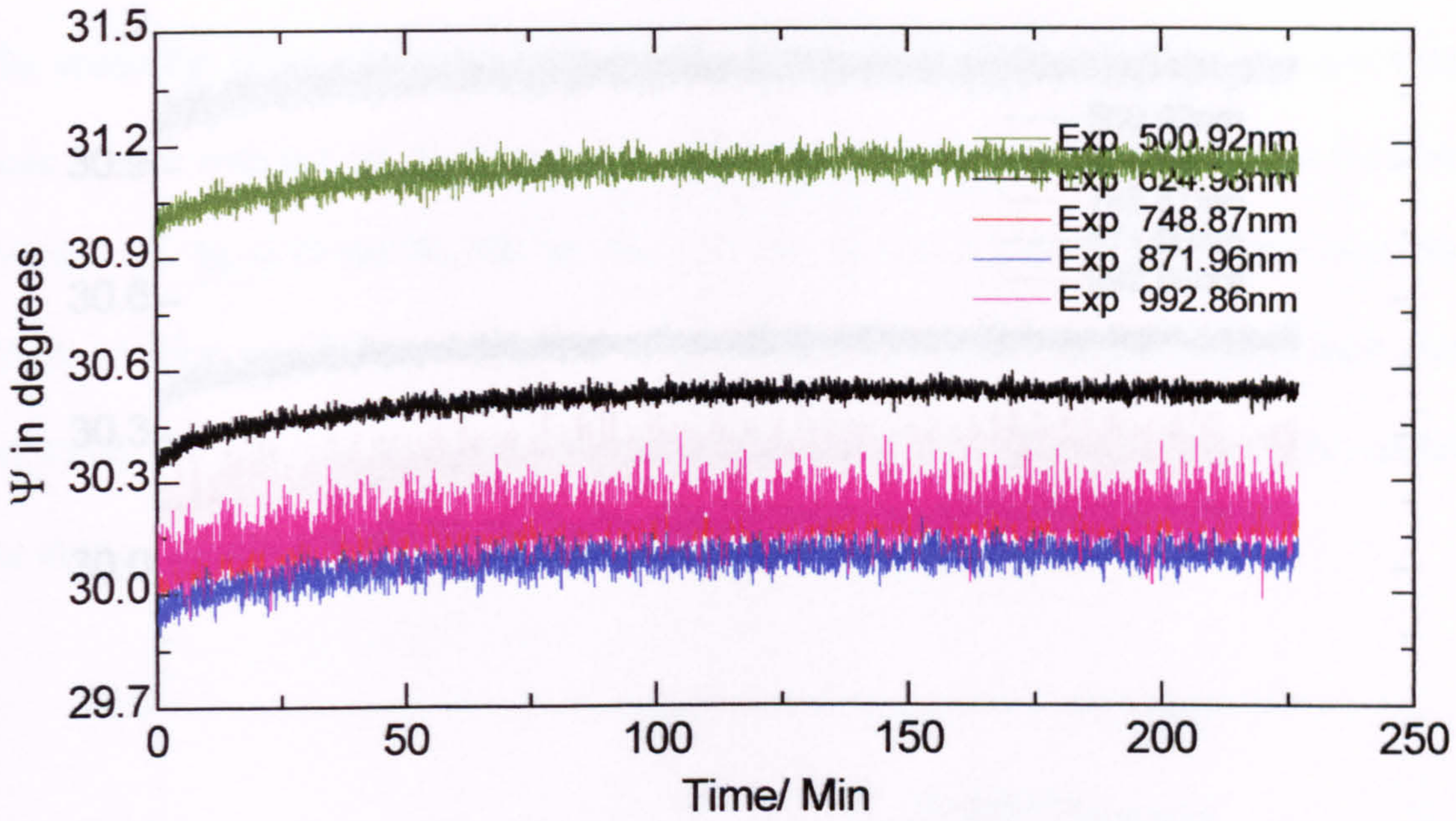

Figure 6.18: Plot of ψ as a function of time for 0.5 wt. % P1 and 1.25 wt. % S2 solution

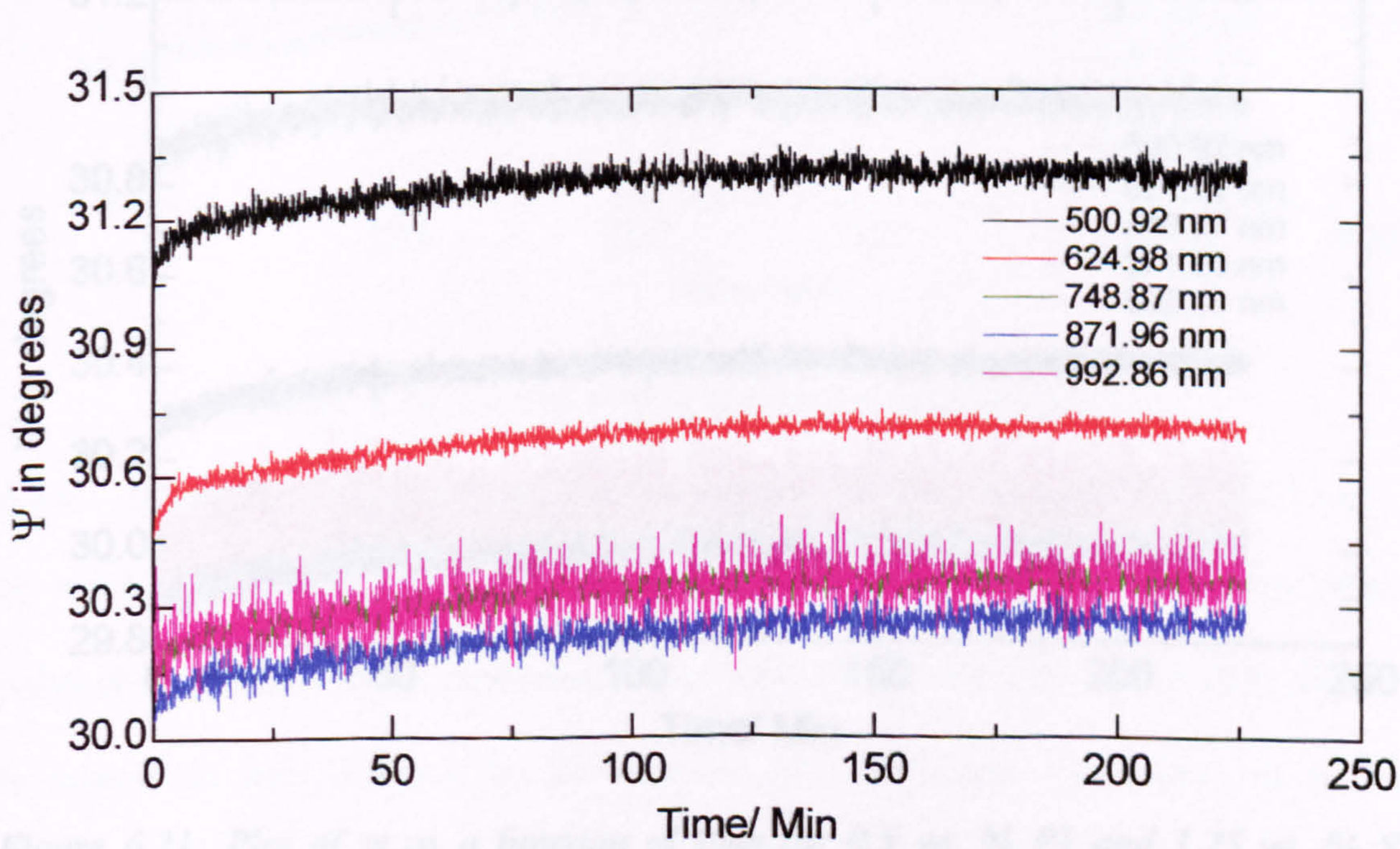

Figure 6.19: Plot of ψ as a function of time for 0.5 wt. % P1 and 1.25 wt. % S3 solution

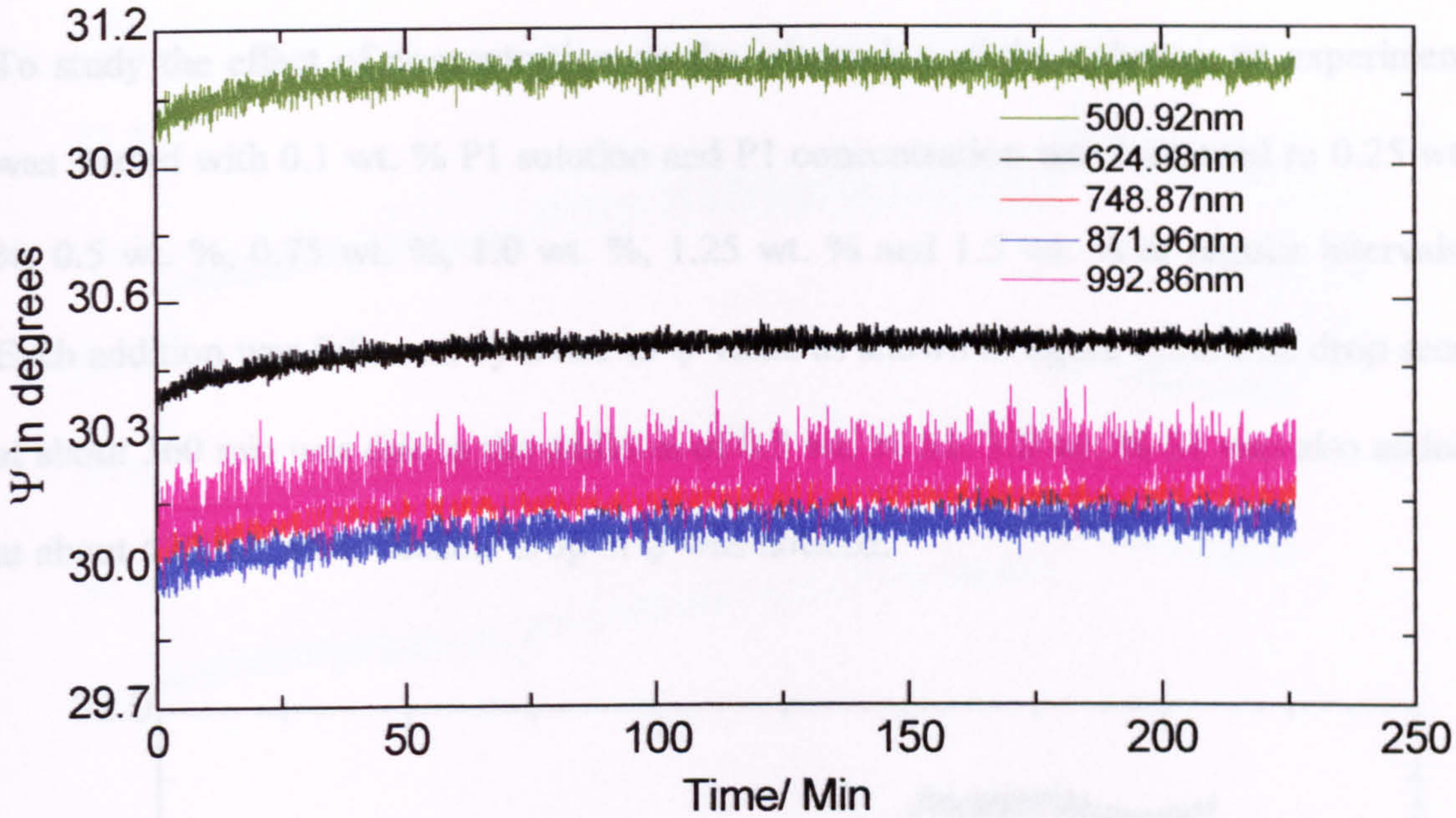

Figure 6.20: Plot of ψ as a function of time for 0.5 wt. % P1 and 1.25 wt. % S4 solution

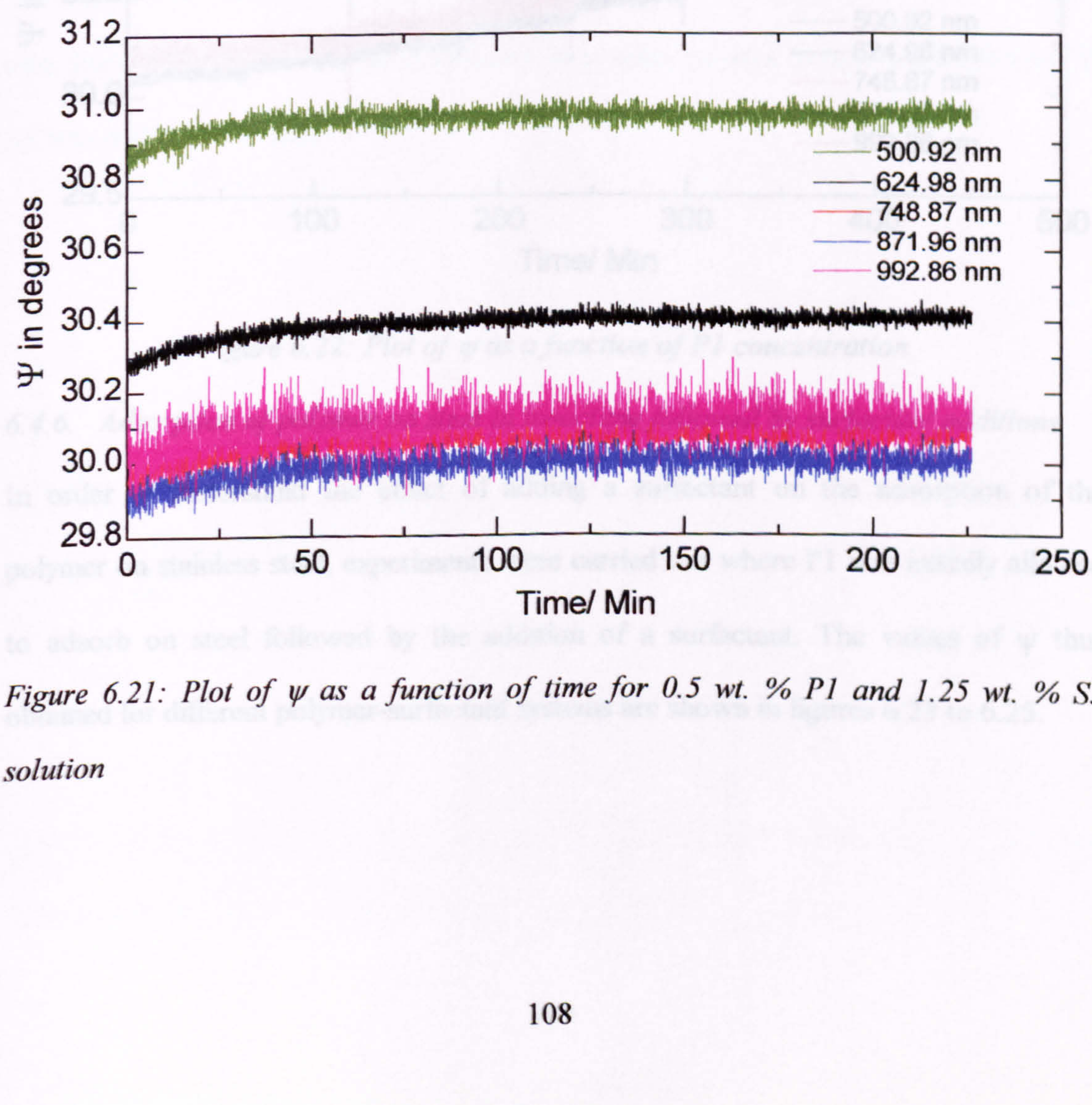

Figure 6.21: Plot of ψ as a function of time for 0.5 wt. % P1 and 1.25 wt. % S5 solution

6.4.5. Adsorption of polymer on steel as a function of concentration in isooctane

To study the effect of concentration on the adsorption of the polymer, an experiment was started with 0.1 wt. % P1 solution and P1 concentration was increased to 0.25 wt. %, 0.5 wt. %, 0.75 wt. %, 1.0 wt. %, 1.25 wt. % and 1.5 wt. % at regular intervals. Each addition was followed by a rise in ψ value as shown in figure 6.22. The drop seen at about 360 min was due to the addition of 0.5 wt. % S1. 1.0 wt. % S1 was also added at about 420 but no noticeable drop in ψ was noticed.

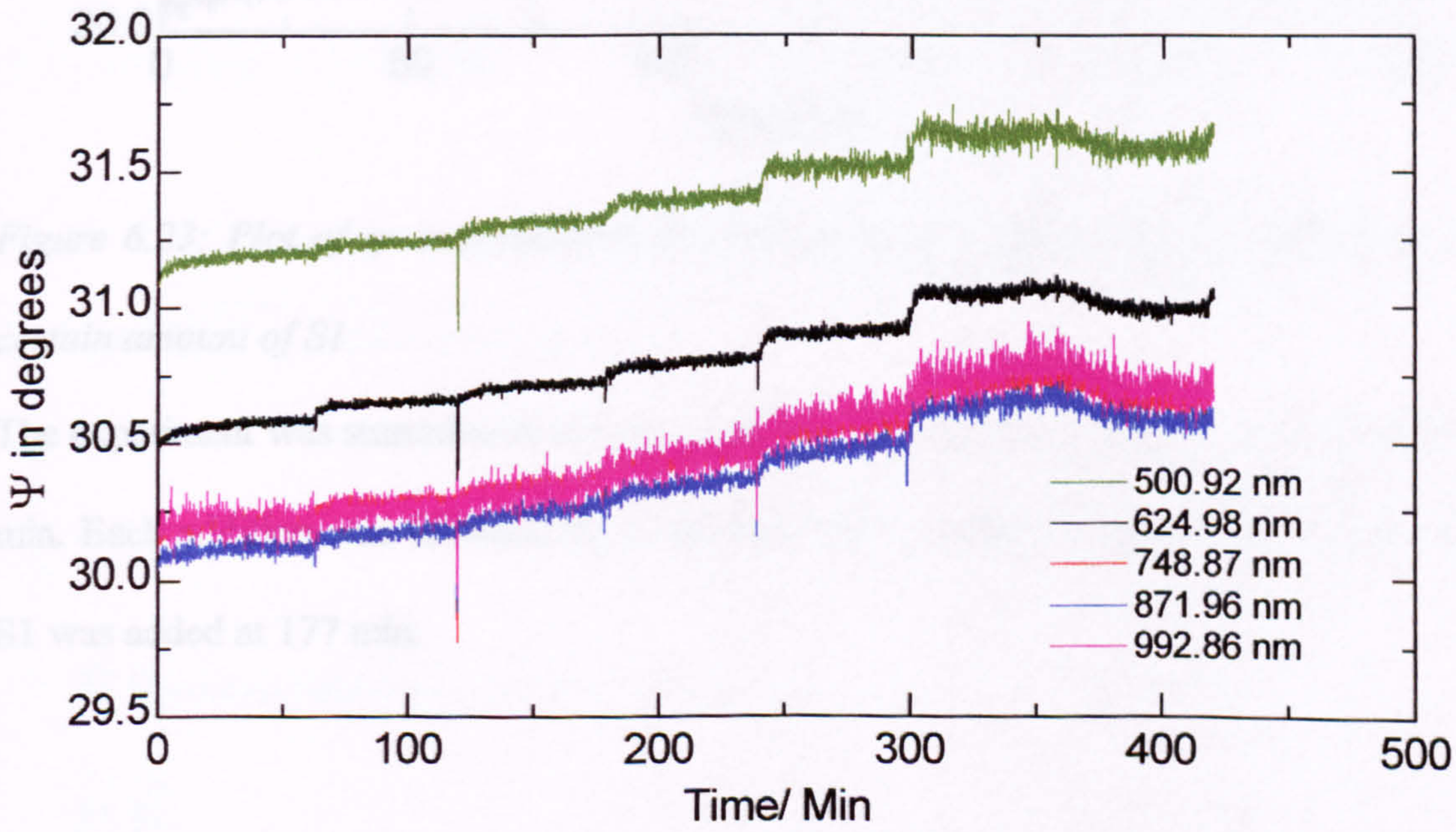

Figure 6.22: Plot of ψ as a function of P1 concentration

6.4.6. Adsorption of polymer on steel in isooctane followed by surfactant additions

In order to understand the effect of adding a surfactant on the adsorption of the polymer on stainless steel, experiments were carried out where P1 was initially allowed to adsorb on steel followed by the addition of a surfactant. The values of ψ thus obtained for different polymer-surfactant systems are shown in figures 6.23 to 6.25.

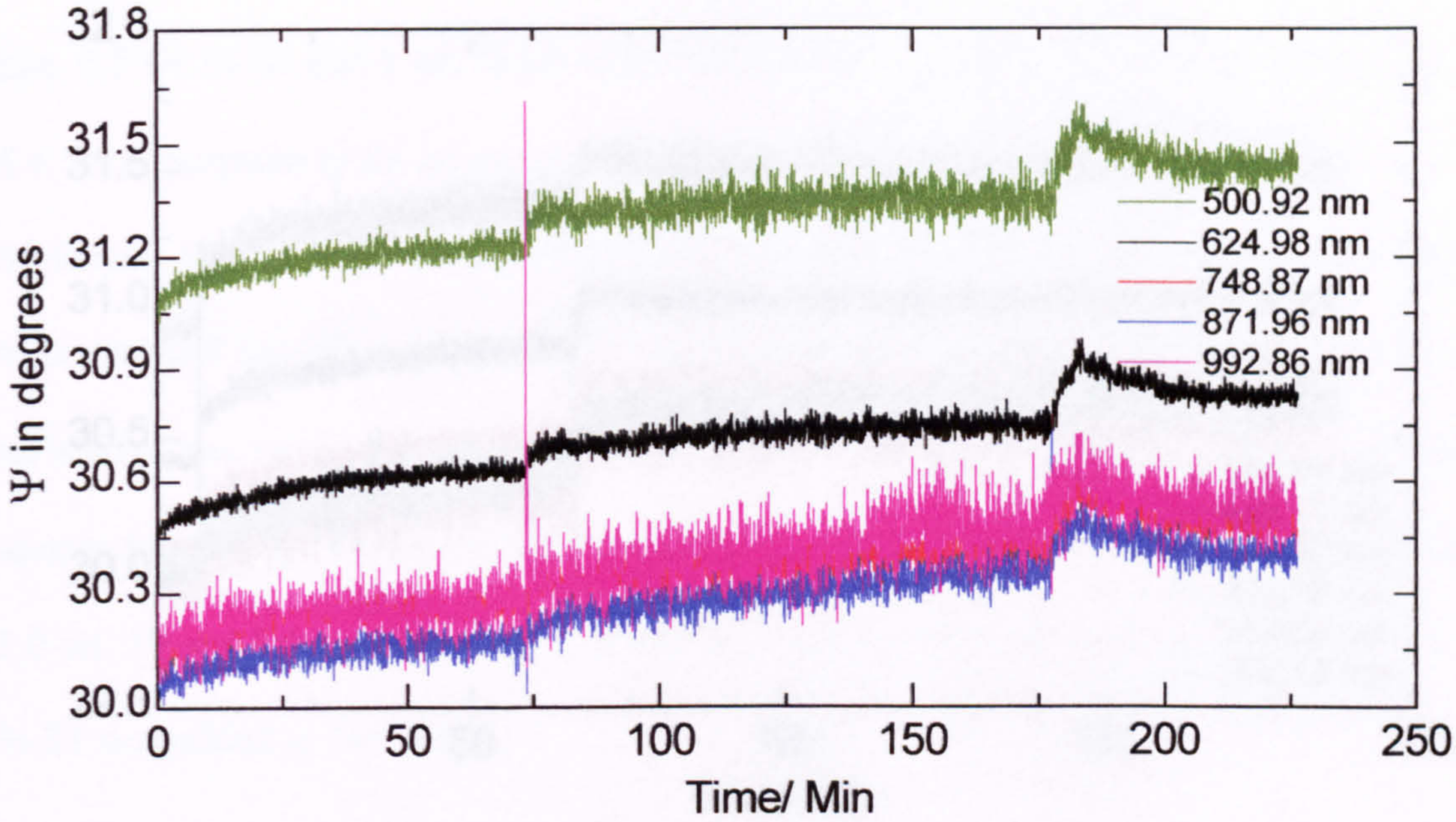

Figure 6.23: Plot of ψ as a function P1 concentration followed by the addition of a certain amount of S1

The experiment was started with 0.5 wt. % P1 solution and increased to 1.0 wt. % at 73 min. Each addition was followed by a rise in ψ value as seen in figure 6.23. 0.5 wt. % S1 was added at 177 min.

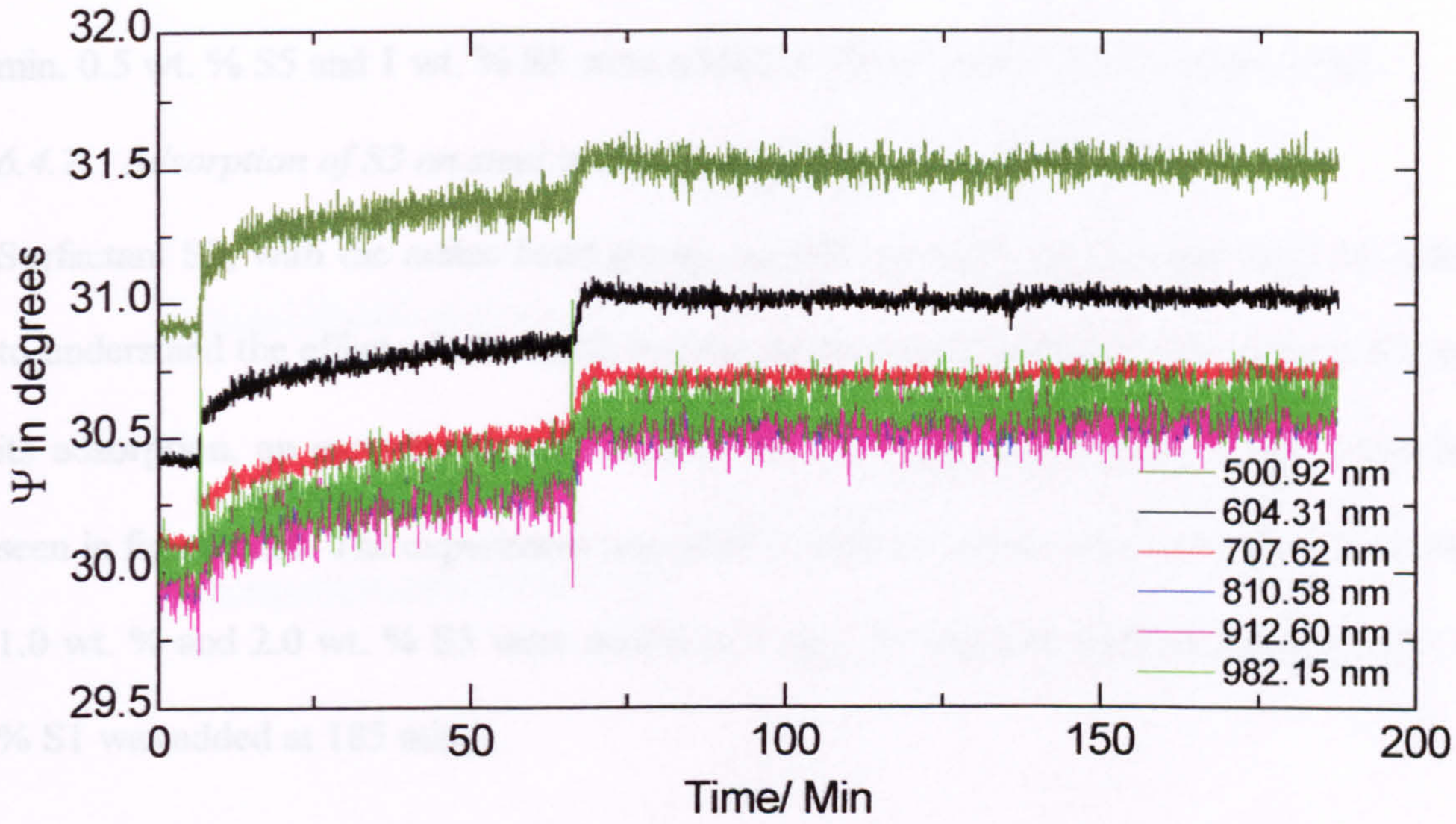

Figure 6.24: Plot of ψ as a function of time at different concentrations of P1 followed by the addition of certain amounts of S3

The experiment was started with isooctane only and then 1 wt. % P1 was added at 6 min. 0.5 wt. % S3 and 1 wt. % S3 were added at 66 min and 135 min, respectively.

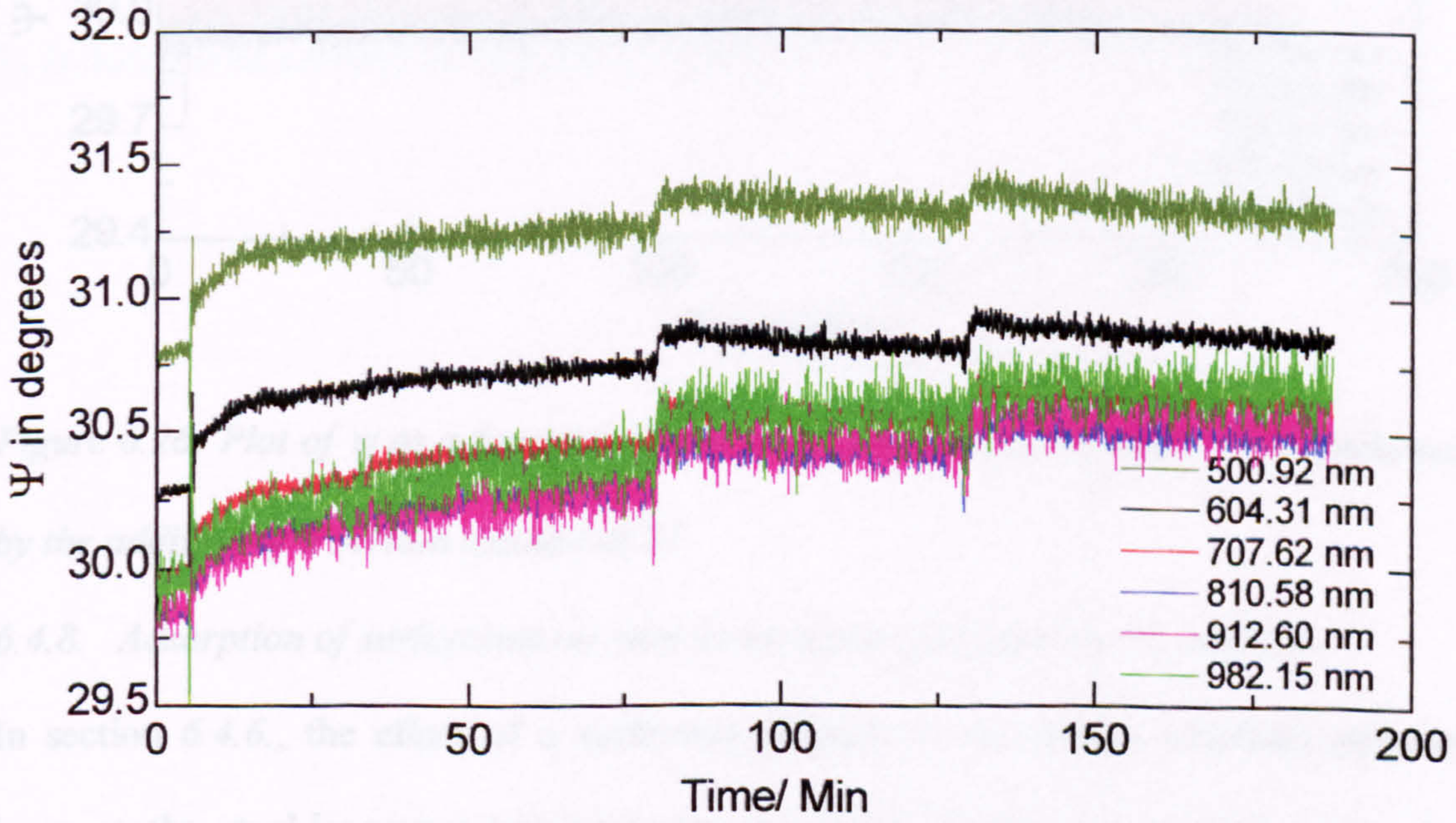

Figure 6.25: Plot of ψ as a function of time at different concentrations of P1 followed by the addition of certain amounts of S5

The experiment was started with isooctane only and then 1 wt. % P1 was added at 5 min. 0.5 wt. % S5 and 1 wt. % S5 were added at 79 min and 128 min, respectively.

6.4.7. Adsorption of S3 on steel in isooctane followed by S1 addition

Surfactant S3, with the amine head group, adsorbs strongly on stainless steel. In order to understand the effect of S1, which has the same number of butoxylate units as S3, on its adsorption, an experiment was carried out. The values of ψ thus obtained can be seen in figure 6.26. The experiment was started with isooctane only and then 0.5 wt. %, 1.0 wt. % and 2.0 wt. % S3 were added at 5 min, 72 min and 122 min, respectively. 1 % S1 was added at 185 min.

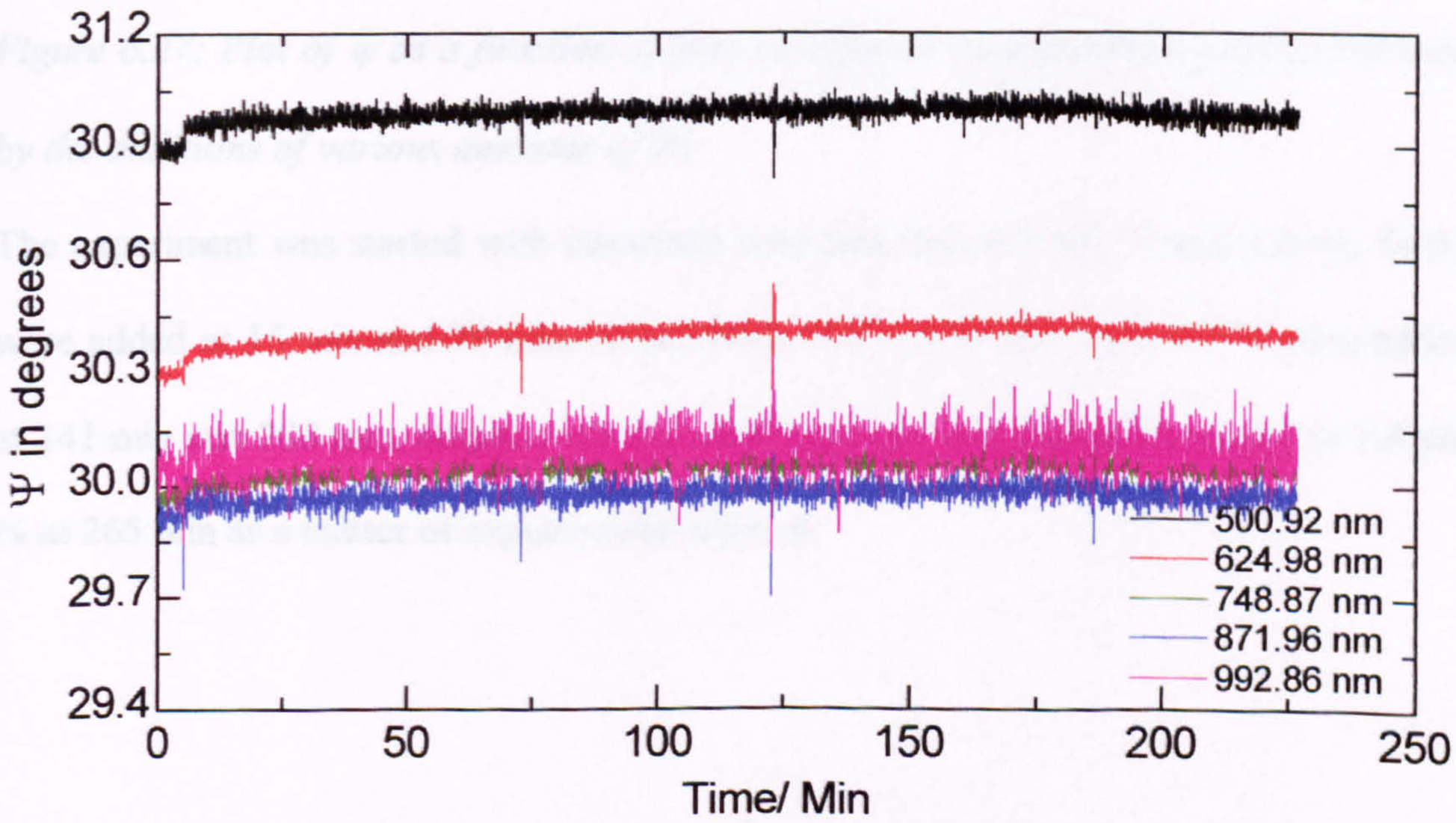

Figure 6.26: Plot of ψ as a function of time at different concentrations of S3, followed by the addition of a certain amount of S1

6.4.8. Adsorption of surfactants on steel in isooctane followed by P1 addition

In section *6.4.6.*, the effect of a surfactant addition to an already adsorbed polymer layer at the steel-isooctane interface was described. Similar experiments were also carried out to study the effect of polymer addition on an already adsorbed layer of a surfactant. The various results obtained are shown in figures 6.27 to 6.29.

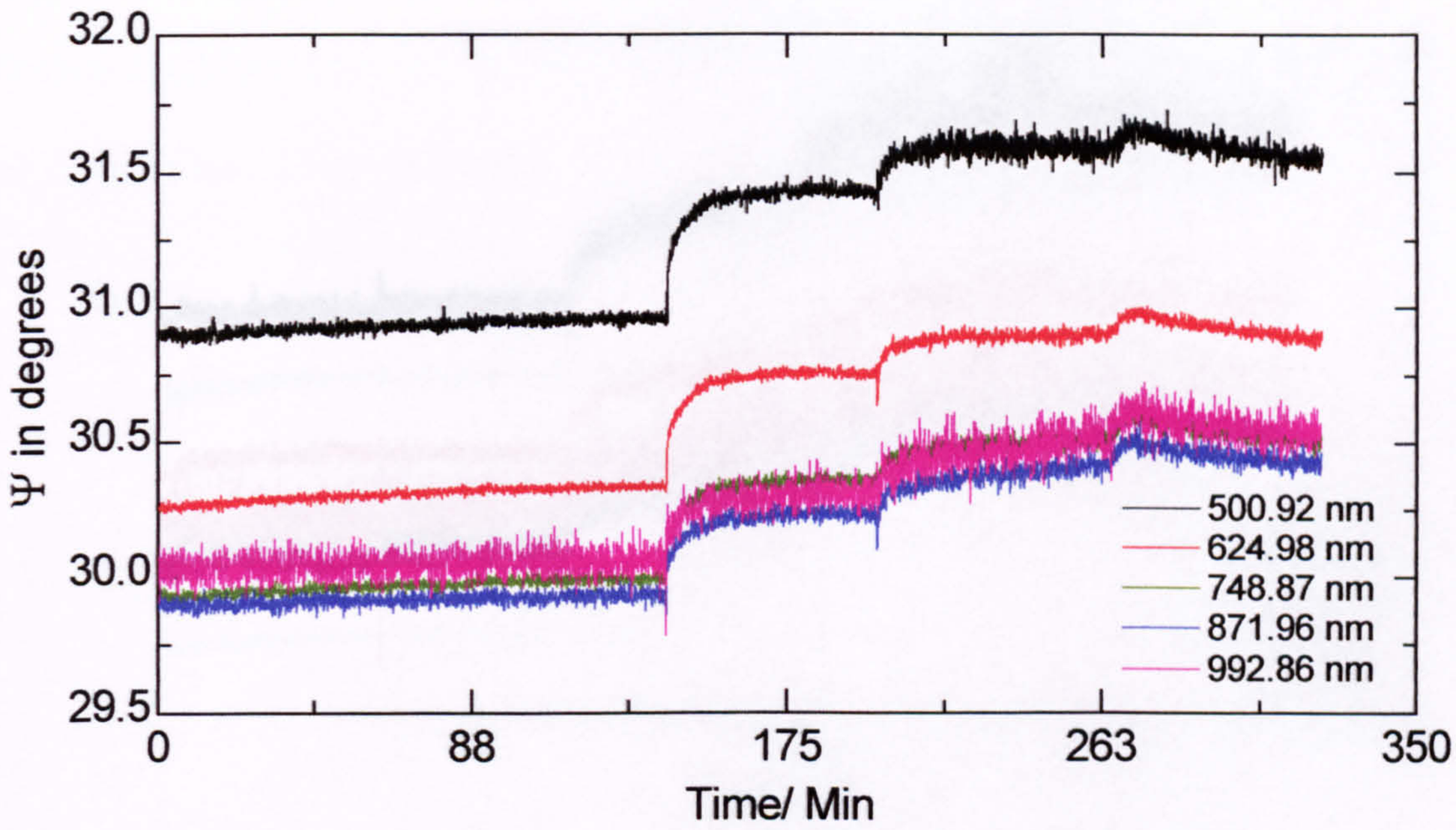

Figure 6.27: Plot of ψ as a function of time at different concentrations of S1, followed by the additions of various amounts of P1

The experiment was started with isooctane only and then 0.5 wt. % and 1.0 wt. % S1 were added at 15 min and 79 min, respectively. 0.5 wt. % and 1 wt. % P1 were added at 141 min and 200 min, respectively. S1 concentration was further increased to 1.4 wt. % at 265 min as a matter of experimental interest.

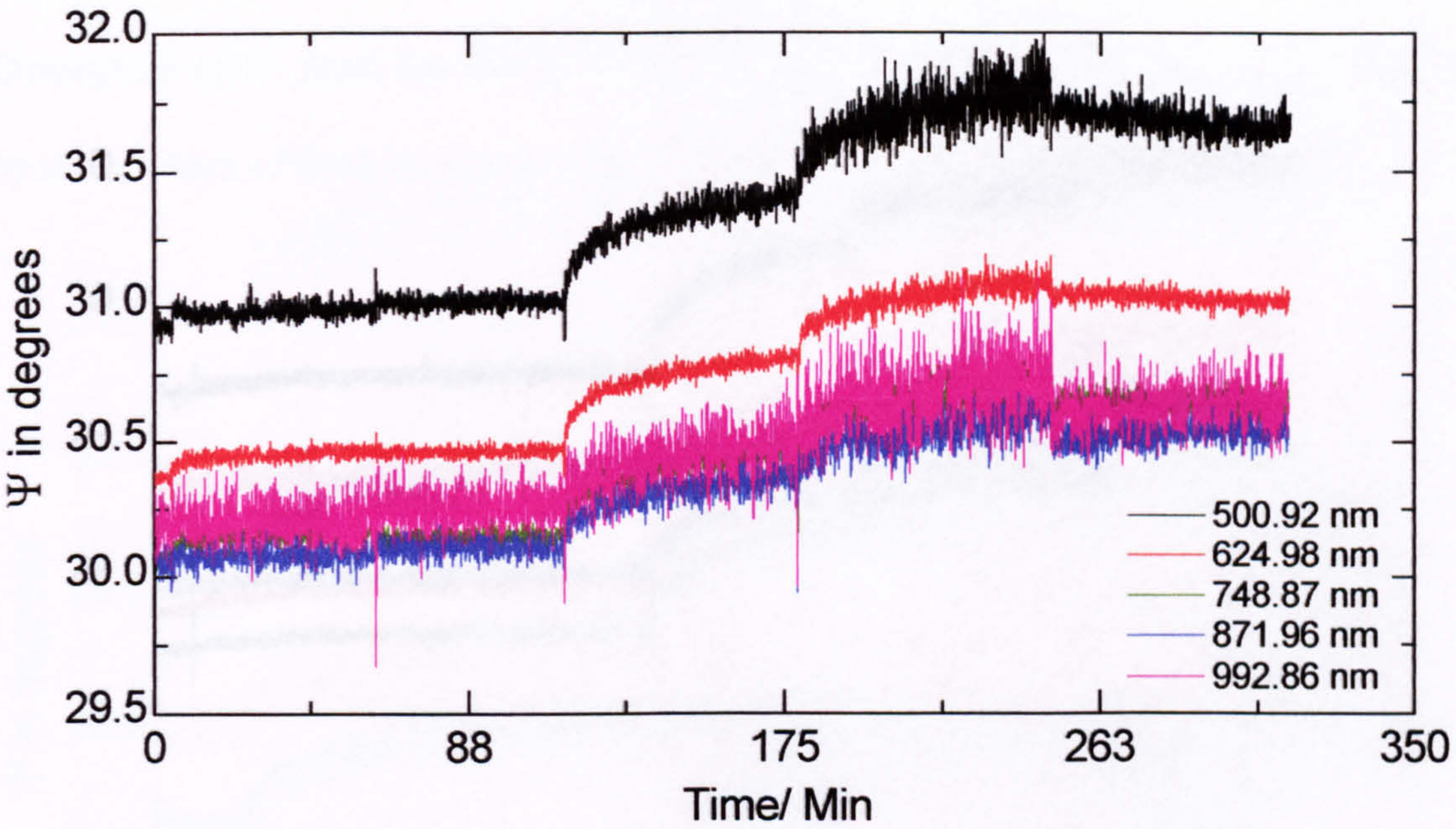

Figure 6.28: Plot of ψ as a function of time at different concentrations of S3, followed by the additions of various amounts of P1

The experiment was started with isooctane only and then 0.5 wt. % and 1.0 wt. % S3 were added at 5 min and 62 min, respectively. 0.5 wt. % and 1 wt. % P1 were added at 114 min and 178 min, respectively. S3 concentration was further increased to 1.5 wt. % at 248 min as a matter of experimental interest.

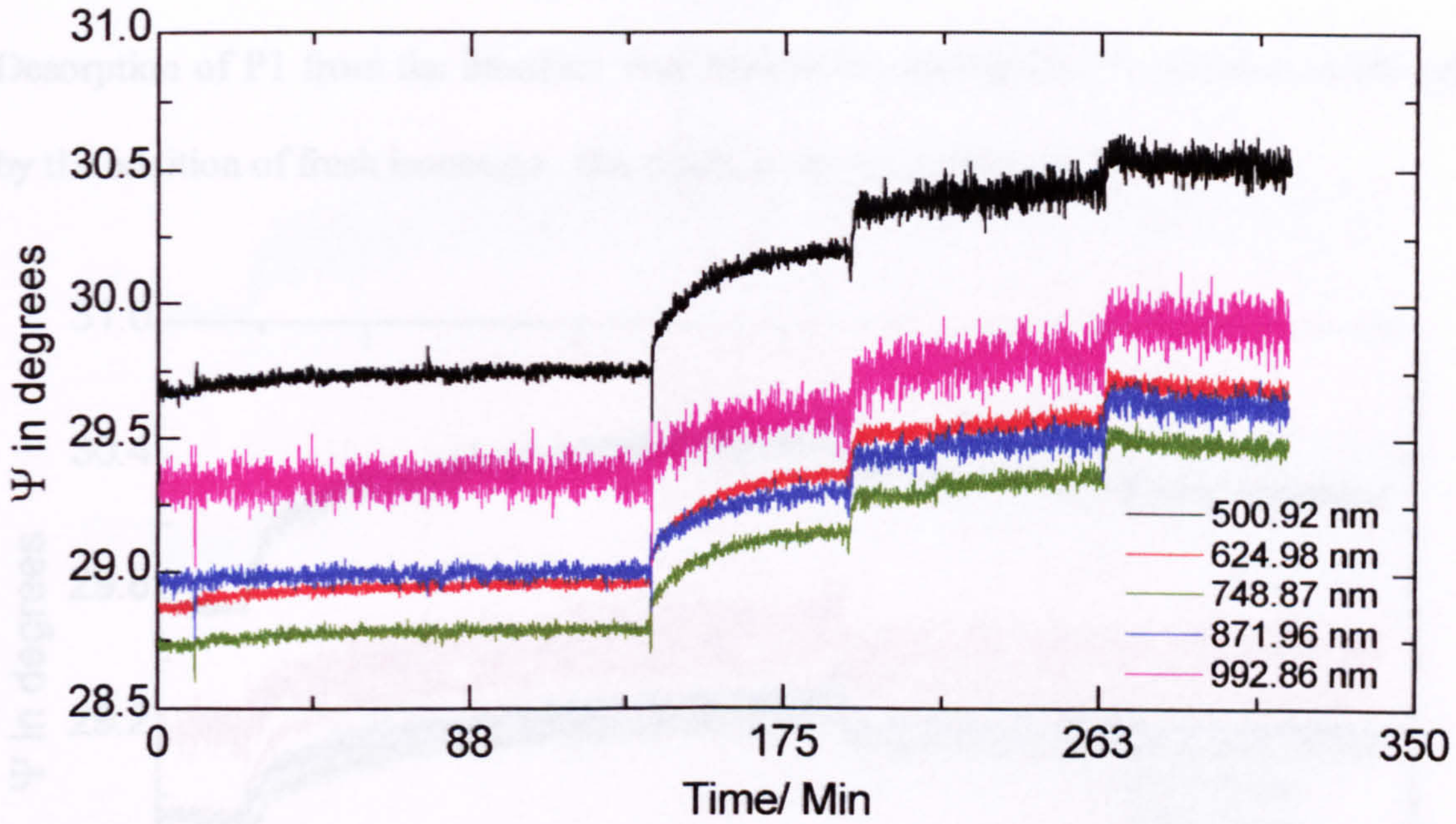

Figure 6.29: Plot of ψ as a function of time at different concentrations of S5, followed by the additions of various amounts of P1

The experiment was started with isooctane only and then 0.5 wt. % and 1.0 wt. % S5 were added at 10 min and 75 min, respectively. 0.5 wt. % and 1 wt. % P1 were added at 137 min and 193 min, respectively. S5 concentration was further increased to 1.5 wt. % at 263 min as a matter of experimental interest.

6.4.9. Desorption of P1 from steel-isooctane interface

Desorption of P1 from the interface was studied by diluting the P1 solution in the cell by the addition of fresh isooctane. The result is shown in figure 6.30.

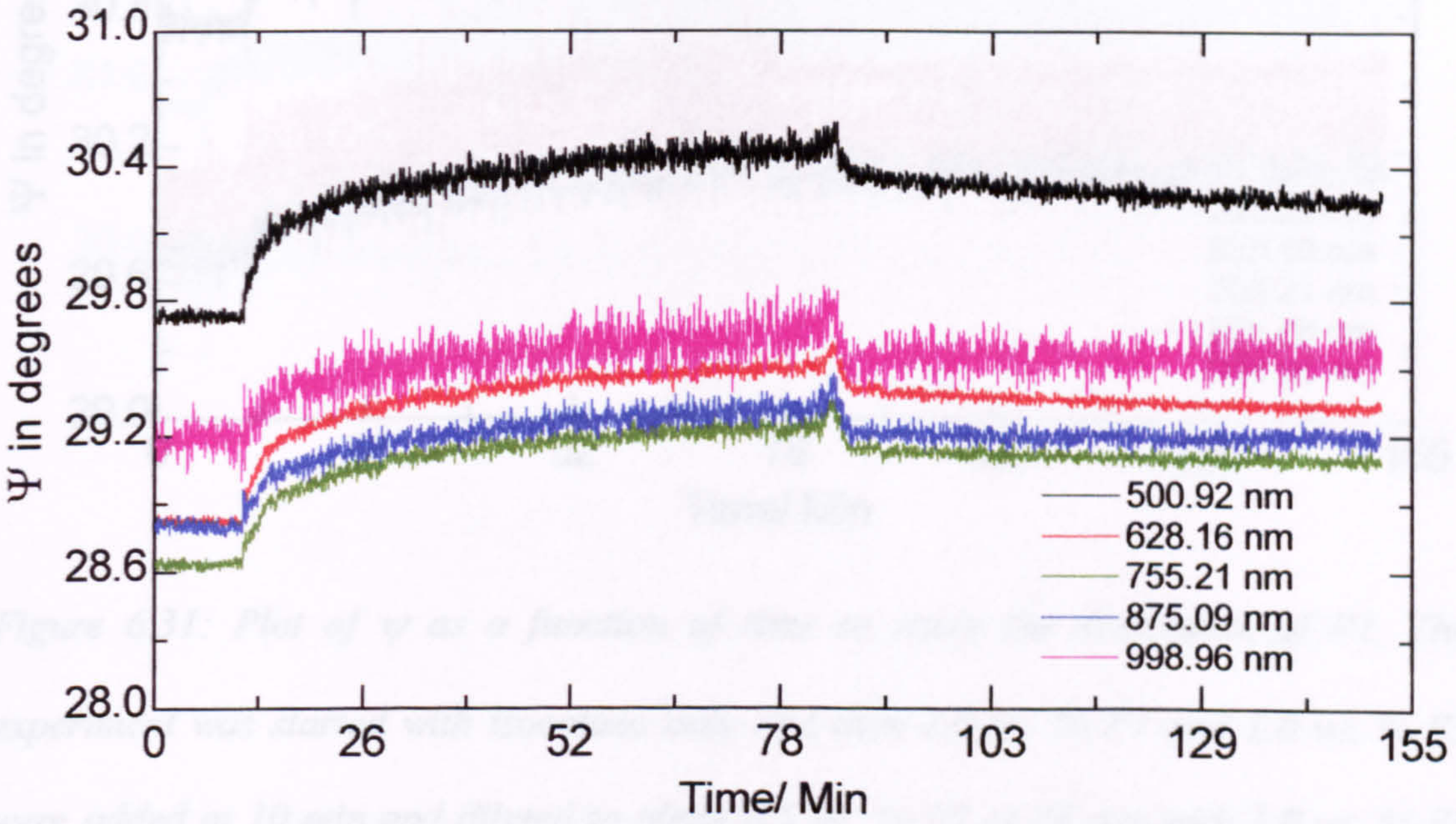

Figure 6.30: Plot of ψ as a function of time to study the desorption of P1. The experiment was started with isooctane only and then 1.0 wt. % P1 was added at 11 min and diluted to 0.62 wt. % at 82 min.

Desorption of 1.0 wt. % P1 and 1.0 wt. % S3 from the interface was also studied by diluting the mixture solution in the cell by the addition of a 1.0 wt. % S3 solution. The result is shown in figure 6.31.

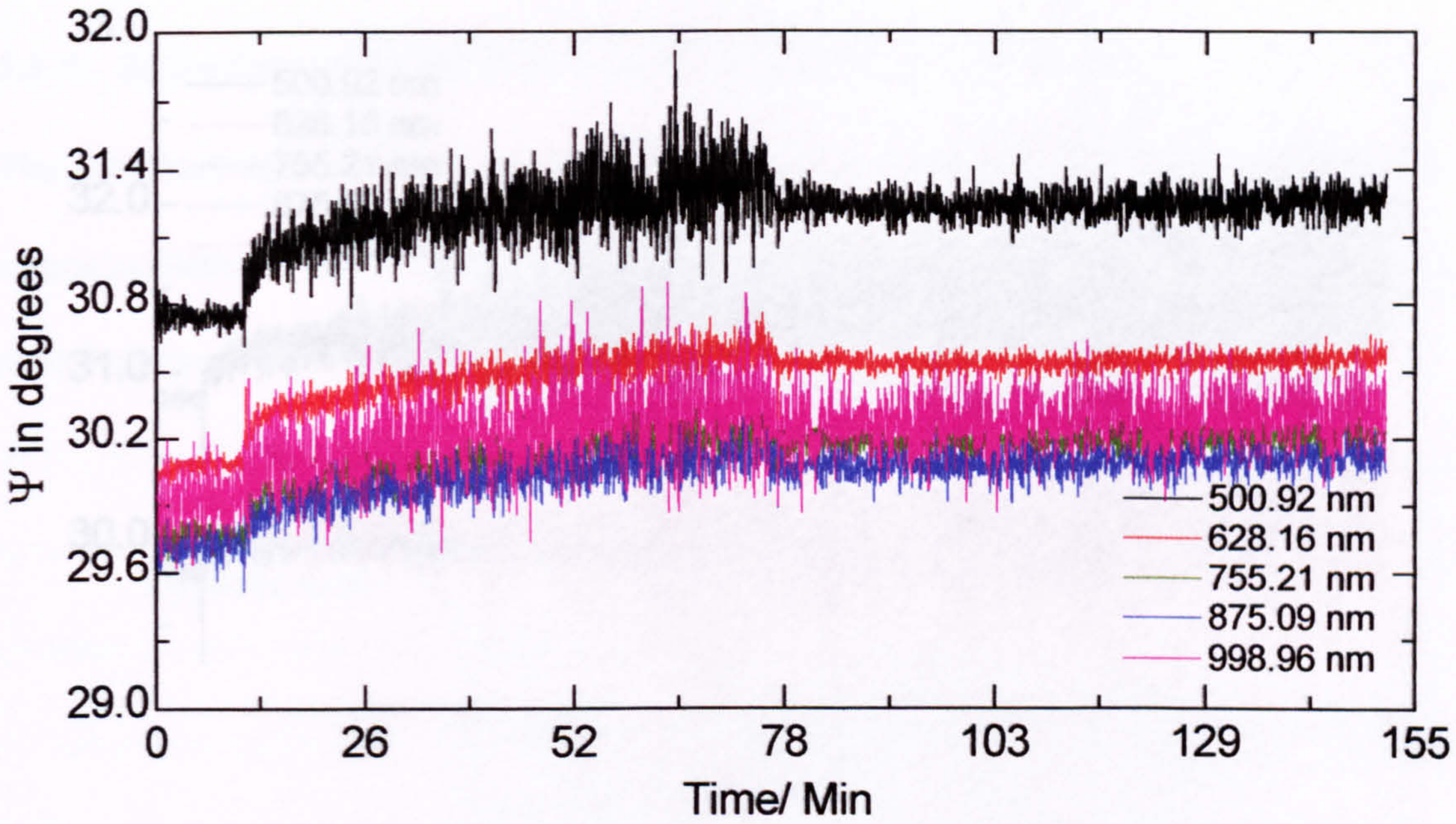

Figure 6.31: Plot of ψ as a function of time to study the desorption of P1. The experiment was started with isooctane only and then 1.0 wt. % P1 and 1.0 wt. % S3 were added at 10 min and diluted to about 0.5 wt. % P1 at 73 min with 1.0 wt. % S3 solution.

Desorption of 1.0 wt. % P1 and 1.0 wt. % S3 from the interface was also studied by diluting the mixture solution in the cell with the addition of a 1.0 wt. % P1 solution. The result is shown in figure 6.32.

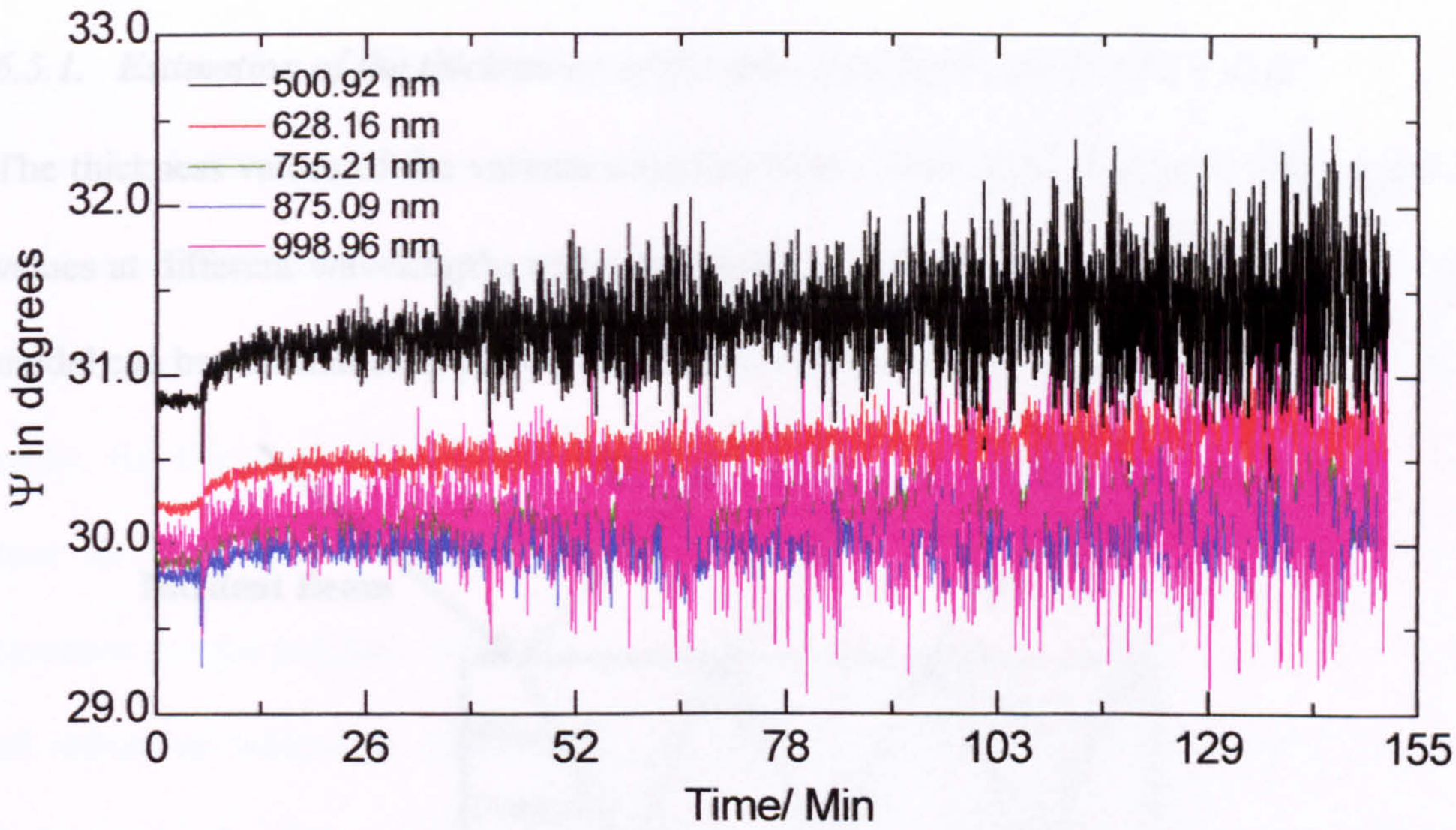

Figure 6.32: Plot of ψ as a function of time to study the desorption of P1. The experiment was started with isooctane only and then 1.0 wt. % P1 and 1.0 wt. % S3 were added at 5 min and diluted to about 0.6 wt. % S3 at 68 min with 1.0 wt. % P1 solution.

6.5. Analysis of results

6.5.1. Estimation of the thicknesses of the adsorbed layers on stainless steel

The thickness values of the various adsorbed layers have been obtained by fitting the ψ values at different wavelengths using the model of an organic film at the interface. This model can be schematically presented as shown below:

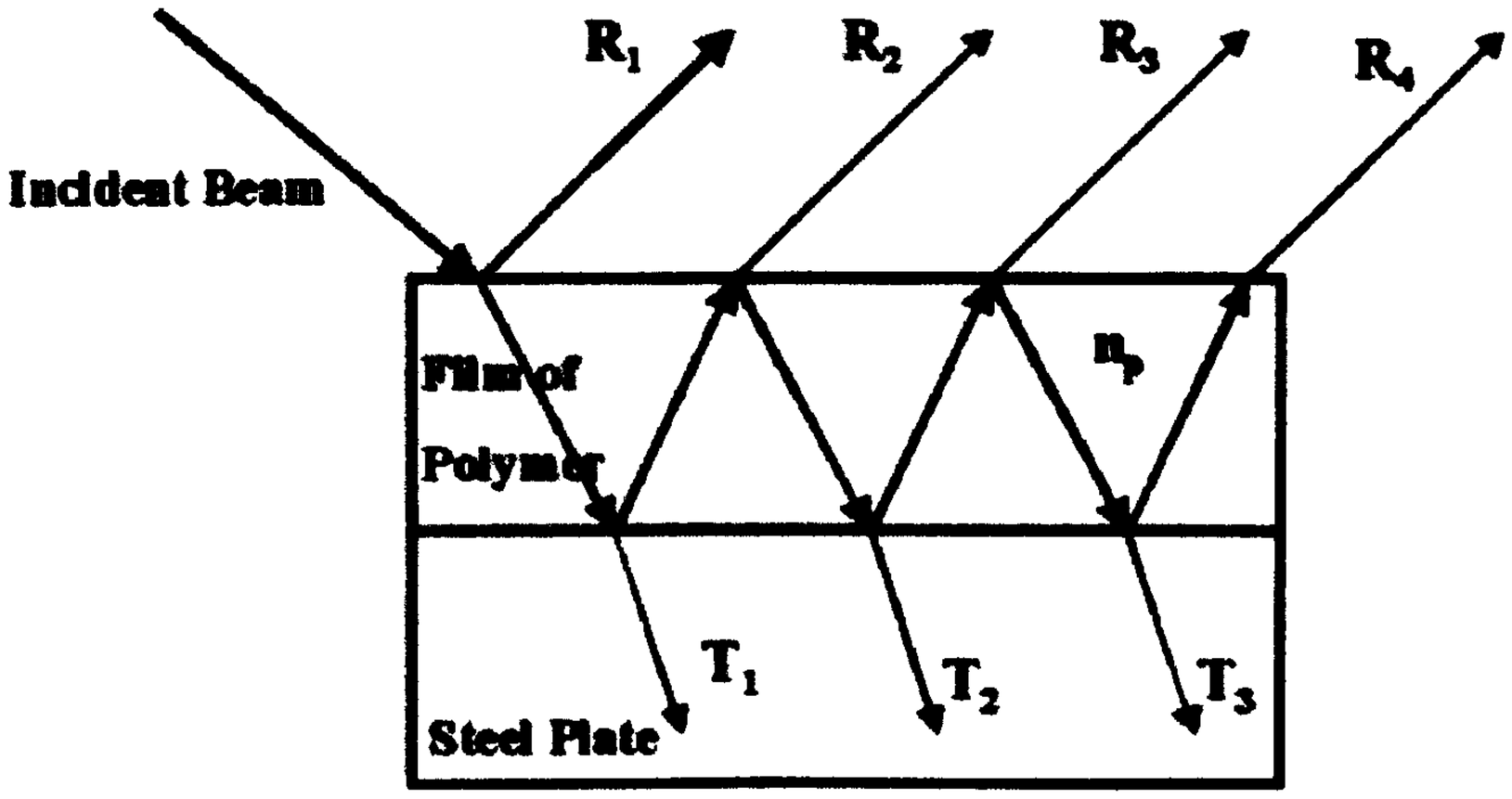

Figure 6.33: A simple model representing multiple reflected and transmitted beams for a single polymer layer at the steel/isooctane interface, assuming that the steel acts as an optically thick substrate

The presence of an adsorbed layer modifies the reflection coefficients so that both Ψ and Δ values change. The reflection of polarised light from the steel plate in isooctane was modelled using a theoretical fit to create a base model for the steel. The difference in the values of Ψ and Δ, as compared to the base model, due to the adsorbed polymer layer can be measured using the ellipsometer. The organic layer model, as shown in figure 6.33, allows the fitting of the values of Ψ in order to derive the thickness and optical properties of the organic film. However, in principle, a multilayer model can be used but this was not attempted in this study. The single layer model appeared sufficient enough to analyse the data obtained, and it is unlikely for such systems in apolar media to form multilayers. It may be noticed from figure 6.33 that there can, in principle, be an infinite number of reflected and transmitted beams. However, the

splitting of the beam into reflected and transmitted components at each reflection would reduce the amplitude of the subsequent reflections such that the reflected and transmitted beams dies out eventually[1]. It was mentioned earlier that the organic layer model was used to fit the experimental values of Ψ. This can be done by varying the thickness, refractive index and the extinction coefficient values of the layer. In this study, the thickness of the theoretical model used for the analysis was varied until the best fit was obtained. The refractive indices at different wavelengths were kept constant for the polymer and the surfactants. The model, however, used a preset range of refractive indices at different wavelengths supplied by the manufacturers of the instrument. A plot of these preset values of the refractive indices at different wavelengths obtained from the theoretical organic layer model is shown in figure 6.34:

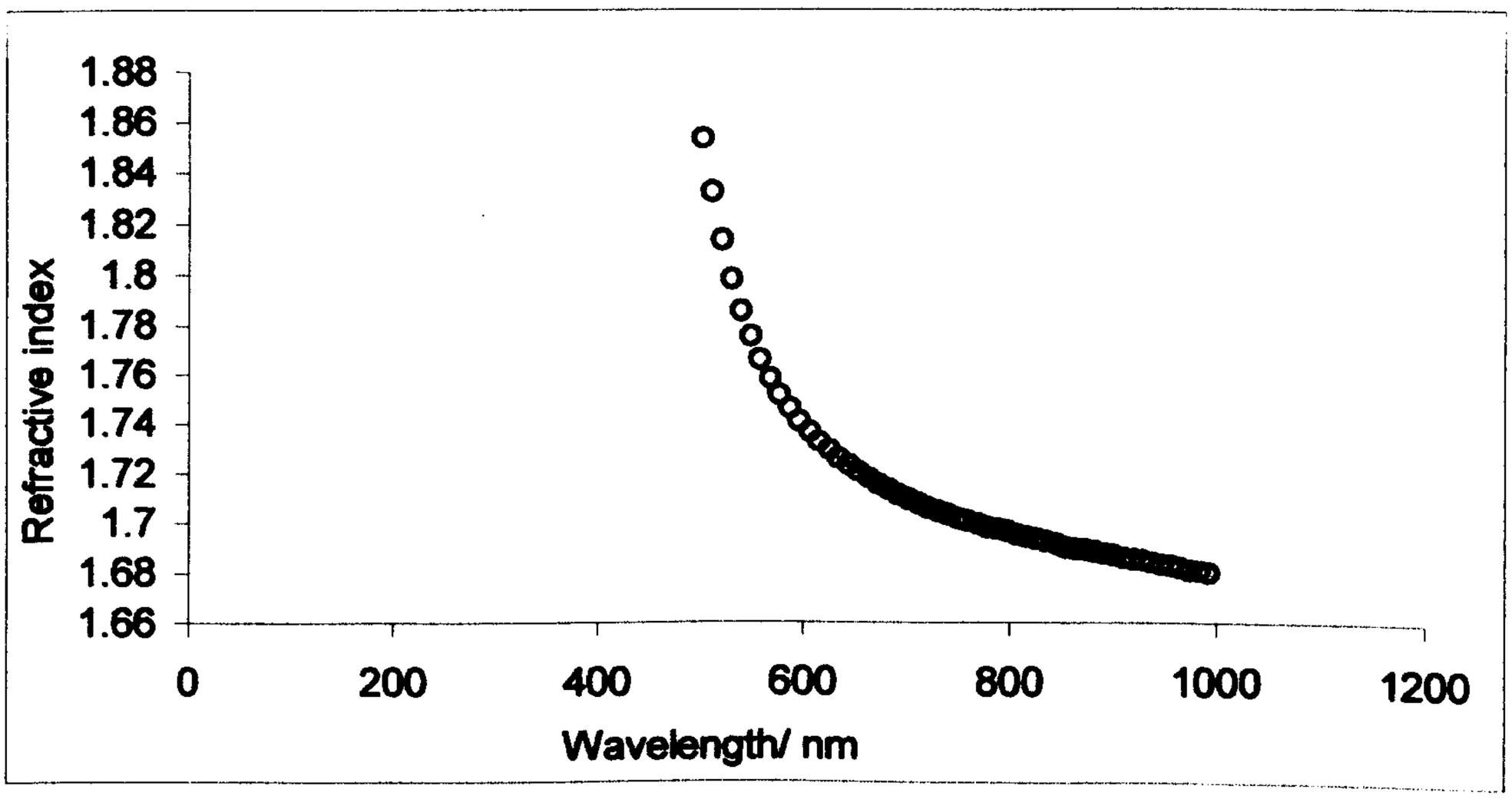

Figure 6.34: A refractive index profile obtained from the polymer layer model

The change in the thickness for the various systems studied are shown in figures 6.35 to 6.38.

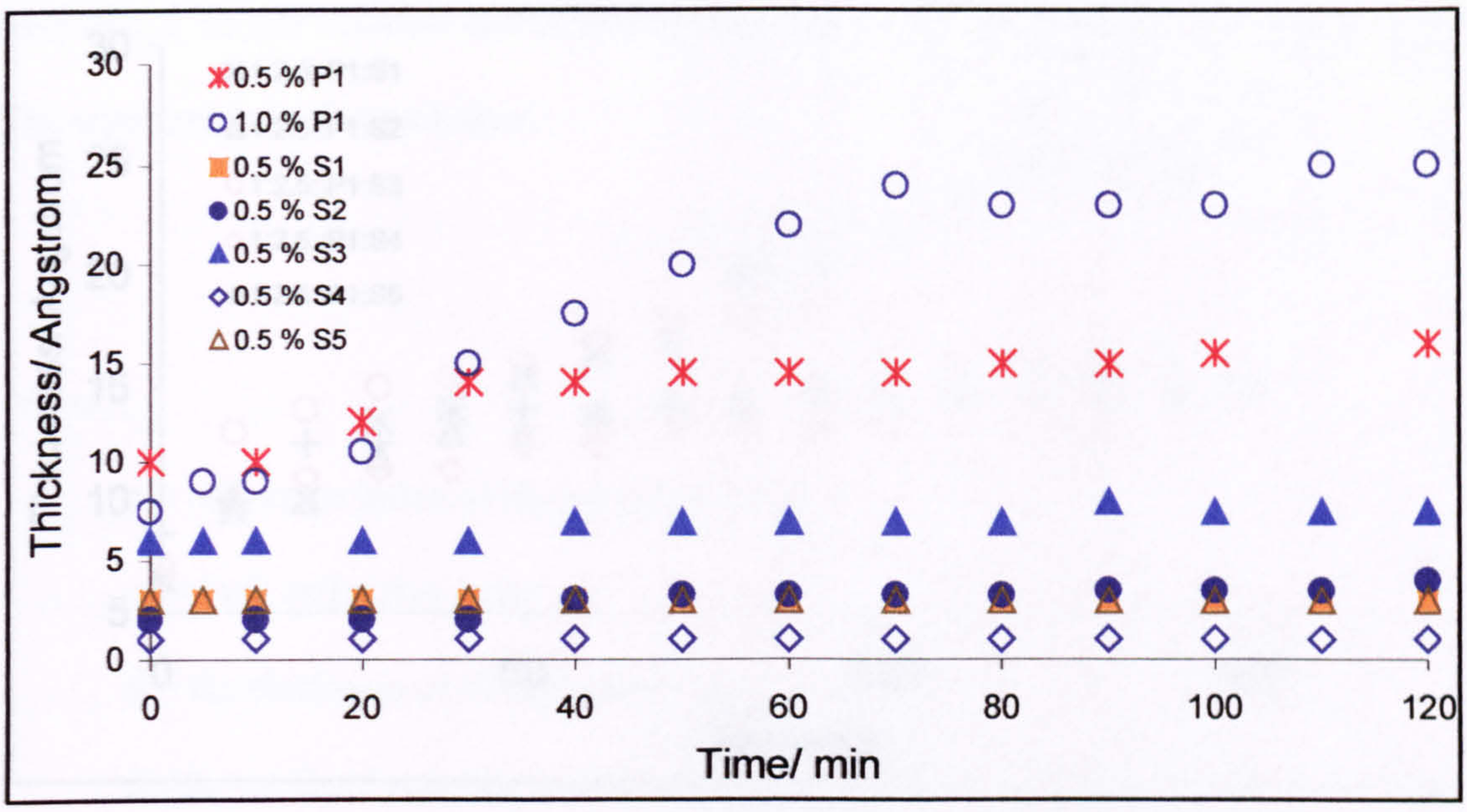

Figure 6.35: Thicknesses of various adsorbed layers at the steel-isooctane interface

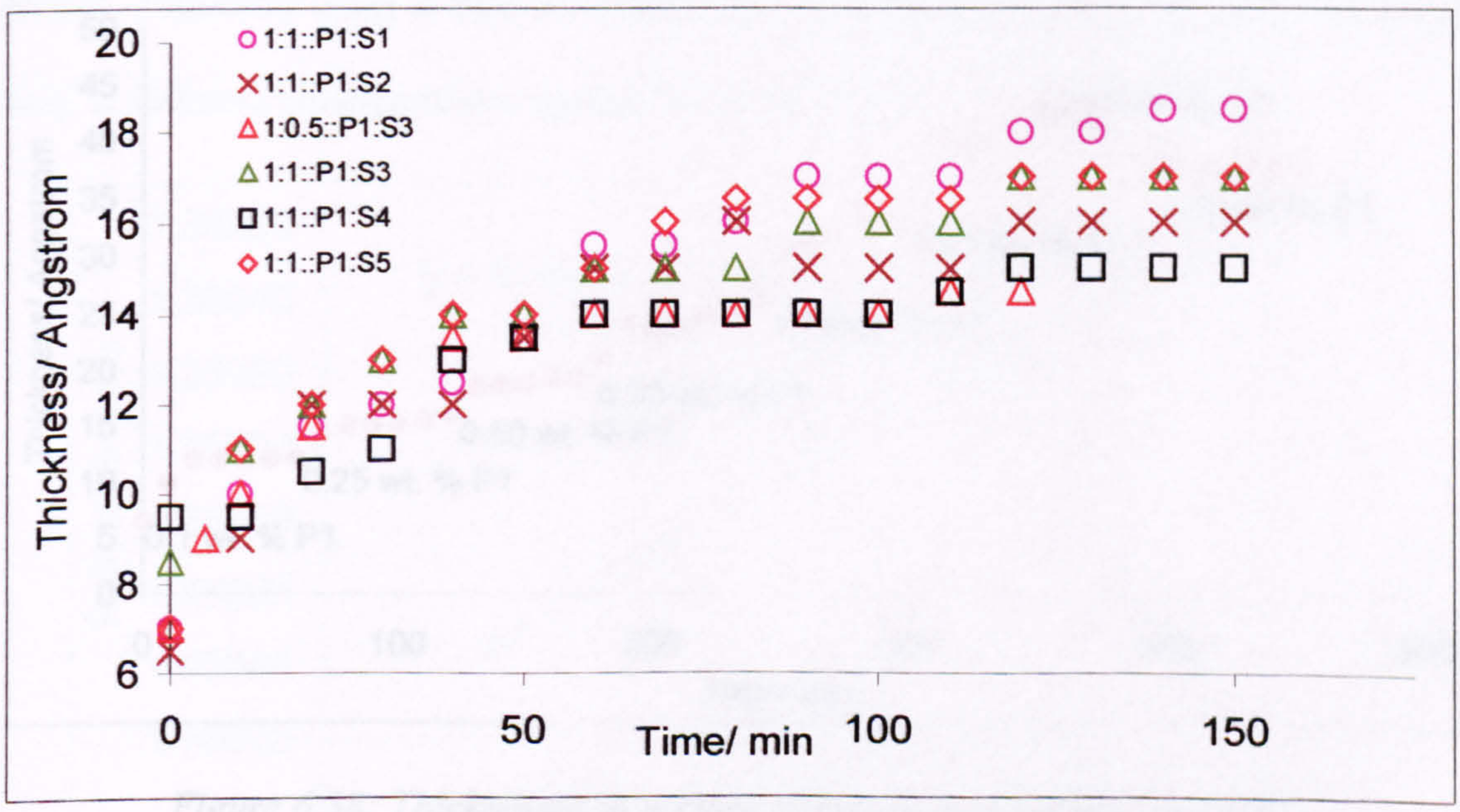

Figure 6.36: Thicknesses of various 1:1 mixtures of the polymer and the surfactants and a 1:0.5 mixture of P1 and S3

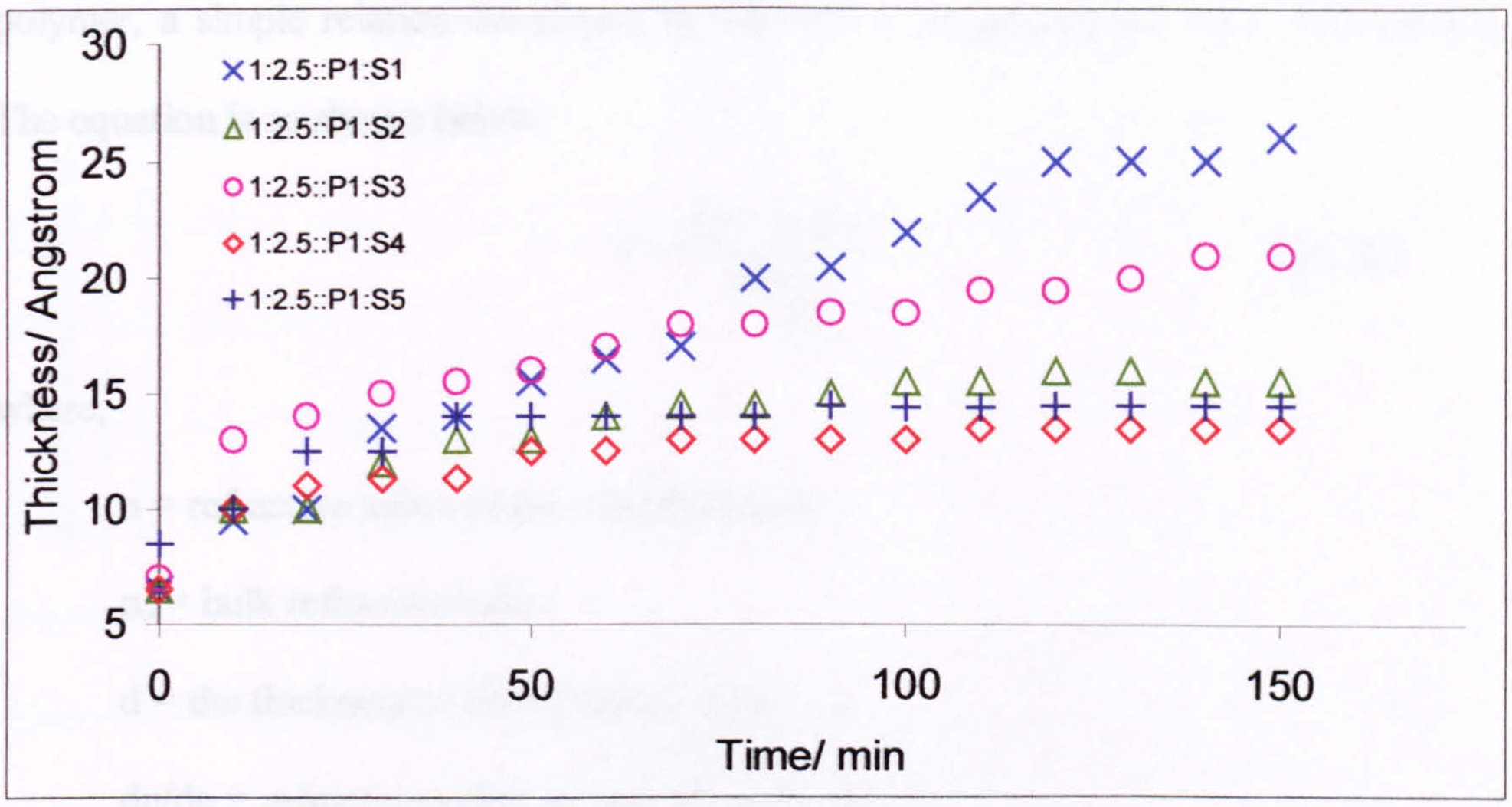

Figure 6.37: Thicknesses of various 1:1.25 mixtures of the polymer and the surfactants

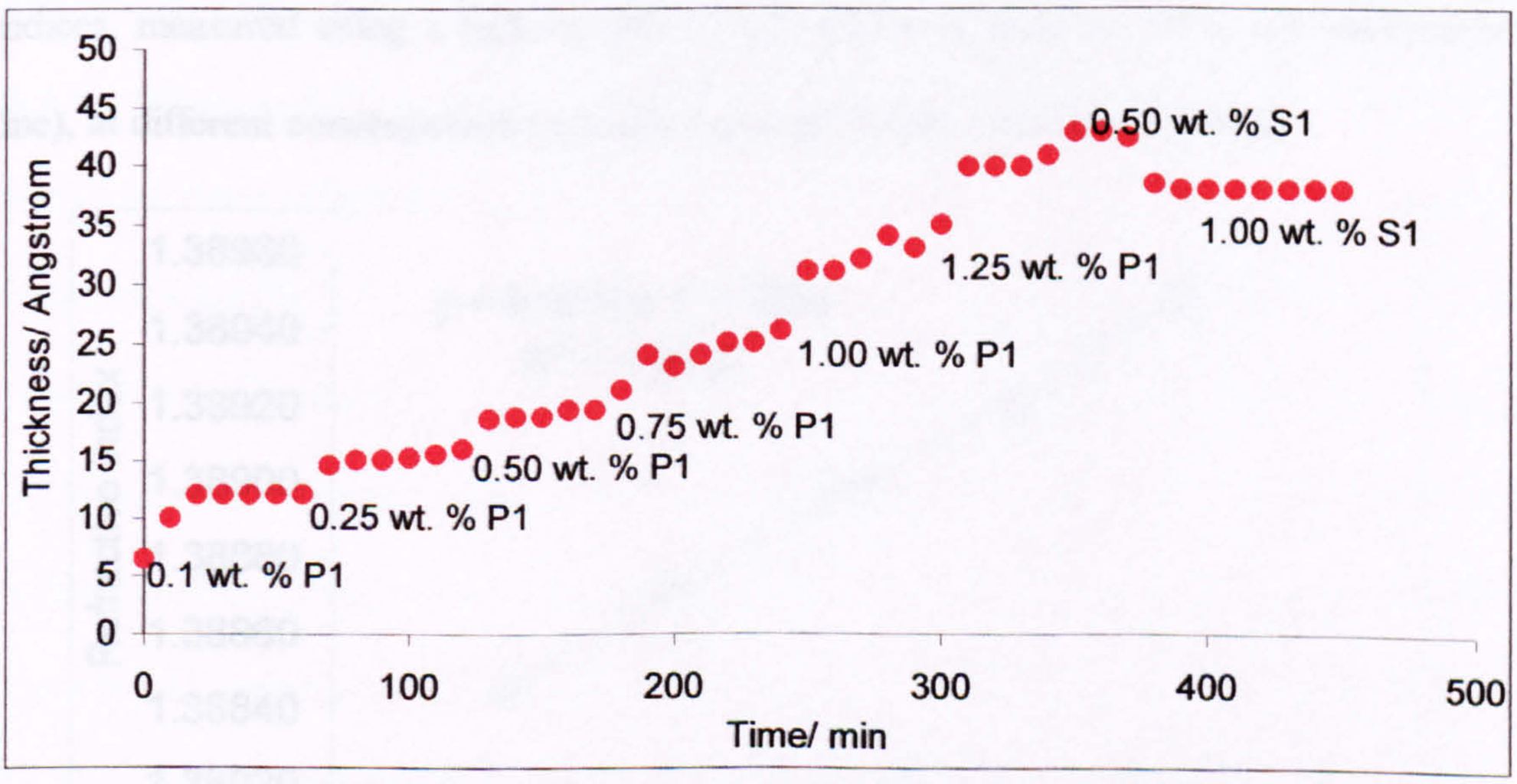

Figure 6.38: Thicknesses at various concentrations of the polymer

In figure 6.38, surfactant S1 was added at the end of the experiment to study its effect on polymer adsorption.

6.5.2. Adsorption isotherm of P1 at the steel-isooctane interface

The thickness of the various adsorbed layers have been obtained by fitting the ψ values at different wavelengths using the model of an organic film at the interface as already explained in the previous section. In order to derive the adsorption isotherm of the

polymer, a simple relation developed by De Feiter, Benjamins and Veer was used[5]. The equation is as shown below.

$$\Gamma = \frac{(n - n_o)\, d}{dn/dc} \qquad \text{Eqn. 6.7}$$

where,

n = refractive index of the adsorbed layer

n_o = bulk refractive index

d = the thickness of the adsorbed layer

dn/dc = refractive index increment of the solute

The refractive index increment of the polymer was obtained by plotting the refractive indices, measured using a high accuracy *Abbe* Refractometer at 589.6 nm (sodium D line), at different concentrations against the concentrations as shown below.

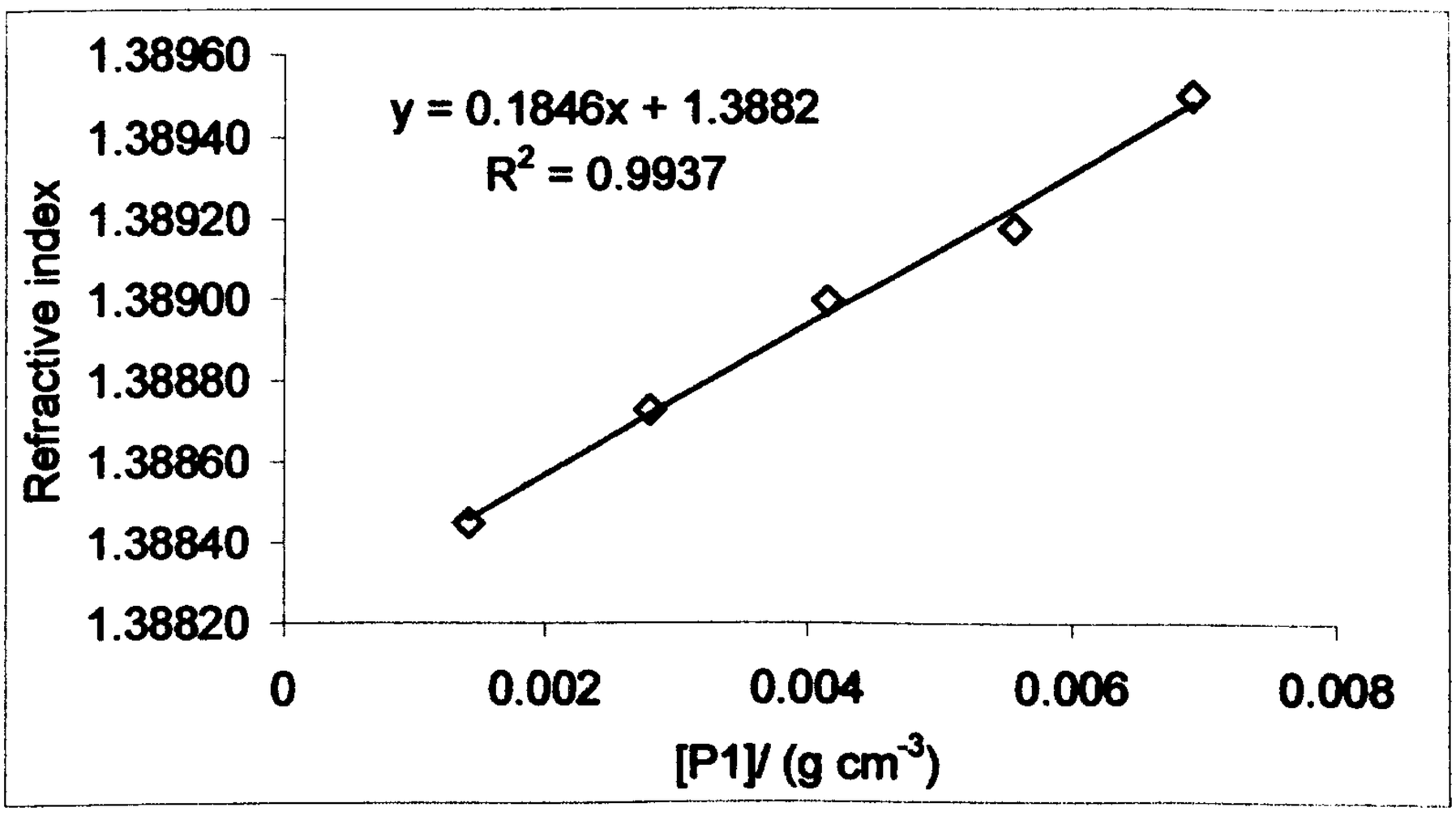

Figure 6.39: Plot of refractive index as a function of polymer concentration

The corresponding adsorption isotherm of the polymer is shown in figure 6.40.

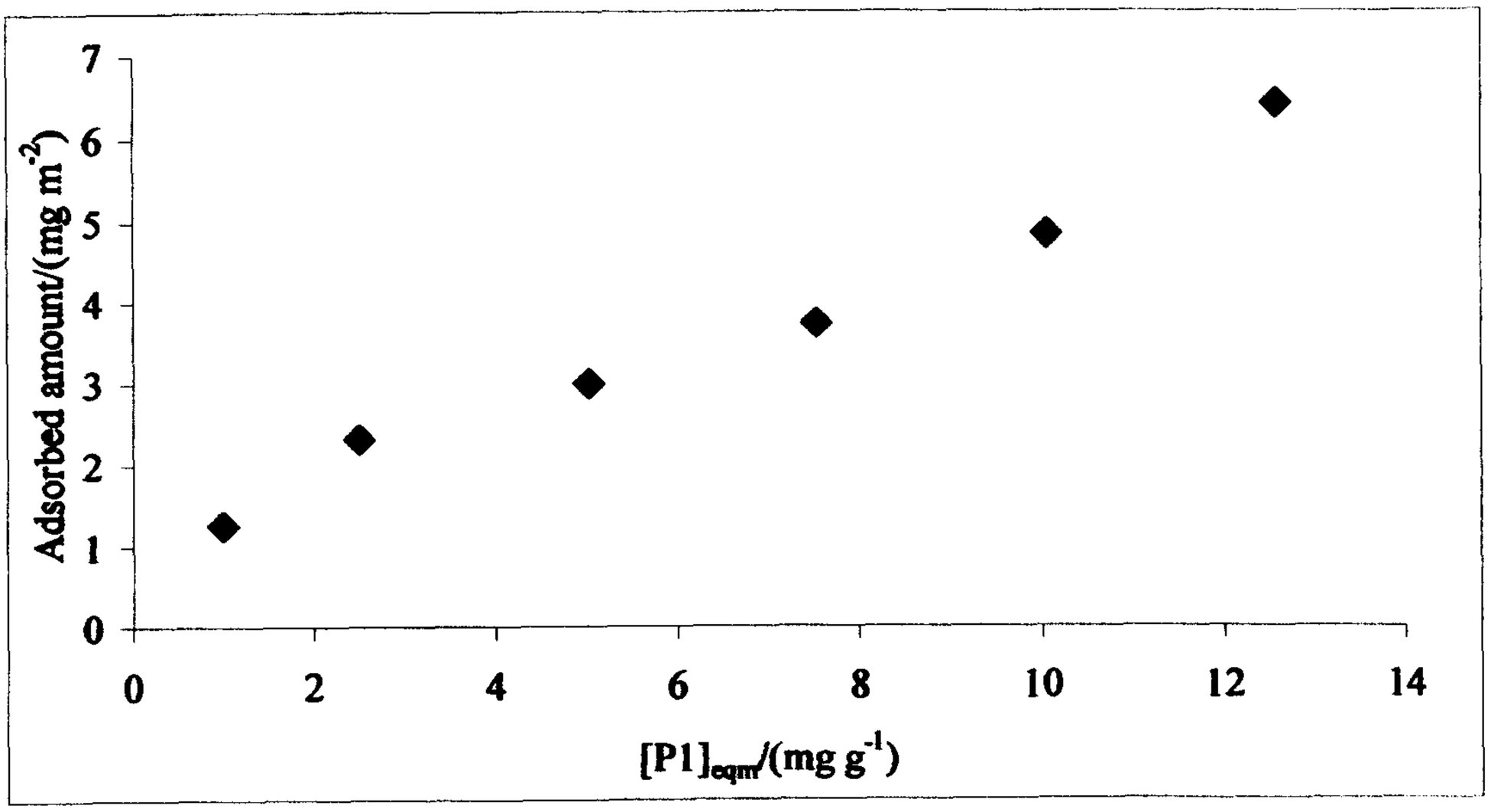

Figure 6.40: Adsorption isotherm of the polymer on stainless steel obtained using ellipsometry

6.6. Analysis and Discussion

The constant values of ψ recorded at different times over the whole wavelength range (figure 6.6) show that the steel/isooctane interface did not undergo any change with time thus excluding effects of surface leaching by the solvent or dissolution of impurities at the interface. Adsorption kinetics measurements showed that polymer adsorption on steel reached equilibrium in less than 90 min (figure 6.7). The kinetics measurement for the surfactant molecules, on the other hand, showed no change in the values of ψ with time suggesting very fast adsorption kinetics with a very small surface density of the surfactants. Such a fast adsorption process was also noticed during kinetic experiments carried out by measuring the surface excess of the polymer (chapter 3). Interestingly, the addition of any surfactant to the polymer, even at high ratios, seemed to have only a minor effect on the kinetics of adsorption of the polymer as can be seen in figures 6.12 to 6.21. It is clear from these figures that P1 was the dominant adsorbing species of all the polymer and surfactants used in this study. The values of ψ also showed a corresponding rise with each addition of the polymer (figure 6.22) suggesting that it continuously adsorbed onto the surface. It is suggested that the polymer molecules most likely formed aggregates at the interface in chapter 3 and this could be an explanation for this rise. Increasing the concentration could be leading to the formation of hemimicelles[11, 12] or hemimicellar aggregates at the interfaces[13]. In the same experiment, it was noticed that the addition of surfactant S1 led to a small rise and then a gradual decrease in the value of ψ, indicating a drop in the adsorbed amount. However, a further increase from 0.5 wt. % to 1.0 wt. % S1 did not have any significant effect on the values of ψ. This behaviour is further confirmed in figure 6.24 and the observation that further addition of the surfactant did not lead to further reduction in the values of ψ is confirmed in figure 6.25. The increase in ψ values was more pronounced for surfactants S3 and S5, which have an amine head group and a

benzene ring respectively. These functionalities could be contributing to the polarisation of the reflected beam leading to an increase in the values of ψ. The second addition of S5 in figure 6.25 led to a more pronounced increase in ψ as compared to the addition of S3 (figure 6.24). This could be due to the fact that S5 has a benzene head group. The repulsion of a polar headgroup by an apolar medium could also explain the minute rise, visible on closer inspection, seen for the second addition of S3 in figure 6.24. After all the additions, there was always an initial rise and then a gradual decrease with time. This could imply a fast interaction/adsorption phenomena occurring at the interface during addition followed by gradual equilibration. Care was taken not to add the polymer/surfactant solutions right on top the steel plate, placed in the middle of the cell, by pipetting in the solutions from the corner of the quartz cell. Surfactant S1 did not seem to affect the adsorption of surfactant S3 as shown in figure 6.26. Previously in chapter 3, it was shown that there was no effect of the addition of S1 on the adsorption isotherm of S3. From these experiments, it was likely that the alkoxylate units of the surfactants lie flat on the surface and interact with the polymer, if present.

Figures 6.27, 6.28 and 2.29 show that the adsorption thickness was independent of which species occupied the surface first. Even though the surfactants had been adsorbed before the polymer, the polymer was the one that gave the thickest layer. However, if the surface had been first occupied by the surfactants, the polymer could only adsorb on the steel surface by displacing the surfactant molecules or by associating with the surfactant molecules to form aggregates. Therefore, it is likely that the adsorbed layer structure is governed by the polymer-surfactant interactions as has been observed in aqueous based studies[4, 9]. Thus, the polymer and the surfactant could be synergistically adsorbing at the interface. From the experiments carried out to understand the effects of dilution of the polymer solution on the adsorbed polymer layer, it appeared as if the polymer is being depleted from the interface (figure 6.30).

Also, this decrease in the value of ψ upon dilution occurred only with the polymer and not surfactant S3 when the two were mixed together (figures 6.31 and 6.32). This could only suggest that the polymer is the primarily adsorbed species determining the layer thickness but it could be easily depleted from the interface by dilution while not being completely displaced.

The thicknesses obtained for the various layers also show that the polymer formed the thickest layer. The thickness was almost double for 1.0 wt. % P1 as compared to that of 0.5 wt. % P1 (figure 6.35). All the surfactants gave very small thicknesses indicating a flat conformation on the surface. However, S3 gave a thicker layer which could be explained by the fact that it has a propylene amine headgroup and an alkane chain which could orient normal to the interface. S5 has twice the number of butoxylate units as S4 and this seems to be reflected in the thickness values too as it always forms a thicker layer. This could be an effect of the higher molecular weight of S5. Similar trends indicating an increase in the adsorbed amount with increasing molecular weight of the adsorbing species have been previously reported[14]. Figures 6.36 and 6.37 also show that surfactant S1 interacts strongest with the polymer thus giving the thickest layers.

The adsorption isotherm obtained from ellipsometry suggest a type II type isotherm indicating aggregation at the interface which ties in well with the assumption that the polymer is forming aggregates at the interface (chapter 3).

6.7. References

1. J. A. Woollam Co., I., *Guide to using WVASE32*. 2001, Lincoln: WexTech Systems, Inc.
2. Hilfiker, J.N., Synowicki, R. A, Bungay, C. L. and Carpio, R., *Solid State Technology*, 1998. 41.
3. Bungay, C., Hilfiker, J., Liphardt, M. and Synowicki, R., *Vacuum & Thinfilm*, Oct. 1999.
4. Joabsson, F., Thuresson, K. and Lindman, B., *Langmuir*, 2001. 17: p. 1499 - 1505.
5. De Feijter, J.A., Benjamins, J. and Veer, F. A., *Biopolymers*, 1978. 17: p. 1759 - 1772.
6. Azzam, R.M.A., and Bashara, N. M., *Ellipsometry and polarized light*. 1988, Amsterdam: North-Holland Physics Publishing.
7. Woollam, J.A., *Ellipsometry, Variable Angle Spectroscopic*, in *Wiley Encyclopedia of Electrical and Electronics Engineering Supplement 1*, J.G. Webster, Editor. 2000, John Wiley & Sons, Inc. p. 109 - 117.
8. Fleer, G.J., Cohen Stuart, M. A., Scheutjens, J. M. H. M., Cosgrove, T and Vincent, B, *Polymers at interfaces*. 1993: Chapman & Hall.
9. Lu, J.R., Thomas, R. K. and Penfold, J., *Advances in Colloid and Interface Science*, 2000. 84: p. 143 - 304.
10. Tomlinson, A., Danks, T. N., Heyes, D. M., Taylor, S. E. and Moreton, D. J., *Langmuir*, 1997. 13: p. 5881 - 5893.
11. Mittal, K.L., *Micellization, Solubilization, Microemulsions*. Vol. 1. 1977, New York & London: Plenum Press.
12. Zhu, B.-Y., Gu, T. and Zhao, X., *Journal of Chemical Society., Faraday Transactions 1*, 1989. 85(11): p. 3819 - 3824.

13. Tiberg, F., Brinck, J. and Grant, L., *Current Opinion in Colloid & Interface Science*, 2000. **4**: p. 411 - 419.

14. Takahashi, A.K., M., Hirota, H. and Kato, T., *Macromolecules*, 1980. **13**: p. 884.

CHAPTER 7: CARBON ADSORPTION/DEPOSITION STUDIES

7.1. Introduction

This chapter is concerned with the investigation of the adsorption and deposition of carbon particles on steel beads and plates. The deposition of carbon particles on stainless steel plates has been studied using a flow cell built in the School of Chemistry at the University of Bristol.

An understanding of particle deposition and removal from surfaces plays an important role in various industrial applications such as particle filtration, paper manufacture, 'soil' release from clothes, etc[1, 2]. Most of the flow cell studies reported have been carried out using aqueous solutions. However, the experiments in this study used a hydrocarbon medium in order to understand the adsorption/deposition of carbonaceous particles, formed during fuel combustion, on engine valves. The removal of particles deposited on the surface under flow was also studied. The role of various polymer and surfactant additives in the deposition/removal process has been investigated. Previous studies have attempted to relate the removal to the flow rate and the adhesion force between the particle and the surface involved[1, 3] in aqueous systems. Investigations into the effect of pH, ionic strength and particle size on the hydrodynamic force required to detach the particles have been carried out[1, 4]. Of particular interest in this present study was the effect of a pre-adsorbed polymer layer on the ease with which the particles could be detached. Such layers may be expected, not only to provide steric stabilisation of particles, but also to act as deposition barriers between the particles and the plate. The affinity of the carbon particles for the beads has also been studied by carrying out adsorption experiments of carbon on steel in the presence of the polymer or surfactant and, polymer plus surfactant mixtures.

7.2. Experimentation

7.2.1. Carbon adsorption on steel

The adsorbed amount of the carbon particles on the stainless steel beads was determined as follows. Dispersions of the carbon particles in polymer/surfactant solutions in isooctane were prepared by dispersing a certain mass of the carbon particles in the polymer/surfactant solution, with the aid of sonication, using an *Ultrawave* sonic bath for 2 min, followed by 20 h of tumbling. To prepare the particle adsorption samples, a certain amount of the concentrated carbon dispersion in isooctane was added to 3 g of stainless steel beads, weighed into a sample vial. Polymer/surfactant solution (in isooctane) was then added to give a total mass of 5.5 g. This procedure was repeated to give various concentrations of carbon particles in the range 0.1 to 1.0 wt. %. The samples were shaken vigorously for 5 min and then tumbled for 20 h. After 20 h the samples were left standing for 30 to 40 min. The steel beads, with a density almost ten times that of isooctane, sedimented rapidly within this period. The supernatant was diluted, as necessary, and the turbidity determined using a *HP 8453* Diode Array UV/Visible spectrophotometer, at a wavelength of 800 nm, to obtain the equilibrium concentration of carbon particles in the supernatant. A calibration plot of the turbidity versus the concentration of carbon particles in the appropriate polymer/surfactant solution was first obtained. The reference used was polymer/surfactant solution tumbled for 20 h with the steel, sedimented and slightly diluted. This would significantly reduce any contribution from any adventitious species which may have leached from the steel beads.

7.2.2. Flow cell studies

In order to carry out the deposition and removal experiments, a flow cell was constructed from a block of Teflon and encased in a metal casket. A schematic diagram of the flow cell is shown in figure 7.1.

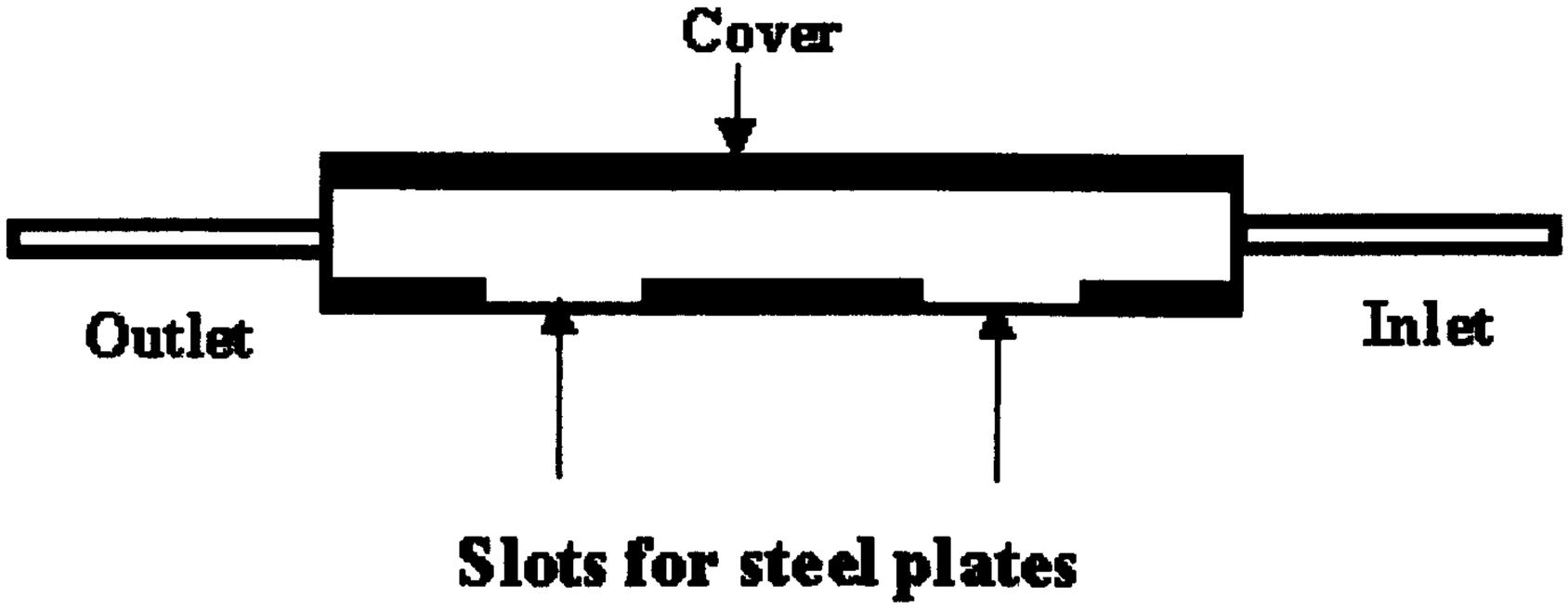

Figure 7.1: Schematics of flow cell for studying carbon deposition on steel plates

The casket also helped in supporting the metal tubes which were used to connect to Teflon tubes. Two 1 cm^2 portions of the bottom of the cell were etched out such that the depth of the pit was the same as the thickness of the steel plates used. The whole apparatus consists of the flow cell, which houses the stainless steel plate, a Braun flow-meter which was set, in the experiments reported here, to operate at a speed of 25 mL h^{-1}, a syringe to hold the carbon dispersion and a sink to collect the output. The various units are linked using Teflon tubes of internal diameter 1 mm and a two-way tap regulates the flow. For the deposition experiments, 10 mL of carbon dispersion was placed in the syringe. A polished steel plate was rinsed in isooctane, dried and then placed in the pit at the bottom of the flow cell. The flow cell top was sealed tightly with Teflon tape. The experiment was started by first switching on the flow meter and then opening the tap. At the end of the experiment, the steel plate was removed, dried and analysed directly using a *JEOL JSM – 5600 LV* scanning electron microscope. To study subsequent particle removal, a second syringe, containing 10 mL of the solvent or the appropriate polymer/surfactant solution was used.

7.2.3. Image analysis

In order to analyse the SEM micrographs in a more quantitative way, *Scion* image-analysis software (beta 4.0.2 version) obtained from Scion Corporation was used. The image was first processed to find the edges of the particles and then the threshold was set automatically. On doing so, the software automatically sets the background level white leaving the areas occupied by the particles as dark spots. Measuring the occupied area and then the surface area of the total image enabled the percentage area covered by the particles to be calculated. This method was considered more reliable as the threshold value was set automatically by the software and thus not prone to human error. However, this method of analysis is susceptible to error if there are particles adsorbed on top of others at the same point.

7.3. Results

7.3.1. Carbon adsorption on stainless steel beads

7.3.1.1. Calibration of carbon particles dispersed in P1 and S3 solutions at 800 nm

Only P1 and S3 (both with the amine head group) were effective in stabilising the carbon particles for a sufficient length of time, and hence withstand sedimentation. Therefore, all the particle adsorption experiments were carried out using only P1 or S3, on their own or in the presence of other surfactants. The concentrations of the carbon dispersions were calibrated by measuring their turbidity at 800 nm, well beyond the absorbance range of the polymer or surfactant. The resultant plots are shown in figures 7. 2 and 7.3.

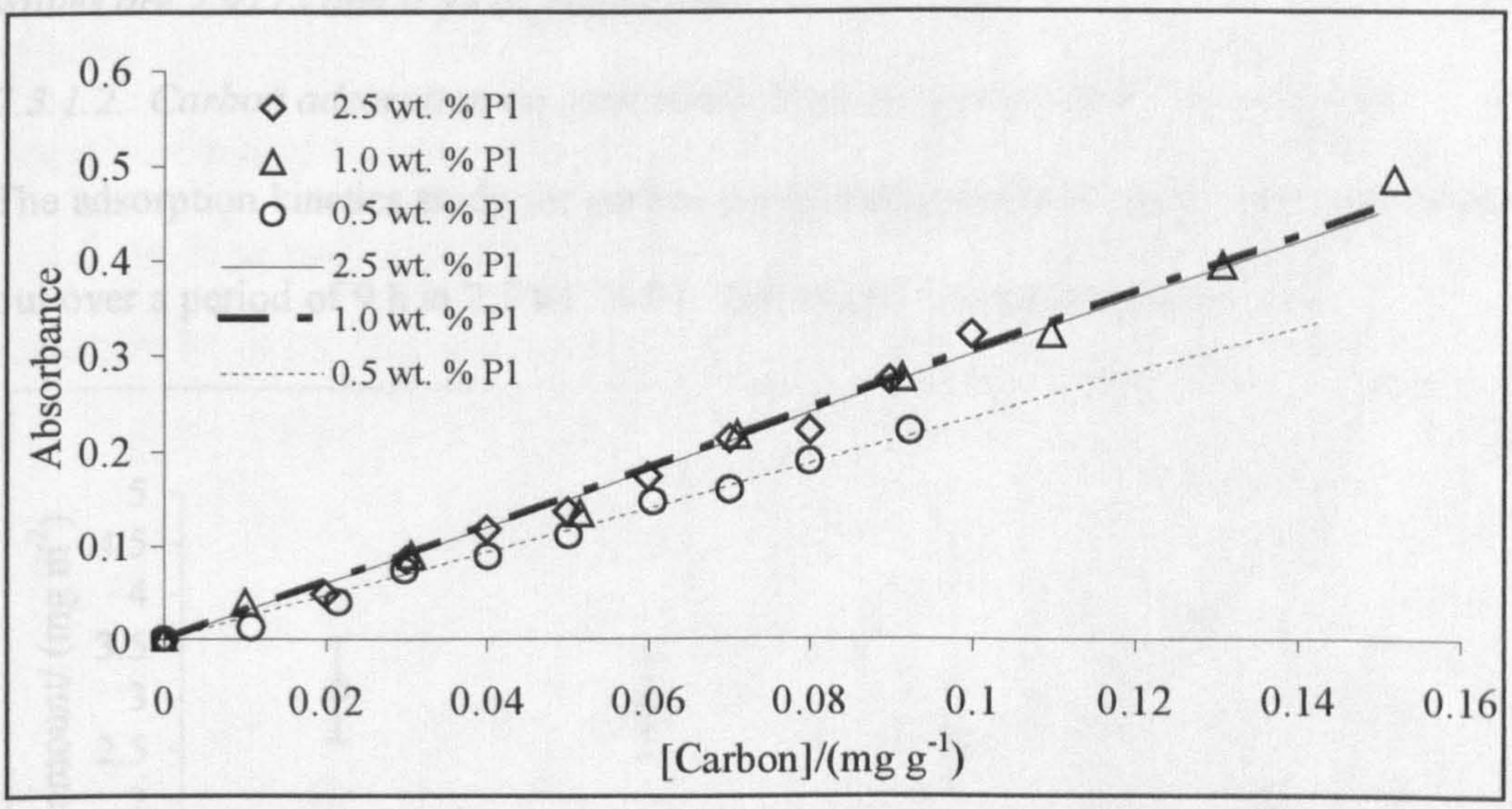

Figure 7.2: Calibration of carbon in P1 solutions. The slope and regression values are 2.9939 and 0.9871, 3.0526 and 0.9944, and 2.3370 and 0.9916 for 2.5 wt. % P1, 1.0 wt. % P1 and 0.5 wt. % P1, respectively.

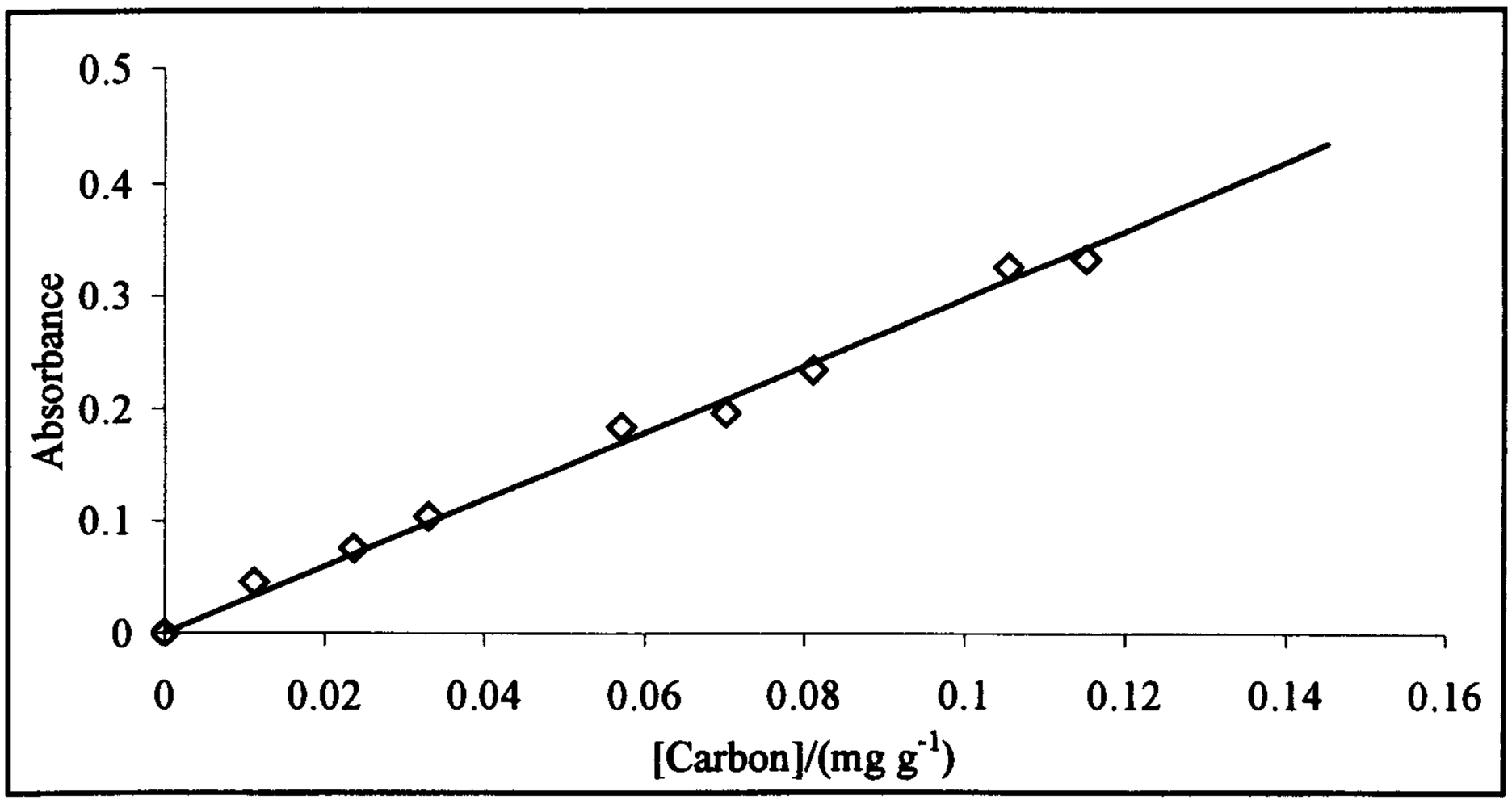

Figure 7.3: Calibration of carbon in 2.5 wt. % S3 solution. The slope and regression values are 2.9775 and 0.9926, respectively.

7.3.1.2. Carbon adsorption on steel beads from dispersions in P1/S3 solutions

The adsorption kinetics study for carbon particle adsorption on steel beads was carried out over a period of 9 h in 2.5 wt. % P1. The results are shown in figure 7.4.

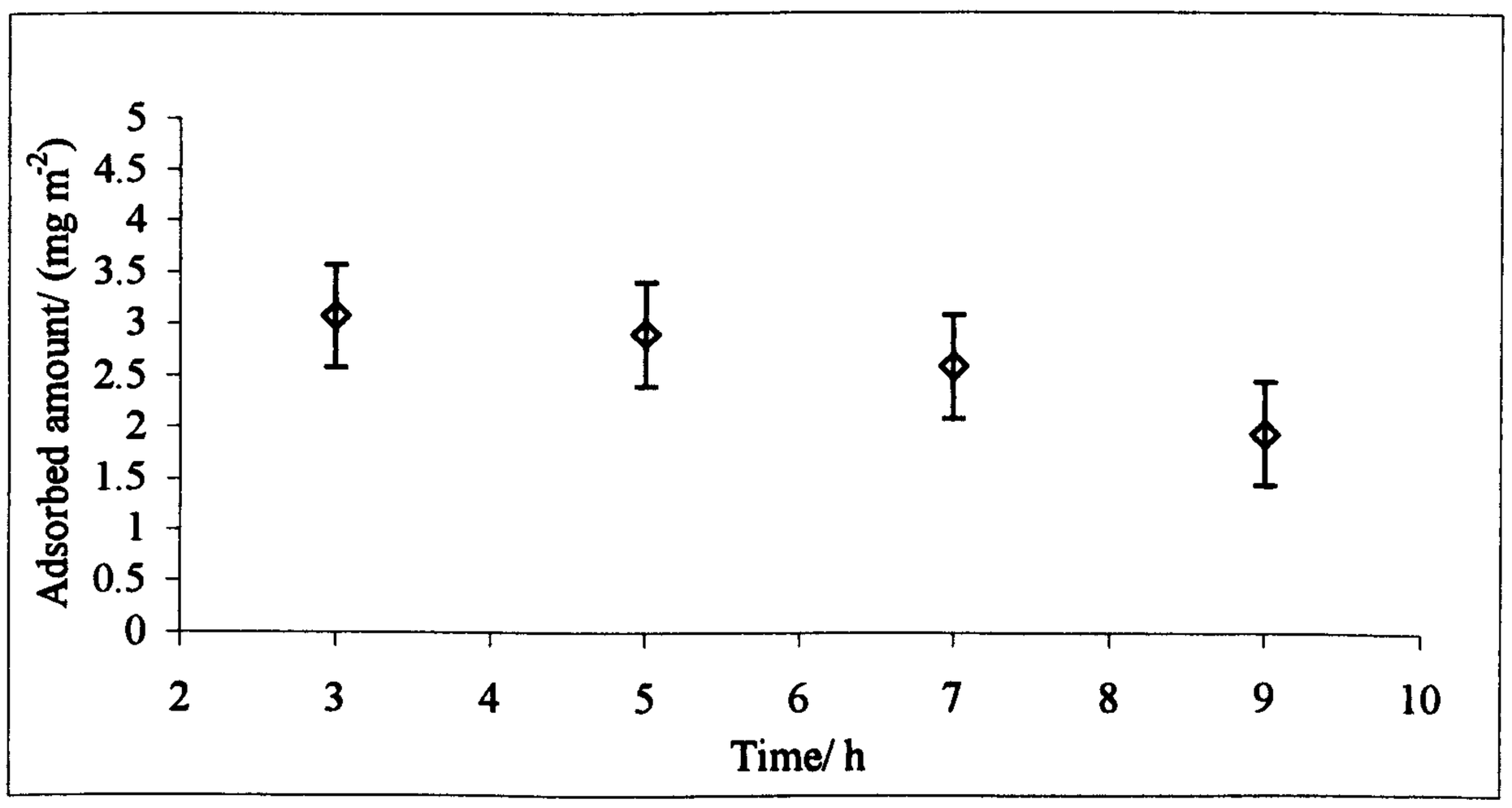

Figure 7.4: Kinetics of carbon adsorption on stainless steel beads

The adsorption of carbon particles on stainless steel beads from dispersion of carbon in 2.5 wt. % P1 solution was determined following the procedure described in section 7.2.1. The adsorption isotherm obtained is shown in figure 7.5.

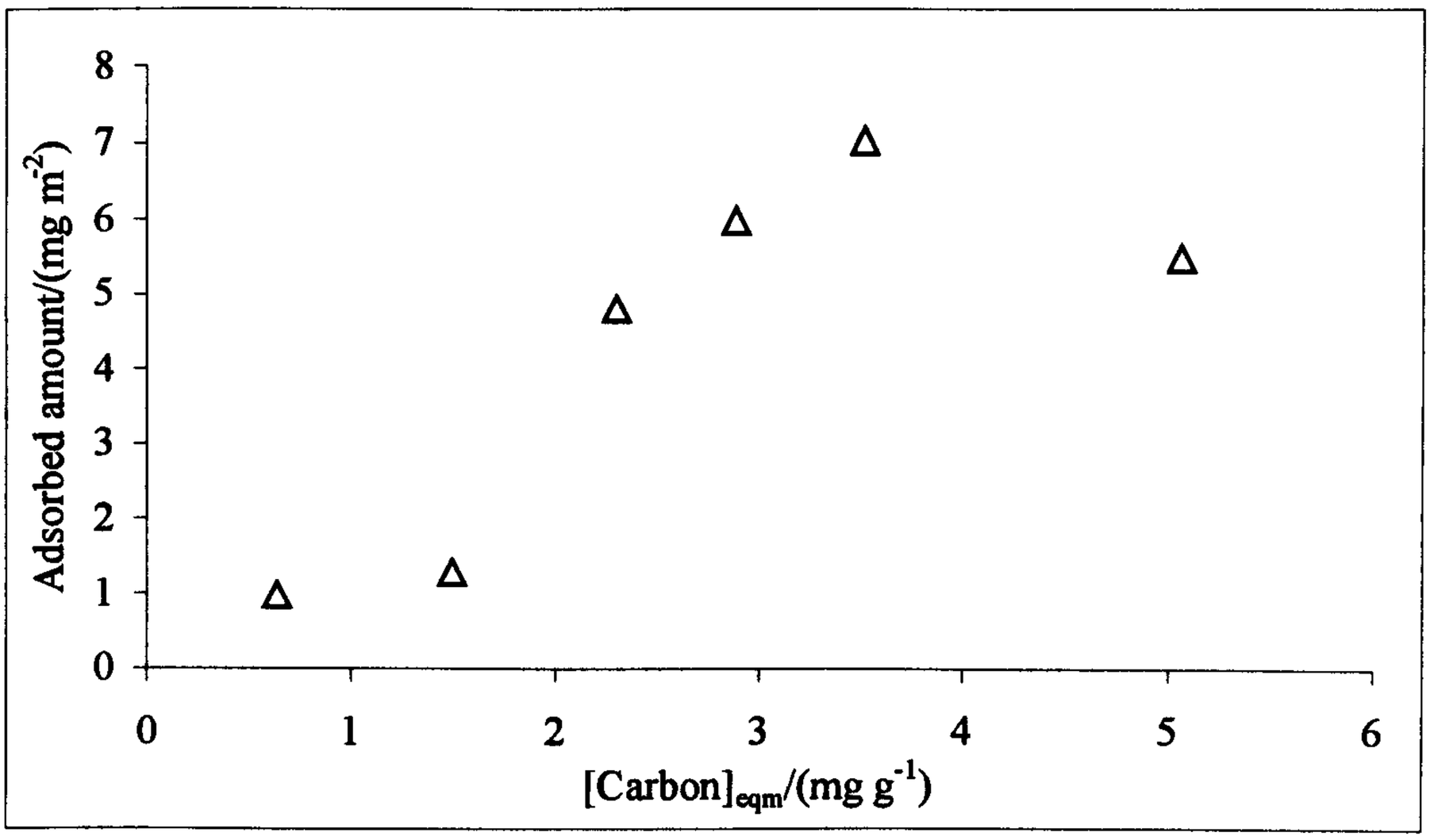

Figure 7.5: Adsorption isotherm of carbon on stainless steel beads in 2.5 wt. % P1 solution

The adsorption of carbon particles on steel beads was also carried out in the presence of 2.5 wt. % of surfactant S3, on its own and in combination with 0.5 wt. % of either surfactant S1 or S5. The isotherms are shown in figure 7.6.

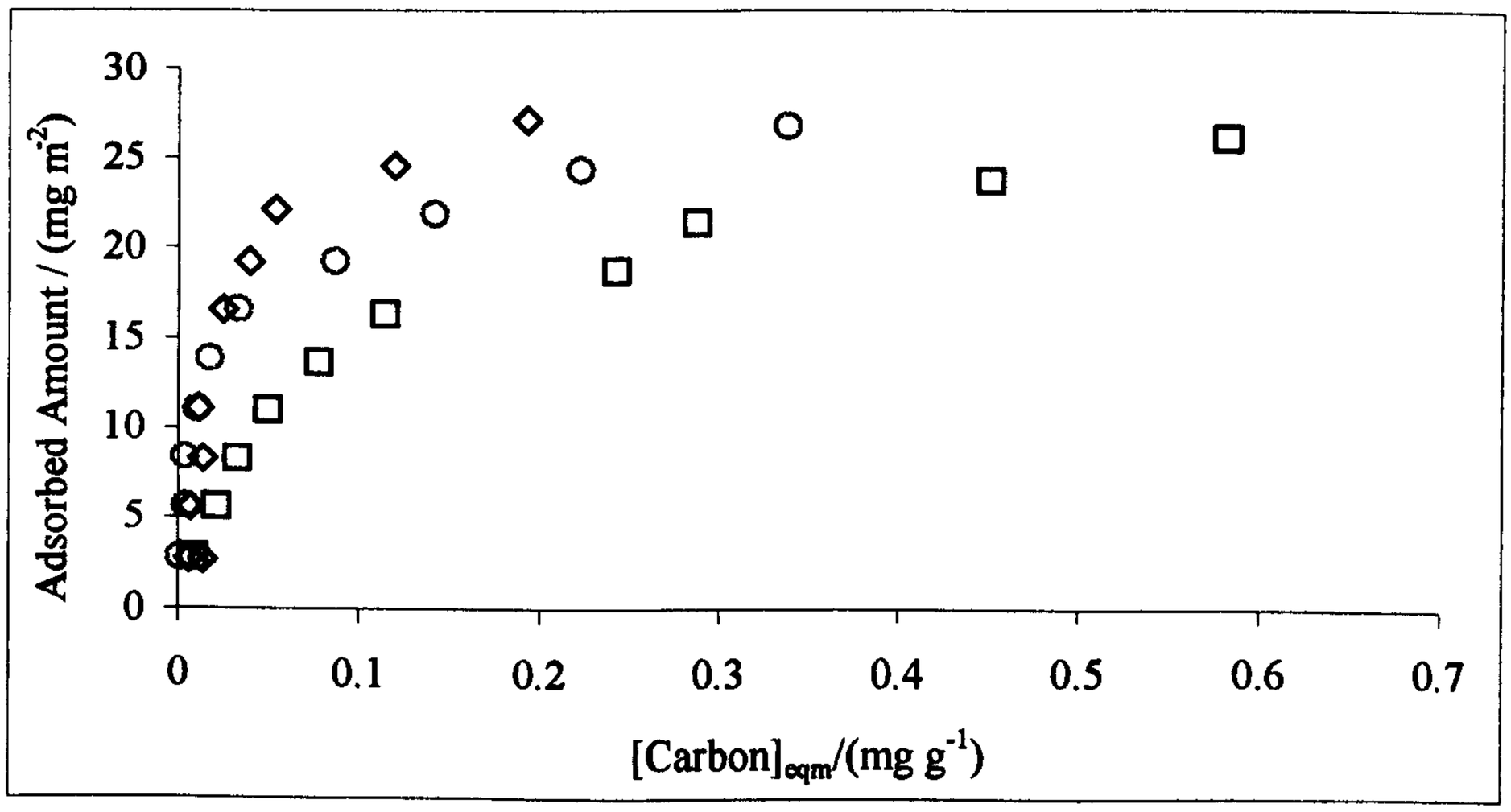

Figure 7.6: Adsorption isotherms of carbon on stainless steel beads in 2.5 wt. % S3 (◊), 2.5 wt. % S3 and 0. 5 wt. % S1 (□), and 2.5 wt. % S3 and 0.5 wt. % S5 (O) solutions

All the adsorption measurements reported here were made after 25 minutes of letting the samples stand, so that most steel beads had sedimented. However, further experiments were carried out in order to investigate the effects of sedimentation on the adsorbed amount. Adsorption experiments were carried out in 2.5 wt. % S3 after 25 min, 4.5 h and 30 h of allowing the samples to stand. The isotherms obtained are shown in figure 7.7.

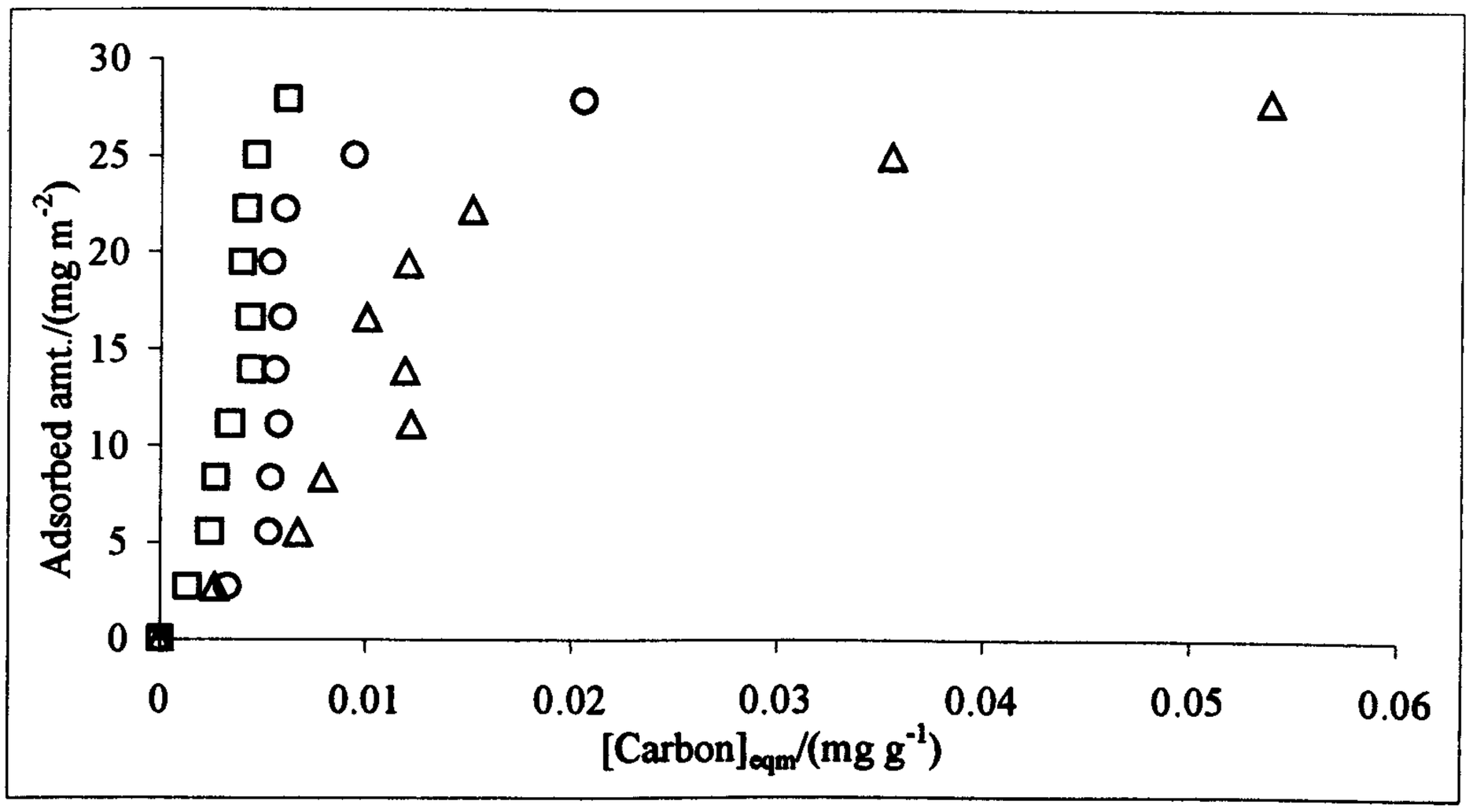

Figure 7.7: Adsorption isotherms of carbon on stainless steel beads in 2.5 wt. % S3 after 25 min (Δ), 4.5 h (O) and 30 h (□) standing

The adsorption isotherm of carbon particles after more than 30 min of allowing the samples to stand are not strictly adsorption isotherms as the effect of sedimentation sets in and the "adsorbed" amount includes carbon particle agglomerates which have sedimented from the dispersion.

7.3.2. Carbon deposition/removal studies using the flow cell

7.3.2.1. Deposition of carbon particles

All the deposition experiments were carried out on finely polished steel plates of area 1 cm^2 which have been prepared as described in section **2.7**. An SEM micrograph of one such plate is shown in figure 7.8.

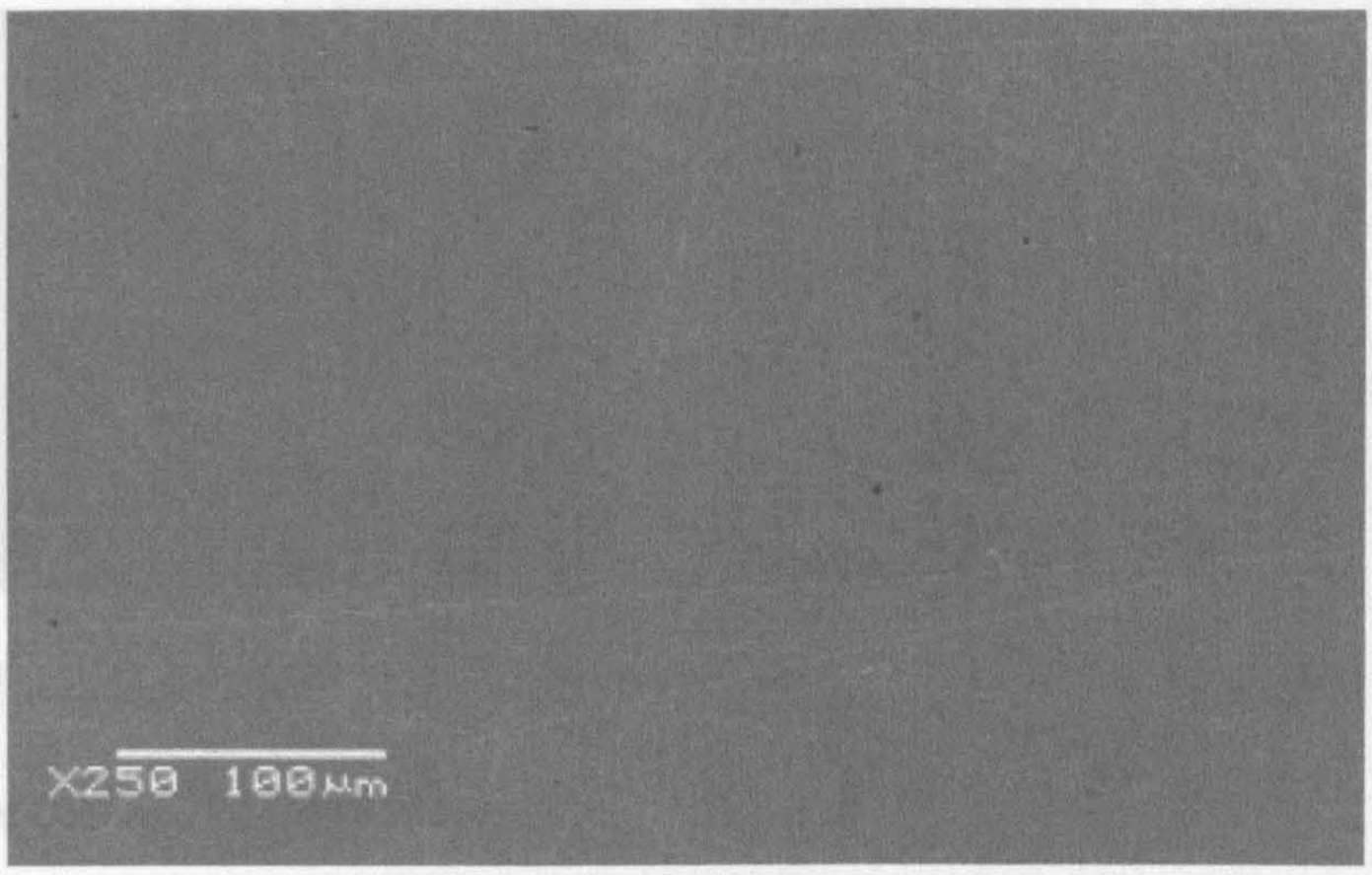

Figure 7.8: SEM micrograph of the stainless steel plate

Flow cell studies were carried out to investigate the deposition of carbon particles on steel plates from 0.1 wt. % carbon dispersions in 2.5 wt. % P1 and 2.5 wt. % S3 solutions in isooctane. The micrographs obtained are shown in figures 7.9 and 7.10.

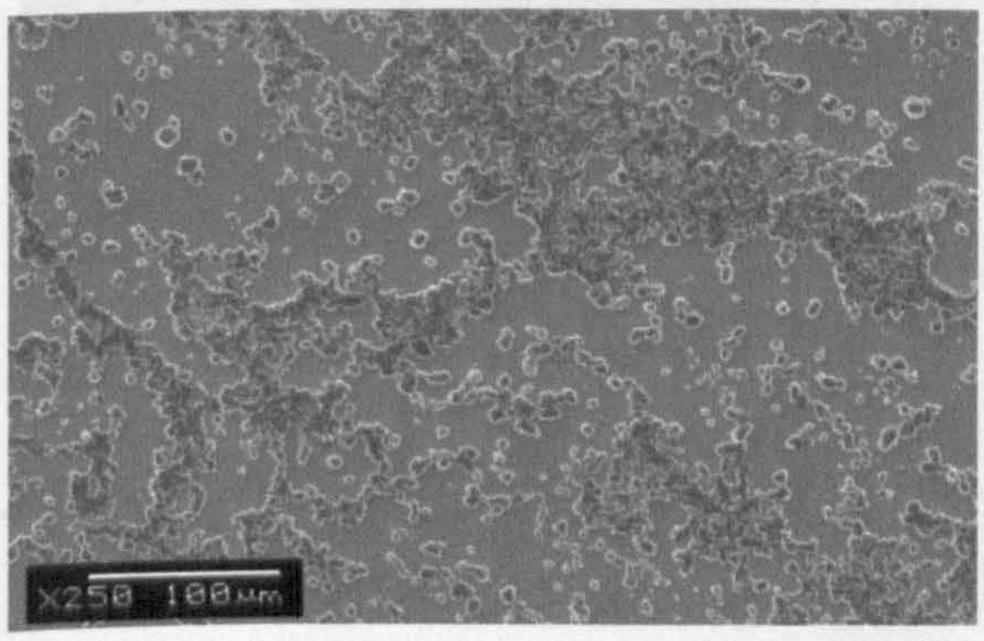

Figure 7.9: Deposition of carbon particles from 0.1 wt. % carbon dispersions in 2.5 wt. % P1 solution

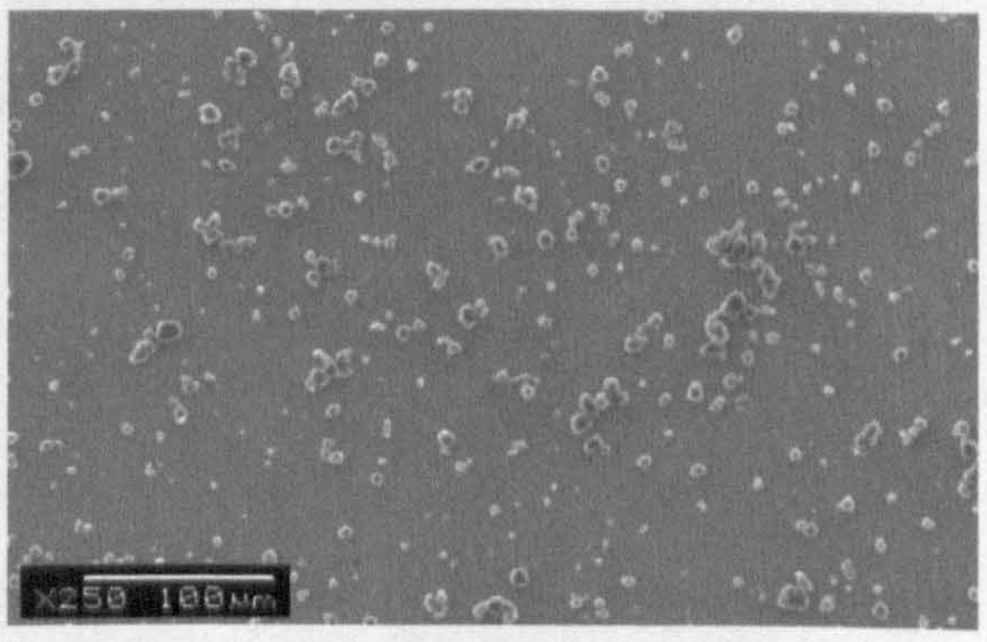

Figure 7.10: Deposition of carbon particles from 0.1 wt. % carbon dispersions in 2.5 wt. % S3 solution

Flow cell studies were also carried out to investigate the deposition of carbon particles on steel plates from 0.1 wt. % carbon dispersions in mixed solutions of the polymer and surfactants, namely 2.5 wt. % P1 and 1.0 wt. % of one of the surfactants in isooctane. The micrographs obtained are shown in figures 7.11 to 7.15.

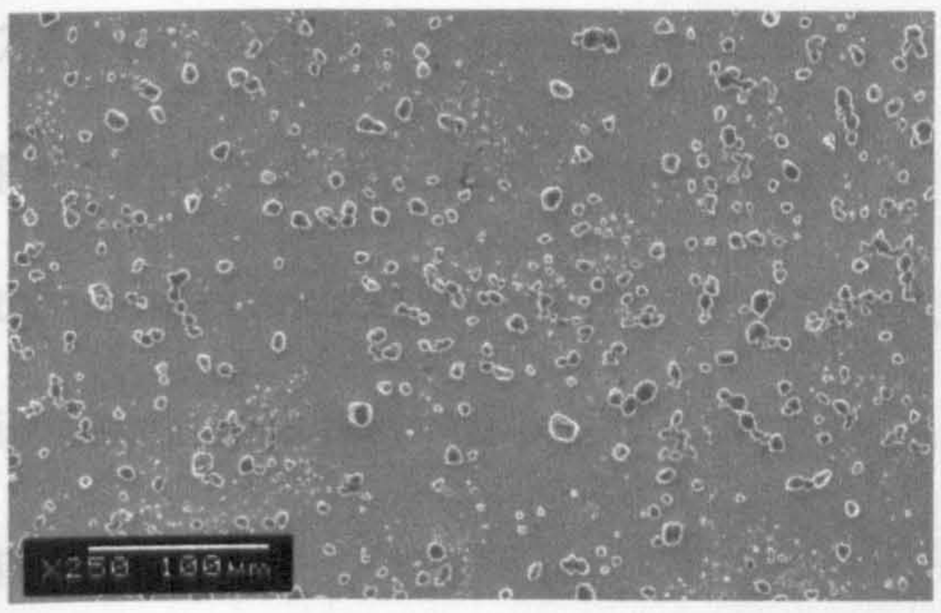

Figure 7.11: Deposition of carbon particles from 0.1 wt. % carbon dispersed in 2.5 wt. % P1 and 1.0 wt. % S1 mixture solution

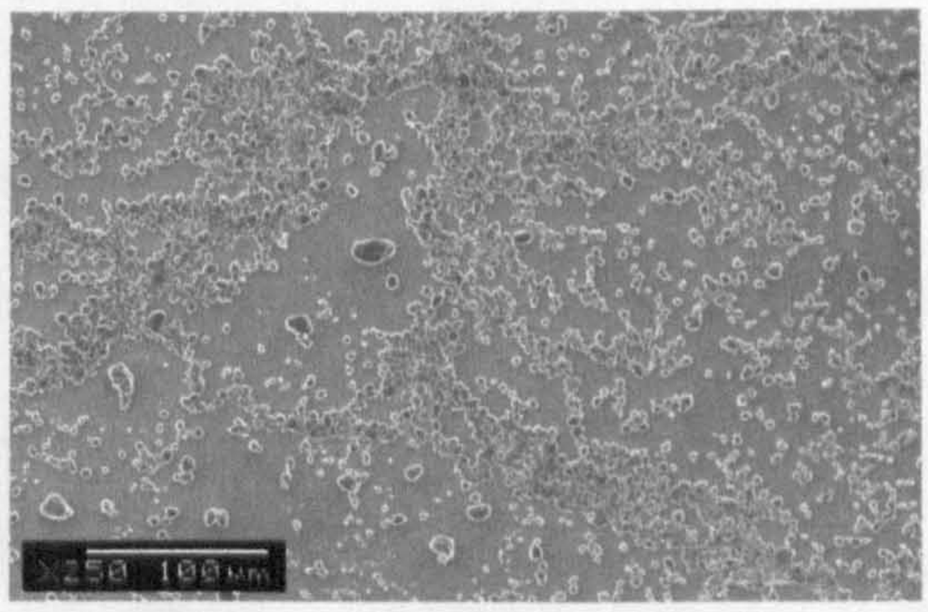

Figure 7.12: Deposition of carbon particles from 0.1 wt. % carbon dispersed in 2.5 wt. % P1 and 1.0 wt. % S2 mixture solution

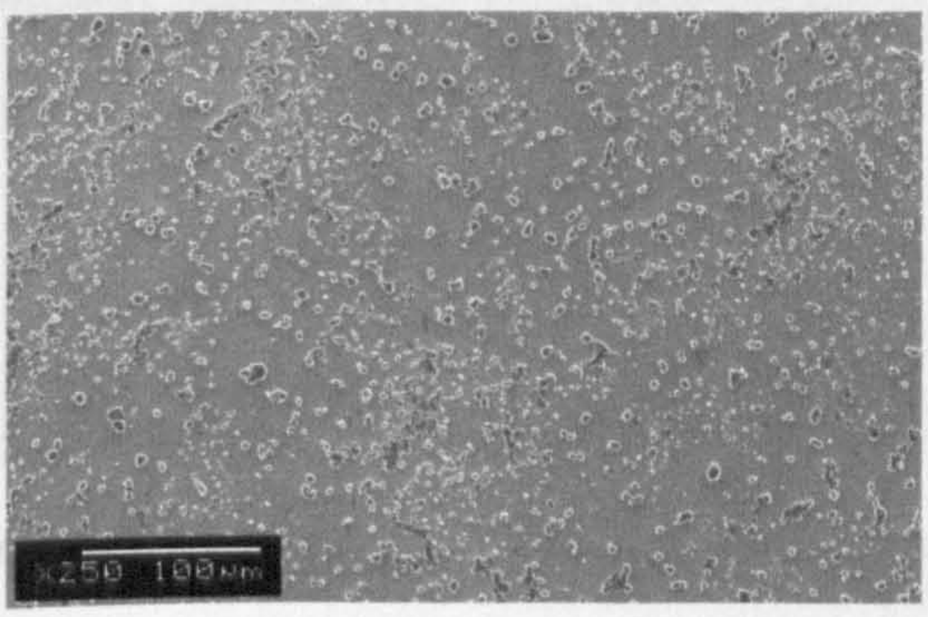

Figure 7.13: Deposition of carbon particles from 0.1 wt. % carbon dispersed in 2.5 wt. % P1 and 1.0 wt. % S3 mixture solution

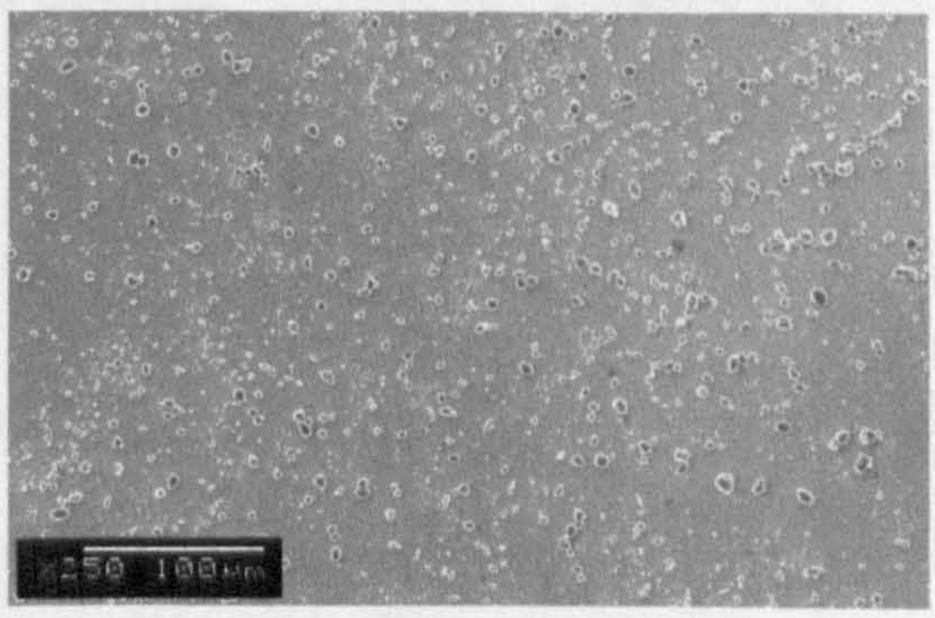

Figure 7.14: Deposition of carbon particles from 0.1 wt. % carbon dispersed in 2.5 wt. % P1 and 1.0 wt. % S4 mixture solution

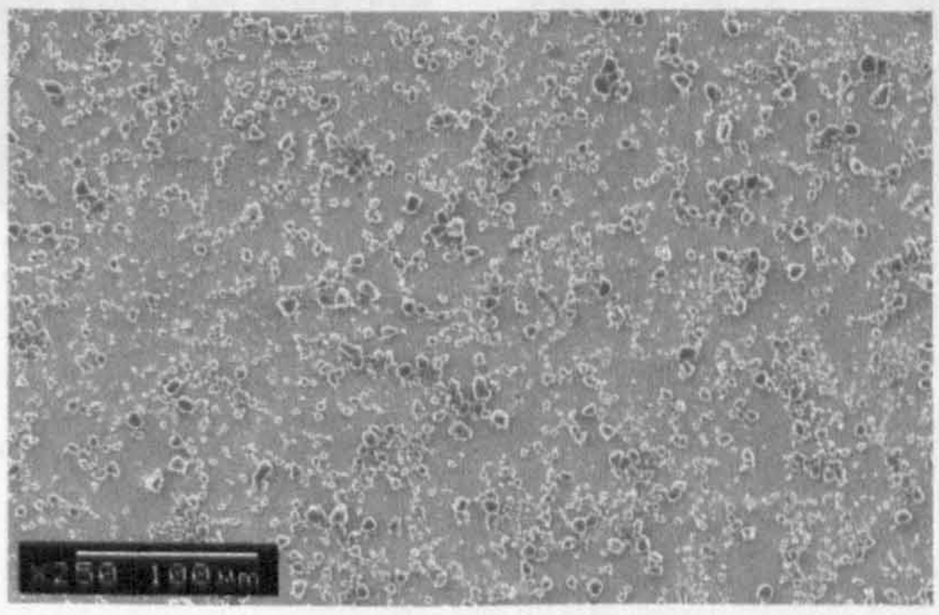

Figure 7.15: Deposition of carbon particles from 0.1 wt. % carbon dispersed in 2.5 wt. % P1 and 1.0 wt. % S5 mixture solution

7.3.2.2. Removal of carbon particles

Following the deposition experiments, removal experiments were also carried out. In these experiments, 0.1 wt. % dispersion of carbon particles in 2.5 wt. % P1 solution in isooctane was allowed to flow through the flow cell to effect the deposition of carbon particles on a steel plate. This was followed by the flow of isooctane to attempt to remove the deposited carbon particles. The procedure was repeated by flowing through 2.5 wt. % polymer solution, and mixtures of 2.5 wt. % P1 and 1.0 wt. % of a surfactant. The micrographs obtained are shown in figures 7.16 to 7.20.

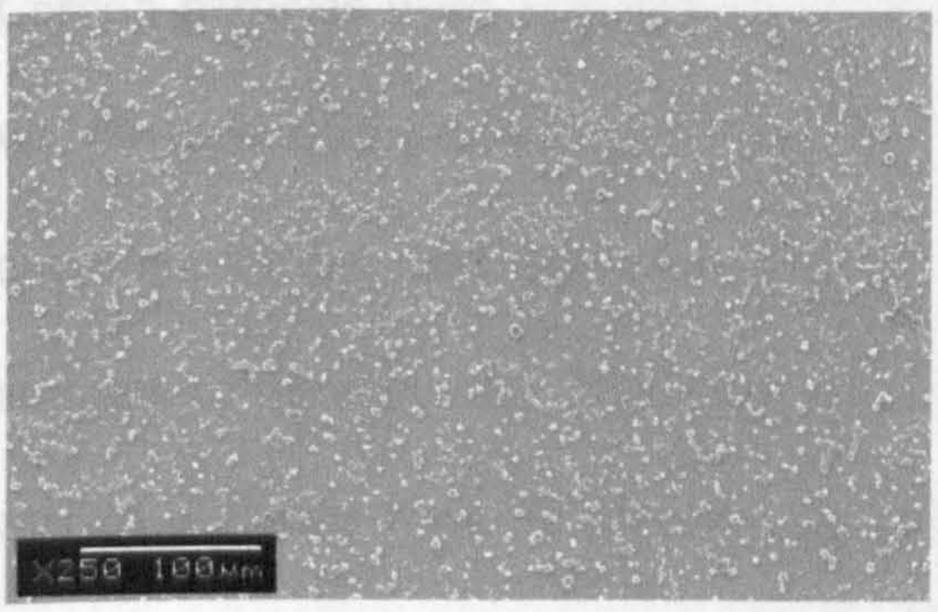

Figure 7.16: Removal of carbon particles by isooctane

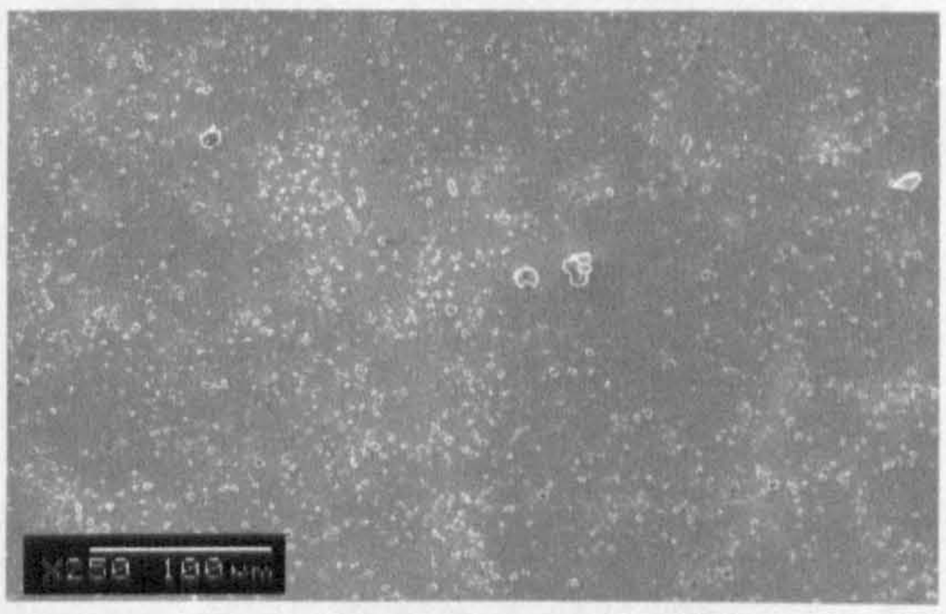

Figure 7.17: Removal of carbon particles by 2.5 wt. % P1 solution

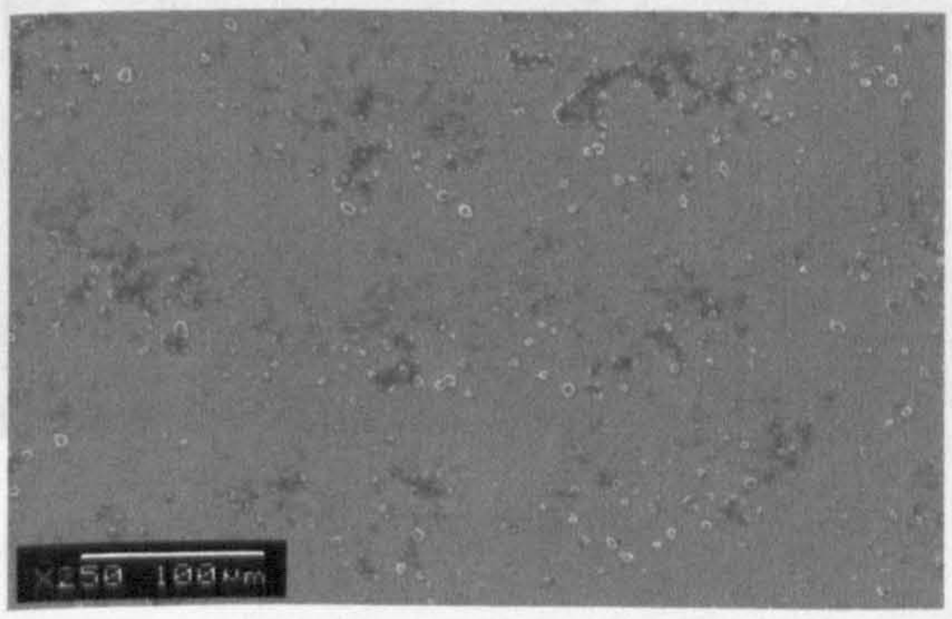

Figure 7.18: Removal of carbon particles by 2.5 wt. % P1 and 1.0 wt. % S1 mixture solution

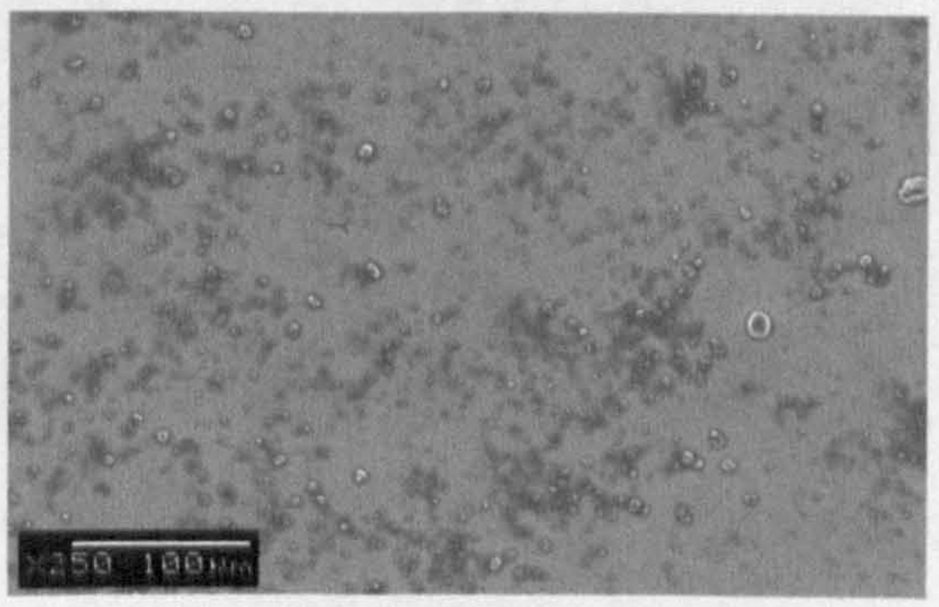

Figure 7.19: Removal of carbon particles by 2.5 wt. % P1 and 1.0 wt. % S3 mixture solution

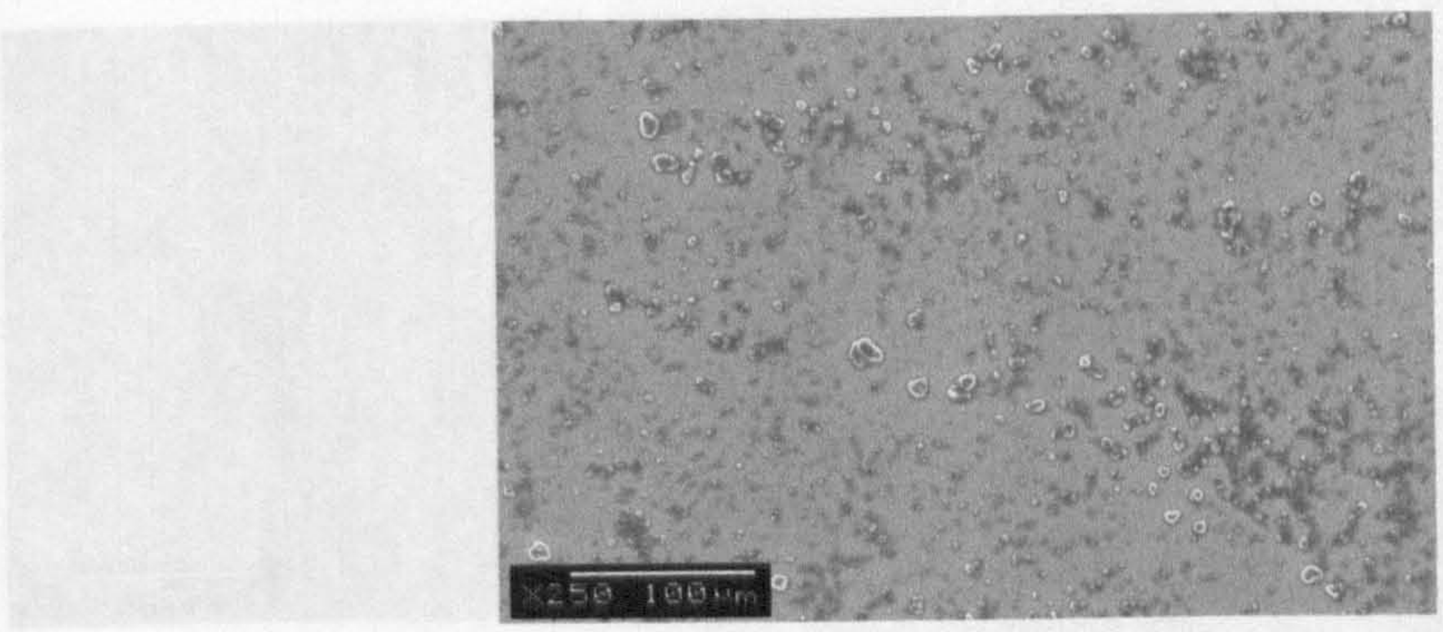

Figure 7.20: Removal of carbon particles by 2.5 wt. % P1 and 1.0 wt. % S5 mixture solution

Carbon particles were also deposited on a steel plate by evaporating two drops of 0.1 wt. % carbon dispersion in 2.5 wt. % P1 solution in isooctane. The plate was left overnight to dry, and then placed in the flow cell. Isooctane was flowed through to attempt to remove the deposited particles. Similar removal experiments were also carried out with 1 wt. % polymer, and 1 wt. % surfactant solutions in isooctane. The micrographs obtained for these removal experiments are shown in figures 7.21 to 7.26.

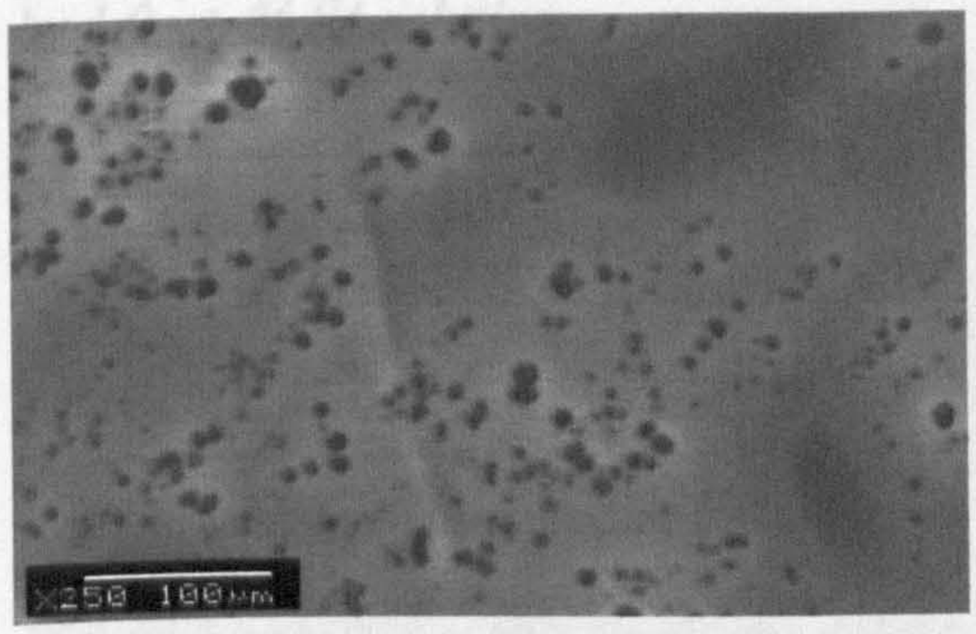

Figure 7.21: Removal of carbon particles by pure isooctane

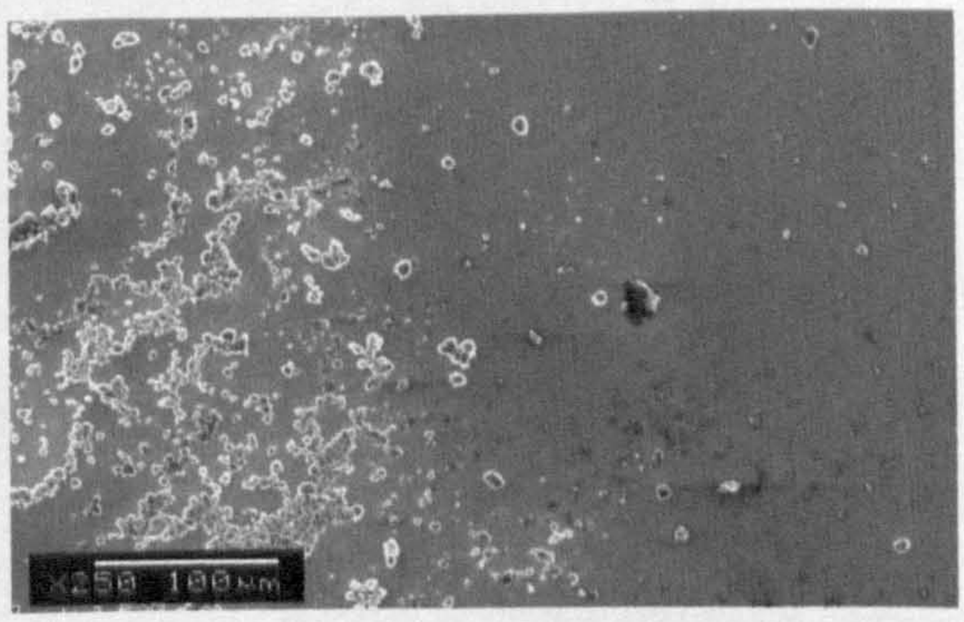

Figure 7.22: Removal of carbon particles by 1.0 wt. % P1 solution

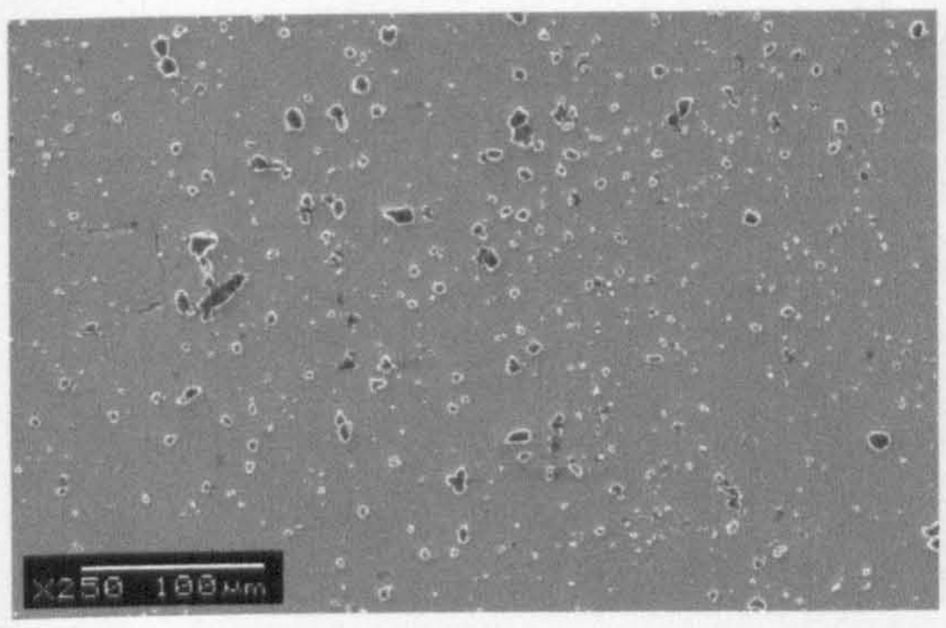

Figure 7.23: Removal of carbon particles by 1.0 wt. % S1 solution

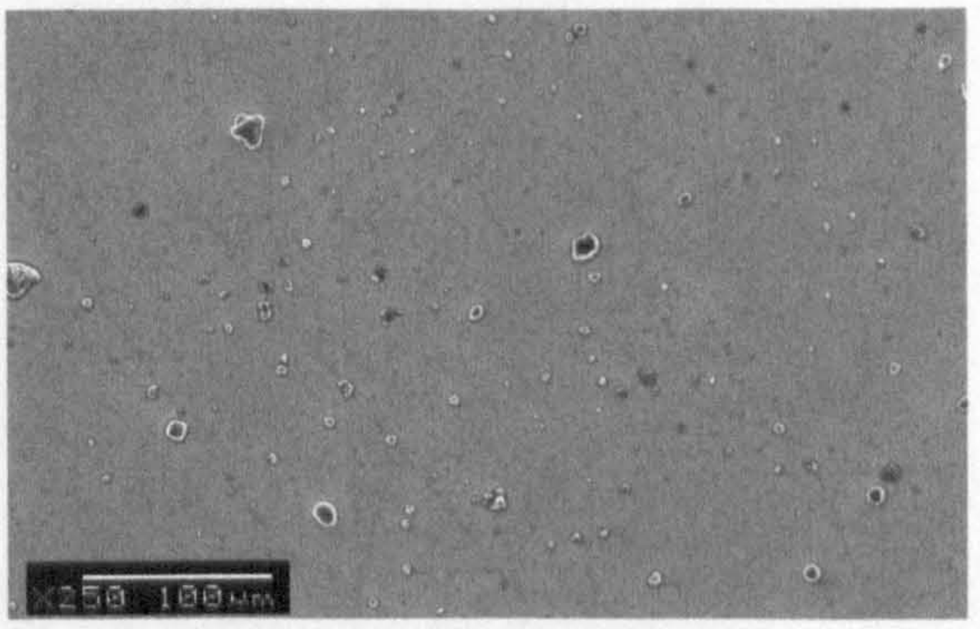

Figure 7.24: Removal of carbon particles by 1.0 wt. % S3 solution

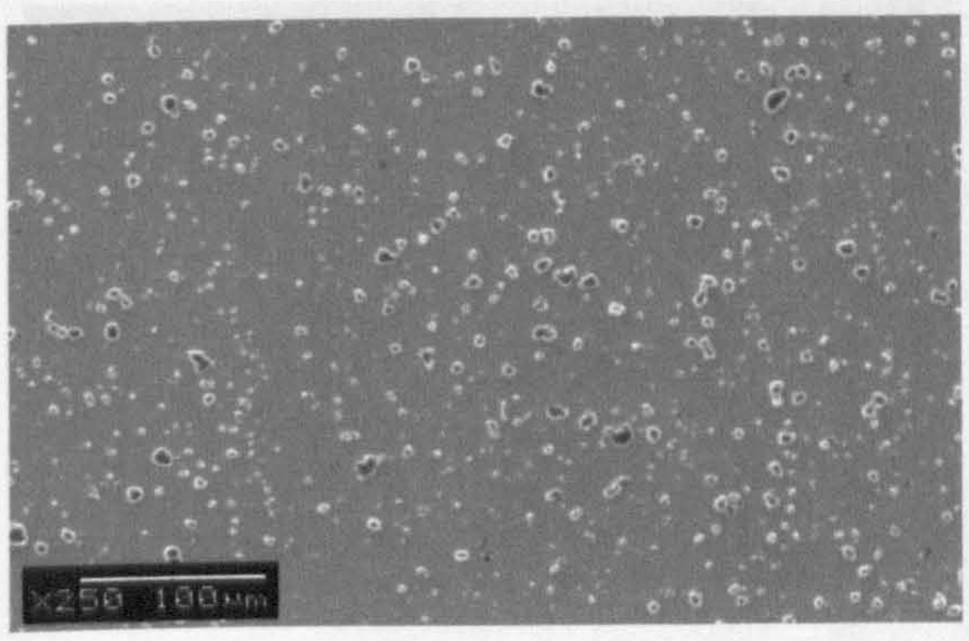

Figure 7.25: Removal of carbon particles by 1.0 wt. % S4 solution

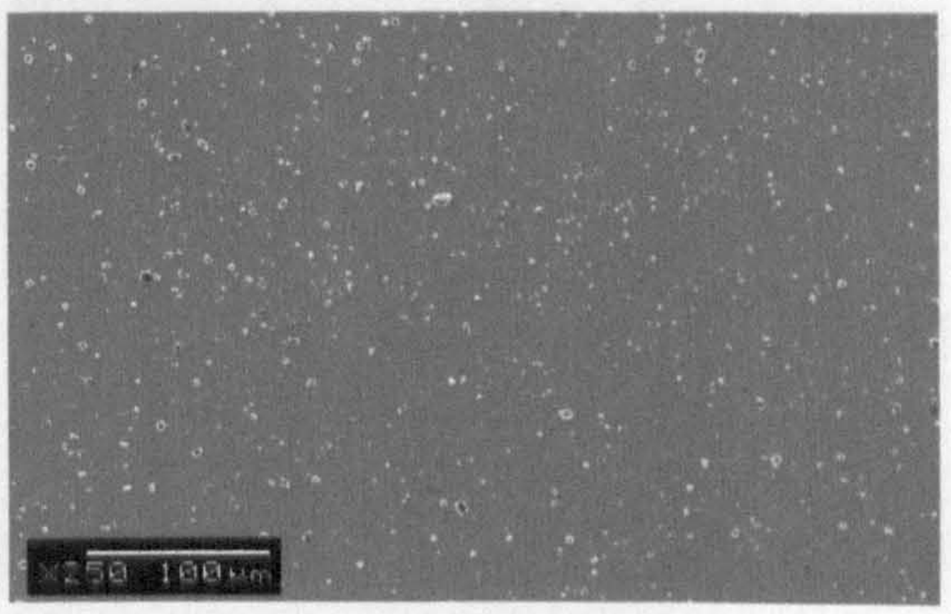

Figure 7.26: Removal of carbon particles by 1.0 wt. % S5 solution

Further experiments were carried out to attempt to remove carbon particles deposited from a 0.1 wt. % carbon dispersion in propan-1-ol. The SEM micrographs obtained for this removal study are shown in figures 7.27 to 7.33.

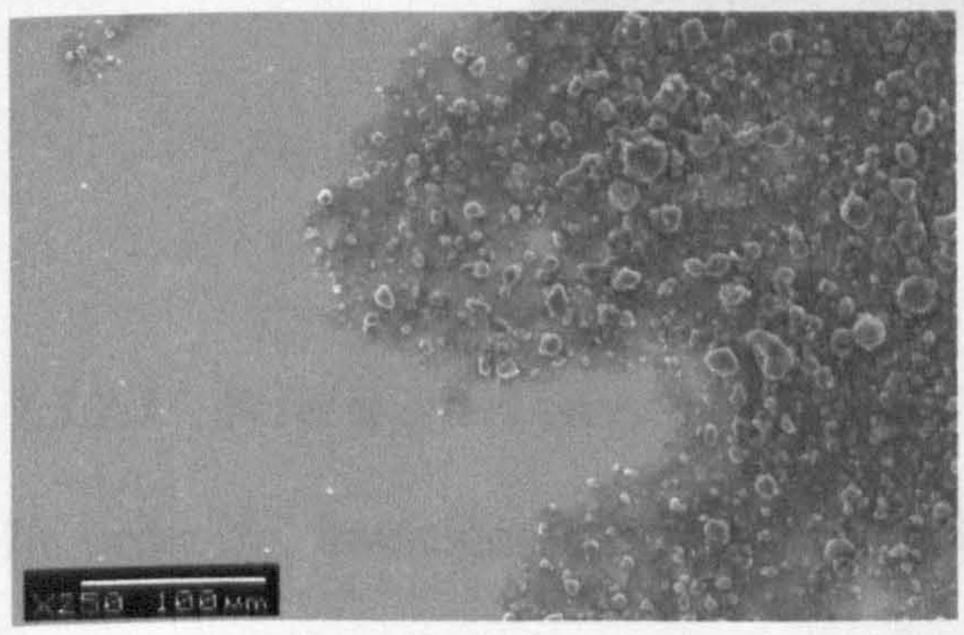

Figure 7.27: Carbon deposited from propan-1-ol dispersion

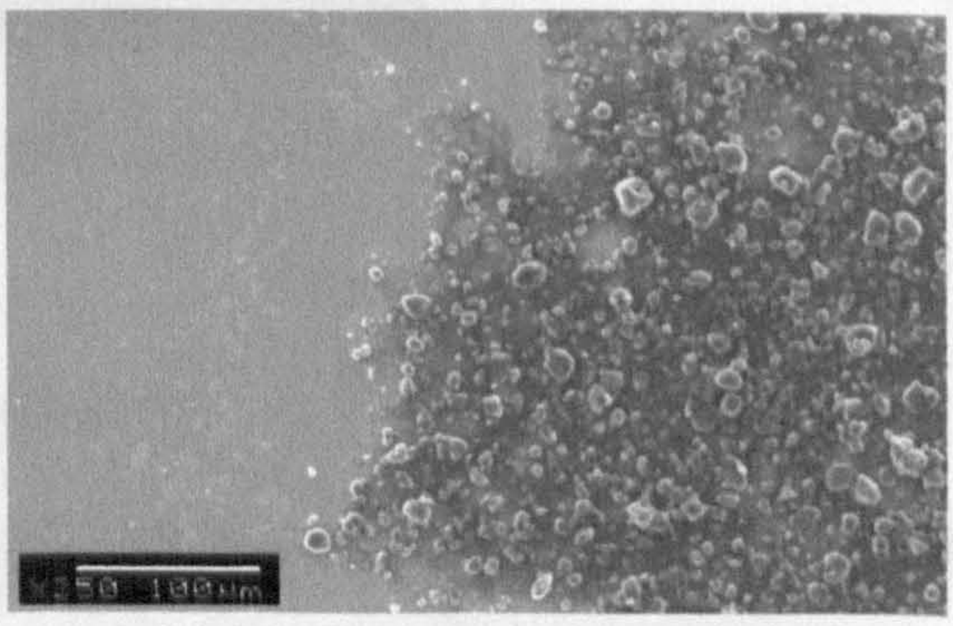

Figure 7.28: Removal of carbon particles by pure isooctane

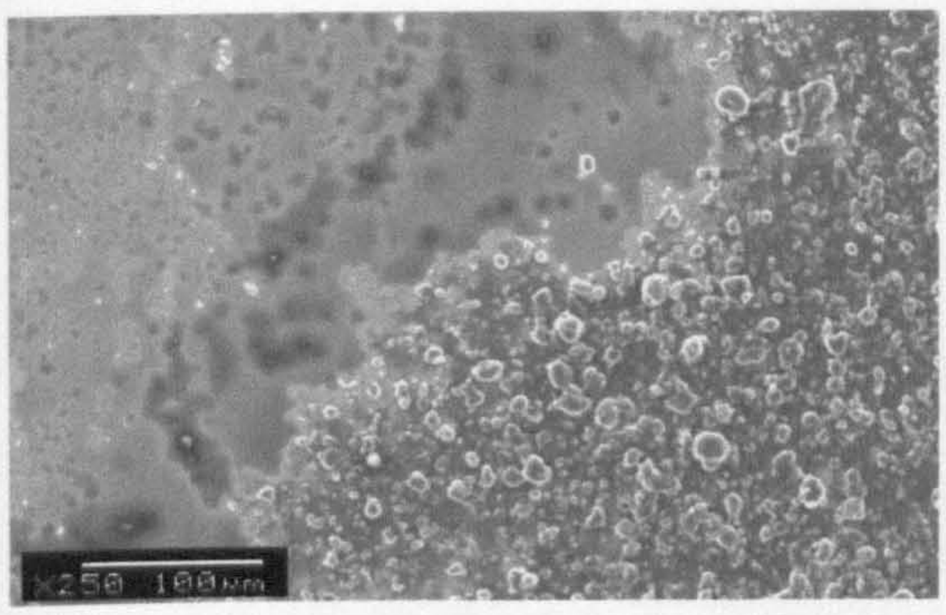

Figure 7.29: Removal of carbon particles by 1.0 wt. % P1 solution

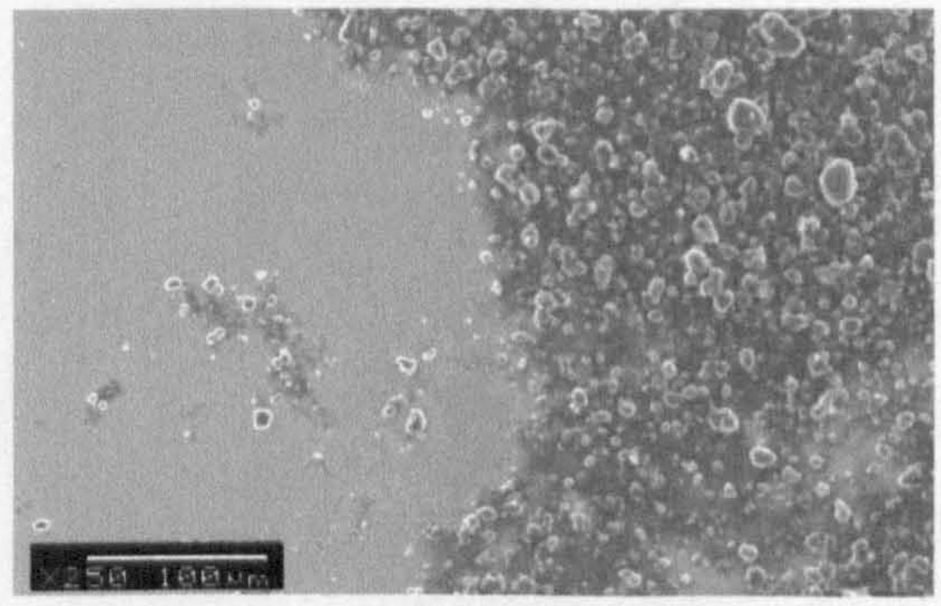

Figure 7.30: Removal of carbon particles by 1.0 wt. % S1 solution

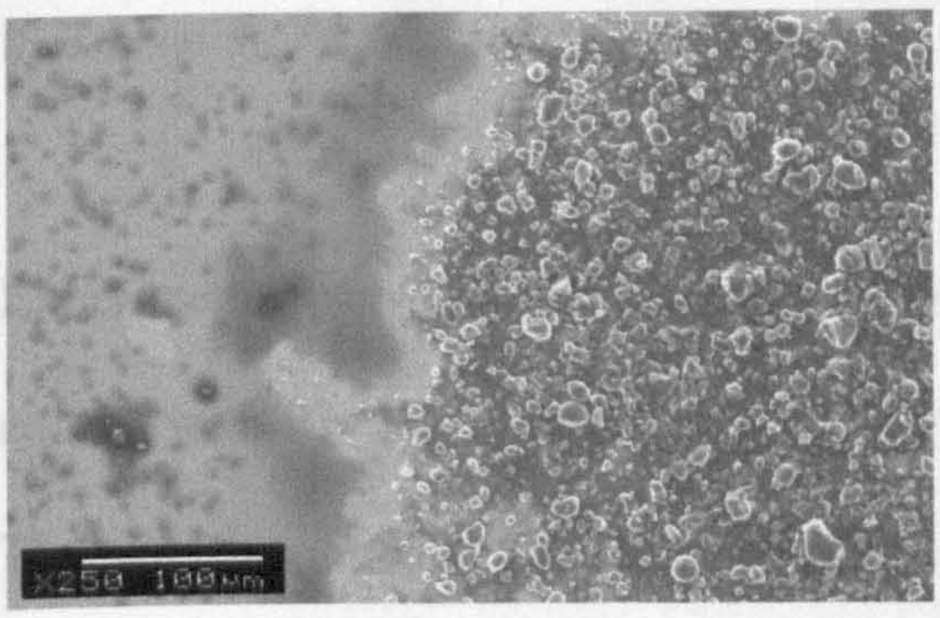

Figure 7.31: Removal of carbon particles by 1.0 wt. % S3 solution

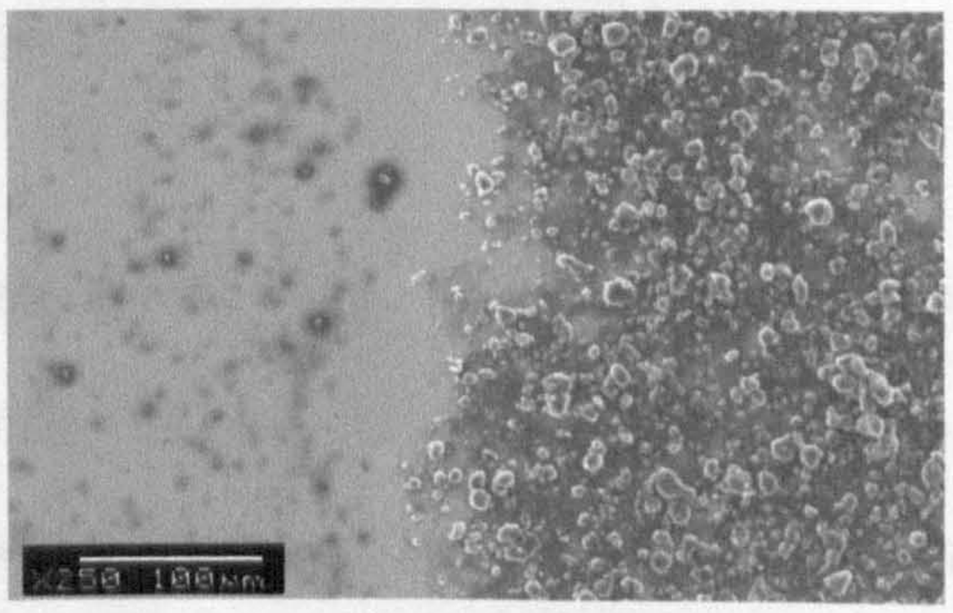

Figure 7.32: Removal of carbon particles by 1.0 wt. % S4 solution

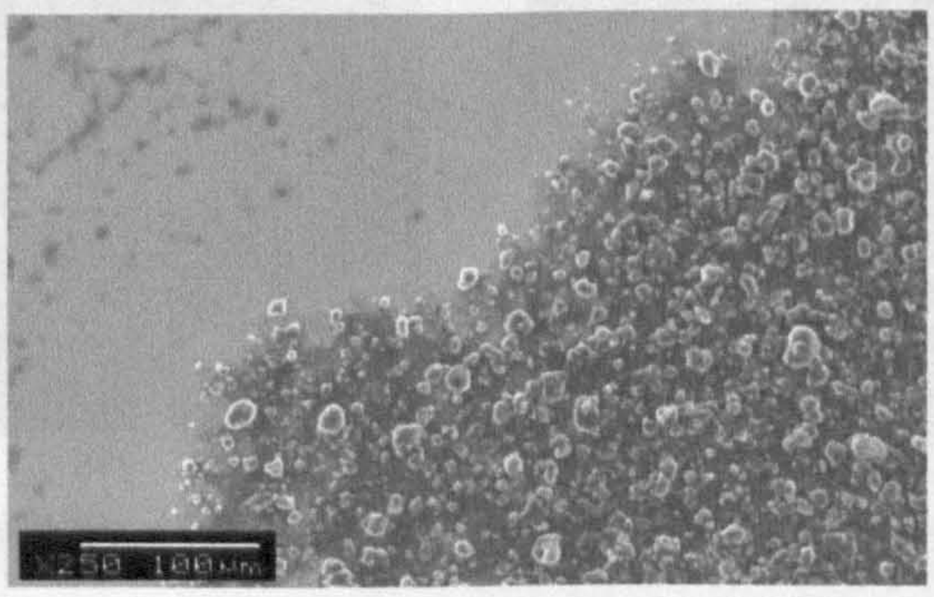

Figure 7.33: Removal of carbon particles by 1.0 wt. % S5 solution

7.3.2.3. Solvent effect on carbon particle deposition

In order to investigate the effect of different solvents on the amount of carbon deposited, flow cell experiments were carried out using 0.1 wt. % carbon dispersions in 2.5 wt. % P1 solutions in toluene and o-xylene. The SEM micrographs corresponding to these experiments are shown in figures 7.34 and 7.35.

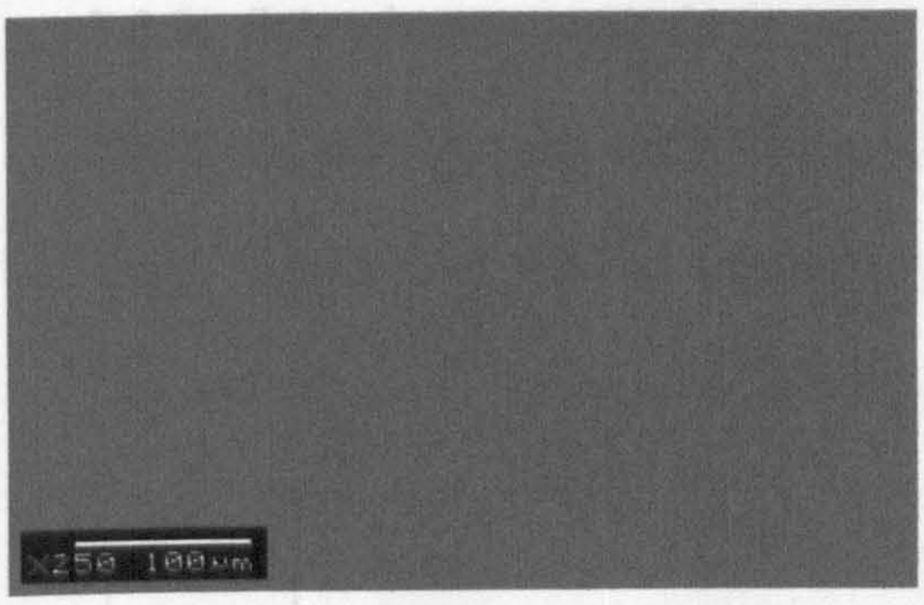

Figure 7.34: Deposition of carbon particles from 0.1 wt. % carbon dispersed in 2.5 wt. % P1 solution in toluene

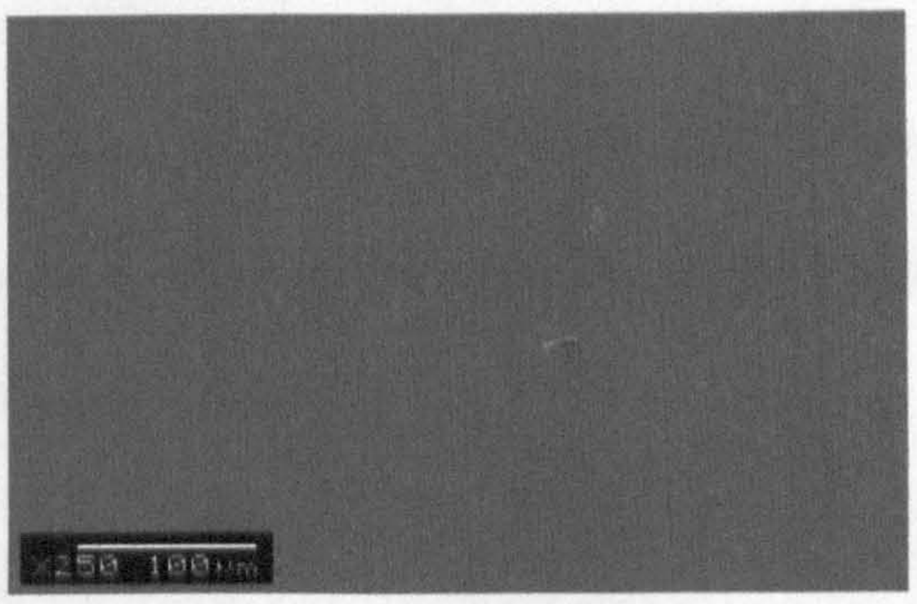

Figure 7.35: Deposition of carbon particles from 0.1 wt. % carbon dispersed in 2.5 wt. % P1 solution in o-xylene

Experiments were also carried out using steel plates whose surfaces had been pre-coated with P1. This was achieved by immersing the plates in a 2.5 wt. % P1 solution. The results obtained from the deposition experiments carried out using these pre-saturated surfaces are shown in figures 7.36 and 7.37.

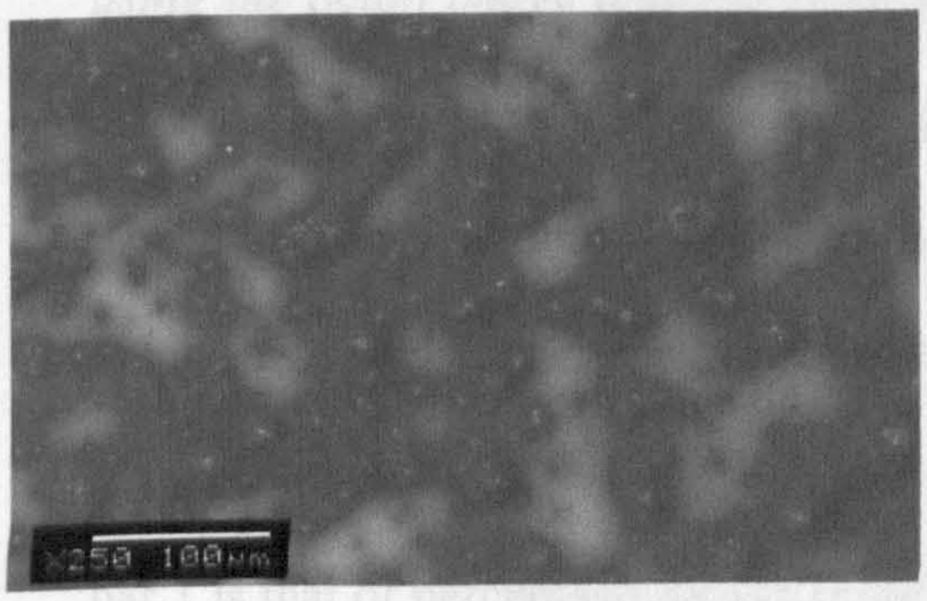

Figure 7.36: Deposition of carbon particles from 0.1 wt. % carbon dispersed in 2.5 wt. % P1 solution in toluene using a pre-coated steel plate

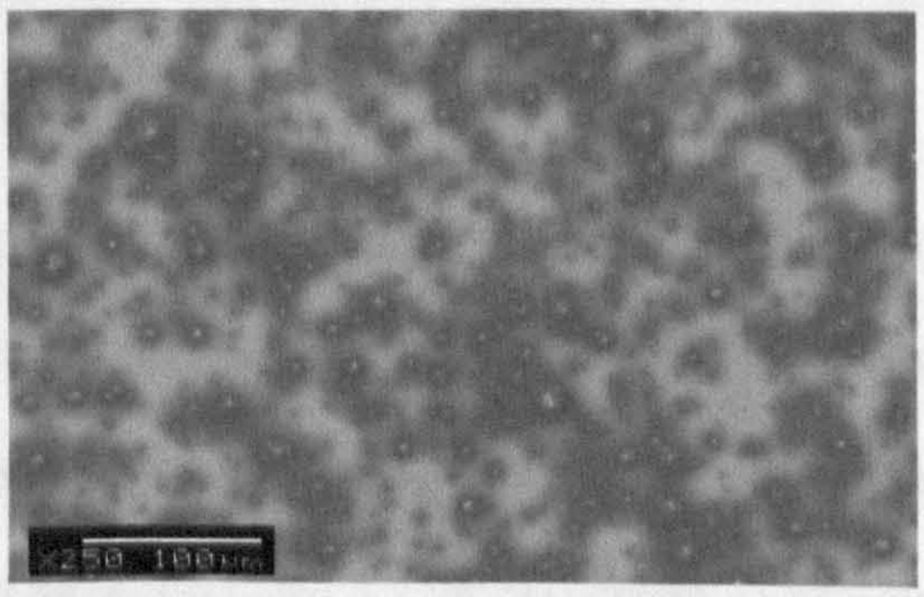

Figure 7.37: Deposition of carbon particles from 0.1 wt. % carbon dispersed in 2.5 wt. % P1 solution in o-xylene using a pre-coated steel plate

7.3.3. Scion image analysis results

The SEM micrographs obtained from the various deposition experiments carried out using P1, S3, and P1 and surfactant mixtures were analysed using the Scion image analysis software. The results obtained are shown in figure 7.38.

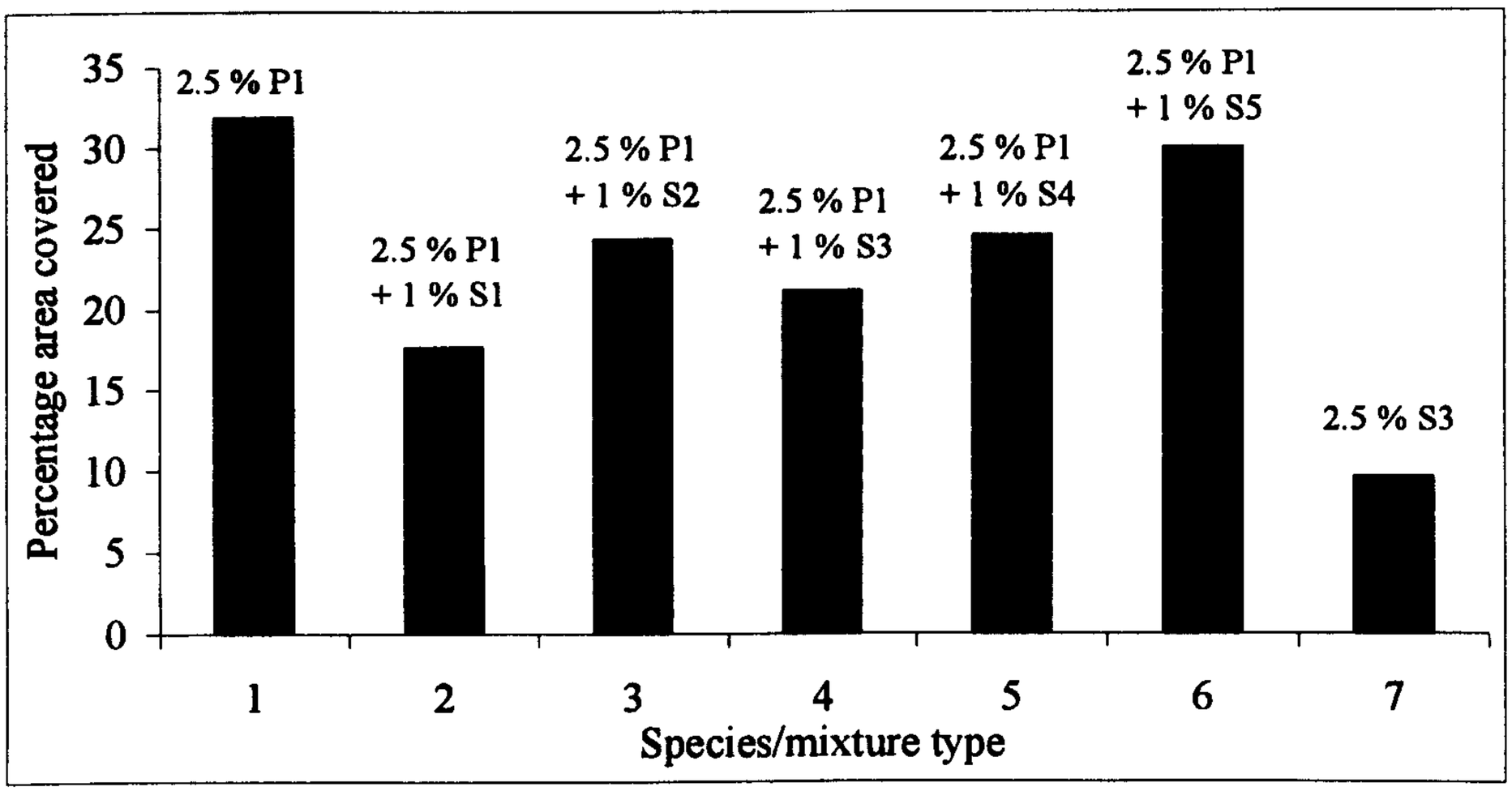

Figure 7.38: Percentage area covered by the deposited carbon particles as calculated using the Scion image analysis software. The species/mixtures used as the dispersant are indicated at the top of the corresponding bar.

The SEM micrographs obtained from the various removal experiments carried out using P1, isooctane, and P1 and surfactant mixtures were also analysed using the Scion image analysis software. The results obtained are shown in figure 7.39. In the figure, bar 1 is that of percentage area covered on deposition from 0.1 wt. % carbon dispersion in 2.5 wt. % P1 solution.

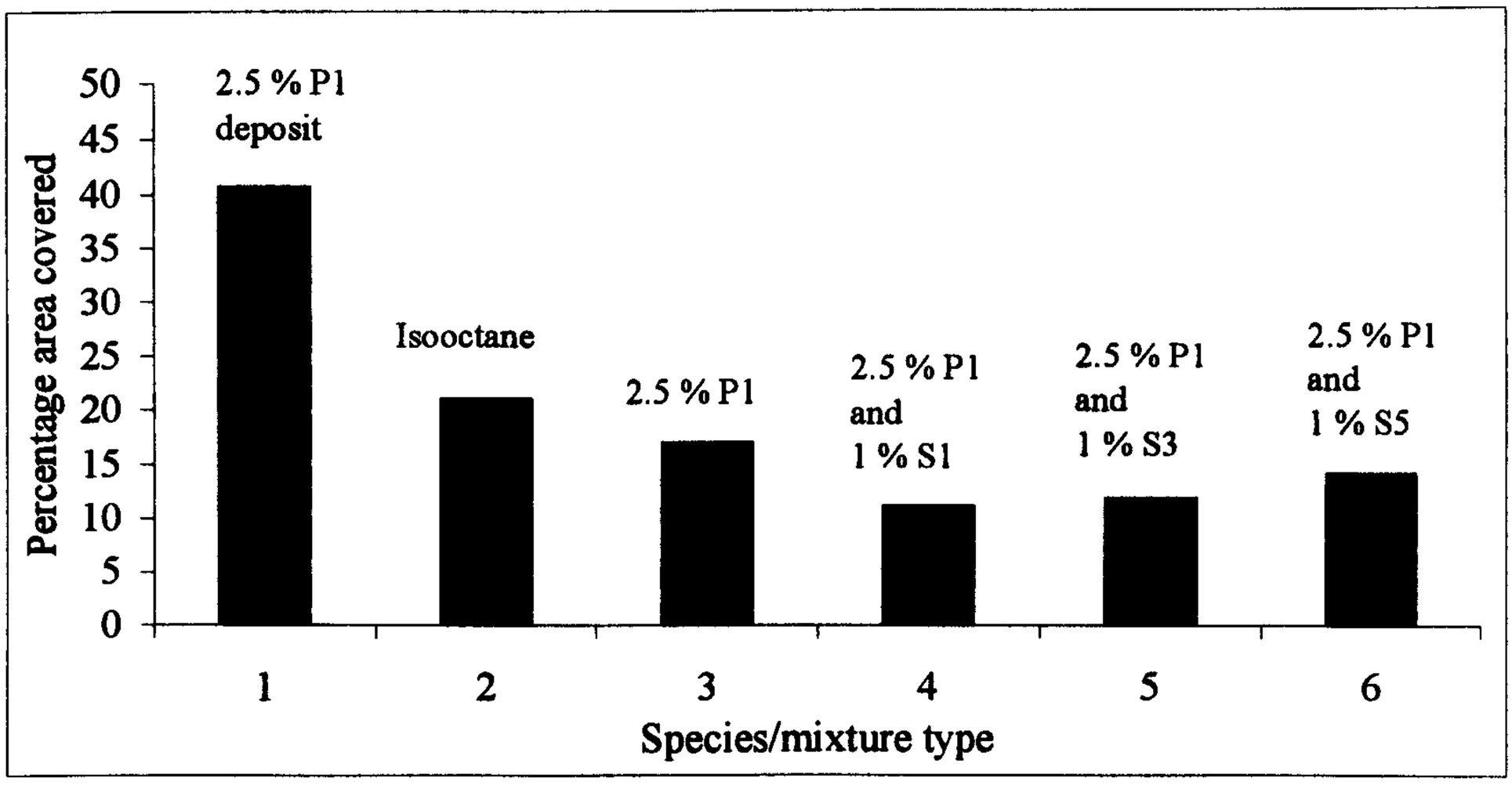

Figure 7.39: Percentage area covered by the carbon particles after the removal experiments as calculated using the Scion image analysis software. The species/mixtures used as the cleaning agent are indicated at the top of the corresponding bar.

The SEM micrographs obtained from the removal studies of carbon particles, deposited by the evaporation of two drops of 0.1 wt. % carbon dispersion in 2.5 wt. % P1 solution, using individual polymer and surfactant solutions were also analysed using the Scion software. The results obtained are shown in figure 7.40.

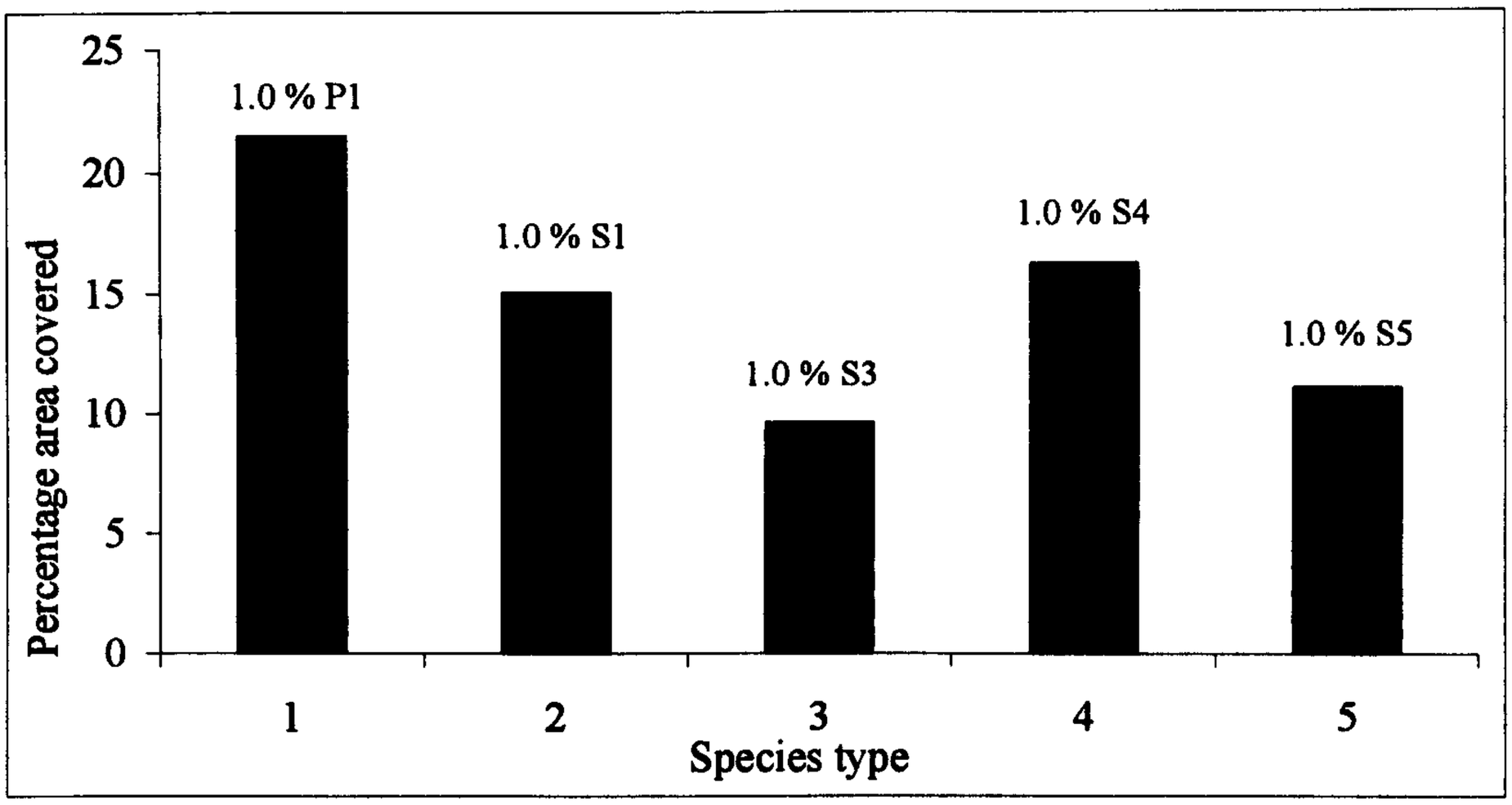

Figure 7.40: Percentage area covered by the carbon particles after the removal experiments using individual polymer and surfactant solutions as calculated using the Scion image analysis software

7.4. Analysis and Discussion

7.4.1. Adsorption of carbon particles on steel beads from dispersions in isooctane solutions

It was observed that the carbon particles could only be successfully dispersed (to the eye) in isooctane using either the polymer (P1) or the S3 surfactant, both of which contain a terminal amine functionality. However, only the particles with adsorbed P1 subsequently remained stable to aggregation for any significant length of time. During the adsorption experiments, the mixture of carbon dispersion in a polymer/surfactant solution and steel beads were tumbled together for 20 h. However, it was found that the adsorbed amount of carbon particles reached a limiting value within a few hours (fig.7.4). The adsorption isotherms of the carbon particles on the stainless steel beads, from dispersions in isooctane containing P1 (fig. 7.5) and S3 (fig. 7.6) indicate that the adsorption of the carbon particles onto the steel beads appears to be much greater in the presence of the surfactant S3 compared to the polymer P1. However, this simply reflects the observation, referred to above, that, although S3 adsorbs onto the carbon particles, it does not stabilise them sufficiently against aggregation. Hence, the carbon particles, in the presence of S3 (either alone, or in mixtures with S1 or S5), are adsorbing onto the steel beads as *aggregates*. The fact that the isotherms obtained in fig. 7.6, are of a "reasonable" form (i.e. the data not too scattered), indicates that the aggregated carbon particle structures are seemingly reproducible. The highest initial concentration of carbon particles used in the adsorption studies was 1 wt. %. If *all* of those carbon particles were to adsorb onto the steel particles then the adsorbed amount would be between ~ 28 mg m^{-2} (based on the B.E.T surface area for the steel balls), and ~ 75 mg m^{-2} (based on the geometric area). The maximum observed adsorbed amount (~ 25 mg m^{-2}) is less than either of these values, so some free (non-aggregated ?) carbon particles remain present in the dispersed phase, as is indeed observed.

Furthermore, if the adsorption isotherms were carried out after longer times of leaving the samples standing (fig. 7.7), the adsorbed amount increased. This can only be due to sedimentation for carbon particles because S3 cannot stabilise them for a significantly long period of time. If the carbon particles were not aggregated, and adsorbed as a hexagonally close-packed monolayer on the steel beads, then the maximum adsorbed amount would be 240 mg m^{-2}, assuming a carbon density of 2 g cm^{-3}. From figure 7.5, it can be seen that the maximum adsorbed amount of carbon particles, in the presence of P1, is considerably much lower than this, i.e. ~ 6 mg m^{-2}.

It is also clear from fig. 7.6 that, as expected, the presence of S1 or S5, together with S3, has very little effect on the adsorption of the carbon particles on the steel beads.

In chapter 3 of this thesis, it was shown that polymer P1 (but not the surfactants) may leach "Fe species" from the surface of steel particles, and hence "distort" adsorption measurements based on turbidity data. That is why isooctane, which had been previously exposed to the steel balls, was used in the reference cell in the turbidity measurements. There may, however, still be some doubt about the reliability of this particular adsorption result. Nevertheless, it is not clear why the adsorbed amount is apparently *so* low, particularly when compared to the large amount of carbon particles *deposited* on the surface of a steel plate, in the presence of P1, to be discussed in the next section (see figure 7.9). Given the relatively high total surface area of steel beads used (compared to the steel plate), it could be speculated that there is little actual adsorption of P1 polymer on the surface of the steel beads, and that the P1-covered carbon particles are adsorbing, therefore, onto essentially *bare* steel surfaces, and this could be why their affinity for the beads is low.

7.4.2. Deposition of carbon particles on a steel plate from dispersions in isooctane solutions

SEM micrographs of the deposition of carbon particles on a polished stainless steel plate from 0.1 wt. % dispersions of carbon particles in P1 solution (2.5 wt. %) show that the surface coverage of P1-coated carbon particles on the steel plate is relatively high as compared to deposition from carbon dispersion in S3 solution (2.5 wt. %). Moreover, it looks as if the carbon particles are aggregated. This is in stark contrast to the adsorption data reported in fig 7.5 for the adsorption of P1-coated carbon particles on the steel beads. However, in the case of the plate, it is likely that the steel surface *is* covered in P1. The total surface area (of steel) available was much lower, and the initial concentration of P1 was somewhat higher, than in the case of the bead experiments. Moreover the steel plate was continuously exposed to fresh P1 solution flowing over its surface. Indeed, the amount of carbon deposited increased when the steel plate was deliberately pre-exposed to P1 solution before commencing the flow experiment (fig. 7.36 and fig. 7.37). The reason for the high adsorbed amounts, and some carbon particle aggregation, on the steel surface, probably has to do with the fact that isooctane (and aliphatic hydrocarbons in general) are actually not that good solvents for PIB chains[5]. Also, changing the solvent to toluene or o-xylene (known good solvents for PIB and benzene is a θ solvent at 24.5 °C[6]) gave a much cleaner surface with minimum deposition as shown in figures 7.36 and 7.37. Thus, although the P1 chains adsorb on the carbon particles (through the terminal amine groups), and the particles indeed appear to be dispersed to the eye, nevertheless, there may be some limited, weak aggregation of the carbon particles in isooctane media, associated with less than totally effective interparticle steric repulsion. This could be due to an insufficiently thick adsorbed layer, or more likely in this case, due to some weak osmotic attraction between the PIB chains on approaching particles. Similar weak

aggregation has been confirmed by rheology and other experiments[7] carried out to study the stability of carbon particles in the presence of related functionalised PIB molecules in aliphatic hydrocarbon media. With the S3 molecules, on the other hand, the more extensive aggregation of the carbon particles, observed over time, is almost certainly due to there being too thin an adsorbed layer (essentially the C_{13} aliphatic chains) on the carbon particles. Aliphatic hydrocarbons are good solvents for the C_{13} chains. The reason for the large adsorbed amounts of the P1-covered carbon particles on the P1-covered steel plates, is probably due also to the weak osmotic attraction between protruding PIB chains on each surface. (Recall that with the steel *beads* – section 7.4.1 - it is likely that the steel surfaces were largely devoid of adsorbed PIB).

When the carbon particles are deposited from S3 solution in isooctane alone (figure 7.10), then a much lower coverage is observed. Some aggregates appear to be present, but, as discussed earlier, the carbon particles were observed to aggregate slowly anyway in isooctane dispersions in the presence of S3. One has to ask why such a low coverage of carbon particles is obtained on the steel plates, compared to the steel beads (fig. 7.6)? It has been shown previously in chapter 3 that S3, and indeed all the other surfactants used in this study, adsorb strongly on steel surfaces. Also, it is known that S3 is indeed a good anti-deposition agent for preventing carbon deposition in engines. Unlike in the "quasi-static" experiments carried out with the steel beads, in the *flow* experiments any large aggregates of carbon particles would simply be "swept off" the surface of the steel plate. The removal force, for a given flow rate, is proportional to particle size. Thus, only singlets and relatively small aggregates remain on the steel surface after the flow experiment.

In figure 7.13, the carbon particles deposited from a mixture of P1 and S3 seem to be slightly greater in number, but perhaps slightly less aggregated, than for S3 alone (fig. 7.10). On the other hand, the deposited amount is less than for P1 alone (fig. 7.9).

Similar results are also obtained for some of the surfactants, especially S1 (fig. 7.11) and S2 (fig. 7.12). Clearly the surfactants are preferentially adsorbed, compared to P1, on the steel plate surface, and this prevents any osmotic attraction between the carbon particles and the steel surface, as was suggested to occur in the presence of P1 alone. However, the P1-coated carbon particles are somewhat more stable in bulk dispersion than the S3-coated particles. Hence, fewer aggregates are seen on the steel surface in the case of the P1+S3 mixture (fig. 7.13) compared to S3 alone (fig. 7.10). The same reasoning can also be applied to explain the lesser aggregation seen in the presence of the other surfactants (figures 7.11, 7.12, 7.14 and 7.15). The relative trend in the percentage area covered on deposition from various systems has been quantitatively obtained using the Scion image analysis software (fig. 7.38). This shows that the deposition is highest in the presence of the polymer and least in the presence of the S3. Also, deposition from a polymer and surfactant mixture system is relatively less than that of the polymer on its own.

7.4.3. Removal of deposited carbon particles from the steel surface

The stainless steel plate with carbon particles deposited from 2.5 wt % solution of P1 in isooctane (i.e. corresponding to fig. 7.9) was subsequently subjected to 'removal' experiments, by passing the solvent or a solution, as appropriate, through the flow cell. In these experiments the steel plate was always covered with liquid, and never allowed to "dry". It was found that "washing" the steel surface with isooctane alone reduced the deposited amount of P1-coated carbon particles. Using the Scion software to analyse the total area occupied by adsorbed carbon particles, the reduction in the amount of carbon deposited was about 50 % (fig. 7.39). The effect of using a solution of P1 (at 2.5 wt %) may be seen directly by comparing fig. 7.17 with fig. 7.9. Again, a significant amount of the deposited carbon seems to have been removed by this "washing" action. Using the Scion software, in this case, the reduction in the amount of

carbon deposited is about 58 %. It is probable that the removal of the particles in the above cases is mostly "mechanical" in origin. When P1+S1, P1+S3, or P1+S5, were used as the "washing" solutions, a greater decrease in the amount of deposited carbon was seen (figures 7.18, 7.19 and 7.20 respectively). Using the image analysis software, the reductions in surface area occupied by the deposited carbon particles were now 73 %, 71 % and 66 %, respectively. In the cases where S1, S3 or S5 is present, these surfactant molecules are probably displacing the more weakly adsorbed P1 molecules from the steel surface, and this is another mechanism for removal of the deposited carbon particles.

The effect of *drying* the deposited particles on the plate, prior to the removal stage, was also studied and these results can be seen in figures 7.21 to 7.26. It was not possible to obtain a picture of the dried particles on the plate because the polymer melted when bombarded by electrons in the SEM. Analyses of the SEM micrographs using the Scion software showed that S3 is the most effective removal agent as compared to the other surfactants studied (fig. 7.40). In a similar set of experiments, carbon particles were dispersed in propan-1-ol, *without* any polymer or surfactant. The particles seemed to be somewhat better dispersed in this more polar solvent than in isooctane alone. However, some aggregates were undoubtedly present. Two drops of this carbon dispersion in propan-1-ol were evaporated onto the surface of a steel plate and allowed to dry. It was noticed that, after evaporation, the carbon particles formed large, separated clusters on the steel surface as shown in fig. 7.27. The steel plate was placed in the flow cell and attempts were made to remove the carbon particles by flowing through isooctane, polymer solution, or a surfactant solution. It was not possible to remove the particles and large clusters of aggregated carbon particles remain on the steel surface as shown in figures 7.28 to 7.33. Clearly, it is important that the carbon particles are more-or-less well dispersed in the solvent, by the adsorption of the

functionalised PIB polymer chains, prior to their deposition on the steel surface. Otherwise, the polymer or surfactant molecules become ineffective as removal agents.

7.5. References

1. Elzo, D., Schmitz, P., Houi, D. and Joscelyne, S., *Journal of Membrane Science*, 1998. **109**: p. 43.

2. Varennes, S., and Van de ven, T. G. M., *Colloids and Surfaces*, 1988. **33**: p. 63.

3. Visser, J., *Journal of Colloid and Interface Science*, 1970. **34**: p. 26.

4. Sharma, M.M., Chamoun, H., Sita Rama Sarma, D. S. H. and Schechter, R. S., *Journal of Colloid and Interface Science*, 1992. **149**: p. 121.

5. Cox, A.R., Mogford, R., Vincent, B and Harley, S., *Colloids and Surfaces A: Physicochemical and Engineering Aspects*, 2001. **181**: p. 205-213.

6. Brown, W., and Zhou, P., *Macromolecules*, 1991. **24**: p. 5151 - 5157.

7. Mogford, R., *The effect of polymer chain architecture on the adsorption properties of derivatised polyisobutylenes at the carbon/n-heptane interface*. To be submitted, University of Bristol.

CHAPTER 8: CONCLUSIONS AND FUTURE WORK

8.1. Conclusions

8.1.1. Materials

The functionalised polyisobutylene and the five different alkoxylate surfactants, all synthesised at Lubrizol UK, were used without further treatment. The BET surface area of the steel beads and the carbon particles were about 0.3 m^2g^{-1} and 210 m^2g^{-1}, respectively. Carbon particles showed a slight hysteresis in the adsorption-desorption isotherms of nitrogen gas indicating a porous surface. The steel beads were found to be around 7 μm in diameter while the carbon particles gave a diameter of around 214 nm.

8.1.2. Adsorption isotherms of the polymer and surfactants

The adsorption isotherms of the polymer and various surfactants on steel beads and carbon particles showed mostly type II and type III BET isotherms suggesting the formation of aggregates or multilayers at the solid/isooctane interfaces. Zhu-Gu model fit studies gave aggregation numbers in the range 2 to 6 for all the species except for S3 on carbon which seemed to form a monolayer, in the concentration range studied. The polymer leached the steel surface of metal ions at high concentrations giving rise to negative values of the adsorbed amount and thus, no model fits could be carried out. The functionalised species namely, the polymer and S3 (an alkyl butoxylate chain with an ethylene amine head group) showed strong adsorption, even at very low concentrations. When polymer and surfactant mixtures were adsorbed on steel beads, a decrease in the adsorbed amount of the polymer was observed signifying that the surfactant either displaced the adsorbed polymer or solubilised the loosely bound polymer molecules into the solution. The molecules may be forming mixed aggregates in solution. However, one surfactant has no such effect on another surfactant.

8.1.3. Aggregation studies

The model fit studies of the adsorption isotherms indicated the presence of aggregates at the solid/isooctane interface. Therefore, it was hypothesised that there would most likely be aggregates in solution too, existing in equilibrium to the adsorbed aggregates. Vapour pressure osmometry experiments were carried out using the polymer and all the surfactants. However, these gave no conclusive results or aggregation numbers. The aggregation in solution was then studied using Rhodamine B, a water soluble dye which can easily solubilise in the polar core of the reverse micelles. Its absorbance was monitored as a function of polymer concentration and this showed evidence of aggregation in solution. The polymer, with the most polar head group, formed aggregates in solution and the addition of a surfactant showed only a slight change.

8.1.4. Atomic force microscopy studies

Atomic force microscopy experiments were carried out using a carbon particle probe measured against a finely polished steel plate in the presence and absence of polymer/surfactant in isooctane. The distance of interaction increased almost linearly with increasing polymer concentration indicating a constant build up of molecules at the interfaces. Though surfactant S5 had twice the number of propoxylate units as compared to S4, the two showed no difference in the distance of interaction signifying that they laid flat at the interfaces. Experiments were also carried out using mixtures of the polymer and a propoxylate surfactant. It was noticed that the distance of interaction decreased with increasing surfactant concentration demonstrating a removal of adsorbed polymer layers or solubilisation of the loosely bound polymer molecules. A similar conclusion was also drawn from the adsorption isotherm experiments.

8.1.5. Ellipsometry studies

Ellipsometry showed a very fast kinetics of adsorption of the polymer at the steel/isooctane interface. The polymer gave the thickest layer and the layer thickness increased continuously with increasing concentration. All the surfactants gave a very thin layer, verifying the conclusions drawn from the atomic force microscopy experiments that they lay in a flat conformation at the interface. Surfactant S3, with an ethylene amine head group, showed a slightly thicker layer than the rest of the surfactants and this was attributed to the added functionality. The addition of a surfactant to an adsorbed polymer layer generally gave rise to a slight increase in thickness initially which then decreased with time. Extra additions of the surfactant molecules did not change the thickness further. This suggested an interaction between the different species at the interface before attaining equilibrium. The adsorbed polymer molecules could also be easily diluted to give a thinner layer by adding the solvent indicating that the polymer molecules are held loosely at the interface. It was also found that the polymer adsorbed at the interface whether a surfactant layer occupied the surface or not. This further justifies the suggestion that the adsorption of the different species involved a synergistic interaction between the different molecules.

8.1.6. Adsorption and deposition of carbon particles

The adsorption of carbon particles on stainless steel beads, in the presence of the polymer and S3, the functionalised surfactant, showed that the adsorbed amounts were much higher in the case of the surfactant. The surfactant, though it adsorbs on the particles, does not stabilise the carbon particles against aggregation. Thus, the particles adsorbed as aggregates on the steel beads. Letting the samples stand for longer time led to an increase in the adsorbed amount indicating the effect of sedimentation of the large agglomerates. The polymer, on the other hand, dispersed the particles very well and little particle adsorption was observed.

A flow cell was built to study the deposition of carbon particles on stainless steel plates. The particles were deposited by flowing a dispersion of the particles in a polymer/surfactant solution and the plates were analysed by using a scanning electron microscope. In this case, larger depositions were observed in the presence of P1 than S3. This was attributed to the fact that particles formed larger aggregates in the surfactant solution which could easily be swept off the steel surface by the flow of the solution.

Extensive deposition and removal experiments were carried out using carbon particle dispersions in various combinations of the polymer and surfactants. The electron micrographs obtained were then analysed by using an image analysis software to obtain the percentage area covered by the particles. The general trend observed was that the particle deposition was reduced in the presence of the surfactants. The polymer and surfactant mixture solutions were also able to remove the particles more efficiently. Changing the solvent from isooctane to o-xylene or toluene in the deposition experiments gave a drastic reduction in the amount of carbon particles deposited. It was also found that the particle deposition increased if the steel plates were pre-coated with a polymer layer. Finally, it was also observed that the particles could not be removed from the surface if they did not have a layer of polymer around them before they were deposited.

8.1.7. Summary

This work has shown that the polymer is the species that provides a steric barrier between the carbonaceous particles, and against the steel surfaces. The presence of the polymer layer is quintessential for the "carrier fluids", or surfactants, and solvent to remove the particles. The surfactant molecules not only help in reducing the deposited amount but also play an active role during removal. They form mixed aggregates with

the polymer in solution and at the interface. This may help disperse the carbonaceous particles in solution easing their removal.

8.2. Future work

During the course of this study, a 'hot box tumbler' was built to help facilitate the investigation of adsorption isotherms at higher temperatures. Unfortunately, the work could not be carried out comprehensively due to the low surface areas of the steel beads and the small volumes involved. The volatile nature of the solvent also made it difficult to go up to higher temperatures. Carrying out the experiments in a high boiling point solvent such as hexadecane and using carbon particles as the adsorbent can overcome this and form the core of future studies.

Similarly, a high-temperature and high-pressure flow cell can also be built to emulate the conditions found inside an internal combustion engine. Further work also can be carried out with the flow cell by using solvents like o-toluene or xylene.

The interactions between the polymer and the surfactant in solution also can be investigated more by using other techniques like neutron scattering and nuclear magnetic resonance.

The role played by the polymer and surfactants in charging the carbon particles and the possibility of electrostatic contributions in particle stabilisation also need further investigation. This can be carried out by using techniques like phase-analysis light scattering and electroacoustic measurements.

The exact role of the polymer head group and the polyisobutylene tail in the adsorption and stabilisation of the carbon particles can also be studied by synthesising polymers with varying head groups and tail units.

Further ellipsometry experiments can also be carried out to study the adsorption and interactions between the different species on a carbon surface. Improvements in the

technique may also help in measuring the orientation of the adsorbed molecules at the solid/liquid interface.